PREDICTING NATURAL VENTILATION IN RESIDENTIAL BUILDINGS IN THE CONTEXT OF URBAN ENVIRONMENTS

by

Adil M. K. Sharag-Eldin

B.Sc. (University of Khartoum) 1983
S.M.Arch.S. (Massachusetts Institute of Technology) 1988

A dissertation submitted in partial satisfaction of the

requirements for the degree of

Doctor of Philosophy
in

Architecture

in the

GRADUATE DIVISION

of the

UNIVERSITY OF CALIFORNIA, BERKELEY

Committee in Charge:

Professor Edward E. Arens, Chair
Professor Charles C. Benton
Professor Robert Reed

Fall 1998

Acknowledgments

I would like to express my gratitude first to Professor Edward Arens, my thesis supervisor for his guidance, friendship, and support throughout the research and writing of this dissertation. His patience and attention to details have helped me to remain on the path during the long and arduous course of my studies. Without him, there would be no dissertation.

My appreciation extends to the members of my dissertation committee, professors Charles Benton and Robert Reed. Their contribution was instrumental in shaping the dissertation the way it is represented here.

I wish also to thank professors Gail Brager and Nezar Al Sayyad for their participation in the Qualifying exam committee. With the members of the dissertation committee, their comments and discussions have enriched and broadened the scope of the research.

I wish to acknowledge Fred Bauman and Charlie Hezinga for their friendship and help in the various stages of the project.

This project has been funded by two grants from the University of California Energy Institute. Without these grants, conducting this project would have been very difficult if not impossible.

Adiyana, my wife, supporter, and friend. Because of her believe in me, I could finish the dissertation despite the hurdles. Without her Love and sacrifices, nothing would have been possible.

Abstract

Predicting Natural Ventilation in Residential Buildings in the Context of Urban Environments

By
Adil M. K. Sharag-Eldin

Doctor of Philosophy in Architecture

University of California, Berkeley

Professor Edward E. Arens, Chair

The objective of this dissertation was to develop, through systematic research and experimentation, a mathematical model for predicting exterior surface pressures and indoor air velocities for small-scale buildings in urban settings. The resulting model is a step-by-step series of functions that produce these results while accounting for various possible geometric relationships between the building and the urban surroundings.

This study was conducted in two phases. The first phase developed an empirical Pressure Prediction Model (PPM) for shielded surfaces using a sequence of wind tunnel tests. The model produces a non-dimensional Pressure Modification Coefficient (C_{pm}) using a set of geometric variables that describe urban surroundings in terms of obstruction blocks and the gaps between them. A number of empirical corrections account for horizontal displacement of obstructions and for wind direction effects. C_{pm} is then used to calculate the average pressure coefficient on shielded surfaces. The wind tunnel tests show that the shielding effect of an obstruction block is significant within a $\pm 70^{\circ}$ arc around the wind direction, and that it is possible to predict the shielding effect of multiple obstruction

blocks within this arc by averaging the shielding effects of individual obstruction blocks and summing the effects of all the gaps.

The second phase concentrated on the development of an Indoor Velocity Prediction Model (IVM). The IVM uses the PPM-predicted surface pressures on shielded walls as input to a model developed by Ernest (1991) to determine the Indoor Velocity Coefficients (IVC). The IVM model also adopts a procedure developed by Arens *et al* (1986) to convert remote weather station data into site-specific wind speeds. Arens' procedure corrects for the differences in height between the weather station and the site, the differences in terrain roughness characteristics between the two locations, and wind acceleration due to site topography.

The PPM was verified against Wiren's (1984) tests of an instrumented model in different arrays of similarly configured obstruction blocks, and against an instrumented model in a more complex layout. The predicted and the measured pressure values showed a reasonably good fit in both cases. The successes and limitation of the model are discussed.

The IVM predictions of interior airflow were not validated here. Ernest has validated his model in both unobstructed and simply-obstructed conditions, and the PPM is not expected to change the nature of the interior flows predicted by Ernest's model.

TOC

Table of Contents

Chapter 5: Implementations of the Prediction Model

LOF

List of Figures

LOT

List of Tables

LOS

List of Symbols

Nomenclature

A_i	= Open inlet area, mm^2 or m^2
A_o	= Open outlet area, mm^2 or m^2
A_w	= Interior area of wall, mm^2 or m^2
A_f	= Face Aspect Ratio, ND
A_s	= Side Aspect ratio, *Equation (4-7)*, ND[a]
C_d	= Discharge Coefficient, ND
C_p	= Mean Surface pressure coefficient, *Equation (4-1)*, ND = $C_{p_{av}}$
C_{p_i}	= Surface pressure coefficient at point i
C_{p_Θ}	= Mean surface pressure coefficient at wind direction Θ, ND
$C_{p(shielded)}$	= Pressure Coefficient on a shielded surface, *Equation (4-2)*, ND
$C_{p(unshielded)}$	= Pressure Coefficient on an unshielded surface, *Equation (4-2)*, ND
C_{pm}	= Pressure Shielding Modification Coefficient *Equation (4-3)*, ND
$C_{pm(ortho)}$	= Pressure Shielding Modification Coefficient, *Equation (4-8)*, ND

$C_{pm_{\alpha d(corr)}}$	= C_{pm} Corrected to account of wind displacement angle α_d effect, *Equation (4-9)*, ND
$C_{pm_{\Theta(corr)}}$	= C_{pm} Corrected to account for wind direction Θ effect, *Equation (4-9)*, ND
$C_{p(Norm)}$	= Normalized Pressure Coefficients, *Equation (4-2)*, ND
C_{sv}	= Coefficient of spatial variation, ND
C_v	= Average velocity coefficient, *Equation (5-29)*, ND
d	= Zero plane displacement height, *Equation (A-1)*, mm
d_m	= Model depth, mm
g	= Gap or spacing between adjacent blocks, *Equation (4-21)*, m or mm
ht_m	= Model height, m or mm
ht_o	= Obstruction height, m or mm
k	= von Karman's constant, *Equation (A-1)*, ND
NC_p	= Normalized surface pressure, *Equation (4-7)*, ND
P_{dyn}	= Mean dynamic pressure at surface, Pa
P_m	= Mean pressure at model surface, Pa
P_n	= Interior partition type, Equation (5-29), ND
P_s	= Mean static reference pressure, Pa
r_{calc}	= Radial coordinate of calculated corner point of an equivalent obstruction block, *Equation (5-9)*, S_o [b]
r_n	= Radial coordinate of point n, expressed in obstruction heights (ht_o), *Section 5.3.1*, S_o

$r_{\frac{w}{2}}$	= Radial coordinate of the point connecting the mid points of both the surface and the equivalent adjacent block, *Equation (5-10)*, S_o
$ROGRAT$	= Roughness wind speed modification factor, Equation *(5-21)*, ND
S	= Spacing or distance between an adjacent block and the surface for which the pressure is predicted, m or mm
S_m	= Spacing expressed in model heights (ht_m), ND
S_o	= Spacing expressed in obstruction heights (ht_o), ND
$SLPFAC$	= Slope wind acceleration factor, Equation *(5-24)*, ND
$S_{\max}$	= Maximum fractional speed-up ratio at ground level, *Equation (5-27)*, m/s
U_f	= friction velocity, *Equation (A-1)*, m/s
V_e	= Mean wind velocity at eave height, *Equation (3-3)* m/s
V_g	= Mean wind velocity at gradient height, m/sec
V_i	= Indoor velocity, m/sec
V_o	= Outdoor velocity, m/sec
V_r	= Velocity at reference height, m/sec
V_w	= Velocity at weather station, m/sec
V_z	= Mean wind velocity at height z, *Equation (A-1)*, m/s
W_m	= Model width, mm
W_o	= Obstruction width, m or mm
z	= Height above ground level, *Equation (A-1)*, m
Z_i	= Height at point *i*, m

Z_g	= Gradient Height, m
z_0	= Roughness length, *Equation (A-1)*, m

a. ND = Non Dimensional.

b. S_0 = Obstruction spacing.

Greek Letters

α	= Velocity profile exponent, *Table B-1*, ND
α_h	= Horizontal angle of obstruction description, *Section 4.6.2.1*, degree
α_v	= Vertical angle of obstruction description, *Section 4.6.2.2*, degree
α_d	= Displacement angle of obstruction block relative to the surface under consideration, *Section 4.6.2.5*, degree
Δ	= Absolute value of difference
Θ	= Wind direction, degree
Θ_{ws}	= Wind direction as presented in weather data (0˚-360˚), *Section 5.3.3.1.1*, degree
Θ_m	= Wind direction used in the prediction model, *Section 5.3.3.1.2*, degree
Θ_{rel}	= Wind direction relative to the surface for which the pressure is predicted, *Section 5.3.3.1.3*, degree
λ_n	= Angular polar coordinate of point n, *Section 5.3.1*, degree
Π	= Multiplication notation
ρ	= Density of air, kg/m^3
Σ	= Summation notation
φ	= Wall porosity (window area/wall area), *Equation (5-29)*, ND

Chapter 1

1

Introduction

1.1 Prelude

Wind is one of the most noticeable of the invisible elements a person may encounter. Throughout history, a general understanding of the effects of wind on shaping human settlements has evolved. This understanding has been *intuitive*, a product of a long trial-and-error process. Since the requirements for human habitability vary for different climates, different architecture and urban plans have evolved in the different climatic regions of the world. These traditional vernacular designs are usually able to provide their occupants with effective thermal comfort, often in spite of constraints in available materials and energy for space conditioning. In many climates, thermal comfort is provided by allowing fresh air to flow into interior spaces (natural ventilation).

Since the introduction of electricity and mechanical air-conditioning, building designers could create islands of indoor comfort isolated from their climates. The result is that the art of designing for comfort via natural ventilation is disappearing among the building design community.

As a result of the technical advances in aerodynamics, *scientific* understanding of natural ventilation has become possible. Engineers have used wind tunnels to study the strength of structures against wind forces by measuring wind pressures on building surface.

Since the second half of the nineteenth century, the engineers have established a link between indoor airflow and surface pressures on buildings. In fact, the earliest recorded use of wind tunnels for studying pressures on model buildings was by W. C. Kernot in Australia and Irminger in Denmark in the 1890's (Ref. 30). Kernot studied building models including the effect of parapet walls and surface pressures on gable roofs of various angles of inclination. In Denmark, Irminger worked on flat plates, airfoil sections, and simple building models[1].

Researchers have used methods developed for studying structural wind problems in natural ventilation studies. These applications began in the 1940's and 50' with the work of J. B. Dick *et al* on the studies of infiltration in houses (Ref. 69), and Smith, White, and Caudill in the Texas Engineering Experiments (Refs. 187, 221, & 47) on natural ventilation. Currently, building aerodynamic studies are concerned with the following aspects of design:

- To provide thermal comfort through allowing cooler outside air to remove solar and internal heat gains.

1-1 From class notes, Prof. Arens, E. 1993.

- To reduce energy consumption by using natural ventilation to cool the structure at night (often applied to hot-dry climates).
- To cool building occupants by air movement (warm humid climates).
- To understand the effects of surrounding buildings and vegetation on airflow through buildings openings.

1.2 General Objectives

The objective of this study is to develop, through systematic research and experimentation, a numerical model for the prediction of natural ventilation in small-scale buildings within urban settings. There are already generic models for predicting natural ventilation, but these models depend on published surface pressure data to predict interior airflow. Most of existing published data have been collected either for isolated buildings or for buildings in highly prescribed layouts of obstruction blocks. This study concentrates on the development of a mathematical model to predict surface pressures on shielded buildings that is independent of layout. This mathematical model is based on a flexible system of obstruction block description that is intended to allow the model to accommodate many urban patterns. The is also developed to be easy to use by designers.

1.3 Scope

The dissertation is divided into three parts. The first part (Chapter 2) uses vernacular examples to illustrate the effect of natural ventilation in shaping architectural and urban designs. The second part (Chapters 3 and 4) deals with developing the

scientifically-based ventilation prediction tools. Wind tunnel testing and mathematical correlation techniques were used to provide functions that can be generalized to apply in a wide variety of urban situations. The third part (Chapter 5) applies the functions to predict natural ventilation for a building located in the heart of complex urban surroundings.

Chapter 2 includes examples of how to incorporate climatic requirements in the design of individual building and urban planning. These examples illustrate the adaptation of environment responsive design features in both hot-arid and warm-humid climates.

Chapter 3 includes a discussion of the requirements for natural ventilation and the mechanisms affecting indoor airflow. The chapter also provides a comprehensive background coverage of natural ventilation research and prediction techniques.

Chapter 4 encompasses the development of the mathematical functions needed for predicting building surface pressures. The experiments were conducted in four phases. The first phase was to establish a basic relationship between measured pressures on the wall surfaces of a target model building and a geometric description of the individual building block obstructing it. The second phase dealt with the displacement of the obstruction block relative to each surface on which pressure was measured. Phase two concluded that the effect of this displacement could be treated as a correction to the functions provided in phase one. The third phase was an added correction based upon the effect of changing the wind direction

relative to the model and its obstruction. The fourth phase involves the effect of multiple obstruction blocks and the spaces between them on the target building. Chapter 4 concludes with the verification of the mathematical model using data obtained from previous experiments and from complex urban patterns tested in the wind tunnel facility.

Chapter 5 discusses the application of the developed mathematical model referred to as the Pressure Prediction Model (PPM). The first part of the chapter deals with the determination of the inputs to the model. These inputs include the development of mathematical and geometric functions for the description of obstruction blocks relative to the target surfaces. Other inputs include weather and pressure data. The application of the mathematical model includes an illustration of a method for transforming weather station data to site specific conditions. The chapter also describes the integration of a mathematical model developed by Ernest (Ref. 74) for the prediction of indoor velocity coefficients using surface pressure data provided by the mathematical model developed in Chapter 4.

Appendix A describes the wind tunnel, the instrumented and obstruction models and the various instruments used throughout the research.

Appendix B describes a detailed calculation of the effect of using different boundary layers from the one used in the experiments. The resulting boundary layer conversion factors are tabulated.

Appendix C is a documentation of pressure measurements on unobstructed models of various sizes and shapes under different wind directions. These unobstructed pressures are the basis for the mathematical functions provided in the PPM.

Appendix D documents test results of shielded surface pressures used in the derivation of the mathematical function in phase one of Chapter 4.

Data used for deriving the displacement corrections are shown in Appendix E .

Appendix F shows the result of changing wind direction on surface pressures for the various tested surfaces and obstruction geometries.

Appendix G illustrates the results of the multiple obstruction study.

Appendix H , demonstrates the use of the mathematical models, its input, and the different phases of calculations used to produce the indoor velocity values. These calculations are performed on the complex model pattern used for the verification of the mathematical model in Chapter 4.

Chapter 2

2

Notes on Natural Ventilation in the Context of the Built Environment

2.1 Introduction

Natural ventilation has always affected the environment within which human settlements have evolved. Among the many physical factors involved in creating buildings, climate plays a major role in shaping the built environment. Natural ventilation has manifested itself in dramatic architectural design solutions (Figure 2-1). However, building layout also affects the movement of wind around and within buildings. This chapter describes the reciprocal relationship between climate and the built form.

Figure 2-1 Cool Towers in Hyderabad, Source: Melaragno (Ref. 161)

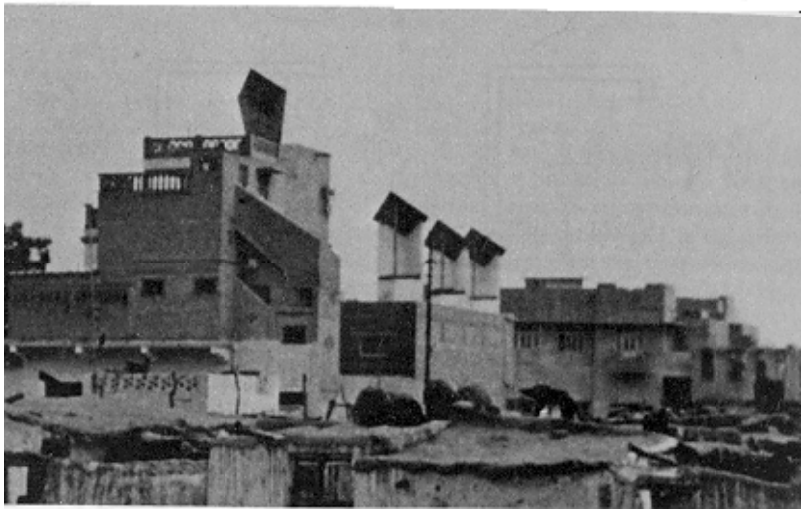

2.2 Climatic Determinants in Architecture and Urban Form

The unique combination of various forces that determine the built form creates an urban context unique to the place and time in which the building is situated (Ref. 279). At the individual building level, climate has an essential role in defining the most suitable architectural form.

Determinants of architectural form can be divided into physical and non-physical components. While the emphasis in this study, is on the role of climate as a force shaping architectural form, the author recognizes the complex interaction between the built form and its many determinants. This understanding is illustrated in the following conceptual model:

Figure 2-2 Determinants of built form.

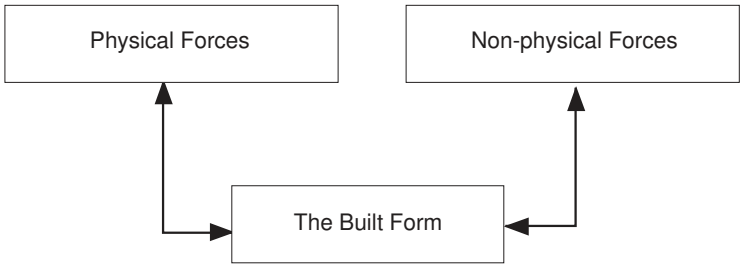

Non-physical forces include defense, religion, and socio-economic factors. Although more difficult to circumscribe than the physical influences, non-physical determinants offer broader range of explanations to match the diversity in the architectural form. In contrast, the physical factors are easy to define and their effects are easy to detect. Climate, site, technology, and other material resources are among those physical forces that determine the built form.

The proposed model shows two-way links between the built form and its determinant forces (Figure 2-2). This two-way

relationship suggests that the built form affects its determinants as well as it is affected by them. With the multiplicity of determinants, the role of each form-generating force is limited to modifying the built form instead of deciding it.

This chapter will concentrate on the role of climate in modifying the built form in both individual and urban scales. Examples of buildings in two climatic regions will be used to demonstrate the range of built form adaptation to climate.

2.3 Climate and The Built Form

Shelter is one of the basic purposes of the house. By definition, it protects against climatic elements and provides comfortable, safe, and defensible domain. Depending on the climatic conditions, the built environment has taken various forms to provide the basic requirements of shelter (Ref. 260).

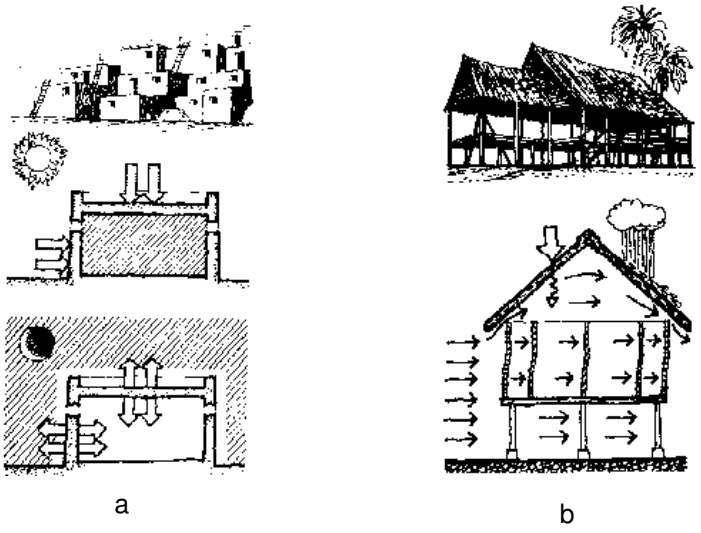

Figure 2-3 Climatic effects on building form. Examples for Hot-dry climate (left), and for Warm-humid region (right). Source: Konya (Ref. 260).

Figure 2-3 shows schematics of two primary patterns of building form adaptation to hot-arid and warm-humid climates. In

order to maintain cool interior surfaces for midday and afternoon indoor space uses, buildings in hot-dry climates require high mass to delay heat transfer to the interiors (Figure 2-3a). Windows in this pattern are as small as possible (Figure 2-4) to reduce passage of hot air and solar radiation (Ref. 282). Another characteristic of the windows in this climate is their location at higher levels in the room to promote a thermal stack effect[1]. Finally, buildings in hot-arid climates are often as compact as possible to reduce the surface area of the structure exposed to the solar radiation and the hot surroundings.

Figure 2-4 Window Configuration in Hot-arid Climates, Source: Norberg-Schulz (Ref. 273).

In warm-humid climates the pattern is more towards the side of lightness and airiness (Figure 2-3b). Examples of this pattern can be found in most parts of the warm-humid regions of

2-1 Thermal stack effect occurs when air is allowed to move freely from an inlet source at low level to the outlet usually at higher level.

the world except in a few cases where cultural and social reasons override environmental requirements[2].

TABLE 2-1 shows a summary of the impact of the hot-dry and warm-humid climates on the built form. These climatic responses carry design decisions that influence the architectural style most suited for each climate.

TABLE 2-1 **Summary of Climatic Impact on Building Form in Selected Hot Climates**

Building Element	Climate	
	Hot Dry	**Warm Humid**
Geometry	As compact as possible	Elongated perpendicular to wind direction
Walls	Massive	Light
Windows	Aperture should be as small as possible	As open as possible to allow for maximum air velocity for occupants' comfort
Shading	Important to shade at all times	Shading is important
Surface to Volume Ratio	As small as possible	not as important
Relation to ground	Close or even underground	Elevated from the ground if possible

2.4 Wind and the Built Form

Although the field of building aerodynamics is relatively new, designing for wind is as ancient as buildings themselves. Since the beginning of human settlements, traditional plans have maintained formal structures that responded to climate. The

2-2 Examples of anticlimatic designs were observed by the author in Java, Indonesia where thermal stack effect is used instead of direct ventilation through windows because of the fear of air penetrating human body and disturbing its balance.

archeological digs of the ancient city of Kahun in Egypt 2000 B.C. showed urban zoning based on separating the city into favorable and unfavorable wind sites. Public buildings and officials' housing were located in zones that enjoy the flow of pleasant northerly winds, while the less affluent groups were housed at the west side of town where they were exposed to the hot westerly wind. In addition, the houses on the west side shielded the more affluent area from the unfavorable wind. Other examples include the Feng Shui principles in ancient China which encouraged the integration of elements of wind and light in building designs. Greek writings also show that the integration of wind in the design of settlements was a conscious decision shared by both the designers and settlers (Ref. 216).

Figure 2-5 Sketch of housing layout at Kahun, Source: (Ref. 30).

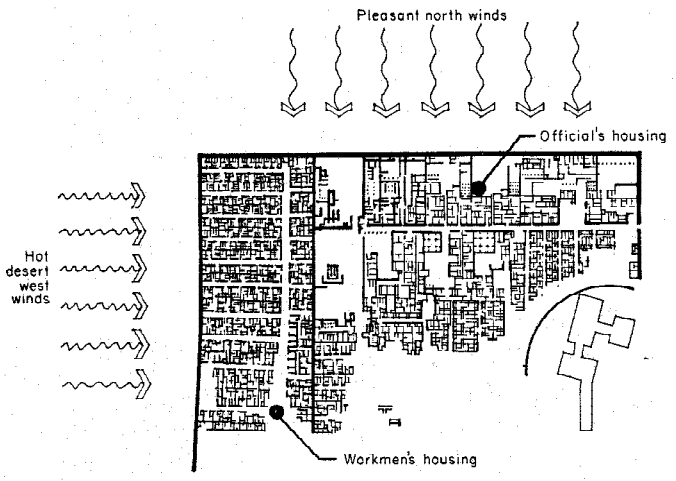

Tests of traditional settlements in Dubai (Ref. 251) show that the orientation, the high and massive walls, the narrow alleys, and the compactness of the open spaces were successful at ameliorating its harsh climate. These elements are typical

urban morphological characteristics of settlements in hot arid climates (Figures 2-6 and 2-7).

Figure 2-6 Settlement in hot dry climate, Source: Koenigsberger et al (Ref. 259).

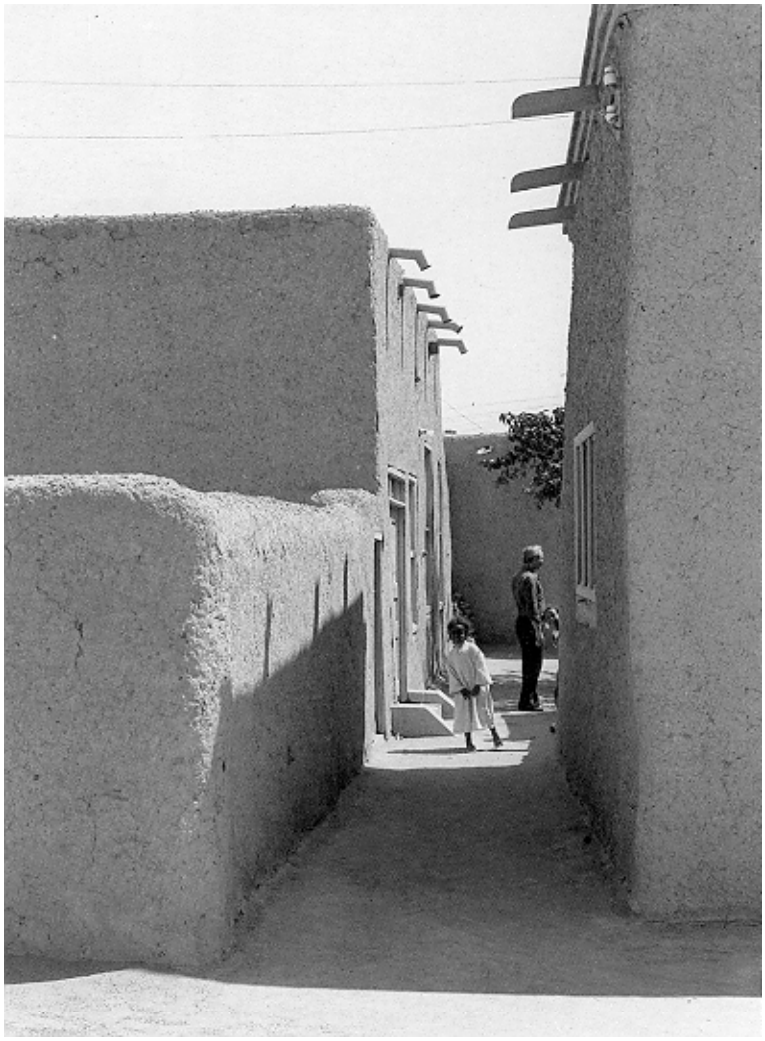

Figure 2-7 Alley ways, Omdurman, Sudan. Dimensions of the alley guarantee shading throughout most of the day hours. Source: Norberg-Schulz (Ref. 273).

In contrast, warm-humid planning strategies involved promoting natural ventilation of individual buildings and increasing wind speeds in outdoor spaces (Figure 2-8).

Figure 2-8 Row Housing in Southeast Asia. Source: (Ref. 34).

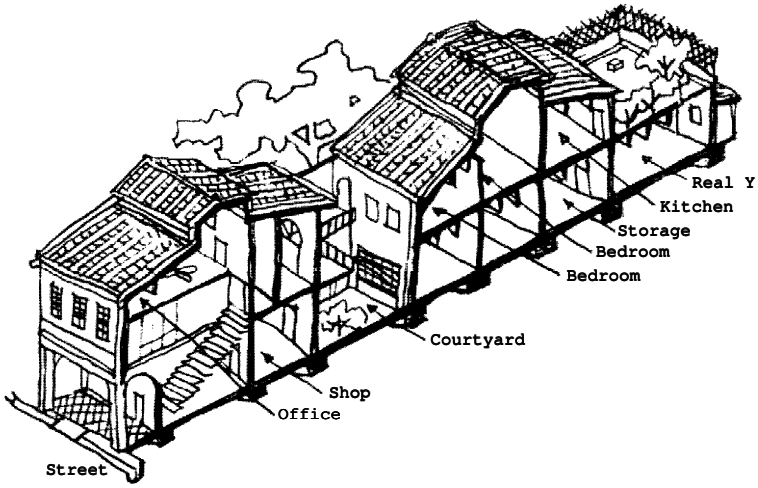

Figure 2-9 Naturally ventilated traditional building, Source: (Ref. 289)

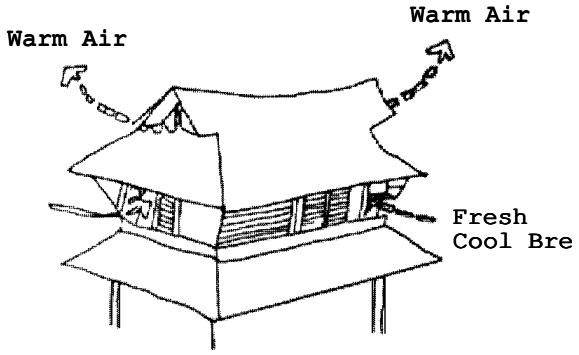

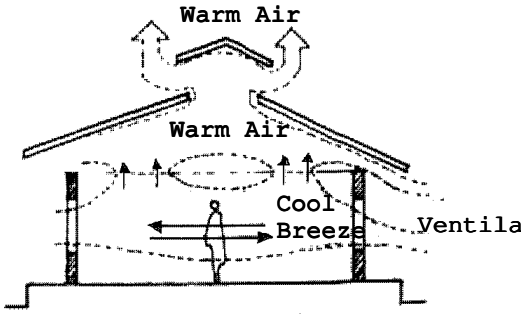

2.5 Examples

This section includes examples demonstrating the influence of wind on traditional Indonesian and Middle Eastern architecture. These examples illustrate the adaptation of architectural elements such as roofs and cool towers to meet the demands of warm-humid and hot-dry climates respectively.

2.5.1 Examples form Warm-humid Climates

The climate of the Indonesian Archipelago is predominantly warm-humid with a brief hot-dry season. The similarity of architectural forms[3] are due to the uniformity of climatic conditions. To provide thermal comfort for building occupants in this climate, traditional buildings have large openings on their exterior walls (Ref. 260 and 240) to maximize indoor airflow[4]. Figures 2-9 to 2-11 show examples of design solutions to provide interior spaces with high airflow rates through large windows, louvered walls and roof openings.

2-3 Based on author's observation.

2-4 Table TABLE 2-1.

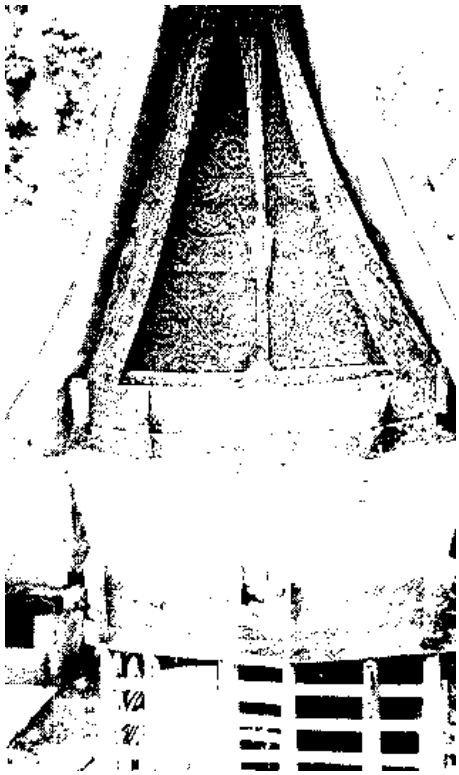

Figure 2-10 House (converted rice granary), Sigumpar, Indonesia, Source: (Ref. 267)

In addition to direct ventilation schemes, examples of thermal stratification-promoting designs can be found in east Java. Removal of the buildup of warm air to provide thermal comfort of occupants is achieved by venting stratified interior air through roofs and high ceilings (Figure 2-9).To maximize airflow through roof openings, many exterior walls in Javanese houses are porous to permit the displacement of indoor hot air with cooler outdoor air (Figure 2-11).

Figure 2-11 Example of porous wall construction in Java, Source: Author's collection.

Figure 2-12 University of Indonesia Campus, Source: Author's Collection.

Figure 2-12 demonstrates an example of the use of traditional Indonesian architectural elements in modern buildings. The building in the University of Indonesia's new campus uses a multi-layered roof configuration to shade the continuous windows on the various floors. The function of the upper roof (cupola) is to create a suction zone similar to the one illustrated in Figure 2-9. The combination of the continuous operable windows at the lower floors and the cupola causes the

wind to flow upwards, replacing hot interior air with cooler outside air.

2.5.2 Examples form Hot-dry Climates

In many locations in the Middle East, North Africa, and the Northwestern corner of the Indian subcontinent, a traditional ventilation and cooling system has developed. This system is known as wind towers or wind catchers (*Malqafs*) in Egypt (Ref. 246), *Badgirs* in Iran the Gulf area (Ref. 238, 6, and 223), and recently referred to as cool towers or ventilation towers (Ref. 282 and 264). These are all vented towers or vertical projections in the roof intended to catch or remove air from the interior spaces (Ref. 237).

Ventilation towers -in most cases- act as wind scoops capturing air at roof level and diverting it to indoor spaces. The temperature of inlet air is sometimes cooled by passing it through underground enclosures. In dry climates, the air is cooled and humidity raised by passing the airflow over water-filled jars or though wetted pads.

The design of the inlet portion of ventilation towers (tower head) depends on the prevailing wind direction. A single-opening tower suits cases where the prevailing wind comes from a single direction, while a multi-opening tower head best suits cases where the wind comes from different compass directions (Figure 2-13).

Figure 2-13 Tower head designs, Source: (Ref. 283).

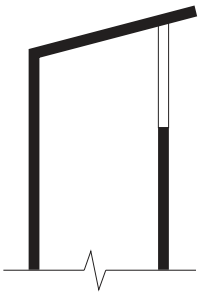

Single-opening Tower Head

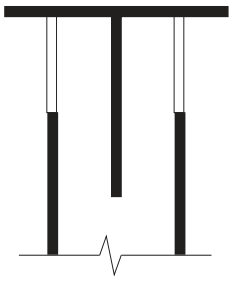

Multi-opening Tower Head

The tower head configuration affects interior and exterior building design. Because it requires maximum exposure to different wind directions, a ventilation tower with a multi-opening head usually becomes a dominant architectural feature (Figure 2-14). This exterior dominance is often reflected in the interior plan. The multi-opening tower is usually connected to a large interior space where the cool air is delivered. In contrast, single-opening towers are usually less prominent in both the exterior and interior plan. This configuration is a product of restricting tower head to a single wind direction. To maximize exposure to prevailing wind direction, the ventilation tower is often located at the perimeter facing the roof of the building instead of the exterior (Figure 2-15). This location allows the wind tower to face the airflow unaffected by surrounding buildings (Figure 2-16).

Figure 2-14 Multi-opening wind catcher in Kerman Bazaar, Iran. Source: (Ref. 238).

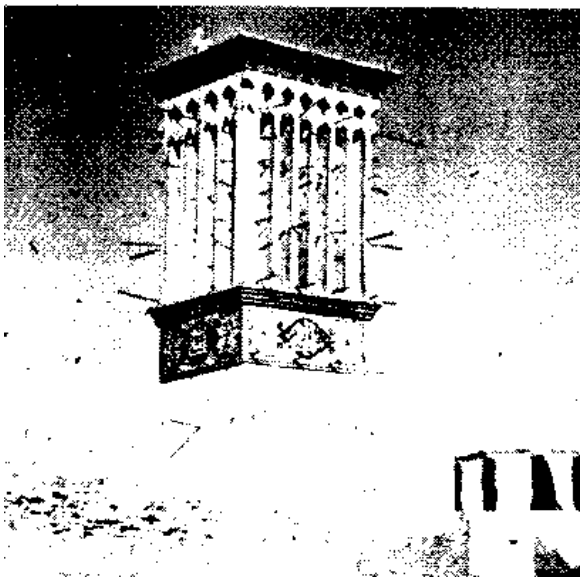

Figure 2-15 Example of a single-opening wind catchers in Al-Kufa, Iraq, Source: (Ref. 246)

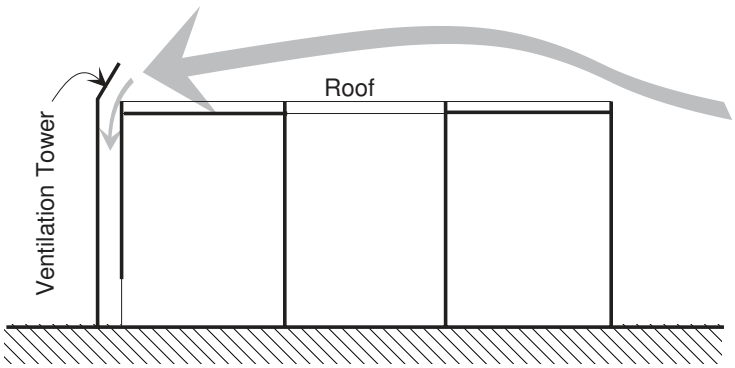

Figure 2-16 Single-opening tower head is located at position where effect of surrounding buildings is minimal.

Hassan Fathy is one of the most influential leaders of the revivalist movement in the Arab world. His traditionalist work exemplified in Gourna (Refs. 247 and 246) involved the reintroduction of construction materials and climate responsive solutions suitable for the project site. Figure 2-17[5] illustrates the use of massive walls, small windows and *mashrabiahs*[6]. This shading device doe not only reduce solar radiation but also provides relatively large openings on building exteriors and/or courtyards.

2-5 Source of Image: "Omaggio ad Hassan Fathy" in *Italian* at http://www.triennale.it/expo/monograph/fathy.htm.

2-6 A mashrabiah is a screen made of timber and located over large windows for privacy and shading.

Figure 2-17 Examples of Hassan Fathy's reintroduction of traditional architectural design features.

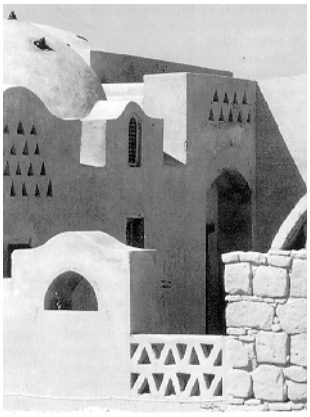

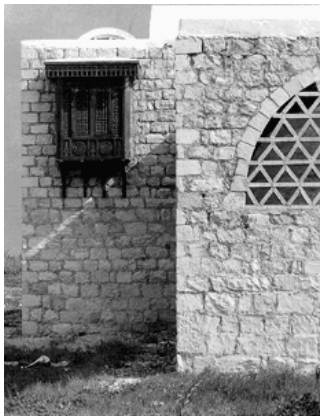

Figure 2-18[7] shows a view from the University of Qatar. The university campus contains design features that reflect revived traditional elements such as wind towers and courtyards. The designers used multi-opening ventilation towers in combination with water fountains to evaporatively cool the interior spaces. Other features include the use of *mashrabiahs* and light towers. The latter is an attempt to minimize the use of windows. This was attained by separating the functions of a window into ventilation and daylighting, each of which is provided by a separate design element. This separation gives the designer the freedom to control airflow for ventilation and cooling of interior spaces without concern about lighting needs through the same opening. The result is an architectural style responsive to the climate and unique in morphology (Figure 2-19).

2-7 Mimar, April 1985, pp. 20-27.

Figure 2-18 Modern Design Solutions, University of Qatar, Source: (Ref. 287).

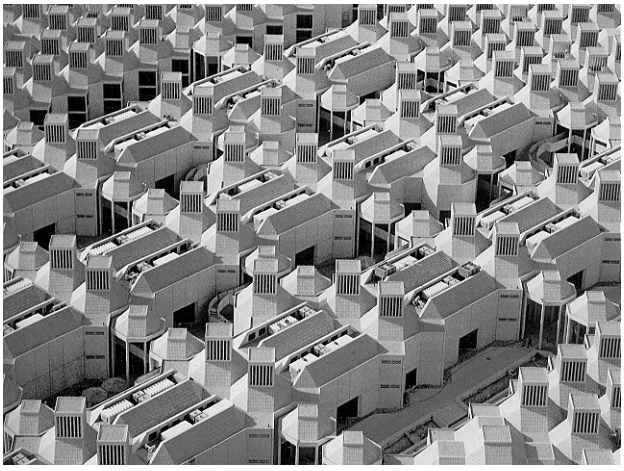

Figure 2-19 Bird's eye-view of the University of Qatar. Source: Ibid.

In all the examples, wind plays an important role in shaping the form of individual buildings as well as the architectural style of the region. The examples also demonstrate the effect of the wind in shaping the urban morphology. To incorporate wind in the design of individual buildings or urban layouts, knowledge of wind behavior around buildings is paramount. Tools and/or algorithms -if available- should be used to predict wind flow patterns in urban areas.

2.6 Conclusion

Traditional buildings provide rich examples to architects and urban planners of how to promote natural ventilation. This chapter gave a few selected examples characterizing ventilation design in the opposite poles of humid and arid climates.

Most the examples discussed in this chapter demonstrate the effect of wind on the built form except the example of the city of Kahun in ancient Egypt (Figure 2-5). The builders of the city used the general layout to direct favorable breezes towards and diverted unfavorable winds from certain sections of Kahun. This exemplifies the use of urban layout to manipulate wind movement around buildings.

Although the effect of wind in determining street sizes and building spacing is generally understood, other factors affecting zonal layout and street pattern often prevail. Designing for natural ventilation in such conditions requires an understanding of the effect of building layouts on wind movement. To provide a comprehensive understanding of wind movement around buildings, wind design should account for the individ-

ual buildings as well as the urban layout. Inversely, relative sizes and shapes of buildings and the spacing between buildings can also be manipulated to produce the desired wind flow patterns. This study will attempt to provide a set of tools to allow the designers to determine indoor airflow of buildings in urban settings.

Chapter 3

3

Ventilation Research: Background

3.1 Introduction

This Chapter deals with the description of natural ventilation and the progression in knowledge leading to the development of a mathematical model for the prediction of indoor air speeds. The chapter begins with a brief description of the uses of ventilation, its requirements, and flow mechanisms. Follows, is a section that discusses the potential impacts of a prediction model on energy, building standards, and thermal comfort.

The subsequent sections of the chapter describe previous research studies that dealt with ventilation prediction directly or indirectly. The indirect methods use wind pressures on building surfaces to compute infiltration and interior airflow through windows located on those surfaces. Finally, the chapter dedicates a section to the variables affecting airflow in urban areas.

3.2 Ventilation

Natural ventilation is defined as desirable air exchange (such as through open windows) capable of cooling either the space,

the structure, or the occupants' bodies. Ventilation cools interior spaces by displacing the hot inside air with cooler outside air. This displacement can be obtained naturally through wind-induced pressure or thermal stack effect.

3.2.1 Airflow Cooling Effects

The amount of heat removed is a function of the ambient temperature, outdoor temperature and airflow rate. Ventilation may be used to cool buildings when the outdoor temperature is less than that of the indoor air. This occurs most often at night. By removing the sensible heat stored in the building mass during nighttime ventilating, interior mean radiant temperature is lowered throughout the early part of the next day. When the outdoor temperature is higher than the indoor temperature, airflow may be cooled evaporatively or through passing air over shaded spaces.

In humid climates, ventilation is most effective in cooling building occupants directly. This takes place through convection and evaporation off the skin.

3.2.2 Ventilation Requirements

The requirements of ventilation can be categorized (Refs. 95 and 200) under *thermal comfort* and *health* (Figure 3-1). By satisfying both requirements, residential buildings can benefit from the potential energy saving of natural ventilation use as an alternative to compressor-based cooling during warm and transitional seasons [Givoni (Ref. 102), Byrne *et al* (Ref. 45), Arens *et al* (Refs. 11 and 13)].

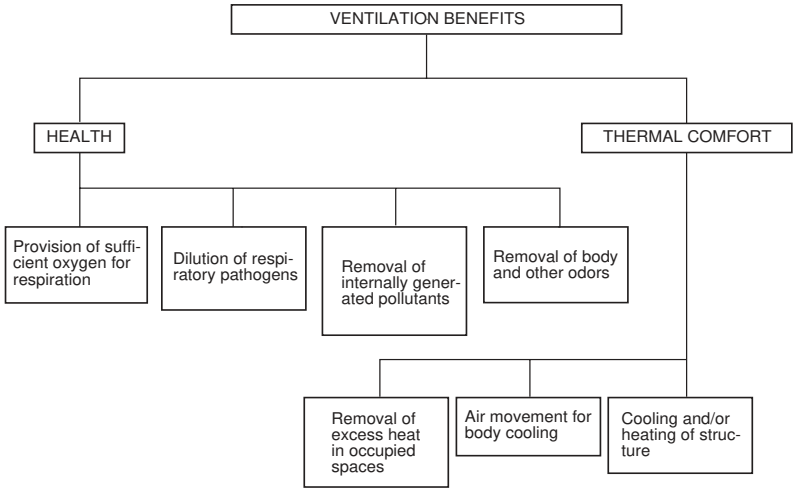

Figure 3-1 Schematic illustration of ventilation requirements, adapted from van Straaten (Ref. 200)

3.2.3 Mechanisms Affecting Natural Ventilation Airflow

Wind-induced airflow is a result of a pressure difference between the outside and inside a structure, or between the surfaces within which fenestration is located. This pressure gradient may be caused either by the difference in interior-exterior temperature (thermal forces) or by external wind flow (wind forces).

3.2.3.1 Thermal Forces

When two openings are at different heights and the indoor temperature is higher than the outside, a pressure gradient is generated causing the inside air to move out of the higher openings and the outside air into the lower openings [Watson and Labs (Ref. 219)]. The airflow in this regime is dependent on the temperature difference between inlet and outlet as well as the aperture difference in height (Figure 3-2).

3.2.3.2 Wind Forces

The difference in dynamic wind pressure creates a potential for the air to flow from a point to another point where the pressure is lower [Givoni (Ref. 102)]. When wind strikes a wall perpendicular to its direction of flow, the surface of the wall

experiences pressure higher than that of the atmospheric pressure. The leeward surface experiences pressures lower than that of the atmosphere with less variation in pressure distribution than the windward side (Figure 3-2). The side walls however, experience negative pressures around the windward edge and positive pressures at the leeward end.

Cross ventilation occurs when a pressure difference exists between two exterior openings, whether they are located in the same or different surfaces. This pressure difference causes the indoor air to flow from inlet/s to outlet/s located in building walls at lower surface pressure. In addition, even when the measured pressure difference between the two apertures is equal to zero, some airflow can still occur as a result of inertia from wind entering the window [Ernest and Evans (Refs. 74. and 78)], or from differences in pressure along the height of each window (Ref. 102).

Natural airflow inside buildings is a combination of the effects of both thermal and wind forces. However, the airflow generated from combing the two forces does not exceed 40% of the windflow generated by the greater force even when the two forces are in the same direction (Ref. 102).

Figure 3-2 Forces Affecting Natural Airflow

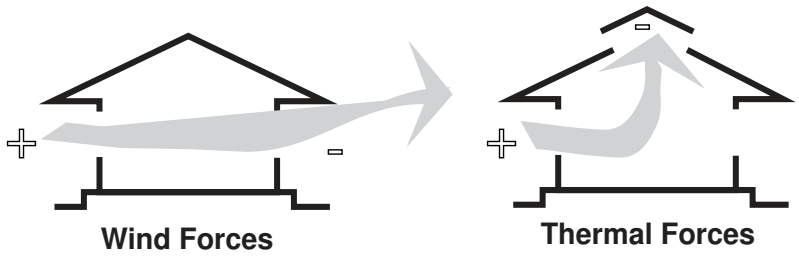

3.3 Natural Ventilation Research

Recent studies have quantified and developed models for:

- Indoor ventilation velocities for occupant cooling [Chand *et al*, Ernest *et al*, Bauman *et al* (Refs. 50, 74-76, 35)].
- Air changes for space cooling [Vickery *et al* (Ref. 215)].
- Heat transfer coefficients for high air change rates to quantify structural cooling under natural ventilation [Pedersen *et al*, Spitler (Refs. 172 and 194).
- Infiltration [ASHRAE (Ref. 19)].

The common denominator for these wind effect models is that the designer needs to know wind pressures on building surfaces to implement these models.

At present, the designer cannot use weather station wind data to obtain pressure distributions on building surfaces because most of the available building pressure data apply to buildings in open terrain conditions. There are, however, models that take into account generalized effects such as the upwind terrain roughness in the surrounding 5 km, the effect of large hills, and the height of the building being modeled above the ground surface (Ref. 19).

Although these are useful models, they describe effects that have little impact on building pressures in most actual building sites. The most important factor influencing wind on buildings is the large-scale obstruction blocks, i.e., other buildings, trees, etc. in the immediate vicinity of the building being modeled. These obstruction blocks cast various forms of wakes downwind. The combined effect of these surroundings shapes wind pressures on other buildings situated within their wakes.

It is not easy to describe these wakes for modeling purposes. For one thing, the number of potential configurations of multiple upwind obstructions is virtually infinite, and to rationalize them into a set of useful dimensions requires some informed decisions about the importance of wake-shaping properties. For another, the building being modeled interacts with the wake from its surroundings, so it is not enough just to characterize the wake-generating properties of the surroundings alone.

Finally, researchers of this subject have not conducted their experiments in a consistent way, but have bounded the problems they worked on in whatever way was convenient for the study at hand. Their studies of wind pressure in built-up surroundings can not be generalized for application in a building energy simulation program such as DOE-2, CALRES or BLAST (Ref. 132).

From the literature review, two categories of empirical ventilation prediction models could be identified;

3.3.1 Mean Wind Speed Coefficient Method

The first category is the Mean Wind Speed Coefficient Method where velocity coefficients are used to predict indoor air speeds. This method relies on data obtained through wind tunnel studies of indoor air velocities and presented as ratios to an outdoor reference velocity [Equation (3-1)]. The reference velocity (V_o) is usually taken at 10 m height above ground (Ref. 25).

$$C_v = \frac{V_i}{V_o}^{1} \quad \textbf{(3-1)}$$

Where

V_i = indoor air speed (m/s)

V_o = wind speed at site (m/s)

C_v = velocity Coefficient (ND)

Models in this category are by Aynsley (Refs. 30 and 27), Givoni (Ref. 102), and Chandra (Ref. 54). Despite the apparent simplicity of the speed coefficient method, obtaining wind tunnel results may be too difficult and costly, especially for small designs.

3.3.2 Discharge Coefficient Method

The second category uses the discharge coefficient (C_d) for the prediction of the natural ventilation. The mean wind speed V_w entering a space is a function of the difference between the windward and leeward pressure Coefficients (ΔC_p), outdoor air velocity (V_o), and the discharge coefficient (C_d):

$$V_w = C_d \cdot [\Delta C_p V_0^2]^{1/2} \quad \textbf{(3-2)}$$

Where

V_w = mean wind speed through an opening (m/s)

C_d = discharge coefficient (ND)

ΔC_p = mean pressure difference coefficient between windward and leeward surfaces (ND)

V_0 = wind speed at site (m/s)

3-1 Source: Aynsley 1977 (Ref. 30).

Wind flow creates pressure differences between the different sides of a building. Surface pressures are usually presented as non-dimensional coefficients relating wind pressures to pressures measured at eave height. The numerical value of pressure coefficients is determined using the following formula:

$$C_{p_i} = \frac{(P_m - P_s)}{(0.5 \cdot \rho \cdot V_e^2)} \quad \textbf{(3-3)}$$

Where

C_{p_i} =mean surface pressure coefficient for each point in the facade (ND)

P_m =mean pressure at each point on the facade (Pa)

P_s =mean static reference pressure (Pa)

ρ =density of air (kg/m^3)

V_e =mean reference velocity at eave height (m/s)

Examples of the discharge coefficient indoor velocity prediction methods are found in Ernest (Ref. 76), Chand (Ref. 52), Allard *et al* (Ref. 5), and Murakami (Ref. 167).

3.4 Shielding Effects

There are a few ways to account for upwind shielding in building energy simulation, but most of these methods do not predict surface pressures. For infiltration calculations, ASHRAE Handbook Chapter 23 describes the approach of the LBL infiltration model, which is implemented in most building energy simulation programs. It uses coefficients based on five local shielding classes[2] which, when multiplied by the square of the

3-2 Tables 6 and 8, ASHRAE Fundamentals Handbook, 1989, pp. 23.17-18.

wind speed, give an estimate of outdoor wind velocity. These shielding coefficients do not consider the effects of any specific obstructions in the vicinity of the building (Ref. 79).

For natural ventilation through large area window openings the situation is equally inadequate. CALRES, for example, uses a single factor to predict the local wind speed from the weather tape values. The local wind speed is then converted to air changes using a simple model for airflow through windows. In energy code simulations using CALRES, little energy effect can be observed from implementing various natural ventilation strategies. The credit given to designers is limited to the potential benefits of introducing natural ventilation on reducing mechanical system requirements of the designed space.

3.5 Methods for Predicting Wind Pressures

Most of the existing wind pressure data have been collected for structural engineering purposes where the interest is in the maximum or minimum pressure values the wind exerts on various building shapes. Such data are therefore obtained from wind tunnel tests on models of unshielded buildings.

3.5.1 Empirical Pressure Models

Swami and Chandra (Ref. 203) summarized many such studies for their applicability to natural ventilation design, and produced functions describing the wind pressures on various unshielded building shapes through the full range of wind approach angles. However, the vast majority of real buildings is shielded from the wind by vegetation, topography, or other

buildings. Such shielding, considerably changes the wind pressures on building surfaces.

Few researchers have studied the effects of obstruction blocks on building surface pressures. Lee and Soliman, Chand, Wiren, and Balazs have studied the pressures on array of cubes, and Ernest and Bauman have studied pressures on rows of buildings. These studies have resulted in coherent relationships defining building surface pressures (C_p), or often the difference between building windward and leeward surfaces (ΔC_p), as a function of array spacing and arrangement of the arrays. According to those studies two or three rows of upwind obstructions were sufficient to define the upwind obstructions (Refs. 13 and 149), similar to the underlining assumption of the program SITECLIMATE (Ref. 10).

The study of Lee *et al* (Ref. 149) analyzed the shielding effects of windward buildings on wind pressure differences (ΔC_p) across the modeled building. In this study, the distance between the model and the windward obstruction was varied until the effect of the windward block was no longer detectable. The experiment showed that three wake flow regimes were formed between the two blocks. The same study showed that for wind direction between 0˚-60˚ from normal, there was little effect on the pressure difference from changing the wind direction. However, when the wind direction exceeded 60˚ from the normal to the surface of the tested model, the pressure difference of the shielded building approached that of the equivalent unobstructed (isolated) model.

Recently, mathematical relationships have been developed to account for the effect of surrounding buildings on building surface pressures. Among those, Swami and Chandra (Ref. 203) used Wiren's set of experiments (Ref. 226) to develop a function that predicts the pressure shielding of any obstruction block based on its position relative to the tested surface. The problem with Swami and Chandra's approach is that it is limited to the specific layouts tested in Wiren's study. Knoll *et al* (Ref. 140), on the other hand, related the surrounding buildings to the tested surfaces through a Cartesian coordinate system. The result is a more flexible model where individual adjacent blocks are considered despite the layout in which the building is set. Knoll's approach is however limited by the inability of the algorithm to take into account complex building shapes and the effects of gaps between the buildings.

3.5.2 Computational Models

Computational Fluid Dynamic Modeling (CFD) is a numerical solution of fluid flow problems using mathematical equations based on fundamental laws of conservation of momentum, energy, and mass (Refs. 131 and 222). Computational techniques for predicting wind velocities, surface pressures and fluid temperature distributions were first developed for nuclear and aerospace industries. With the advancement of computational speeds and capacities, these methods have found their way into building-oriented applications.

CFD models in buildings may be used to determine the following (Ref. 131):

- Thermal comfort parameters such as air speed and temperature.
- Effectiveness of ventilation systems.
- Efficiency of energy distribution in spaces.

3.5.2.1 Advantages

In general, current models are capable of simulating most typical indoor airflows. However, a limited set of outdoor wind environments may be simulated with reasonable resemblance to results obtained from wind tunnel comparisons [Gadilhe *et al* (Ref. 90)]. These models offer the following advantages over other ventilation prediction tools;

- CFD models do not require physical modeling such as in wind tunnels.
- They are usually less expensive than full-scale experiments.
- They proved to be useful in parametric studies (Refs. 137 and 195).

3.5.2.2 Disadvantages

Computation Fluid Dynamic models require specialized expertise to run, monitor, and analyze generated results. In addition, substantial computing power and time are needed to run them. With the advancement in computers, however, CFD models may represent attractive alternatives to other prediction tools in the future. Currently, these algorithms are mainly used in research instead of design because of the following;

- The difficulty to input and establish boundary conditions which have major effects on the simulation.
- The difficulty to validate results of the simulation.

3.5.3 Field Measurements at Full Scale

Full scale measurement studies use full-scale models or actual structures to test parameters that cannot be modeled at smaller

scale (Ref. 187). Indoor airflows can be measured directly or through the detection of the decay of a tracer gas introduced into the space in question. Pressure sensors can also be attached to building surfaces both inside and outside buildings (Ref. 112).

3.5.3.1 Advantages

- High confidence in results.
- Used for the verification of other prediction methods; e.g., wind tunnel and CFD methods [Ashley (Ref. 15), Katayama *et al* (Ref. 133)].

3.5.3.2 Disadvantages

- For design purposes, field measurements are usually more costly to do than simulation (mathematical or wind tunnel modeling).
- Limited parameters for generalized studies.
- Often difficult to maintain steady state conditions throughout tests (Ref. 217).

3.6 Summary of Variables affecting Airflow

Despite the large number of variables that can affect airflow around buildings (and consequently the airflow inside buildings), four general categories of variables can be identified. These are the pattern of urban layout, the compactness of the layout, terrain effect on the boundary layer, and the porosity of obstructions such as trees.

3.6.1 Layout Patterns

Because of the enormous number of possible urban layouts, only few regular layouts have been tested (Figure 3-3). The predominant layouts are; normal patterns (Grid-iron) and staggered patterns. Examples of these configurations are described in Soliman (Ref. 191), Wise (Ref. 228), Wiren (Ref. 225), and

Chand *et al* (Ref. 50). Their studies prove that wind pressures of shielded building surfaces are drastically different from those of unshielded buildings.

Figure 3-3 Tested Patterns in Shielded Studies

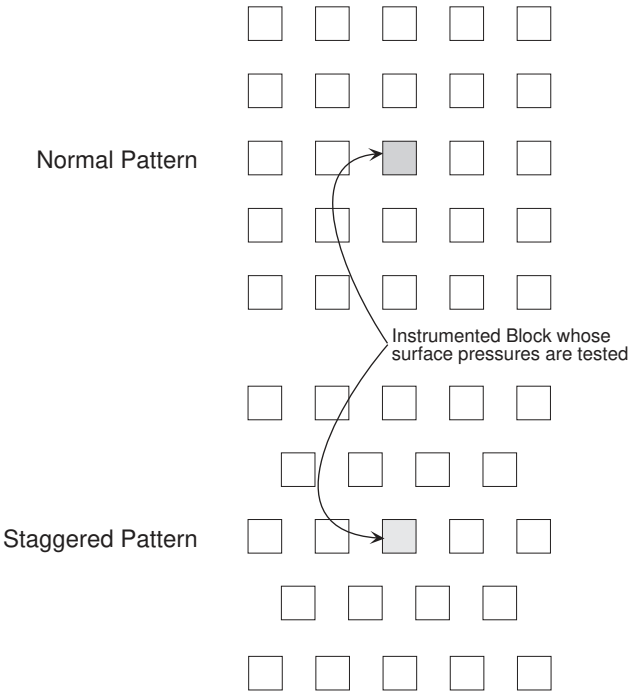

3.6.2 Compactness of Layout

Compactness of the layout is a general term that includes the distances between the obstruction blocks and the tested surfaces as well as the spaces between the blocks themselves (Refs. 149 and 192). In general, the more compact the layout, the lower the local wind speeds and surface pressures. Since the compactness of layout is a function of the spacing between blocks, it can be concluded that there is an inverse relation between wind speeds and surface pressures and the spacing between blocks.

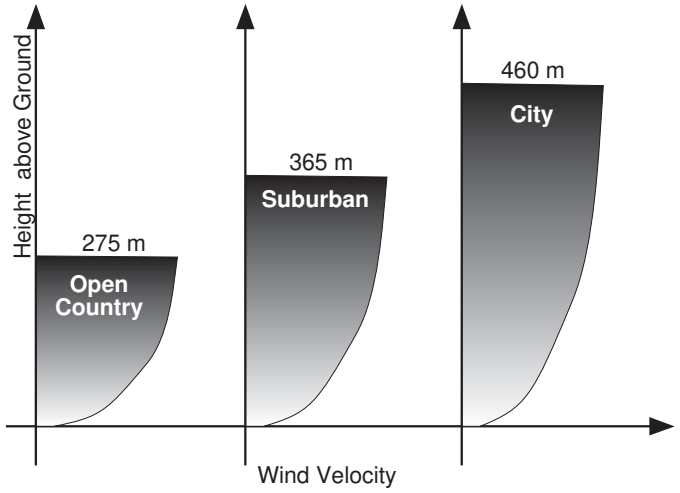

Figure 3-4 Gradient height depends on the roughness of the terrain.

3.6.3 Boundary Layer and Terrain Effects

The terrain affects the degree of exposure of the site under investigation. Different terrain roughnesses generate different boundary layers and exponential functions can be used to determine wind speeds at any height from a known location at reference height. These characteristic boundary layers are shown in Figure 3-4.

Effects of terrain on boundary layers are well documented and can be estimated using any of the methods suggested by ESDU (Refs. 72 & 73), Murakami *et al* (Ref. 168), Arens *et al* (Ref. 10), or Aynsley (Ref. 24)].

Local topography such as hills and valleys also can have a strong influence on the boundary layer. Such non-flat surfaces redirect the airflow, changing its strength, steadiness and direction (Refs. 12, 96, &127).

3.6.4 Effects of Vegetative Windbreaks

Some studies have been conducted to assess the effect of trees on the wind environment, particularly of shelterbelts for the

reduction of ground wind speeds over crops. Shelterbelts are also applicable in areas where pedestrians and other human activities might be adversely affected by high wind levels.

Wind speeds downwind of shelterbelts are reduced (from 15%–68%) depending on their density or permeability (Ref. 161). The higher the density of the vegetation, the shorter the distance to where the wind regains most of its energy (this occurs 8–17 times the height of the wind screen). Robert White's investigation (Ref. 221) of the effect of trees, shrubs and hedges on the natural ventilation of buildings found that the type of vegetation, and its distance from the openings greatly influences the airflow inside the sheltered structures.

The analysis of the effect of vegetation on airflow is a complex issue (Ref. 96). However, some studies have established empirical coefficients through which the wake behind a shelterbelt can be predicted (Ref. 10). These estimates are based on the freestream wind speeds, profile, density of vegetation and the distance behind the shelterbelt. Seasonal corrections may be applied to account for leaf loss of deciduous trees in winter.

3.7 Conclusion

The wind is an integral ingredient in the determination of thermal comfort for the occupants of a naturally ventilated building. Early consideration of thermal comfort may be necessary if acceptable climate responsive solutions are desired.

Recently, mathematical models have been developed that apply building surface pressure data to predict indoor air

velocities, and flow patterns in simple single and partitioned spaces. However, very few surfaces pressure data are available for situations where the building is surrounded by other buildings that affect the wind on its surfaces. The few databases of measured pressures are limited by the specificity of the tested layout configurations.

Computational fluid dynamics methods, on the other hand, are in most cases inaccessible to the designers by virtue of their complex input and the computation time they require.

The few available pressure prediction models that consider the shielding effects of surroundings are simple and do not address the complex variations in urban form that might confront the modeler.

Chapter 4

4

Development of an Empirical Model for the Prediction of Surface Pressures in Shielded Environments

4.1 Introduction

Pressure differences on building surfaces drive the airflows through openings in those surfaces. The distribution of wind pressure on building walls and windows varies with the geometry of the building, wind direction, the adjacent roof shape, and the surrounding building blocks. The wakes generated behind windward obstruction blocks cause the pressures on surfaces falling within these wakes to vary significantly from surface pressures in similar unshielded circumstances. The shielding effect is a factor of the number of obstruction blocks, their size, and position relative to the surface.

This chapter describes the development of a mathematical model to predict the pressures on wall surfaces located within wakes of windward buildings. The model is based on empirical results of wind tunnel tests, developed in a stepwise manner to retain simplicity in the final mathematical model.

4.2 The Proposed Model

The general objective of the intended model is to predict the effect of the surrounding buildings on the indoor airflows

through building fenestration. To do this, new work was required for predicting wind pressures on building exterior vertical surfaces behind or adjacent to obstruction blocks.

To be useful in design, the pressure prediction model (PPM) should use simple techniques for characterizing the surrounding buildings. The method should not require from the designer any knowledge of the fundamentals of architectural aerodynamics. The input should be limited to a description of the surrounding buildings in terms that can either be easily taken off site plans or measured using conventional site surveying methods.

The model should be in the form of an algorithm compatible with existing wind databases so it can be used with energy analysis programs. The model should allow direct estimates of the effect of wind shielding on building surface pressures, given the configuration of surrounding obstructions, and the terrain roughness. The outcome of such an algorithm should be hourly pressure values in a format matching that of recorded hourly wind speed and direction data.

Finally, as a by-product of the physical experiments needed to produce this model, an extensive database of surface pressures could be accumulated.

4.3 Approach

The first step in developing the algorithm for the prediction of surface pressures was to investigate the validity of using a single obstruction block to represent multiple rows of obstruction blocks.

The second was to establish a simple-to-obtain and easy-to-use set of model variables. These variables were based on angular description of individual obstruction blocks relative to the surface on which air pressure was to be determined.

Third, in developing a non-dimensional coefficient for studying the shielding effects, a function for predicting pressure coefficients of the unobstructed instrumented surfaces was needed. This was done by adapting a mathematical relationship developed by Lee *et al* (Ref. 149).

Fourth, these simple relationships were studied for various arrangements of the instrumented model and a single windward obstruction block. Both the width of the obstruction block and the distance from the instrumented model surface were varied. In these tests, the center-to-center line between the model and obstruction block was parallel to the wind direction[1]. Variables such as the obstruction height and depth, the size and shape of the instrumented model, and the boundary layer characteristics were kept constant.

The fifth step involved varying the displacement of the obstruction block so that the center-to-center line was no longer parallel to the wind direction. This was achieved by sliding the obstruction block parallel to the instrumented surface and simultaneously maintaining both blocks perpendicular to the wind direction.

4-1 This setup is referred to as the orthogonal Configuration (Section 4.12).

Sixth, the effect of changing the wind direction was analyzed under two scenarios. These scenarios based on whether the obstruction is parallel to the instrumented model or not. The two scenarios involved rotating both the instrumented model and obstruction block on the wind tunnel turntable (Figure A-1) to simulate wind direction change.

The seventh step was the study of the effect of multiple obstructions blocks on the instrumented surface. This was accomplished by comparing the shielding effect of individual blocks to the measured pressure values of the multiple blocks. These tests involved rotating two obstruction blocks of variable gap widths, spacing, and displacement from the instrumented surface.

Eighth, the mathematical model needed to include the effects of roof shapes and more complex building plan forms. Both had been analyzed in previous research and could be incorporated into the algorithm.

The ninth step was to verify the resulting mathematical model. This verification used results from two sources. The first data were obtained from a study conducted at the *National Swedish Institute for Building Research* (Refs. 225 and 226). The second source of data was a wind tunnel study of a complex urban setting, conducted by the author.

4.4 Background

A number of research studies have analyzed the shielding effects of surrounding buildings on wall surface pressures [Lee *et al* (Ref. 149), Hussain *et al* (Ref. 124), Ernest (Ref.

74), and Wiren (Ref. 225)]. To take urban layouts into account, they tested standardized configurations; e.g. grid-iron (normal), staggered, and free layouts (Figure 3-3). The results of the different studies vary because of the difference in tested model configurations. The variation can be attributed to the many variables involved in describing the surrounding building configurations, e.g. spacing between model and obstructions, relative position of obstruction to model, and the number of windward blocks (Figures 4-3, 4-2, and 4-4).

Figure 4-1 Comparison between examples from Hussain et al, Wiren, and Ernest shielding experiment results

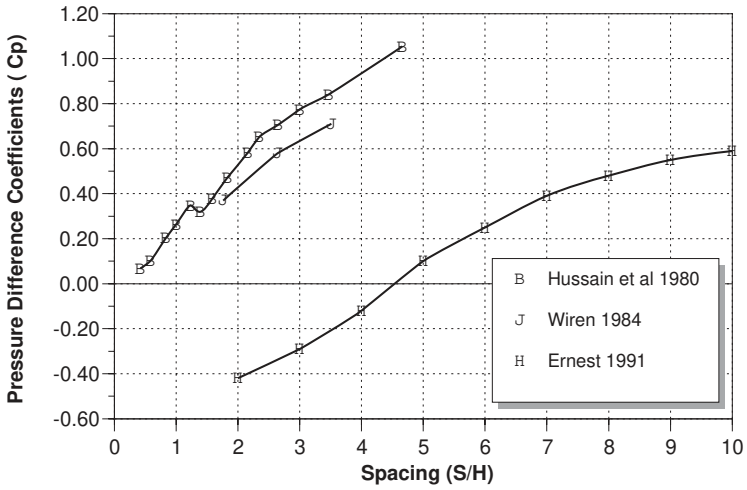

Figure 4-1 shows a comparison of the results obtained from urban layout effect studies conducted by Hussain *et al* (Ref. 124), Wiren (Ref. 225), and Ernest (Ref. 74). The data in the graph are represented in pressure coefficient differences[2] as a function of the distance between the instrumented models and

4-2 The pressure coefficient is a non-dimensional ratio between the average surface pressure and wind pressure at a specific reference height (Eq.3-3). *Pressure coefficient difference* in these studies refers to the absolute value of the pressure coefficient difference between the windward and leeward surfaces of the instrumented models.

the obstruction blocks[3]. Ernest's results are noticeably different from the other two studies. This difference can be attributed to differences in the test models and in the number of obstruction blocks. Wiren's results[4] were obtained by testing a gable-roofed model amid a normal layout (Figure 4-2) of three rows of identical obstruction blocks. Hussain's experiment tested a cubic model with a flat roof in the middle of similarly configured array of obstruction blocks (Figure 4-3). The similarity in configuration between these two experiments resulted in an almost identical distribution of surface pressures over spacing[5] despite the differences in roof shapes. Ernest's tests, on the other hand, used a single flat-roofed obstruction block extending the width of the wind tunnel (200 cm) upwind of a flat-roofed model. The long obstruction block causes a fundamentally different shielding effect.

This result demonstrates the problems of applying prediction models based on specific layouts such as the one suggested by Lee *et al* (Ref. 149). However, all studies showed that the outer or peripheral obstruction blocks and rows did not affect the pressure values on the measured surfaces. Moreover, increasing the number of rows of obstruction blocks (upstream) showed little effect on surface pressures after the third row (Refs. 34, 225, and 212). This means that adding more blocks beyond the closest rows of obstructions does not

4-3 The distance was expressed as spacing, or the ratio between the distance between the instrumented model and the obstruction blocks and the height of the obstruction block/s.

4-4 Wiren's experiments are described in details in Section 4.17.1.

4-5 Data are corrected for boundary layer characteristics and reference pressure at eave height.

significantly change the shielding effect of the surroundings (Figure 4-7).

Figure 4-2 An example of Wiren's test configuration (the one-row Grid-iron pattern)

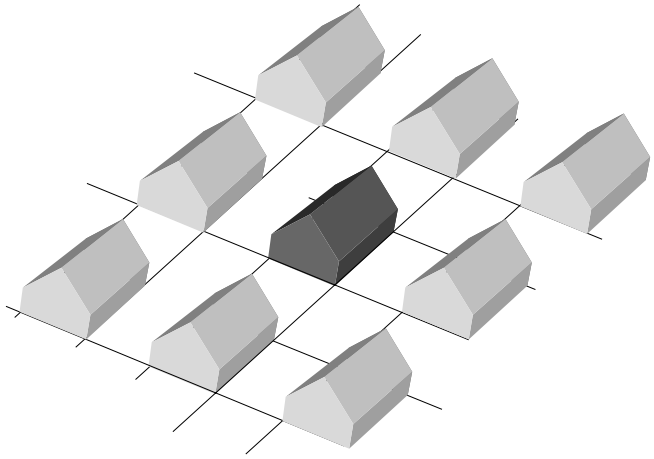

Figure 4-3 An example of Lee et al experiment (the Normal Pattern)

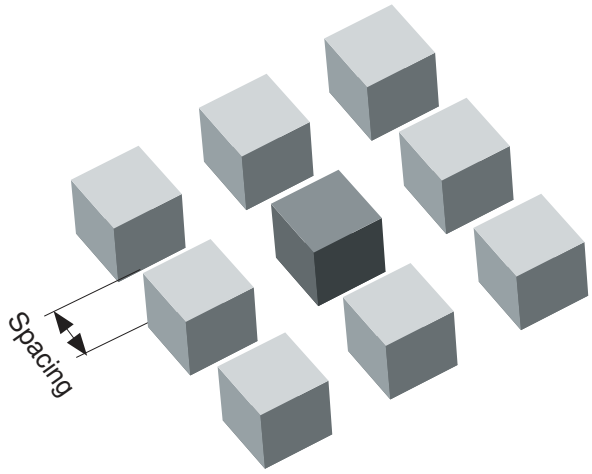

Figure 4-4 Ernest's shielded model configuration

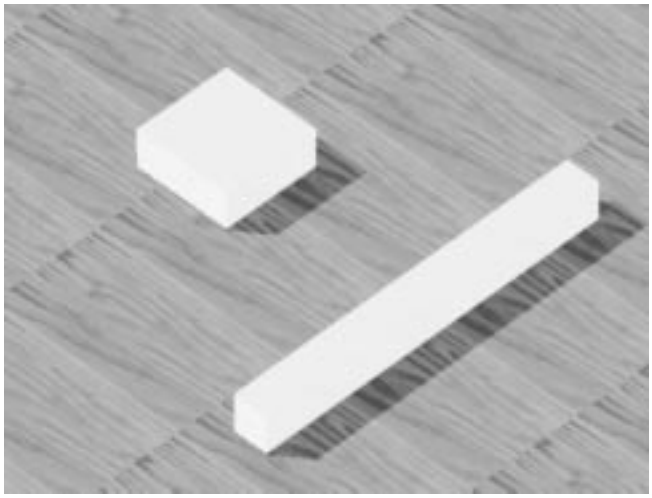

In summary, most of the available prediction models apply to specific urban layout configurations. These models use variables such as the spacing and the number of upwind obstruction rows to predict surface pressure in a shielded environment. However, they do not address other factors such as; the effect of changing the position of the individual obstruction blocks relative to the instrumented surface, the effect of multiple blocks of different size and shapes, and the size and position of the gaps between these blocks.

4.5 Multiple Rows of Obstruction Blocks

As described above, beyond three rows of windward obstruction blocks there was no effect on the pressure on the instrumented surface. This might be attributed to the apparent impermeability of the windward obstructions despite the fact that the blockage was formed by several discrete blocks (Figure 4-5). The question would then be, should only the obstruction blocks visible to the surfaces under consideration

be included in the definition of obstruction blocks in predicting the shielding effects?

Figure 4-5 Multiple discrete obstruction windward blocks.

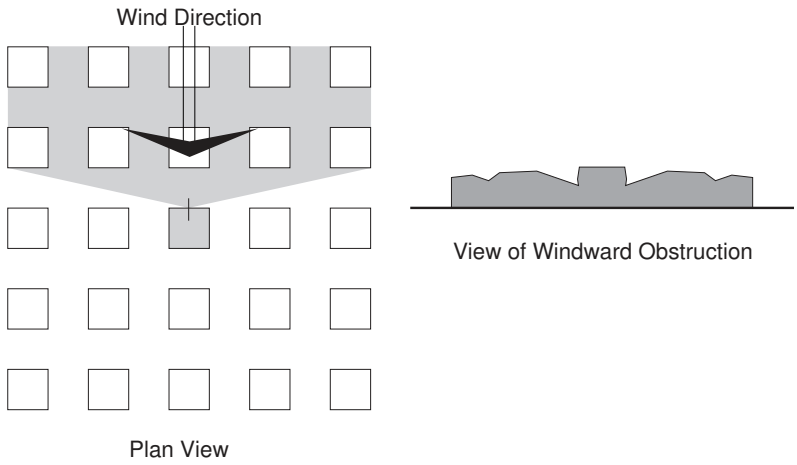

4.5.1 Tsutsumi *et al*'s Experiments

In a series of experiments conducted by Tsutsumi *et al* (Ref. 212), surface pressures were measured for a block embedded within arrays of identical blocks in normal grid and staggered layouts (Figure 4-6). The number of rows and the spacing between the block were varied to evaluate their respective effects on measured surface pressures.

Figure 4-6 Tsutsumi et al experimental setup (Ref. 212).

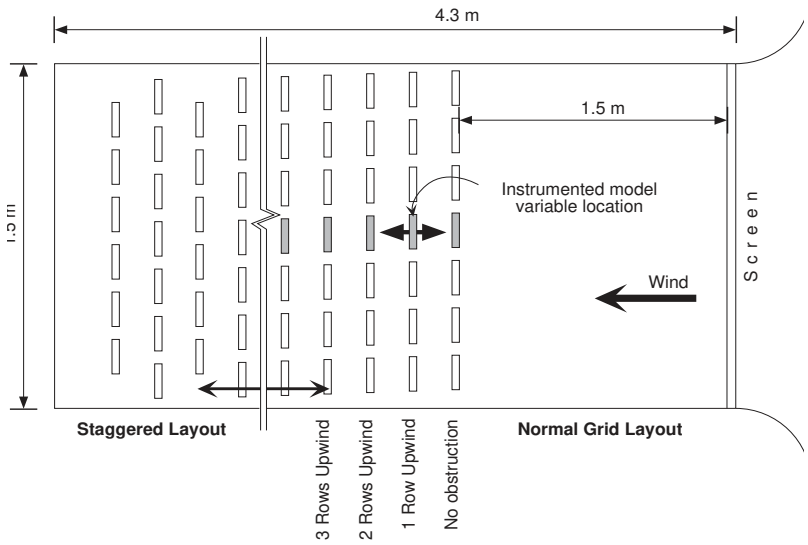

The results shown in Figure 4-7 indicate that adding more rows beyond the first or second does not significantly affect the surface pressures. However, Figure 4-7a shows a noticeable jump in the measured pressures between one and two rows of upwind obstruction blocks. This might be caused by the conditions of this experiment. There are no windward roughness elements for simulating a boundary layer on the windward section of the wind tunnel (Figure 4-6).

Figure 4-7 The result of increasing the number of obstruction blocks. Source: Tsutsumi et al (Ref. 212).

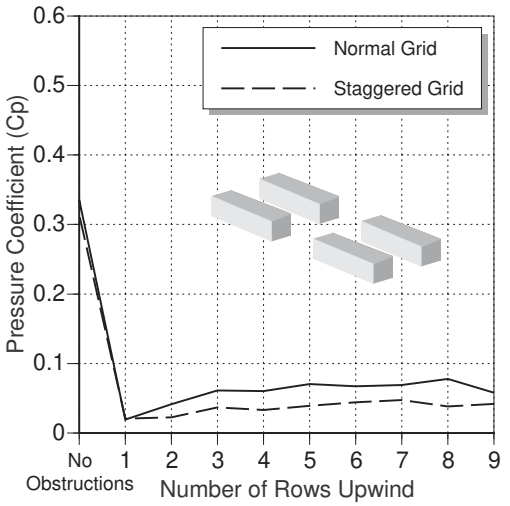

(a) Width-to-height ratio =4

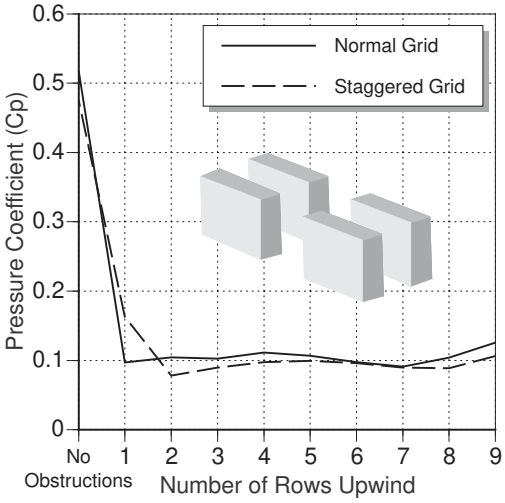

(b) Width-to-height ratio =1.3

The resulting high wind speed incident on the first row of windward obstructions causes a large wake within which there are low surface pressures on the second row (one row upwind of the model in Figure 4-7a). A fully developed boundary layer appears to be generated only beyond three upwind rows of obstruction blocks. This can be attributed to the development of a flow regime where the distance between the upwind

elements allows stable vortices to form between the elements (Figure 4-8c). This flow pattern is similar to the skimming regime described by Lee *et al* (Ref. 149) and shown in Figure 4-8. With multiple rows of obstruction blocks, a boundary layer develops where stable pressure coefficients are measured on the instrumented model surfaces.

Figure 4-8 The three airflow regimes between two identical blocks, Source: Lee et al (Ref. 149)

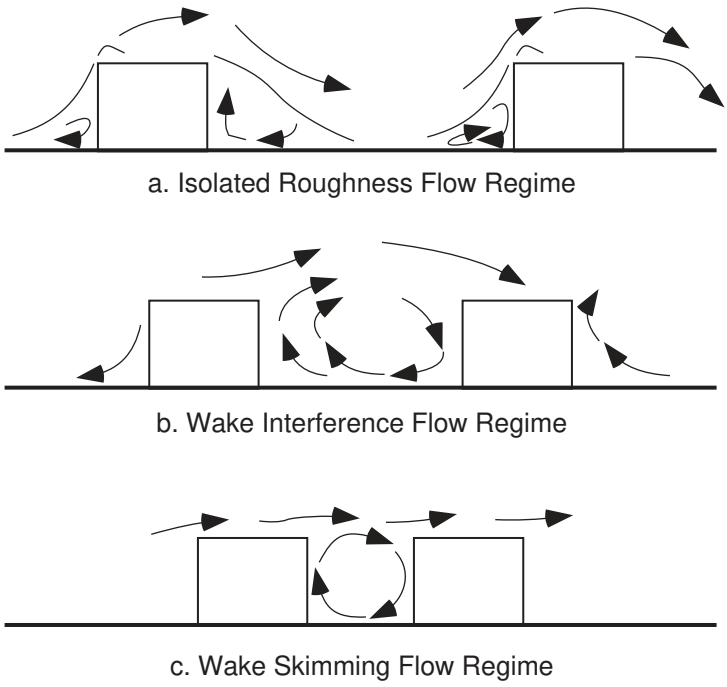

Figure 4-7a shows that wind pressures measured on the model surface in the staggered layout experiments were consistently lower than in the normal grid layout. By staggering the obstruction blocks, the wind was less able to flow through the gaps than in the case of normal grid layout where the wind is channeled through the gaps.

Figure 4-7b, on the other hand, does not show significant variations in the measured values of surface pressures on the

instrumented model after the first row (normal) or second row (staggered). Unlike the smaller obstruction blocks (Figure 4-7a), the tested configuration blocks in Figure 4-7b generated skimming airflow regimes very early in the wind tunnel. The staggered grid needed two rows to stabilize while the grid-iron layout needed one. This is because the staggered layout needs two rows upwind to have one obstruction directly upwind.

4.5.2 Verifying the Effect of Multiple Obstruction Rows

In order to determine the possibility of substituting an array of discrete obstruction blocks with a single block, the author conducted a number of preliminary wind tunnel tests. Figure 4-9 shows the variables tested in these experiments. These are the obstruction widths (20 and 61 cm), number of rows (one, two, and three), the spacing (S_m) between the instrumented model and the first windward row[6] (2, 3, 4, and 6 Spacings), and the spacing between the first and second rows[7] (2, 3, and 4). To avoid the anomalous first two rows described in Tsutsumi's experiments, the setup of experiments included a fully developed boundary layer upwind of the instrumented model.

4-6 Spacing#1 (Figure 4-9).

4-7 Spacing#2.

Figure 4-9 Setup of an initial experiment to study the effect of windward multiple rows on surface pressures.

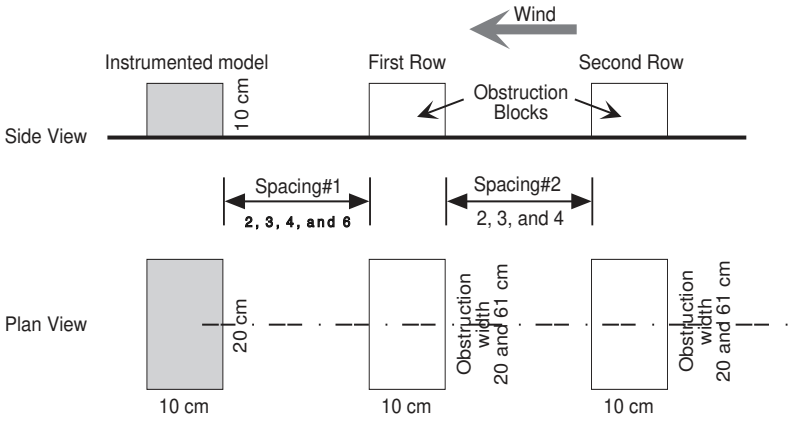

Figure 4-10 Surface pressure measurement results for obstruction width=20 cm

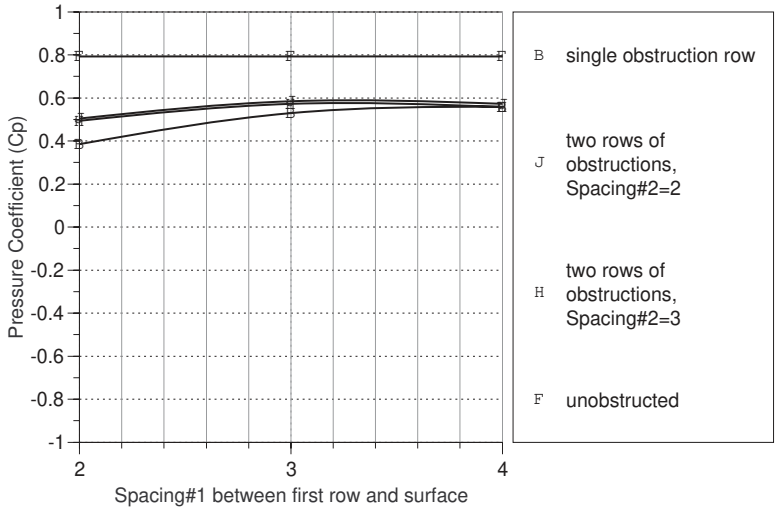

Figure 4-11 Surface pressure measurement results for obstruction width=61 cm

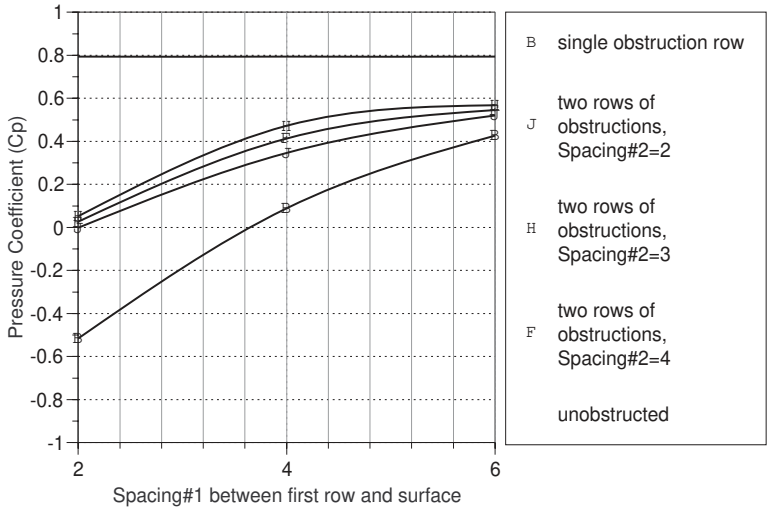

Figure 4-10 shows that upon adding a second row of obstruction blocks (20 cm in width), surface pressures on the instrumented model increased by a maximum of 20% (from 0.4-0.5 C_p) above those measured when using a single obstruction row. The maximum difference in pressure between obstructed and unobstructed models occurred when Spacing#1 and Spacing#2 were equal to 2. At all tested spacing#1, the effect of increasing the spacing between the obstruction rows (spacing#2) was negligible.

When the obstruction block width was 61 cm, the effect of adding a second obstruction row at spacing#1 equals to 2, was very apparent (Figure 4-11). This effect diminishes with the increase of the spacing#1. This can be attributed to formation of airflow regimes similar to those described in Lee *et al* (Ref. 149). Figure 4-12a shows that when spacing of obstruction rows was small, the two rows acted as a single row. As a result, the wake behind the two rows is smaller than that of a single

block (Ref. 79). Figure 4-12c represents a flow regime where the wake generated behind the first row does not interfere with the one behind the second row. As a result, the wake generated behind the second row is similar to one behind a single row (Figure 4-12d). Figure 4-12b represents a flow regime where the space between the two rows is not small enough to develop a stable vortex and at the same time not large enough for isolated roughness flow regime to take place. These results agree with the conclusions of Gowda *et al* (Ref. 108).

Figure 4-12 Flow regimes around lows of long obstruction blocks.

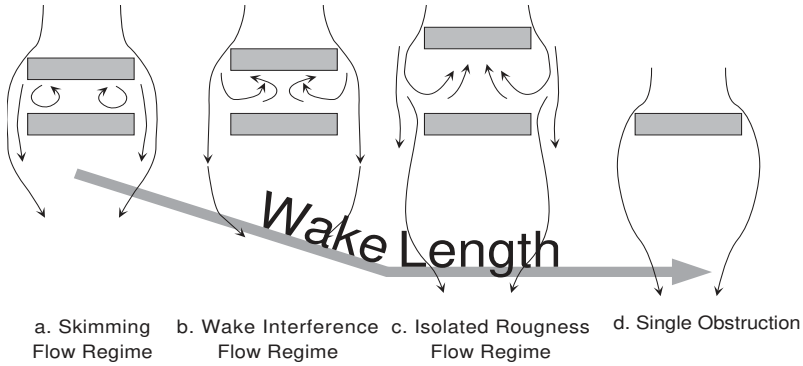

In conclusion, additional rows of obstruction blocks can be ignored in any proposed mathematical model if the obstruction blocks have the same widths as the model of concern. This is especially true for any obstruction block not visible from the instrumented surface. The proposed mathematical model however, should account for the effect of multiple rows of obstruction blocks when wake interference and isolated roughness flow regimes are encountered.

An additional conclusion that can be interpreted from the previous study is that a single windward obstruction block may

be used to predict the effect of an array of windward obstruction blocks when the array forms an impermeable barrier windward of the building (Section 4.5). This conclusion agrees with the supposition set by Ernest (Ref. 75).

4.6 Definition of Variables

The following sections describe the general definition of the variables and terminology used throughout the study. The definition of some of these variables is refined in later sections to account for complexities in the mathematical model.

4.6.1 Wind Direction Angle (Θ)

The wind direction angle is defined in this study as the angle (in degrees) between a line denoting the wind direction and a line perpendicular to the surface of interest. The angle is measured clockwise and ranges between 0˚-360˚ (Figure 4-13).

Figure 4-13 Definition of Wind Direction angle

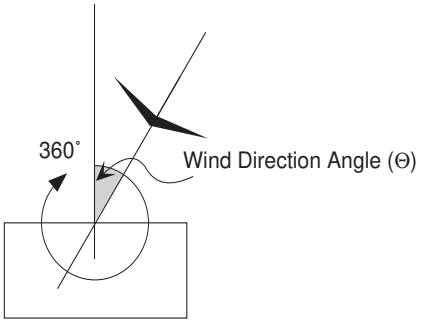

4.6.2 Obstruction Block Description

Individual obstruction blocks are described using geometric angles from a point established at the bottom center of the obstruction-facing surface (Figure 4-14). Figures 4-15 to 4-18 represent the four geometric variables used in this model.

Figure 4-14 Location of representative point on instrumented Surface

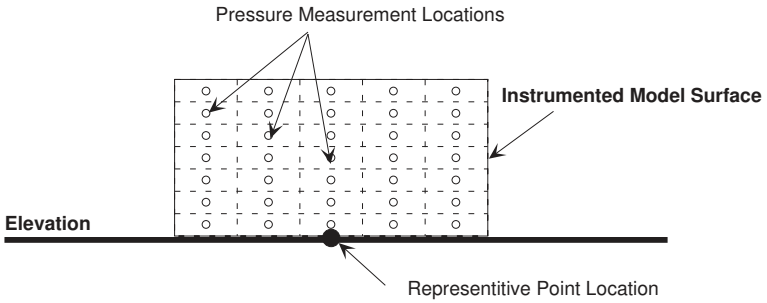

4.6.2.1 Horizontal Angle (α_h)

The horizontal angle (α_h) is defined as the angle originating from the center of the instrumented surface and encompassing the visible limits of the obstruction block from the center of the instrumented model (Figure 4-15).

Figure 4-15 Basic variables: Horizontal Angle (α_h)

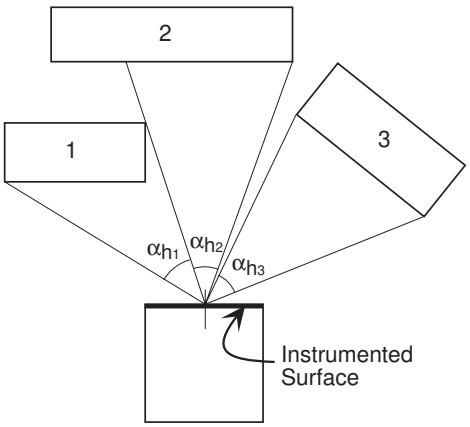

4.6.2.2 Vertical Angle (α_v)

The definition of the vertical angle (α_v) is that angle between a line connecting the bottom center of the instrumented surface to the center of the obstruction block and a line that encompasses the highest visible edge on the vertical plane of the obstruction block (Figure 4-16).

Figure 4-16 Basic variables: Vertical Angle (α_v).

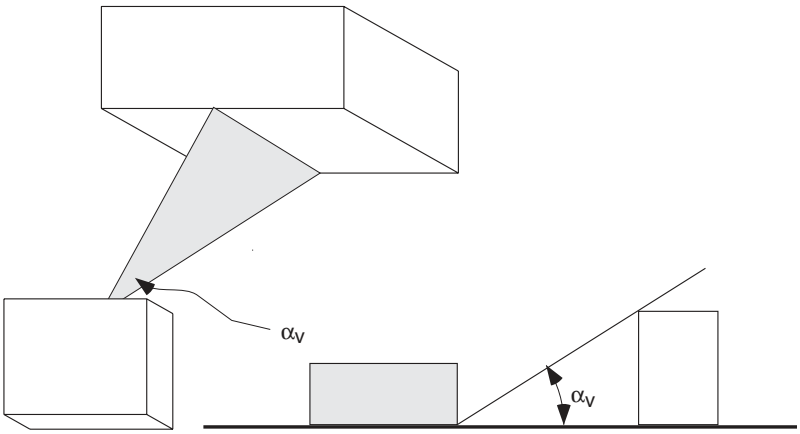

4.6.2.3 Model Spacing (S_m)

Model spacing is defined as the perpendicular distance from the center of the instrumented surface to the center of the obstruction block divided by the height of instrumented model (Figure 4-17).

Figure 4-17 Basic variables: Spacing (S_m).

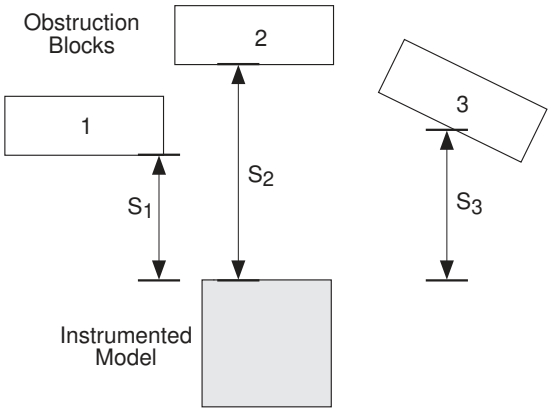

4.6.2.4 Obstruction Spacing (S_o)

The obstruction spacing represents the same distance described in Section 4.6.2.3 divided by the height of the obstruction block instead of the instrumented model. When the line connecting the two centers coincides with the normal wind direction, the obstruction spacing can be expressed as a function of the vertical angle as follows:

$$S_o = \tan(\alpha_v)^{-1}$$

4.6.2.5 Displacement Angle (α_d)

The displacement angle α_d (Figure 4-18) is defined as the angle between the wind direction and the line bisecting the horizontal angle (α_h) of an obstruction.

Figure 4-18 Basic variables: Displacement Angles

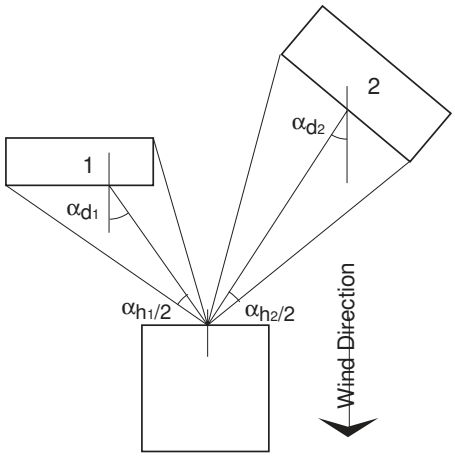

The choice of the these angles was based on a number of preliminary experiments. The criterion for choice was the sensitivity of measured surface pressures to changes in the specific geometric variable.

4.7 Angular Description of Obstruction Blocks

Figure 4-19 shows a comparison between the pressure coefficient C_p results obtained from shielded model experiments by Ernest and Wiren (Refs. 74 & 225). These experiments involved locating models with instrumented surfaces behind windward obstruction blocks. The shown pressure coefficient values were measured at the windward shielded surfaces plotted against obstruction spacing. By comparing the effects of the single obstruction on pressure coefficient values in both experiments the following can be observed:

At C_p equal to about 0.0 (points A and B in Figure 4-19), the corresponding values of spacing on the x-axis were 2.3 and 7.4 in Wiren's and Ernest respectively. Both these spacing values corresponded to geometric relationships illustrated in Figure 4-20. This relationship can also be described in terms of obstruction angles from a representative point on the instrumented surface (Figure 4-14). The measured obstruction angles both configurations are described in TABLE 4-1 .

Figure 4-19 Comparison of Ernest's and Wiren's experiments

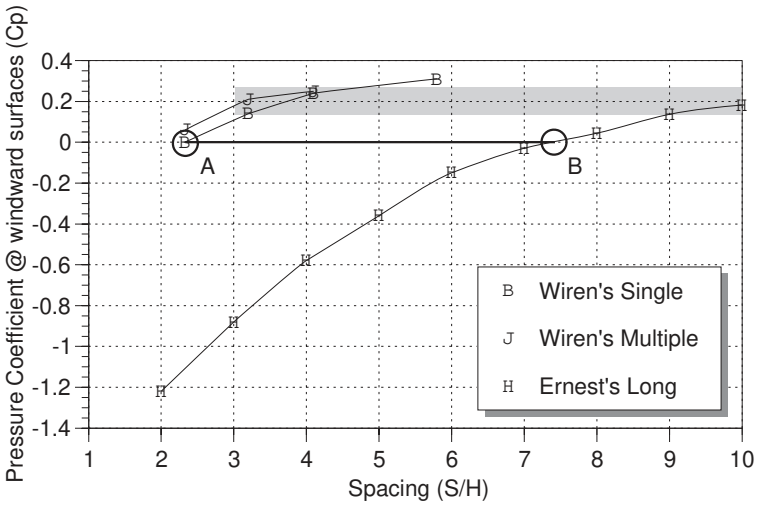

Figure 4-20 Ernest's and Wiren's tested configurations

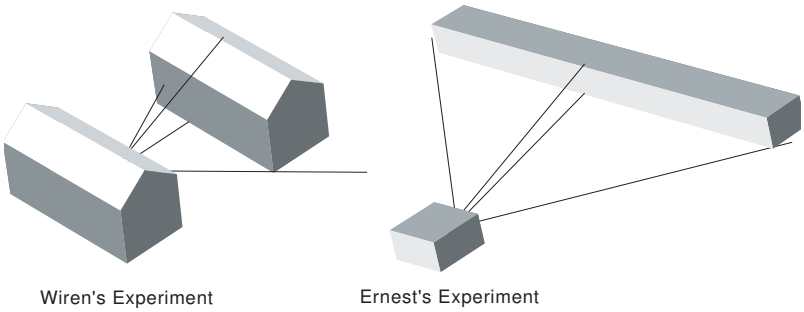

TABLE 4-1 **Angular Description of the Obstruction in tested Configurations**

Experiments	Horizontal Angle of View	Vertical Angle of View
Ernest	110˚	40˚
Wiren	7˚	23˚

In addition to Ernest's and Wiren's experiments, the author tested surface pressures on an instrumented model behind an 89 cm wide obstruction block. The spacing between the obstruction block and the instrumented model was varied until the measured pressure coefficient C_p was equal to zero. The angles of view at that location were measured and plotted against Ernest's and Wiren's experiments (Figure 4-21). The three points can be connected with straight line where $C_p = 0$. This simple relation may indicate a relationship between surface pressures and the proposed angles of description of the windward obstruction blocks.

Figure 4-21 Obstruction angles coincident with measured surface pressure coefficients (C_p)=0

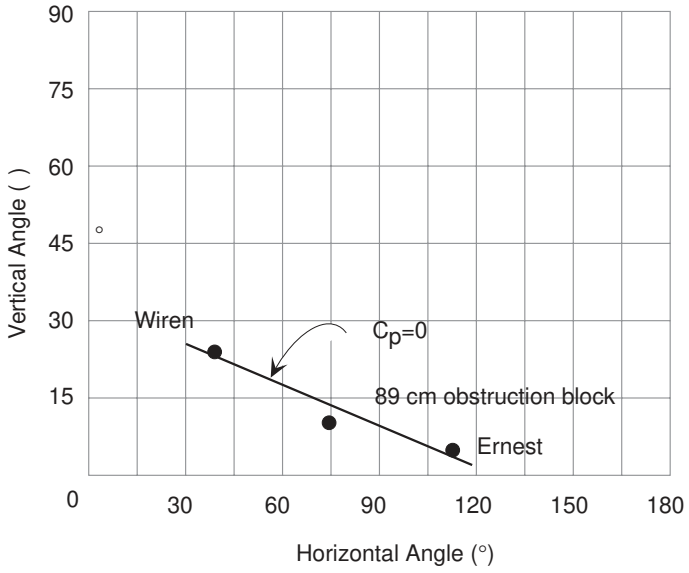

4.8 Summary and Conclusions

The following are four points that can be concluded from the analysis thus far:

- In most cases only visible obstruction blocks affect the pressure values on surfaces of concern.
- In most cases, multi-row obstruction blocks can be represented by a single block located at the location of the closest obstruction block.
- If an array of obstructions form an impermeable blockage in the windward direction, a single obstruction block can be used to represent the array.
- A number of geometric angles may be used to predict the effect of obstruction blocks on the surfaces of concern.

4.9 Developing the Mathematical Model

The following sections describe the development of a mathematical model to predict mean surface pressures on shielded surfaces.

Based on the premise that a smaller or a distant obstruction block produces less shielding effect on an instrumented model than a close or a large one (Ref. 10), the mathematical model was structured in such way that the average surface pressure is determined by averaging the shielding effects of the obstruction blocks visible from the instrumented model (Figure 4-22). The prediction of the shielding effect of individual obstructions is based on the solid angle describing each block.

Figure 4-22 The Shielding Effect of an Obstruction Block.

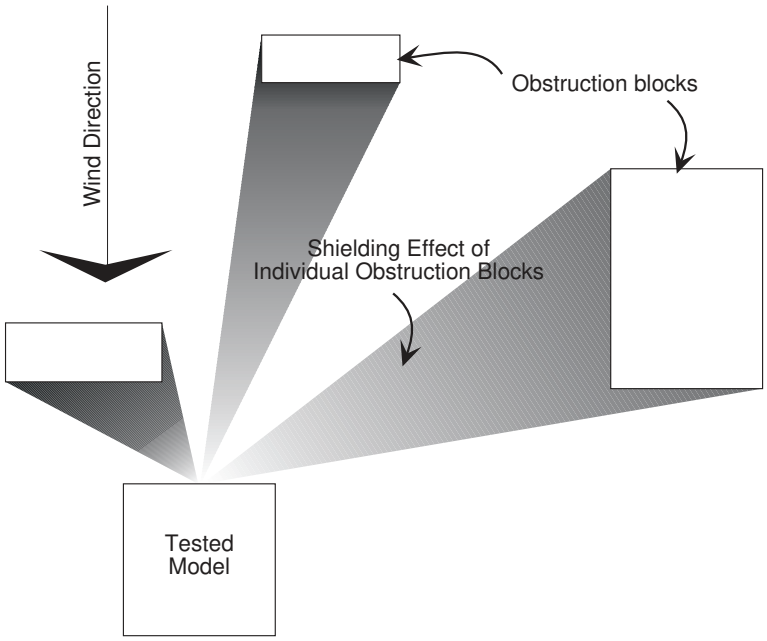

The proposed mathematical functions were built upon three components:

- Surface pressures on the unobstructed block (Section 4.11).
- Surface pressures on the shielded bock (Section 4.12).
- The development of a non-dimensional factor that uses the ratio two above pressures (Section 4.10).

4.10 Pressure Shielding Modification Coefficient C_{pm}

Swami and Chandra (Ref. 203) showed that the proportions of a building surface affect the values of wind pressure incident on that surface. To eliminate the effects of differences in surface dimensions, Swami *et al* used a non-dimensional factor. This factor is calculated by normalizing the average surface

pressure coefficients (C_p) to those at wind direction (Θ) = 0°[8].

In their model, the mean Pressure Coefficient (C_p) is an arithmetic average of individual pressure coefficients measured in an even array on the surface of the instrumented models [Equation (4-1)]. The local Pressure Coefficient for each point on the surface (C_{p_i}) is defined as a non-dimensional ratio of the surface dynamic wind pressure averaged over time to the free-stream dynamic pressure at the model eave height[9]. For this work, the dynamic pressure of the free-stream wind tunnel at eave height was obtained in a separate wind tunnel test. The pressure coefficient for each point at the instrumented surface was calculated according to Equation (3-3).

The Pressure Coefficient averaged for the whole facade is determined using the following function:

$$C_p = \frac{\sum_{i=1}^{n} C_{p_i}}{n} \qquad \textbf{(4-1)}$$

In order to describe the shielding of surrounding buildings, the measured pressure coefficient had to be referenced to the pressure coefficient on the same instrumented model without upstream obstructions. For any wind angle Θ, the mean pressure coefficients of shielded instrumented surfaces could be

4-8 In Swami and Chandra's (Ref. 203), Normalized Pressure Coefficient was defined as $\frac{C_{p_\Theta}}{C_{p \text{ at } \Theta = 0°}}$.

4-9 Eave height is 3.0 m or 10 cm model at scale (Section A.3 in Appendix A).

divided by the mean pressure coefficient on the unshielded model resulting in normalized mean pressure coefficients ($C_{p(Norm)}$ in Equation 4-2).

$$C_{p(Norm)} = \frac{C_{p(Shielded_{\Theta})}}{C_{p(Unshielded_{\Theta})}} \quad \textbf{(4-2)}$$

Examining wind direction effects on $C_{p(Unshielded_{\Theta})}$ showed that zero pressure coefficients can be found. To avoid dividing by zero, Equation (4-2) was modified to an exponential form. This form has the added advantage of being more sensitive to variation in small values of the unshielded surface pressures than is the normalized form. The result is a non-dimensional coefficient that characterizes the degree of shielding of an obstructed building surface compared to an identical unobstructed surface in similar boundary layer conditions. The Pressure Modification Coefficient (C_{pm}) is defined mathematically as follows:

$$C_{pm} = \frac{e^{C_{p(Shielded_{\Theta})}}}{e^{C_{p(Unshielded_{\Theta})}}} = e^{[C_{p(Shielded_{\Theta})} - C_{p(Unshielded_{\Theta})}]} \quad \textbf{(4-3)}$$

Where

C_{pm} = Pressure Modification Coefficient

$C_{p(Shielded_{\Theta})}$ = Pressure Coefficient on shielded surfaces at wind direction Θ

$C_{p(Unshielded_{\Theta})}$ = Pressure Coefficient on unshielded surfaces at wind direction Θ

from Equation 4-3:

$$\text{when } C_{p(Shielded)} = C_{p(Unshielded)} \quad \therefore C_{pm} = 1 \tag{4-4}$$

$$\text{when } \left|C_{p(Shielded)}\right| > \left|C_{p(Unshielded)}\right| \quad \therefore C_{pm} > 1 \tag{4-5}$$

$$\text{when } \left|C_{p(Shielded)}\right| < \left|C_{p(Unshielded)}\right| \quad \therefore\ 0 < C_{pm} < 1 \tag{4-6}$$

4.11 The Unobstructed Model

Today, there are numerous sources of pressure data on unobstructed building surfaces. The following sections describe a mathematical function that uses these data to estimate the effects of wind direction and building geometry on the pressure coefficients.

4.11.1 Swami and Chandra's Model

Swami and Chandra of the *Florida Solar Energy Center* (Ref. 203) consolidated a large database of measurements obtained from wind tunnel experiments. The purpose of their work was to establish a relationship between average wind pressure measured on building surfaces and wind direction and building geometry. Their derived function for $C_{p(Unshielded)}$ demonstrated that an empirical function can be constructed to predict the average surface pressure coefficients.

Because of the diverse datasets from which the relationship was derived, and the sensitivity of the proposed C_{pm} to small changes in $C_{p(Unshielded)}$, Swami *et al*'s function needed be refined for use in the proposed model. A new set of experiments was conducted in a controlled wind tunnel environment.

The following section describes this set of experiments and addresses the derivation of a new ($C_{p(Unshielded_{\Theta})}$). This modification of Swami and Chandra's model involved changing their equation coefficients.

4.11.2 The Modified Unobstructed Model

The experiments devised to predict the wind direction effect on model surface wind pressure involved testing unshielded instrumented models of different geometries.

4.11.2.1 Setup of Experiment

Nine model configurations were tested relative to 13 wind directions (0˚-180˚ in 15˚ intervals). The difference in model configuration was expressed in terms of the Side Aspect Ratio (A_s) or ratio between the length (L_m) to the width (W_m) of the model (Figure 4-23).

Figure 4-23 Definition of the Side Aspect Ratio (A_S)

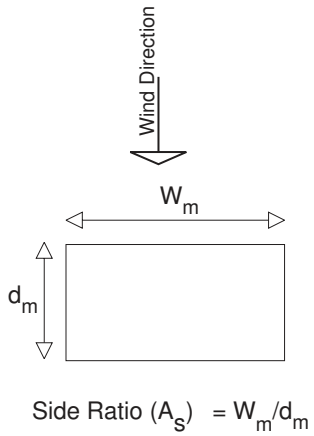

The following table shows the tested configurations:

TABLE 4-2 **Tested Configurations for the Unobstructed Model (13 Wind Directions)[a]**

	Unobstructed Block Configurations				
Dimensions	25×25	25×37.5	25×50	25×62.5	25×75
Side Ratios (A_S)	1:1 (1.0)	2:3 (0.67)	1:2 (0.50)	2:5 (0.40)	1:3 (0.33)
Dimensions	_____	37.5×25	50×25	62.5×25	75×25
Side Ratios (A_S)	_____	3:2 (1.50)	2:1 (2.0)	5:2 (2.50)	3:1 (3.0)

a. The total number of tests in this experiment was 117.

4.11.2.2 Results

Figure 4-24 shows the effects of changing the wind direction on the mean Surface Pressure Coefficients (C_p). It should be noted that the C_p values at wind direction ($\Theta = 0^\circ$) may be divided into two groups. The first group corresponds to configurations with Side Aspect Ratios $A_s \leq 1.0$, while the second applies when $A_s > 1.0$. All the values of $C_{p_{\Theta = 0}}$ in the first group had the same value (Figure 4-24). This should be expected since all tested configurations had the same Face Aspect Ratio (A_f) or windward surface dimensions (25 long $\times$ 10 high) cm. The Face Aspect Ratio is defined as the ratio between the width and height of the wind-facing surface. The second group of configurations ($A_s > 1.0$) showed variation at $C_{p_{\Theta = 0}}$ caused by the difference in their corresponding A_f.

Figure 4-24 Effect of Side Aspect Ratio (A_s) on average pressure coefficients relative to wind direction

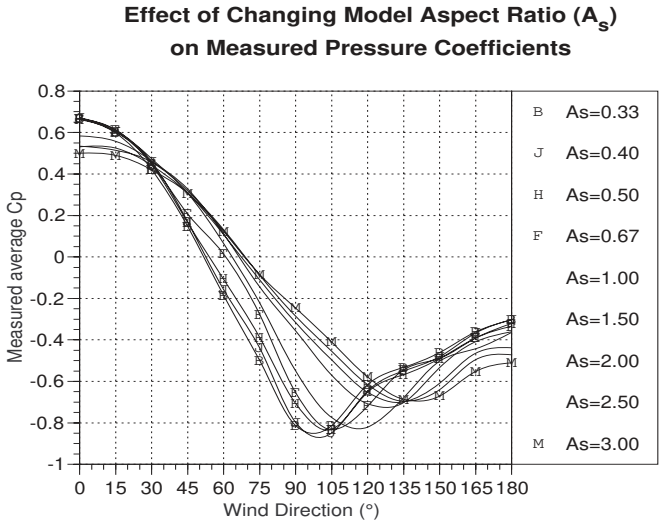

Figure 4-25 Effect of Side Aspect Ratio on mean normalized pressure coefficients relative to wind direction

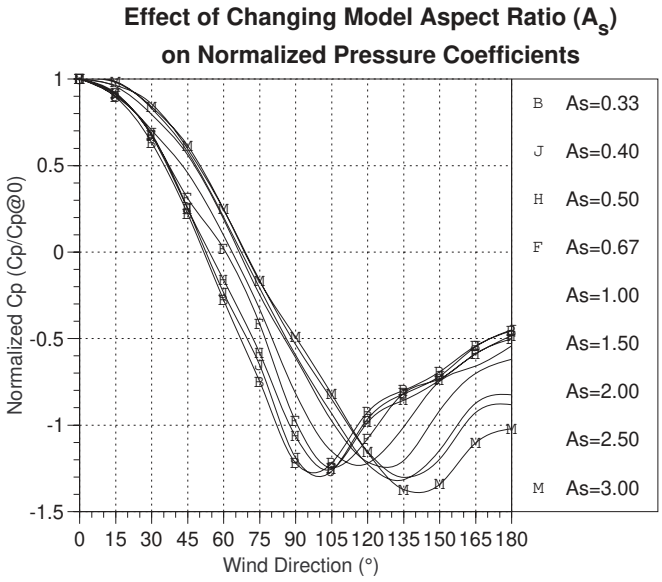

Figure 4-24 represents the same data in Figure 4-25 expressed as NC_p values. The latter Figure shows consistently lower values of NC_p when $A_s \leq 1.0$ than when $A_s > 1.0$ between $0^\circ = \Theta \leq 90^\circ$. However, at $120^\circ \leq \Theta \leq 180^\circ$, the configurations with $A_s \leq 1.0$ maintained higher NC_p values. This behavior at $120^\circ \leq \Theta \leq 180^\circ$ can be explained by the large

self-shielding where $A_s > 1.0$. This in effect tends to reduce the values of measured NC_p below those with smaller Side Aspect Ratios (Figure 4-26). On the other hand, at $0^\circ = \Theta \leq 90^\circ$, the relatively large wind-facing surface in configurations where $A_s > 1.0$ causes the values of NC_p to be higher than those with smaller Side Aspect Ratios (Figure 4-27).

Figure 4-26 Self-shielding when wind direction ≥120˚

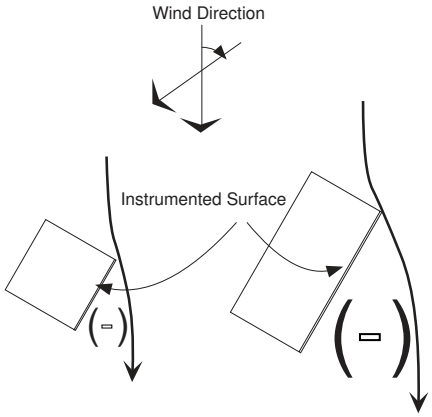

Figure 4-27 Pressure Coefficient of windward surface is relative to the Side Aspect Ratio of the model

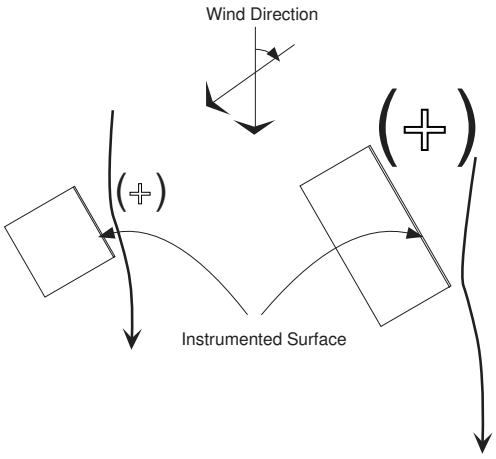

4.11.2.3 Relating NC_p to Wind Direction and Side Aspect Ratio

In order to neutralize the Face Aspect Ratio[10] (A_f) effect and in agreement with Swami and Chandra (Ref. 203), the deci-

4-10 The Face Aspect Ratio is the ratio between the model length to its height.

sion was made to normalize the values of the pressure coefficients to the value of C_p at $\Theta = 0°$ or (NC_p).

In the interest of modifying Swami and Chandra's function instead of proposing a new one, the same variables were used. These variables are the Side Aspect Ratio (A_s) and the wind direction. As a result, new coefficients were introduced to achieve the desired degree of refinement. A linear regression routine was used to determine the equation coefficients giving the highest fit between the measured data and Swami and Chandra's function (Ref. 203):

$$NC_p = \ln\left(C_0 + C_1 \cdot \sin\left(\frac{\Theta}{2}\right) + [C_2 \cdot \sin(\Theta)]^2 + C_3 \cdot [\sin(2 \times \Theta \times G)]^3 + C_4 \cdot \cos\left(\frac{\Theta}{2}\right) + C_5 \cdot G^2 \cdot \left[\sin\left(\frac{\Theta}{2}\right)\right]^2 + C_6 \cdot \left[\cos\left(\frac{\Theta}{2}\right)\right]^2\right\} \quad \textbf{(4-7)}$$

where;

NC_p = Normalized C_p
Θ = Wind direction in degrees
$G = \ln(A_s)$
A_s = Side Aspect Ratio

The new coefficient of Equation 4-7 are:

$$C_0 = 2.295$$
$$C_1 = -1.768$$
$$C_2 = -0.935$$
$$C_3 = 0.147$$
$$C_4 = 0.483$$
$$C_5 = -0.034$$
$$C_6 = -0.006$$

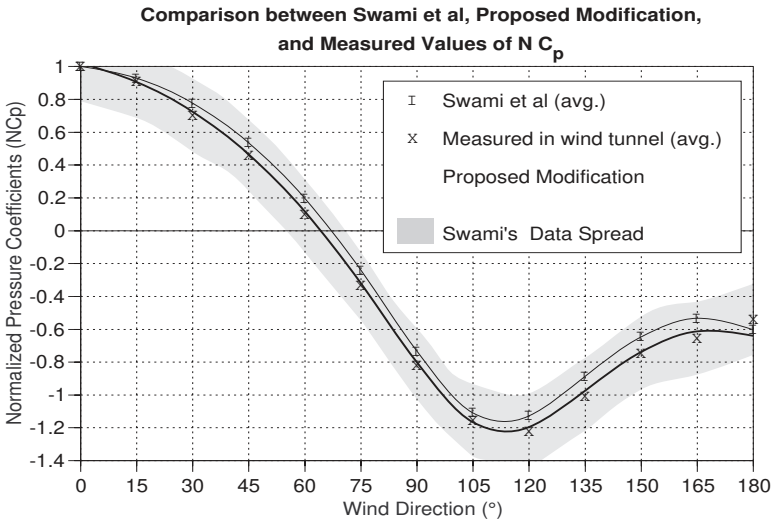

Figure 4-28 Effect of changing wind direction on surface pressure coefficients. A comparison between the existing and proposed models.

Figure 4-28 shows a comparison between Swami and Chandra's mathematical relationship and the modified version developed in this section applied to the same configuration. The adoption of the modified version of the equation in consequent analyses provides consistency in the data used throughout the development of the shielded-surfaces-pressure-prediction model.

4.12 The Orthogonal Configurations

The number of different positions of an obstruction block relative to the surface of concern can be infinite. With such positional changes, all four geometric variables describing the location of the obstruction block (Section 4.6.2) will vary. However, changing one variable such as the spacing (S_o) between the obstruction block and the instrumented surface involves changing derivative variables such as the horizontal (α_h) and vertical (α_v) angles.

At this stage of investigation, the research was restricted to configurations in which the model and obstruction blocks were always perpendicular to the wind direction. These configurations are referred to in the study as the Orthogonal Configurations and the mathematical relationship produced by these tests is described as the orthogonal model.

This section includes a description of the orthogonal model in terms of the tested configurations, variables, and derivation of a mathematical function. The orthogonal configurations in this research were defined as those which fulfill the following geometric criteria (Figure 4-29):

- Only one obstruction block was tested. The initial tests had shown that a single windward block causes most of the shielding for the surface of interest (Section 4.5).
- Both model and obstruction block were placed with centerlines aligned with the wind direction (Figure 4-29). Incidences when the instrumented model and obstruction block were not symmetrical were discussed as a part of the expansion of the model to include non-orthogonal configurations. Thus;

- The wind direction was always 0°. Effect of changing wind direction will be discussed in later stages of the research.
- Finally, both the instrumented surface and the obstruction surface facing it remained parallel to each other. Additional configurations where the two blocks were not parallel are handled in later experiments.

Figure 4-29 Orthogonal configurations.

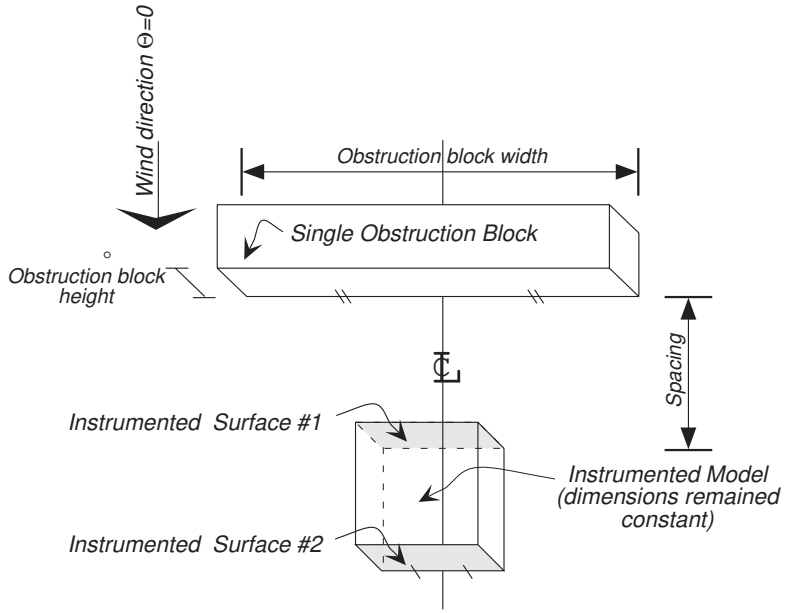

4.12.1 Tested Configurations

The following table (TABLE 4-3) lists the tested variables in the orthogonal configurations.

TABLE 4-3 **Tested Orthogonal Configurations with Variable Spacings (S_m)[a]**

Obstruction Model Height (cm)	Obstruction Block Width (cm)				
	200	150	89	61	25
7	-	-	-	-	X[b]
10	X[c]	X[c]	X[b]	X[d]	X[b]

TABLE 4-3 **Tested Orthogonal Configurations with Variable Spacings (S_m)[a] (Continued)**

Obstruction Model Height (cm)	Obstruction Block Width (cm)				
	200	**150**	**89**	**61**	**25**
17	-	-	-	-	X[b]
25	-	-	-	-	X[c]

a. Refer to definition in Section 4.6.2.3.
b. Spacings =1-10.
c. Spacings =2-10.
d. Spacings = 2, 3, 4, and 6.

A total of 61 tests were performed resulting in 122 values of the mean Pressure Modification Coefficient (C_{pm}) for both windward and leeward surfaces of instrumented model.

To understand the effect of obstruction width, five blocks with the same height 3.0 m (10 cm model scale) and varying widths were tested (TABLE 4-3). The effect of obstruction block height was analyzed using four obstruction configurations with a single width 7.5 m (25 cm) and four heights 2.1, 3.0, 5.1, and 7.5 m (7, 10, 17, and 25 cm respectively). In addition to width and height of the obstruction blocks, the effect of spacing from the instrumented model was also considered. Figures 4-30 and 4-31 show the tested obstruction configurations and the instrumented model. In order to comply with the angular description concept discussed in Section 4.7, height, width, and spacing of the obstruction width were expressed in angular format (α_h and α_v).

Figure 4-30 Tested obstruction widths (Orthogonal configurations)

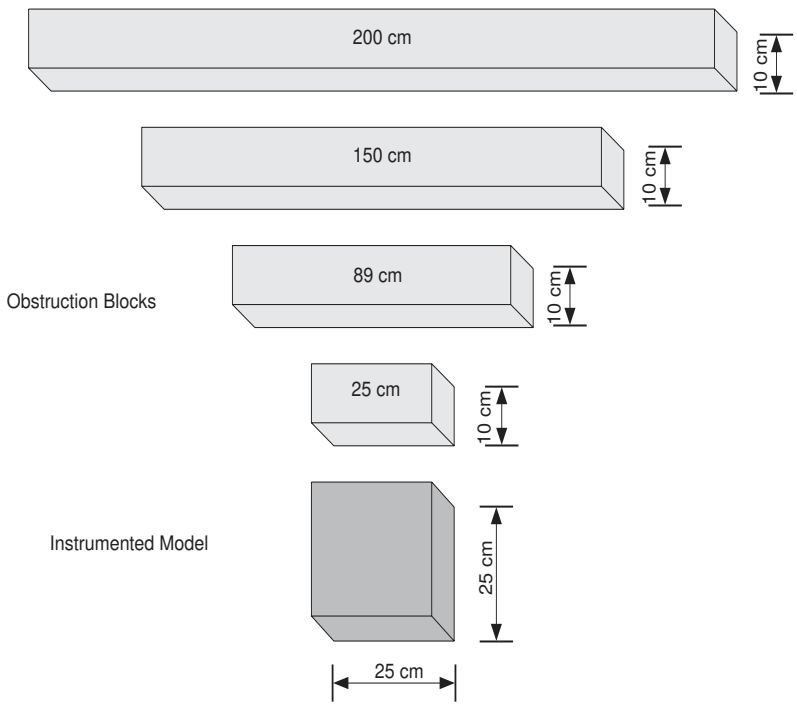

Figure 4-31 Tested Obstruction Heights (Orthogonal Configurations)

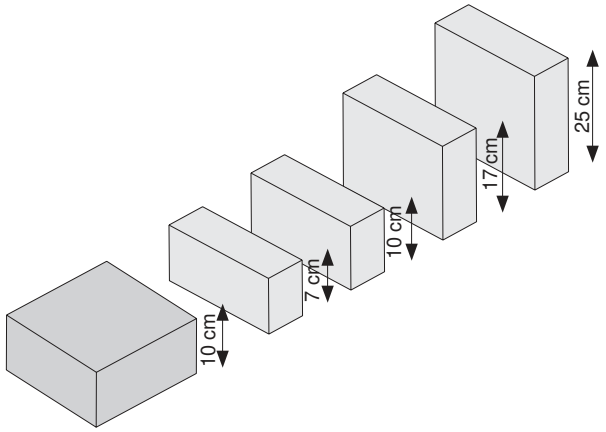

4.12.2 General Discussion

Appendix D contains the results of the 122 surface measurements using the orthogonal configurations. The collected C_p and C_{pm} values in Appendix D, Figures 4-32 and 4-33 represent the arithmetic mean of 27 measurement points on each surface (Equation 4-1).

4.12.2.1 Effect of Spacing on Pressure Coefficients

Figures 4-32 and 4-33 illustrate the relationship between the surface pressures and model spacing (S_m)[11]. The highest pressure modification coefficient values (C_{pm}) were obtained behind the smallest obstruction block (25×7) while the lowest C_{pm} values were measured when the widest block (200×10) was tested.

Figure 4-32 Pressure coefficient on windward side (ww)

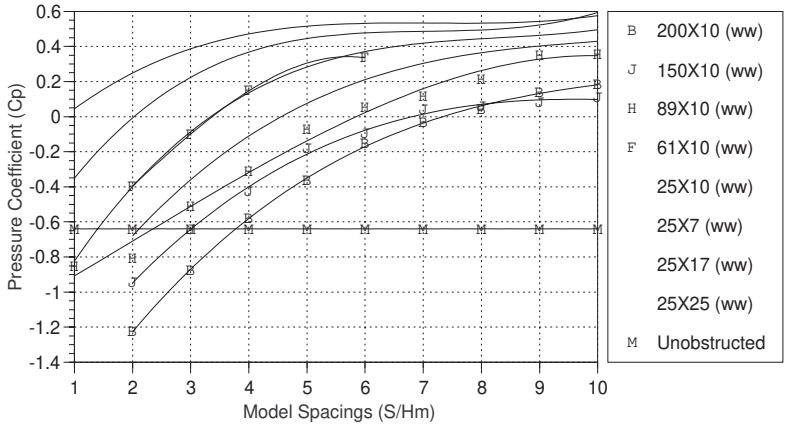

Key:
Configuration wXs
Where:
w=obstruction width
s=spacing

Figure 4-33 Pressure modification coefficients on windward side (ww).

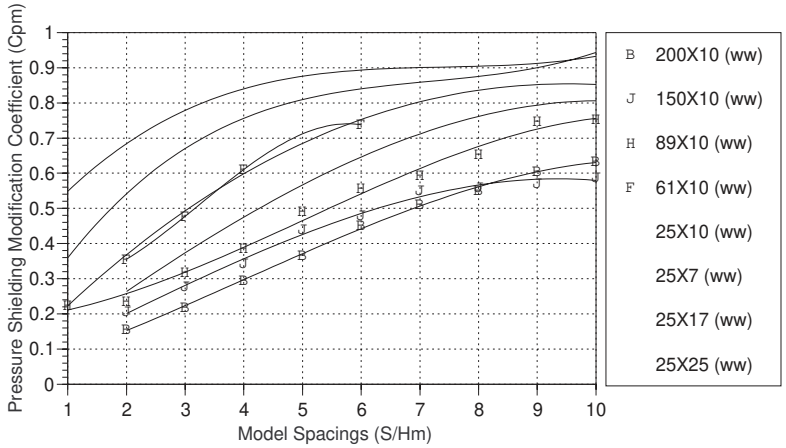

4-11 Definition in Section 4.6.2.3, page 66

At the same spacing, measured C_{pm} values on the instrumented model were almost identical for both obstruction blocks 61×10 and 25×17 (Figure 4-34). This may be attributed to an equality caused by a similar combined effect of the two angles of obstruction. This supports the discussion in Section 4.7 in which a function based of the combination of the angles of obstruction was suggested to determine the shielding effect of an obstruction block.

Figure 4-34 The only test condition when C_{pm} values of two obstruction blocks were identical with reference to Spacing.

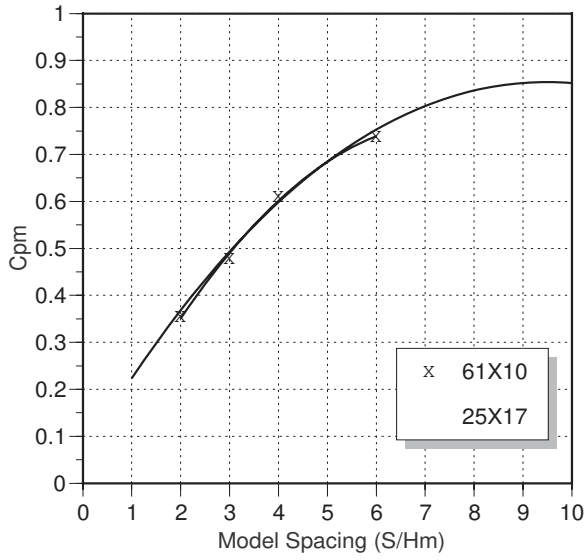

Surface pressures measured at the leeward side of the instrumented model were virtually unaffected[12] by the windward obstruction configuration and spacing (Figure D-15 to Figure D-18 in Appendix D). The only exception was when the obstruction block extended across the whole wind tunnel width[13]. This long obstruction block is referred to in the rest

4-12 Confirming Givoni 1981 (Ref. 102), page 283.

4-13 Obstruction width equals 200 cm.

of the study as the *infinitely long obstruction block*. It could represent a row-housing type of development where the deflected wind does not have a chance to reattach from the sides. The only reattachment of the wind possible was over the top of the obstruction block (Figure 4-35). The C_p values (Figure D-15) measured behind the 200×10 obstruction block at the closest Spacing (S_m=2) from the instrumented surface showed about a 20% reduction when compared with spacings ≥ 5. This was caused by the extraordinarily long wake generated behind the block. Other smaller blocks (which might represent more realistic adjacent buildings) did not show any effect on the C_p values measured in the leeward surface of the instrumented model.

Figure 4-35 The long wake generated behind an infinitely long obstruction block.

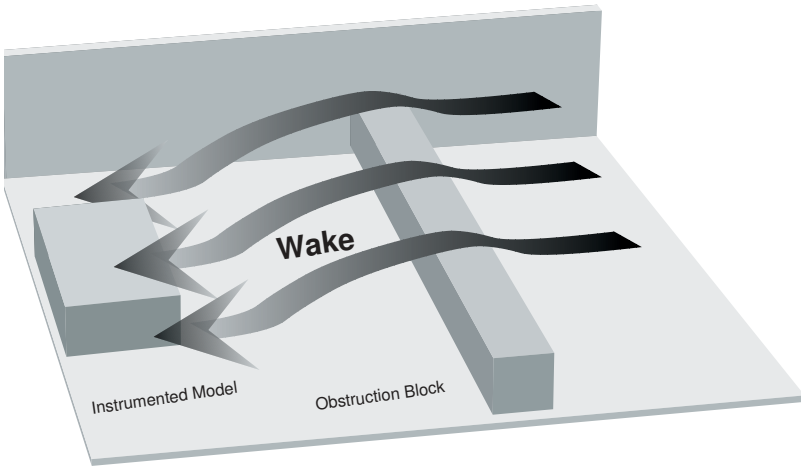

Figure 4-36 The relatively short wake generated behind a small obstruction block.

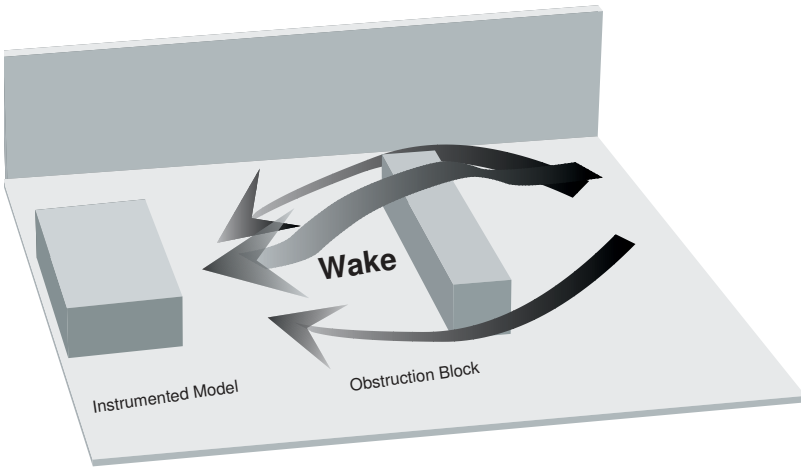

4.12.2.2 Changing the Horizontal Angle of Obstruction

Based on the definition of the horizontal angle in Section 4.6.2.1, the variation in the value of the horizontal angle (α_h) can be achieved through one of two ways;

- by physically varying the obstruction width and,
- by varying the distance of obstruction from the instrumented model (Spacing).

Both techniques were used in the experiments to produce Figure 4-37 in which Normalized Pressure Coefficients ($C_{p(Norm)}$) were plotted against the Horizontal Angle of Obstruction (α_h).Values of $C_{p(Norm)}$ were calculated from the relationship described in Equation (4-2).

4.12.2.2.1 Results

The complete results of varying the Horizontal Angle of Obstruction (α_h) are documented in Appendix D (Figure D-19 to Figure D-22).

Figure 4-37 Effect of varying the horizontal angle of obstruction

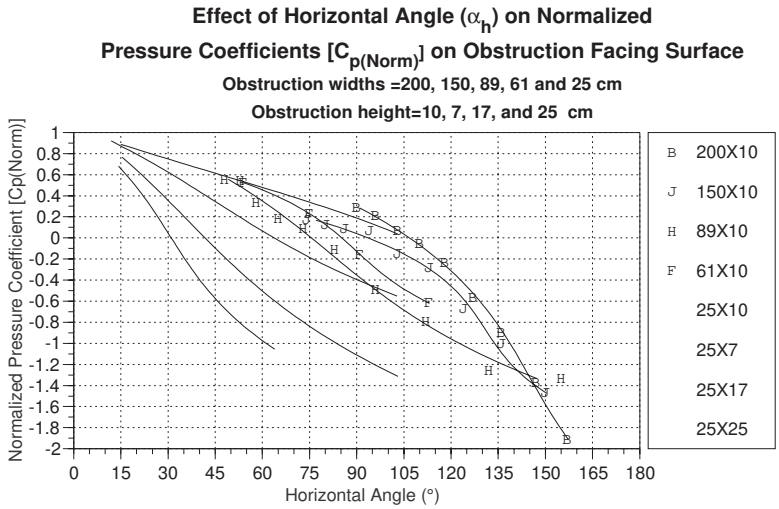

4.12.2.2.2 Discussion

Plotting the Pressure Coefficients $C_{p(Norm)}$ against the Horizontal Angle of Obstruction (α_h) shows the following:

- The data points where the Horizontal Angle lies between 15˚ and 140˚ ($15° < \alpha_h < 140°$) show that $C_{p(Norm)}$ values tend to decrease with the increase of α_h. As the value of α_h decreases, $C_{p(Norm)}$ approaches unity[14].
- When $0° \le \alpha_h < 15°$, neither the size of obstruction block nor its distance from the instrumented surface affects the pressure coefficients. This range of α_h coincides with Lee *et al*'s Isolated Roughness Flow Regime (Ref. 149).
- In most of the obtained values, at $\alpha_h > 140°$, an increase in obstruction width or reduction of spacing does not affect the $C_{p(Norm)}$ value. When α_h exceeds 140˚, the resulting airflow behind the obstruction block is similar to that of the skimming flow regime discussed in Lee *et al* (Figure 4-8). This skimming flow phenomenon can occur in spite of the

4-14 The only exception is when testing the infinitely long obstruction block at the smallest spacings (2).

spacing. The 140˚ arc within which most pressure coefficients values are affected will be referred to as the *Shielding Effectiveness Zone* (SEZ) of the surface under consideration (Figure 4-38).

- At $15° < \Theta < 140°$, the measured $C_{p(Norm)}$ values represent the Wake Interference Regime (Figure 4-8). This zone contained the highest density of points (Figure 4-37). It should also be noted that the largest variation in values of $C_{p(Norm)}$ occur in this zone.

Figure 4-38 The shielding effectiveness zone.

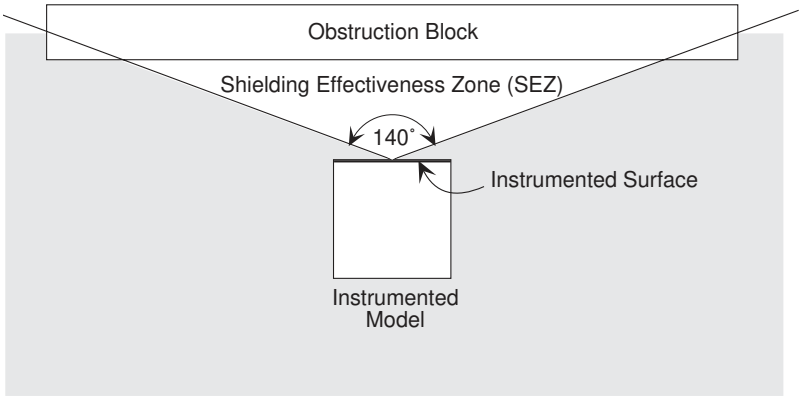

4.12.2.3 Changing the Vertical Angle of Obstruction

The variation of the vertical angle of obstruction α_v, as defined in Section 4.6.2.2, can be obtained through the variation of the inter-model spacing and the height of the obstruction block. The experiments included the two approaches to study the role of the vertical angle in shielding effect of obstruction block.

4.12.2.3.1 Results

The effect of varying the vertical angle on the value of $C_{p(Norm)}$ is plotted in Figure 4-39 as well as Appendix D (Figure D-23 to Figure D-26).

Figure 4-39 The effect of varying vertical angle of obstruction

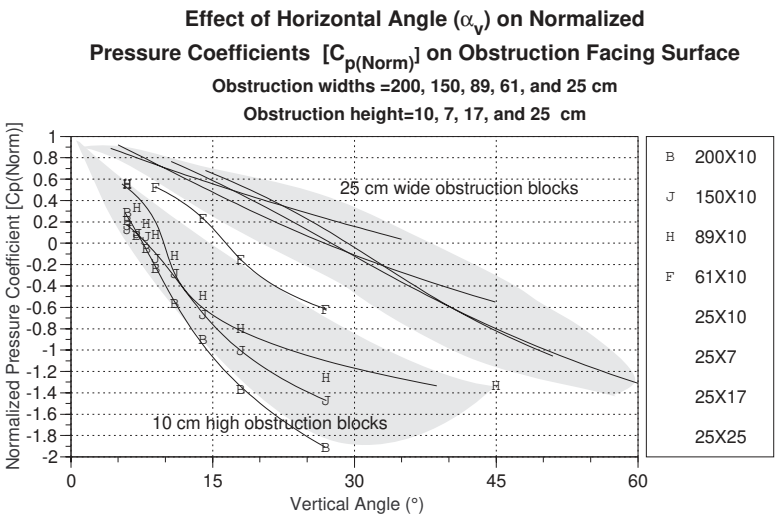

4.12.2.3.2 Analysis

Arthur Bowen of the *Conseil National de Researches* in Canada (Ref. 42) conducted experiments that determined surface pressures for four model-building heights. His measurements of surface pressures clearly demonstrated an inverse relation between the height of the model and the surface pressures at the leeward side. As the height of instrumented block increases, the surface pressure measured at its leeward side is reduced and consequently the length of the wake behind it is increased[15]. The longer the wake behind a block, the larger the magnitude and extend of its shielding effect (Figure 4-40).

4-15 This is also evident from Evans experiments (Ref. 79).

Figure 4-40 The wake length is proportional to obstruction height.

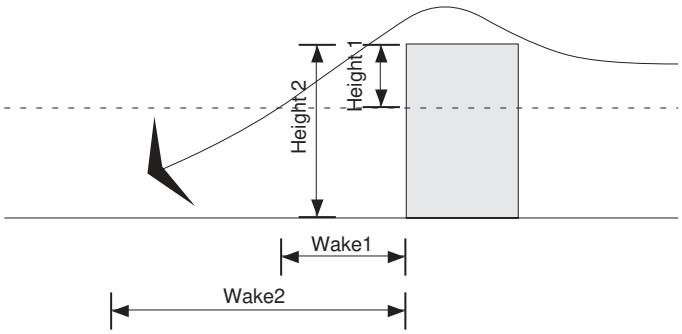

My tests (Figure 4-39) supported Bowen's conclusion. In analyzing the measured $C_{p(Norm)}$ values, the following could be observed:

- There is an inverse relationship between the surface pressure coefficients and the vertical angle describing the windward obstruction block.
- At $0° < \alpha_v < 25°$, which is equivalent to Lee *et al* 's (Ref. 149) *Isolated Roughness Flow Regime* at 2.6 model spacing (S_m), no noticeable shift could be observed in the obtained data. This shows that neither the spacing nor the vertical angle alone can fully describe the wake generated behind an obstruction block. The spread of Normalized pressure data demonstrates the significance of the width and the horizontal obstruction angle of the obstruction block.
- There were not enough data points of $C_{p(Norm)}$ at $\alpha_v > 45°$, which corresponded roughly to the 1.2 spacing *Skimming Flow Regime* at Lee *et al* 's experiments, to observe any shift in the measured surface pressures.
- Similarly, the $25° > \alpha_v > 45°$ range which corresponded to the *Wake Interference Flow Regime*, showed not significant difference from the rest of the measured vertical angles.

It should also be noted that regardless of the obstruction height, the 25 cm wide obstruction block maintained virtually the same $C_{p(Norm)}$ values with the same α_v This means that for the same vertical angle, $C_{p(Norm)}$ value remains unaffected by a small change in the horizontal angle Figure 4-41.

Figure 4-41 For the same obstruction vertical angles, C_{pm} remained largely unaffected by the obstruction height.

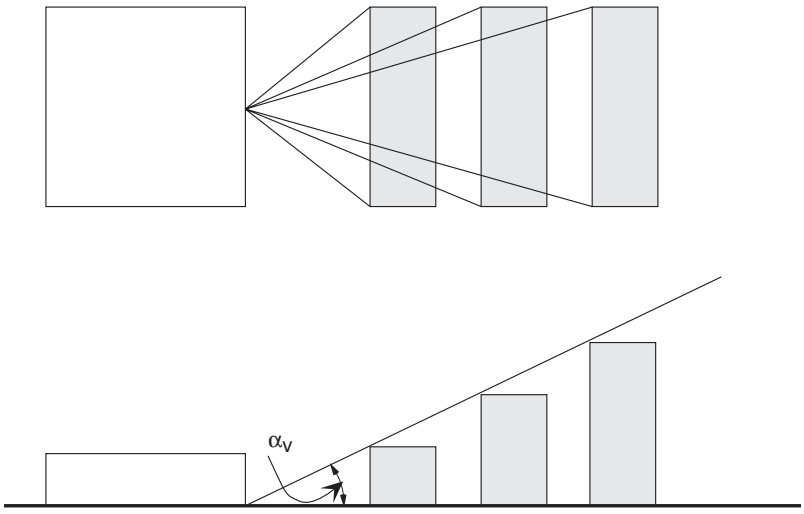

4.12.3 Deriving the Model

As seen in Figure 4-1, expressing C_p in terms of the model spacing (S_m) did not explain the differences between the results of the three experiments[16]. The angular description of the obstruction blocks from the vantage point of the surface in question, on the other hand, has provided the proposed prediction model with a more comprehensive set of variables (Section 4.7). In addition, the identification of the *"lines of sight"* to the obstruction block enhances the ability of the designer to input the actual description of the surrounding blocks.

4-16 Wiren's, *Lee et al* and Ernest.

I proposed a formula using the two angles required to describe the outline of the obstruction block in an orthogonal configuration[17]. The generic form was as follows:

$$C_{pm(ortho)} = C_i, f(\alpha_h,\alpha_v) \quad \textbf{(4-8)}$$

In the cases when the centerlines of the obstruction block and the instrumented surface do not coincide with the wind direction i.e. the obstruction asymmetrically shields the surface in question, I suggest the following correction function (*generic form*):

$$C_{pm\alpha d(corr)} = f(C_{pm(ortho)}, \alpha_d) \quad \textbf{(4-9)}$$

Where (Equations 4-8 and 4-9)

$C_{pm_{\alpha d(corr)}}$ = Displacement-corrected Modification Coefficient

C_{pm} = Pressure Modification Coefficient

C_i = Formula Constants

i = 0, 1, …, N

α_h = Horizontal Angle

α_v = Vertical Angle

α_d = Displacement Angle

Figure 4-42 shows a contour graph of the Pressure Modification Coefficients (C_{pm}) of the tested configurations plotted against both angles of description (α_h, α_v). It can be noted that the C_{pm} values formed two shapes around the line where;

4-17 Refer to the discussion in Section 4.12 on page 81.

$$\alpha_v = \frac{\alpha_h}{2} \quad \textbf{(4-10)}$$

The lines connecting the C_{pm} values above the bisection line were all convex while those below the line were concave. This means that above the bisection line, values of C_{pm} were less sensitive to α_v with the increase of α_h. On the other hand, below the line, with the increase of α_h, C_{pm} became very sensitive to the increase in the value of α_v. Thus, the bisection line describes the zone where the value of C_{pm} is neutral to the acceleration of both angles of view. Consequently, a function was developed based on the relationship between α_h and α_v shown in Equation (4-10).

Figure 4-42 Measured pressure modification coefficients for orthogonal configurations.

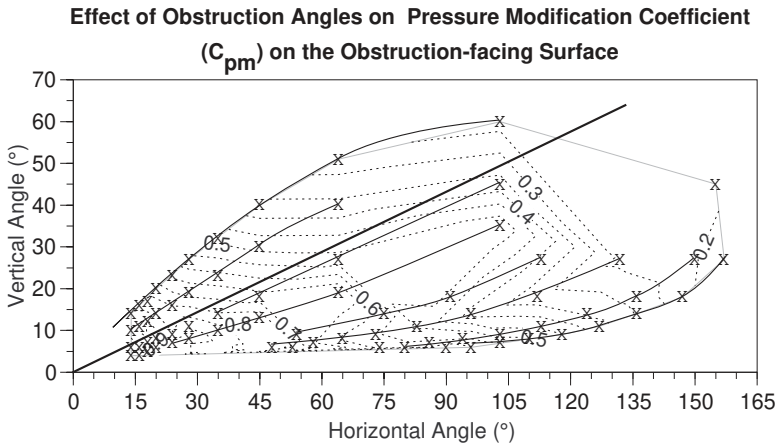

4.12.3.1 Analysis of Variables:

The function coefficients were determined using a stepwise nonlinear regression routine[18] in which the parameters in Figure 4-43 were used.

4-18 Software used in the statistical analysis of the data is SPSS 6.0 Graduate package for the Macintosh platform.

Figure 4-43 Basic variables in orthogonal function

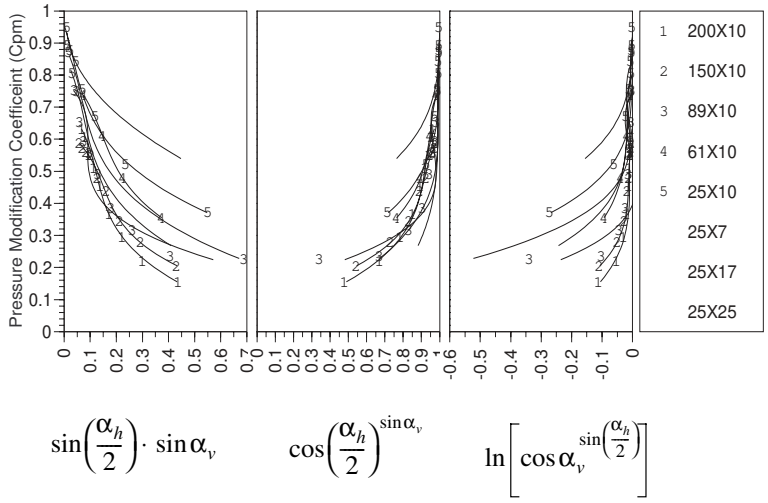

4.12.3.2 The Functions

The stepwise regression analysis was conducted twice resulting in two Functions. The first function would suffice as an easy-to-use, simple, and less accurate (adjusted $R^2 = 0.967$) function for hand and quick calculations [Equation (4-11)].

$$C_{pm(ortho)} = C_0 \cdot \sin\left(\frac{\alpha_h}{2}\right)\cdot \sin(\alpha_v) + C_1 \cdot \cos\left(\frac{\alpha_h}{2}\right)^{\sin(\alpha_v)} + C_2 \cdot \ln\left[\cos(\alpha_v)^{\sin\left(\frac{\alpha_h}{2}\right)}\right] \quad \textbf{(4-11)}$$

where

$$C_0 = -0.8548$$
$$C_1 = 0.7677$$
$$C_2 = -0.6261$$

The second function resulted in a lengthy expression with high-fitting regression value (adjusted $R^2 = 0.995$)[19]. The more complex relationship would be suitable for computer applications and is documented in equation (D-1) in Appendix D.

Figure 4-44 Predicted vs. measured values of surface pressure coefficients- Equation (4-12).

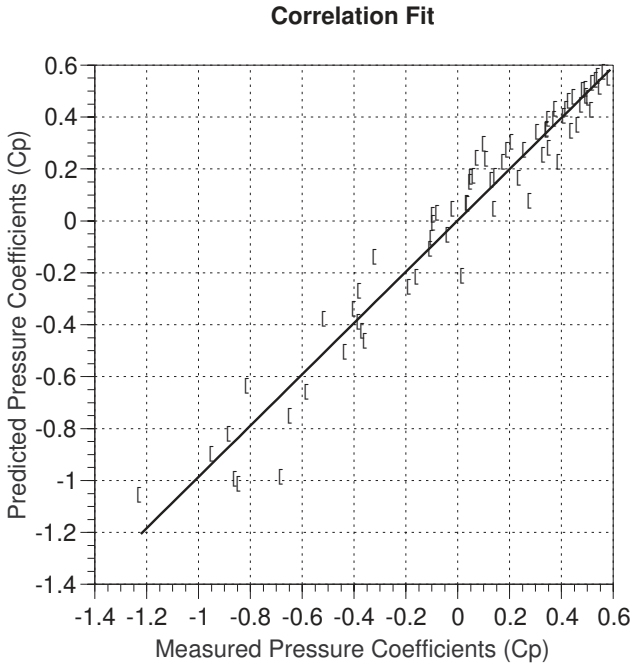

The more complex of the two equations was used in plotting the contour diagram shown Figure 4-45. This diagram can be used to graphically predict $C_{pm(ortho)}$ knowing both α_h and α_v. Based on the parameters of the experiments, the angular variables of Equations (4-11) and (D-1) were bounded by the following limits:

4-19 Figure 4-44

$$0° \le \alpha_h \le 140°$$
$$0° \le \alpha_v \le 60° \quad \textbf{(4-12)}$$

Figure 4-45 Model contour graphically represents the mathematical function in Equation (D-1).

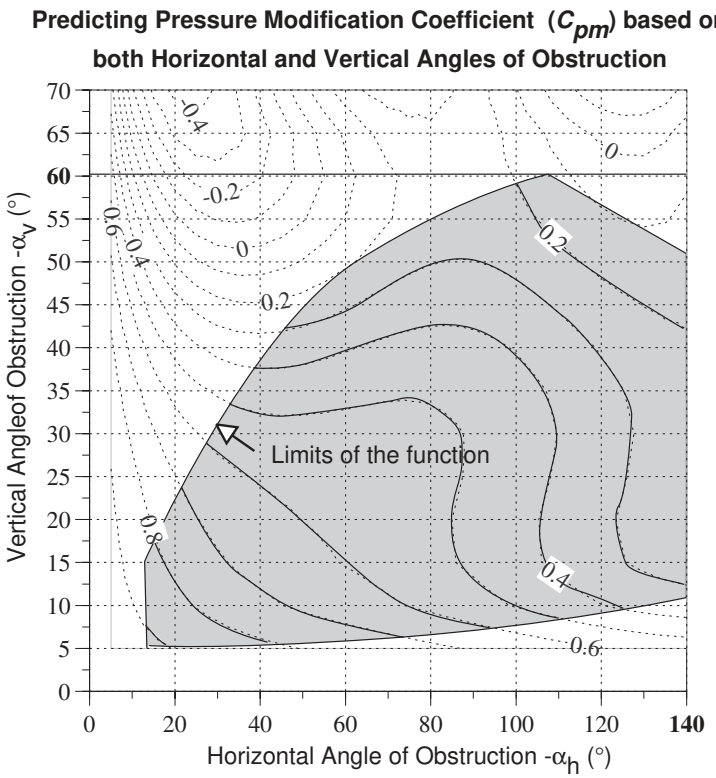

4.12.4 Limitation of the Orthogonal Model

The limitations of the mathematical orthogonal model can be summarized in the following:

- The model is based on tests conducted on cubical models that represent single-floor buildings.
- Tested obstruction blocks had the same depth (10 cm). Deeper obstruction blocks have shorter wakes and less shielding effect than shallower blocks with similar angular description (Ref. 79). However, some initial tests were conducted with a deeper block (25 cm) and the pressure coefficients on the instrumented surface varied only slightly from those of the 10 cm deep block.

- The orthogonal model -by definition- cannot predict surface pressures on occasions when the obstruction block is not symmetrical around the line connecting the mid points of the block and the instrumented model. The primary example of this asymmetry would be a horizontal displacement of the obstruction block from the center line of the instrumented model.
- Since the derived orthogonal model was based on configurations where wind direction was always perpendicular to both the obstruction block and the instrumented model, the effect of the wind direction on the values of C_{pm} was unaccounted for.
- The effect of multiple obstruction blocks on C_{pm} was not considered in the orthogonal model.

4.13 The Displacement Correction

Displacement as defined in Section 4.6.2.5, occurs when the instrumented surface does not fall directly behind the obstruction block thus causing misalignment between the obstruction block and the model (Figure 4-18).

4.13.1 Varying Displacement Angle

Increasing the displacement angle (α_d) shifts the obstruction block laterally relative to the instrumented model surface (Figure 4-46). The premise under which the displacement effect was studied is as follows;

With the increase in α_d angle, the Pressure Modification Coefficient C_{pm} increases until it reaches unity or the unshielded condition (Figure 4-46). As the displacement angle increases, the portion of the instrumented surface falling under the obstruction block wake is reduced (Figure 4-47). The

result is an average C_{pm} value between those obtained from an unshielded surface and a symmetrically shielded surface[20] in similar terrain conditions.

Figure 4-46 Varying the displacement angle.

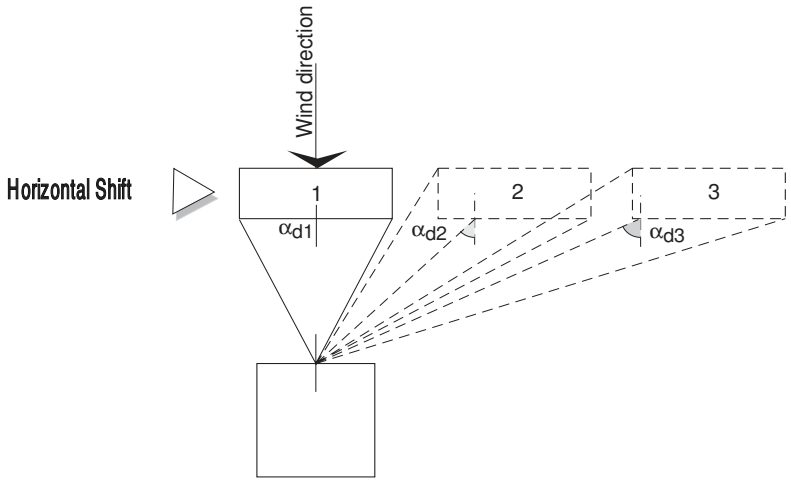

Figure 4-47 Shielding Effect of displacement of obstruction block.

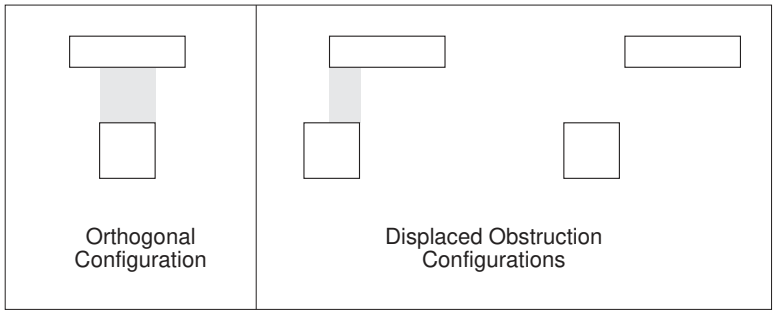

4.13.1.1 Setup of Experiments

A total number of 63 experiments were conducted to determine the effect of varying the displacement of the obstruction block. TABLE 4-4 lists the tested configurations. Three variables were tested (Figure 4-48): the obstruction width, the spacing, and the *horizontal shift of obstruction block*. The latter is defined here as the distance between the mid points of the obstruction block and the instrumented surface. In the

4-20 Orthogonal configuration.

analysis however, the horizontal displacement will be expressed in angular terms (α_d)[21]. The dimensions of the instrumented model in all experiments remained constant.

TABLE 4-4 **Displacement Experiments Setup**[a]

Obstruction Width (cm)	**25**					**61**					**86**	
Spacing (S_m) **Shift (cm)**	**2**	**3**	**4**	**6**	**Shift. (cm)**	**2**	**3**	**4**	**6**	**Shift. (cm)**	**2**
0.0	X	X	X	X	0.0	X	X	X	X	0.0	X
6.25	X	X	X	X	7.63	X	X	X	X	21.5	X
12.5	X	X	X	X	15.25	X	X	X	X	43.0	X
18.75	X	X	X	X	22.88	X	X	X	X	-	-
25.0	X	X	X	X	30.5	X	X	X	X	-	-
31.25	X	X	X	X	38.13	X	X	X	X	-	-
37.5	X	X	X	X	45.75	X	X	X	X	-	-
-	-	-	-	-	53.63	X	X	X	X	-	-

a. Figure 4-48 illustrates the definitions of the experiment's three variables.

Figure 4-48 Displacement configuration variables.

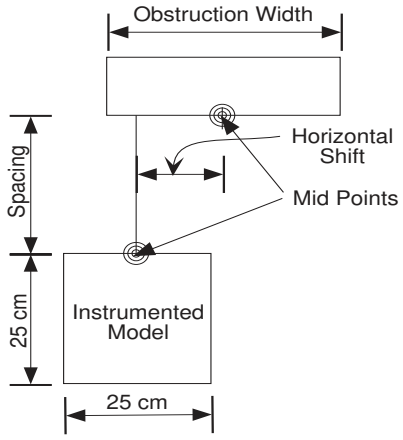

4-21 The displacement angle is defined in Section 4.6.2.5.

4.13.1.2 The Choice of the Displacement Angle

Before starting the discussion of the tests results, it is essential to explain the reason for defining the displacement angle as a bisecting of an obstruction's horizontal angle of view (Section 4.6.2.5). This definition is more sensitive to horizontal shifts than to an asymmetrical elongation of the obstruction block (Figure 4-49). The shielding effect of a displaced obstruction block is lower than that of a fully obstructing block (Figure 4-49a). On the other hand, the shielding effect of a long asymmetric obstruction block is not much different than that of an obstruction block in orthogonal relationship with the instrumented surface (Figure 4-49b). The suggested definition of the displacement angle α_d is responsive to both requirements mentioned above.

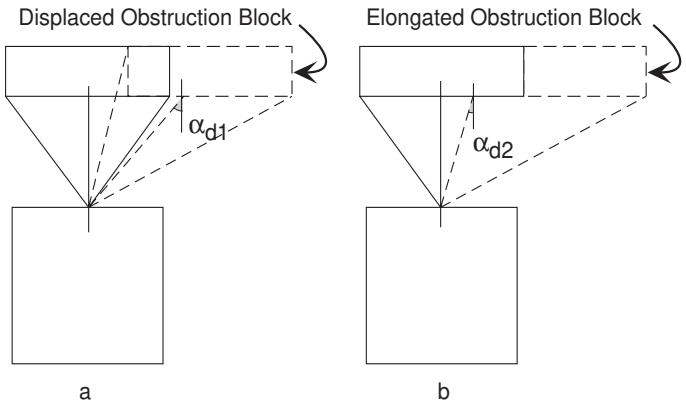

Figure 4-49 Displacement angle (α_d) growth relative to obstruction block.

Preliminary tests verified the sensitivity of α_d as compared to the equivalent angle using the actual center of the obstruction block. That alternative definition exaggerates the effect of obstruction elongation (Figure 4-50), relative to its actual shielding effect.

Figure 4-50 Alternative definition of α_d.

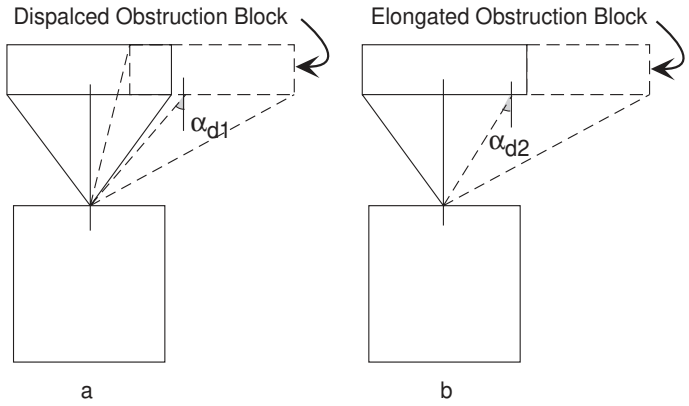

4.13.1.3 Results

The results of Displacement experiments are documented in detail in Appendix E and summarized in Figures 4-51 and 4-52.

Figure 4-51 Effect of displacement angle (α_d) on the pressure coefficients.

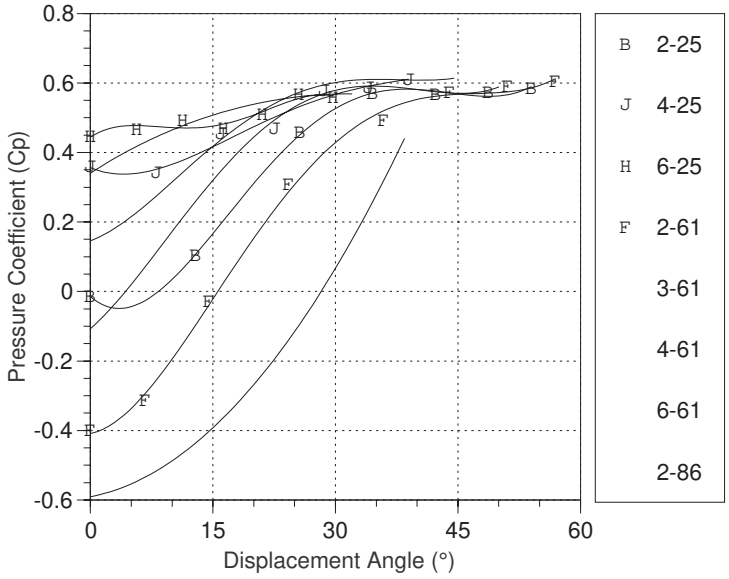

Key:
Configuration s-w
Where:
s=spacing (TABLE 4-4)
w=obstruction width

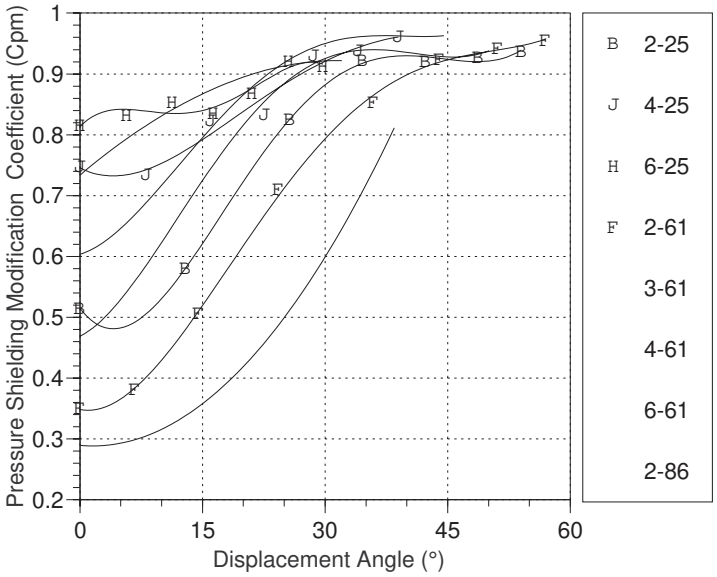

Figure 4-52 Effect of displacement angle α_d on the pressure modification coefficients.

4.13.1.4 Discussion

The results shown in Figures 4-51 and 4-52 support the premise suggested in Section 4.13.1 about the relationship between surface pressures and displacement angles. The values of C_{pm} approached 1.0 with displacement angles $\alpha_d > 40° - 50°$. In addition, measured C_{pm} values were influenced by the size of the obstruction block as well as the spacing from the instrumented surface.

Since both the size of the obstruction and its spacing can be expressed using the angles of obstruction description, an orthogonal value of C_{pm} can be predicted. Figure 4-53 is a contour graph demonstrating the error/correction when the orthogonal prediction was used for a displaced obstruction block. It should be noted that at values of $0° < \alpha_d < 15°$, the orthogonal model did not greatly overestimate C_{pm}. However, with the increased α_d, C_{pm} values quickly approached unity.

Figure 4-53 Displacement correction of C_{pm} values as predicted by the Orthogonal Model.

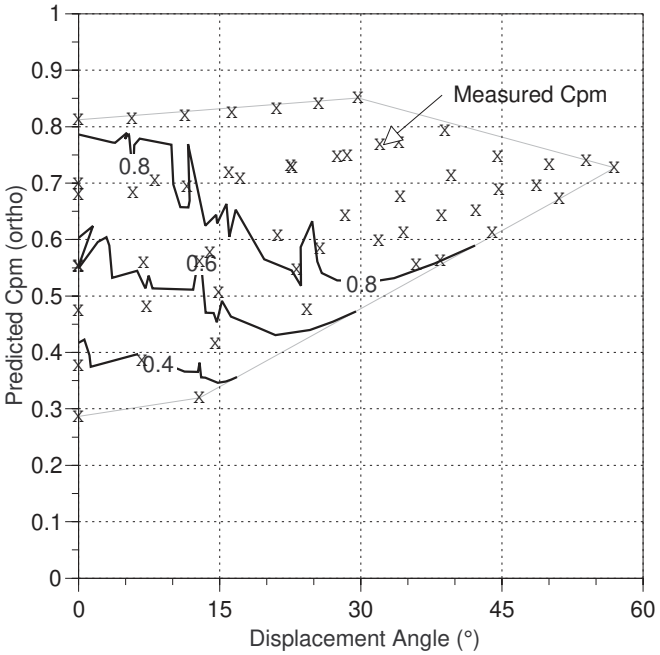

Appendix E contains graphs illustrating the $C_{p(Norm)}$ profiles on both the obstructed and unobstructed surfaces. Analysis of these results demonstrates that the wake behind the obstruction block maintains its rectangular shape even when the instrumented model is located within it. As a result, the pressure profile on the obstruction-facing surface was divided -in most of the tested configurations- into two sections. These two parts were directly related to the wake created by the obstruction block wake. This was demonstrated in Figure E-2 to Figure E-8 where $C_{p(Norm)}$ value on the unshielded[22] portion of the surface equaled unity. The shielded portion, on the other hand, was affected by the windward shielding effects similar to the orthogonal configurations.

4-22 Presented in Appendix E with a shaded area.

4.13.2 Deriving the Correction Function

Based on the above discussion, only two variables are needed to correct for the displacement effects. These variables are the orthogonal estimation of the Pressure Modification Coefficient ($C_{pm(ortho)}$) and the displacement angle. Accordingly, the following function was developed using a stepwise regression routine, resulting in a correlation fit with an adjusted R^2=0.94 (Figure 4-54):

$$C_{pm_{\alpha d(corr)}} = C_{pm(\text{ortho})} + C_1 \cdot \sin(2 \cdot \alpha_d) + C_2 \cdot [\sin(2 \cdot \alpha_d)]^2 + C_3 \cdot \left\{1 - e^{[\sin(2 \cdot \alpha_d)]^{C_{pm(\text{ortho})}}}\right\} \quad \textbf{(4-13)}$$

Where

$$C_1 = 0.5046$$
$$C_2 = 0.2216$$
$$C_2 = 0.4718$$

and;

$$0° \le \alpha_d < 90°$$

It should be noted that if;

$$C_{pm} = 1.0$$

therefore;

$$C_{pm(\text{corr\_d})} = C_{pm} = 1.0$$

and if;

$$\alpha_d = 0°$$

therefore;

$$C_{pm(\text{corr\_d})} = C_{pm}$$

Figure 4-54 Predicted vs. measured C_{pm} values.

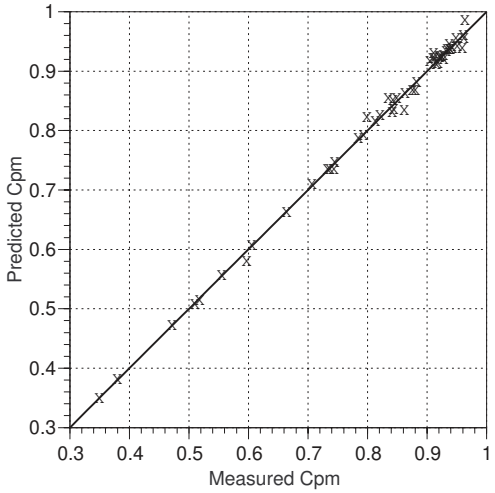

Figure 4-55 shows a graphical representation of equation (4-13) where the displacement corrected C_{pm} was plotted against the displacement angle (α_d). This graph can be used - within the limits of its variables- to manually determine the displacement correction.

Figure 4-55 Correcting C_{pm} value based on displacement angle.

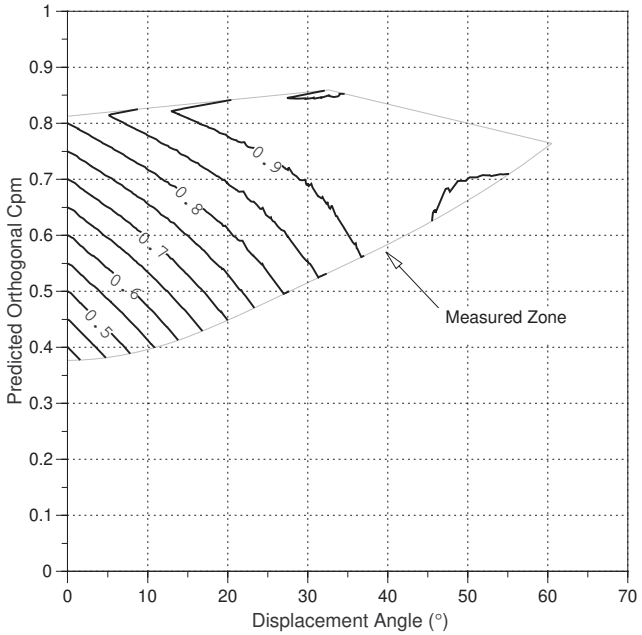

4.13.3 Effect of Roof Shapes

Even though in all of the experiments both the instrumented model and the obstruction block had flat roofs, the proposed prediction model suggests the following;

- In case of an obstruction block with a gable roof (non-flat roof), the vertical angle (α_v) is to be measured from the highest visible point (ridge line). The corresponding horizontal angle (α_h) is then taken off at the location of the ridge line on the plan (Figure 4-56). As a result, the higher the roof pitch, the higher the α_v and the longer its wake (Evans 1974, Ref. 79). This proposition has been tested in Section 4.17.1 with reasonable success.
- Ernest's experiments[23] 1991 (Ref. 74) showed that on the windward side of an instrumented unobstructed surface, roof shape and slope have minimal effect on the average surface pressures. Similarly, Kindangen *et al*'s (Ref. 137) CFD[24] calculations showed insignificant variation in the average velocity coefficient in most of the studied roof geometries[25].
- Both Evans and Ernest[26] agreed that extended eaves have very limited effect on surface pressure coefficients measured at the surface under the eave. In the prediction model, the eave is neglected in describing both the obstruction block and the building under investigation.

In conclusion, the proposed prediction model will not take into account the effect of roof shape aside from extending the viewable plane to the ridge or to the highest viewable line on the obstruction block. The horizontal angle may be slightly

4-23 pp. 58-61.

4-24 Computational fluid dynamics.

4-25 The only significant variation was found at wind direction $\Theta=0^{\circ}$

4-26 pp. 77-78.

reduced in this definition because it extends the obstruction plane to the ridge line instead of the closest surface of obstruction block.

Figure 4-56 Gable roof angular description.

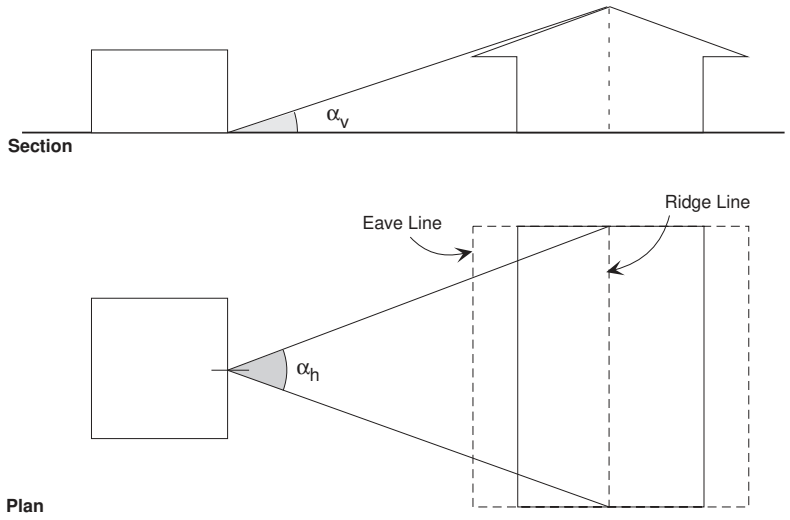

4.13.4 Additional Corrections

Three additional corrections to the pressure prediction model were studied:

- The effect of changing the wind direction on the value and distribution of the pressure coefficients (Section 4.14).
- The shielding effects of multiple windward obstruction blocks (Section 4.15).
- The effect of the geometry of the instrumented model (Section 4.16).

4.14 Effect of Changing the Wind Direction

In all the previous experiments wind direction was constant at $\Theta=0^{\circ}$. Based on the definitions of the angles of obstruction (Section 4.6), a change in the wind direction from 0° will affect the angles of view in the following ways:

- Wind direction is not included in the definition of the Horizontal Angle[27] (α_h). However, since there exists a 140˚ arc (SEZ) within which the shielding effect is most prominent[28], the following should be considered. If the limits of the SEZ arc extend over the arc encompassing the horizontal angle (α_h), the horizontal angle will only be measured within the SEZ (Figure 4-57).
- The vertical angle is reduced as a consequence of the reduction in width of the obstruction block (Figure 4-58). The effect was found to be insignificant.

Figure 4-57 The relationship between the (SEZ) and the horizontal angle.

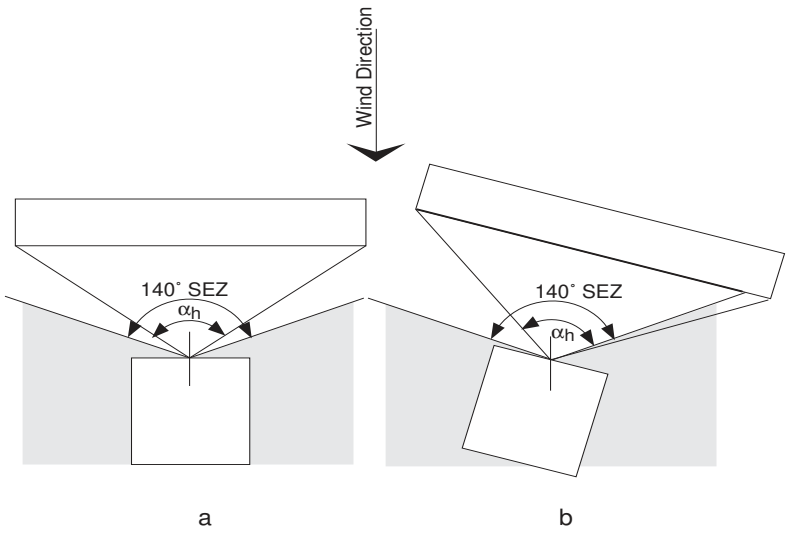

4-27 Section 4.6.2.1, page 65.

4-28 Refer to Section 4.12.2.2, page 88.

Figure 4-58 Spacing correction as a result of wind direction changes.

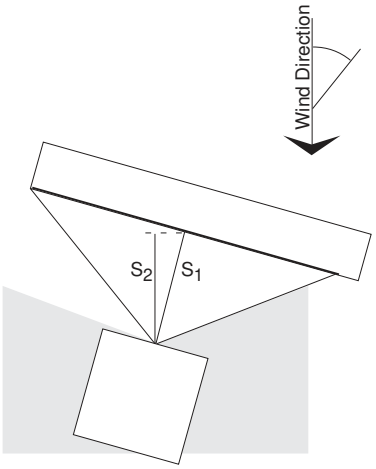

4.14.1 Wind Direction Scenarios

Because wind direction experiments involve the rotation relative to the wind direction, of the model and/or the obstruction, three scenarios could be envisaged (Figure 4-59);

In the first scenario, the obstruction block is positioned parallel to the instrumented model and the wind changes with respect to both instrumented model and obstruction block (Figure 4-62). In the second scenario, the obstruction block remains perpendicular to the wind direction while the wind changes only with respect to the model. In this scenario, a non-orthogonal (non-parallel) relation exists between the instrumented model and the adjacent surface.

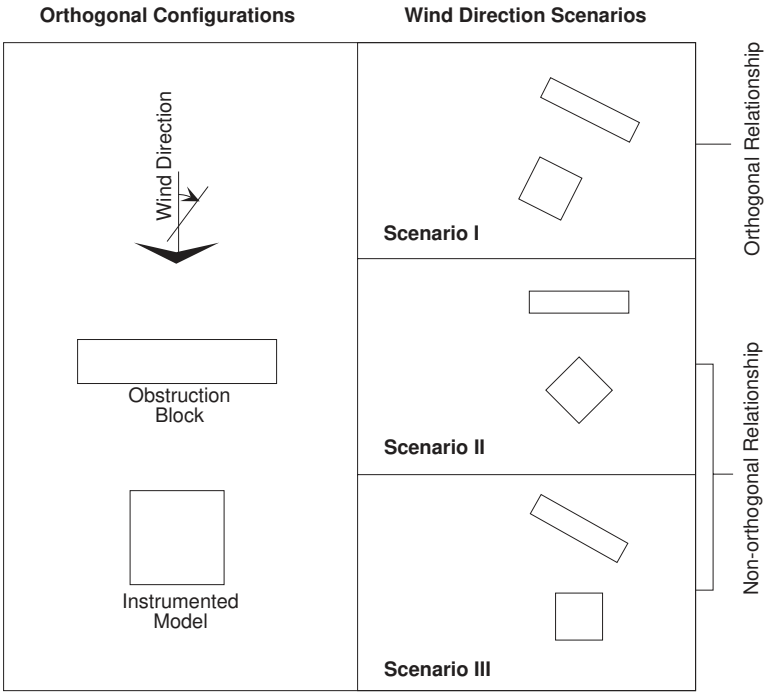

Figure 4-59 The possible instrumented model-obstruction block relationship with respect to wind direction.

Similar to the second scenario, the third scenario involves a non-orthogonal relationship between obstruction and model. However, in this case, the wind direction remains constant relative to the instrumented model rather than the obstruction block. As can be seen in Figure 4-60, scenario III is a combination of scenarios I and II. The prediction model corrections can therefore be based on tests of the two scenarios.

Figure 4-60 Scenario III represents a combination of Scenarios I and II.

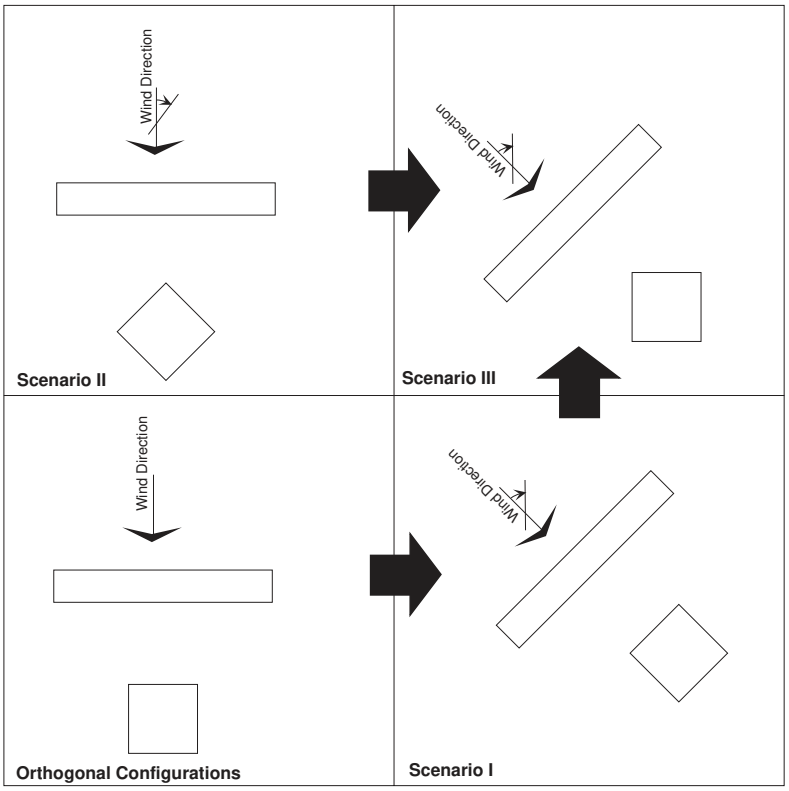

4.14.2 The Equivalent Obstruction Block

The two-steps of the orthogonal model (Section 4.12) corrected for horizontal displacement (Section 4.13) might be called the Displacement Pressure Prediction model. The orthogonal model was developed from tests of obstructions that were always perpendicular to the wind direction. An imaginary equivalent obstruction plane could be used to represent the rotated obstruction block (Figure 4-61). This plane has the same horizontal angle(α_h) of the actual obstruction block and differs only in the fact that it always remains perpendicular to the wind direction.

4.14.2.1 Premise of Wind Direction Analysis

The premise of my research at this stage was that the equivalent orthogonal plane can mathematically substitute for the actual obstruction block when the latter was not perpendicular

to the wind direction. Thus, by simplifying the relationship between the obstruction block and instrumented model, the mathematical model can use the orthogonal algorithm as a basis for wind direction effect prediction.

Figure 4-61 The equivalent obstruction retains the same horizontal angle.

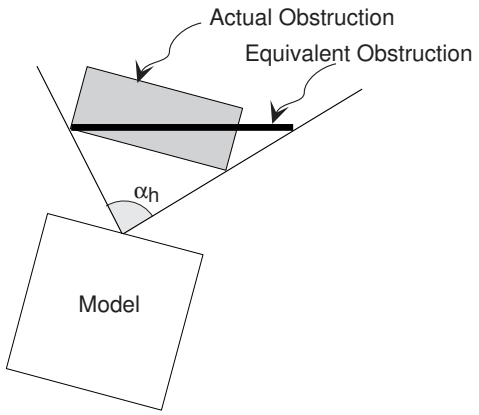

4.14.2.2 Redefining the Angles

Based upon an approach of the equivalent obstruction (Figure 4-61), the definition of the angles of obstruction (Section 4.6) will be measured from the equivalent rather than the actual obstruction blocks. As a result, the vertical and displacement angles of the Equivalent Obstruction Block (EOB) are slightly different from those of the real obstruction block. Additional refinements will be discussed when the need arises in the next sections.

4.14.3 Scenario I: Wind Direction Change with respect to both Model and Obstruction

In scenario I the windward obstruction block is parallel to the instrumented model (Section 4.14.1). In this case, the wind flows onto both the shielding block and model at the same angle.

4.14.3.1 Experiment setup

In the boundary layer wind tunnel, wind direction change was achieved through the rotation of the models on the turntable (Figure A-1). The following variables were tested (Figure 4-62):

- Three actual obstruction widths W_o (25, 61, and 86 cm).
- Four spacings (S_m) between the model and the obstruction block (2, 3, 4, and 6).
- Seven wind directions (Θ = 0°-180° in 15° intervals.)

Surface Pressure Coefficients were measured on two surfaces on opposite sides of the model. One surface always faced the obstruction block while the opposite side never '*saw*' the block (Figure 4-62).

The total number of tested configurations was 12, tested under seven (7) wind directions, and for two (2) surfaces (a total of 168 surfaces were measured).

Figure 4-62 Experiment setup for scenario I.

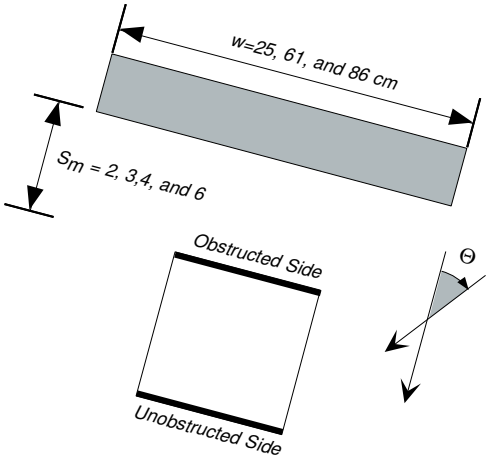

4.14.3.2 Discussion of the Results

Figures 4-63 and 4-64 show the Pressure Coefficients (C_p) and Pressure Modification Coefficients (C_{pm}) measured at the obstructed surface while Figures F-2 (a and b) in Appendix F show C_p and C_{pm} values presented in polar plots.

Figure 4-63 Pressure coefficients variation with wind direction.

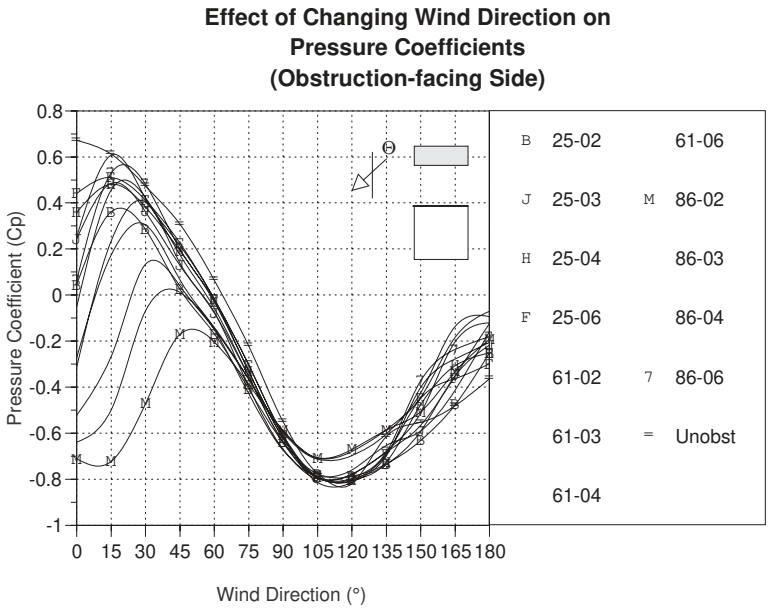

Key:
Configuration w-s
Where:
w=obstruction width
s=spacing

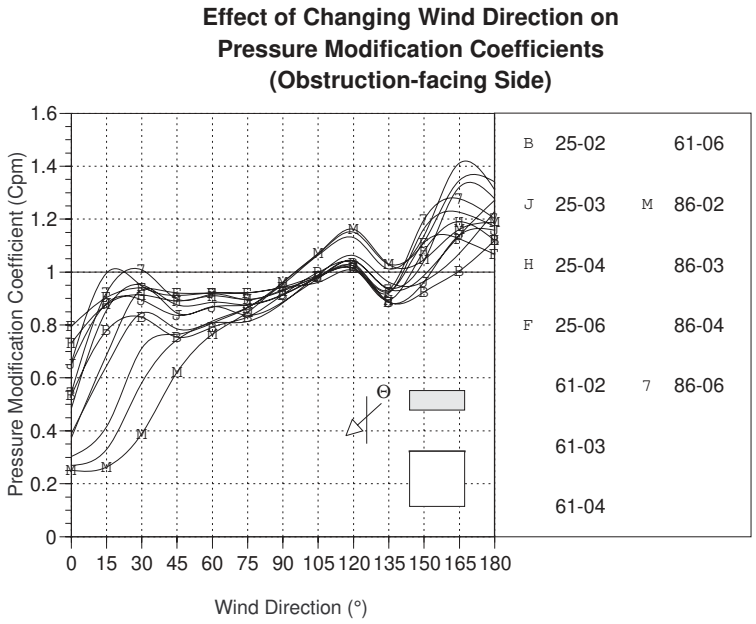

Figure 4-64 Most of the variation in the value of C_{pm} occurs between 0°-60° and 140•-180•.

In all figures, the graphs are divided into three sections. Figure 4-63 shows that between wind directions 0˚ to 60˚, C_{pm} values rapidly increased to peak in all tested configurations between 15˚-45˚. The variation of the Pressure Modification Coefficients in this sector of wind direction was due to the shielding effect of the obstruction block and its location relative to the instrumented surface. Obstruction blocks with the largest obstruction angles maintained the lowest C_{pm} values while smaller blocks produced the highest values of C_{pm}.

Limited variation could be observed in the tested configurations for wind directions 60˚-140˚. The lack of variation can be attributed to the decrease in the values of both the horizontal α_h and vertical angles α_v for the EOB with the rotation of the wind beyond the 60˚ mark. This was true regardless of the size and distance of the block from the model (Figure 4-57).

The same was true for the unobstructed side or the side for which both α_h and α_v are equal to zero (Figures 4-66 and F-2 c and d).

Figure 4-65 Pressure coefficients variation with wind direction (unobstructed side).

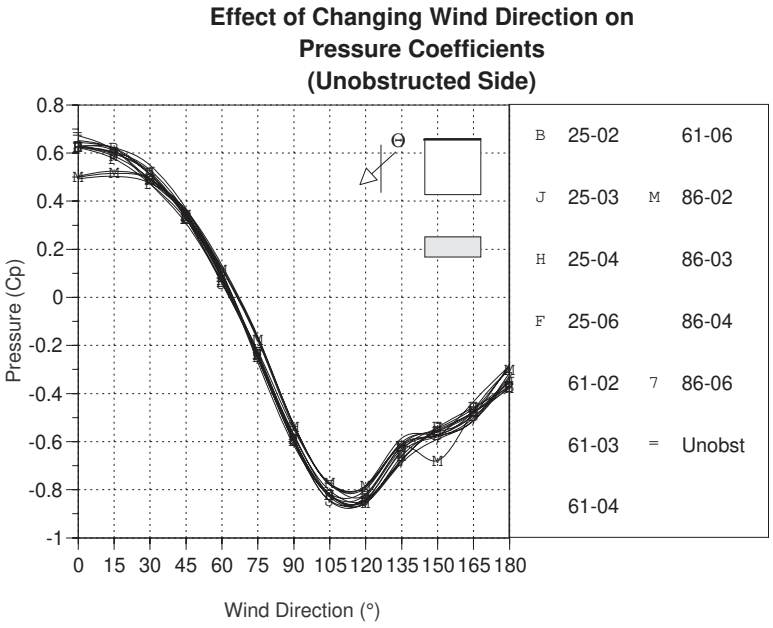

Figure 4-66 Except for few exceptions, the unobstructed side is not affected by the shielding block on the opposite side.

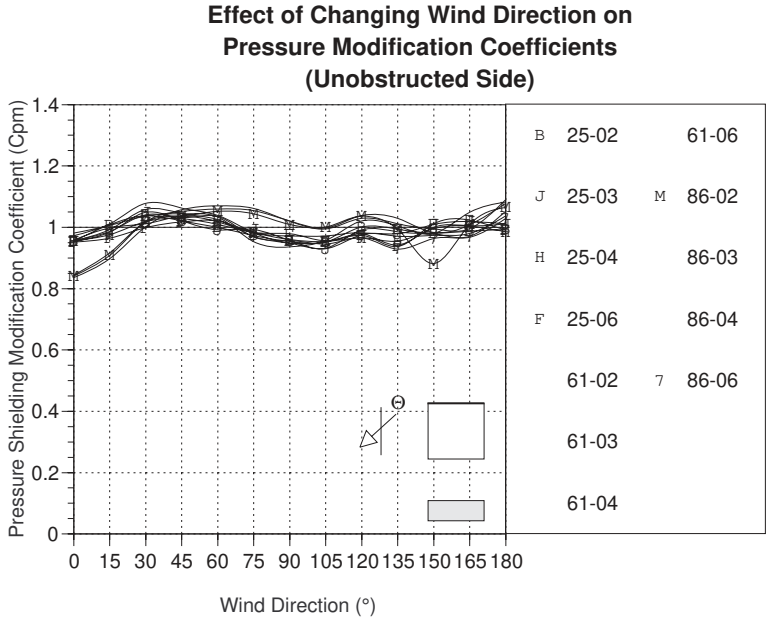

When wind direction was $140^{\circ} \leq \Theta \leq 180^{\circ}$, most of the measured surface pressures for the obstructed surface exceeded those of an unshielded block i.e $C_{pm} > 1.0$ (Figure 4-64 and F-2 b). The reason for such an increase in C_{pm} can be attributed to the increase in pressure caused by the leeward obstruction that obstructs the flow and directs it to the enclosed area between the two blocks (Figure 4-67). The resulting pressurization is related to the width of the leeward block, with the longest blocks causing higher pressure coefficients than smaller ones (Figure 4-64).

Figure 4-67 Leeward blocks increase the pressure at the obstruction-facing surface.

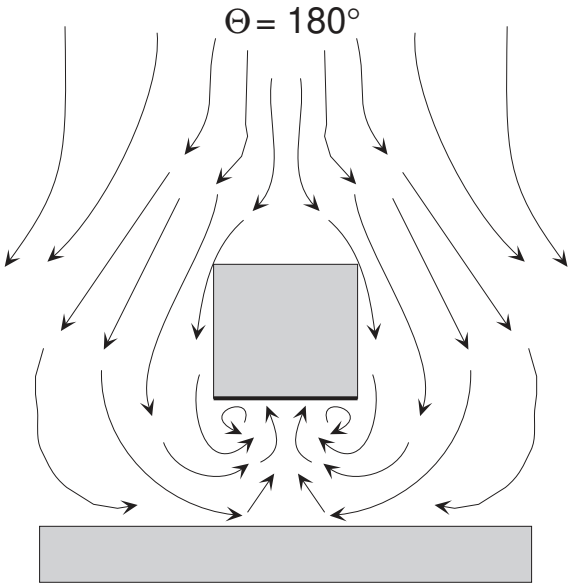

The width of obstruction blocks does not affect the Pressure Modification Coefficients C_{pm} on the unobstructed side in all wind directions except normal (Figure 4-66). At this wind direction, the wake of the long obstruction block (86 cm) casts a long wake within which even the leeward side falls, thus reducing its pressure.

4.14.3.3 Redefining the Angles of Obstruction

As mentioned in Section 4.14.2.2, when rotating the obstruction block relative to the wind direction, some of the angles of description had to be modified. This modification was done in such a way that did not overrule the previous definitions but rather encompassed the orthogonal model in the modified definition.

4.14.3.4 Corrected Displacement Angle $\alpha_{h(\mathrm{corr})}$

Based on the research premise discussed in Section 4.14.2, the horizontal angle remains the same after using an equivalent obstruction block within the SEZ's 140˚ arc (Figure 4-68). However, on increasing the wind direction, more of the obstruction block falls outside the SEZ and consequently the value of $\alpha_{h(\mathrm{corr})}$ gets smaller than α_h.

Figure 4-68 Modified angles of obstruction.

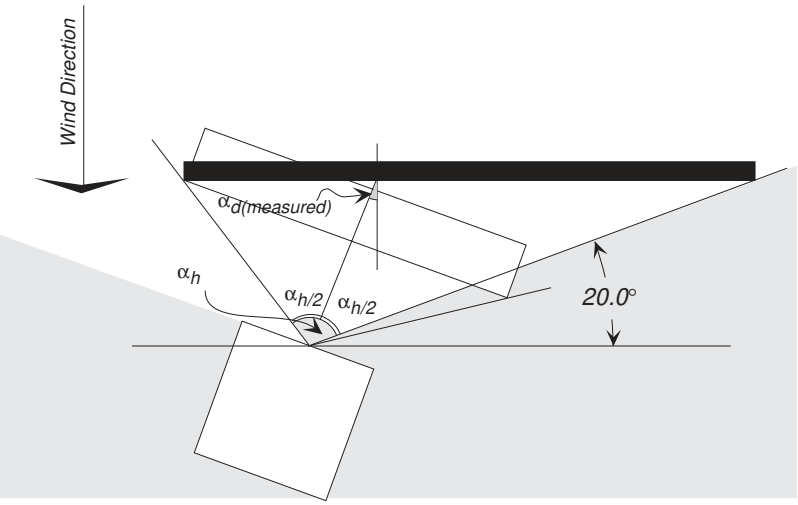

4.14.3.5 Corrected Displacement Angle $\alpha_{d(\mathrm{corr})}$

On the other hand, the definition of the displacement angle α_d on the equivalent obstruction block does not take into account the rotation of the obstruction block relative to the wind direction. This rotation causes the wind to flow behind the shielding block and to flow parallel to the model. This in turn, results in

further reducing the shielding effect as compared to the orthogonal Obstruction block (Figure 4-69).

Figure 4-69 Wind flows behind rotated obstruction block raising surface pressure coefficients.

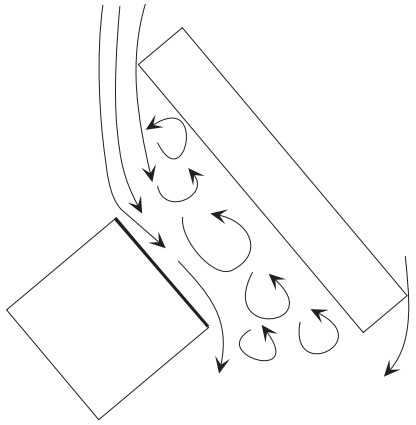

In order to estimate the pressure effect of this flow channeling around rotating obstruction block, the following correction was devised:

$$\alpha_{d(\text{corrected})} = \alpha_{d(\text{measured})} \cdot \cos\alpha_{h/2} \quad \textbf{(4-14)}$$

This correction should be used in calculating the Pressure Modification coefficient correction $C_{pm_{\alpha d(corr)}}$ by replacing α_d with $\alpha_{d(\text{corrected})}$ in Equation (4-13). The correction provides the function in equation (4-13) with the accelerated growth in surface pressure brought about by the wind direction change. The resulting correction in equation 4-14 does not affect the orthogonal configurations since α_d will be equal to zero.

4.14.3.6 Corrected Vertical Angle $\alpha_{v(\text{corr})}$

In addition to the effect of the corrected α_d, the vertical angle had to be corrected to account for the perceived reduction in height of the obstruction block (Figure 4-70). This effect

causes the vertical angle to appear to diminish with the increase in wind direction as viewed from the instrumented surface.

Figure 4-70 The vertical angle appears to diminish with increase in wind direction relative to normal and displacement angle.

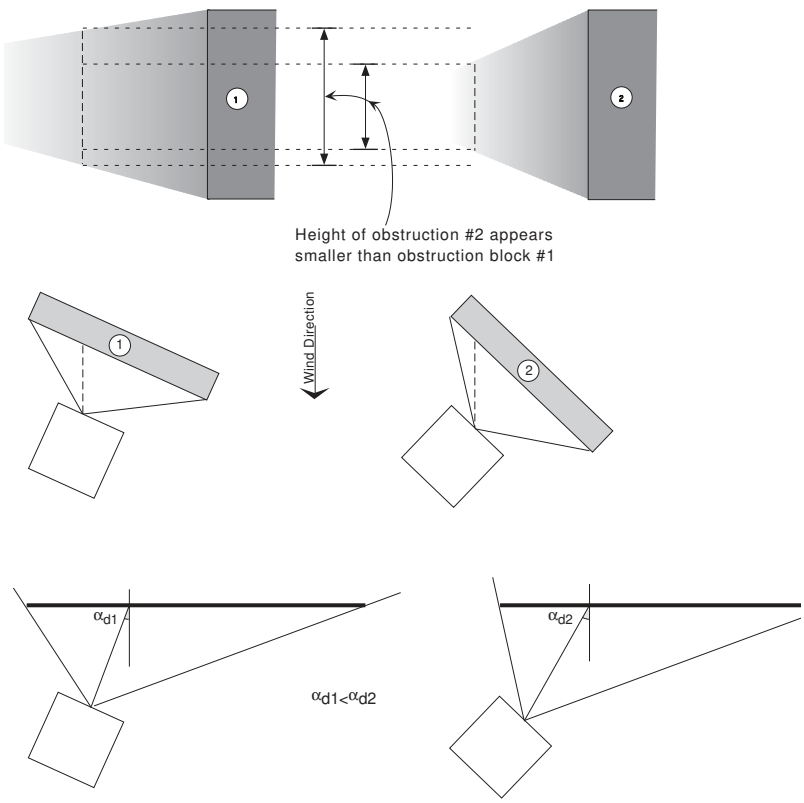

Because of the diminishing effect of the rotating obstruction block, the Vertical Angle α_v has to be corrected to reflect the perspective effect. This correction was determined by correcting the measured α_v based on the degree of displacement of the obstruction block (Figure 4-70). The correction of the α_v uses expressed as follows:

$$\alpha_{v(\mathrm{corr})} = \alpha_v \cdot \cos\alpha_{d(\mathrm{corr})} \quad \textbf{(4-15)}$$

This correction should be used in the orthogonal model in Equations 4-13 and (D-1), substituting either the calculated or

measured values of α_v by $\alpha_{v(\mathrm{corr})}$. The wind direction corrected version of the orthogonal model is as follows[29]:

$$C_{pm_{\Theta(\mathrm{Corr})}} = C_0 \cdot \sin\left(\frac{\alpha_{h(\mathrm{corr})}}{2}\right) \cdot \sin(\alpha_{v(\mathrm{corr})}) + C_1 \cdot \cos\left(\frac{\alpha_{h(\mathrm{corr})}}{2}\right)^{\sin(\alpha_{v(\mathrm{corr})})} + C_2 \cdot \ln\left[\cos(\alpha_{v(\mathrm{corr})})^{\sin\left(\frac{\alpha_{h(\mathrm{corr})}}{2}\right)}\right] \quad \textbf{(4-16)}$$

It should be noted that if $\cos\alpha_d = 0$ in the orthogonal model, therefore $\cos\alpha_{d(\mathrm{corr})} = 1$, and consequently $\alpha_{v(\mathrm{corr})} = \alpha_v$.

Figure 4-64 is a plot of C_{pm} measured values of on the shielded surface for all (12) tested configurations. Correcting both α_d and α_v as shown in Equations 4-14 and 4-15 was found to suffice with an adjusted R^2 equal to 0.96 for the first two parts of the curve i.e. ($0^\circ \le \Theta < 140^\circ$). At wind directions $90^\circ \le \Theta < 140°$, the obstruction block can not be seen within the SEZ ($\alpha_h = 0°$). As a result, $C_{pm_{\Theta(\mathrm{corr})}}$ values always equals to 1.0.

4.14.3.7 Predicting Accelerated Effects

At Θ ($140° < \Theta \le 180°$), the wind-direction-corrected Pressure Shielding Modification Coefficient curve ($C_{pm_{\alpha d(\mathrm{corr})}}$) is above unity. This pressurization is caused by redirecting the wind to the obstruction-facing surface between the obstruction block and the model and is proportional to the horizontal angle α_h. As the obstruction block gets larger or closer, the

4-29 Use the same equation coefficients of Equation (4-13).

catchment area of airflow is increased (Figure 4-67). The expression that was derived to predict the pressure build-up accounting of changes in wind direction is as follows:

When $140^{\circ} \leq \Theta < 180^{\circ}$

$$C_{pm_{\Theta(\text{corr})}} = C_{pm_{\alpha(\text{corr})}} + C_1 \cdot \cos\alpha_{h/2} + C_2 \cdot \cos\Theta + C_3 \cdot (\cos\alpha_{h/2})^{\cos\Theta} \quad \textbf{(4-17)}$$

Where

$$C_1 = -0.6364$$
$$C_2 = -1.0530$$
$$C_3 = -0.2610$$

Because of the way the simulation model is structured[30], the calculated value of $C_{pm_{\alpha d(\text{corr})}}$ at $140^{\circ} < \Theta \leq 180^{\circ}$ will always equal 1.0, therefore equation 4-17 will be:

$$C_{pm_{\Theta(corr)}} = 1.0 + C_1 \cdot \cos\alpha_{h/2} + C_2 \cdot \cos\Theta + C_3 \cdot (\cos\alpha_{h/2})^{\cos\Theta} \quad \textbf{(4-18)}$$

The resulting total fit of the data has an adjusted R^2 value of 0.96 and is represented in Appendix F in Figures F-2 to F-7.

It should be noted that the pressurization of the leeward surface facing a downwind obstruction block occurs only when the obstruction block falls directly behind the instrumented surface. If the block is displaced relative to the surface, there will be no pressurization at the surface and therefore $C_{pm_{\Theta(corr)}} = C_{pm_{\alpha d(\text{corr})}}$ (Figure 4-71).

4-30 The model assumes that if the obstruction does not fall within the 140˚ SEZ, the obstruction block has no shielding effect on the instrumented model.

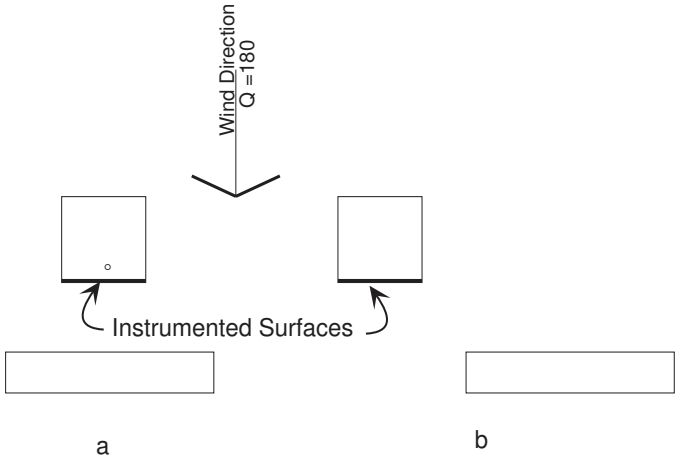

Figure 4-71 Pressurization of leeward surface depends on the relative position of the adjacent block and wind direction.

4.14.4 Scenario II: Wind Direction Change with respect to Model only

This set of experiments was designed to account for the types of urban layout in which the building of interest is not parallel to the surrounding buildings. Even though the mathematical model thus far can substitute an obstruction block that is not perpendicular to the wind direction with an equivalent obstruction[31], the dynamic relationship between the wake behind the obstruction block and the instrumented surface makes it necessary to consider special corrections in these circumstances.

4.14.4.1 Experiment Setup

The second scenario was envisaged to contain a non-parallel model-to-obstruction relationship. However, in this configuration, the wind changes its direction with respect to the instrumented model only in 15˚ increments while the obstruction block remains perpendicular to all wind directions. An additional obstruction block (200 cm) was tested to simulate an infinitely long obstruction of which no edges could be '*seen*'

4-31 Section 4.14.2.

within the 140˚ viewing Shielding Effectiveness Zone (SEZ)[32]. The following is a description of the tested variables in this set of experiments:

- Four obstruction widths (25, 61, 86, and 200) were tested.
- For all obstruction widths except the 200 cm block, five spacings between the obstruction block and the instrumented model (2, 3, 4, 6, and 8) were tested. The 200 cm block was tested under 9 spacings (2-10 in intervals of 1 Spacings).
- Due to the asymmetry of this setup (Figure 4-72), 13 wind directions were tested for each configuration (0˚-180˚ in 15˚ intervals).

The resulting total number of tested configurations was 312 or (624 surfaces).

Figure 4-72 Experiment setup for scenario II

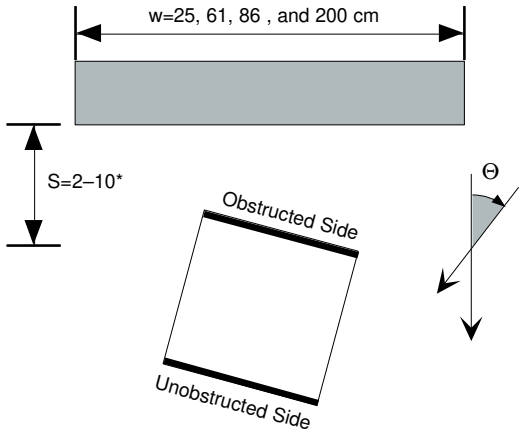

*3, 5, 7, 9 Additional spacing (S) for obstruction width = 200 cm only

4.14.4.2 Discussion of the Results

Graphs demonstrating the effect of changing the wind direction on the surface pressure coefficients (C_p) and Pressure

4-32 The cross section width of the wind tunnel is approximately 210 cm, thus a 200 cm wide obstruction entirely blocks the flow of air around its sides.

Modification Coefficients (C_{pm}) are documented in Appendix F (Figure F-10).

Similar to scenario I (Section 4.14.3), all curves representing the Surface Pressure Coefficients (C_p) demonstrate the same behavior in terms of being composed of two parts (Figure 4-73). However, the following is observed:

- Unlike Scenario I, the separation points between the two parts do not always fall at 140˚ wind direction (Figure 4-73). Instead, it varies with the horizontal angle of view α_h (Figures 4-74 to 4-81). The point separating the two curves coincides with the point where the obstruction block can no longer be seen within the Shielding Effectiveness zone. This is true for values of horizontal angle $0° \leq \alpha_h \leq 10°$.
- Branching out from the above observation, the right part of the curve ($\alpha_h = 10°$) is affected by the spacing rather than by angles of view since α_h -according to the definition- equals to zero.
- C_{pm} at the left part of the curve however, is a function of the shielding effect as well as of the wind direction.
- The infinitely long obstruction (200 cm) demonstrates similar two-part behavior at spacings 6-10 (Figures 4-80 and 4-81). However, at small spacings (2-5), the curve is much flatter and the two sections of the graphs were hardly distinguishable. This can be explained by the lack of airflow from the sides. This in turn, prevents the wake from diminishing by forcing the air to flow only over the top of the obstruction model. The result is a much larger wake zone behind the infinitely long obstruction.

Figure 4-73 The Pressure coefficients lines in Scenario II consist of two parts.

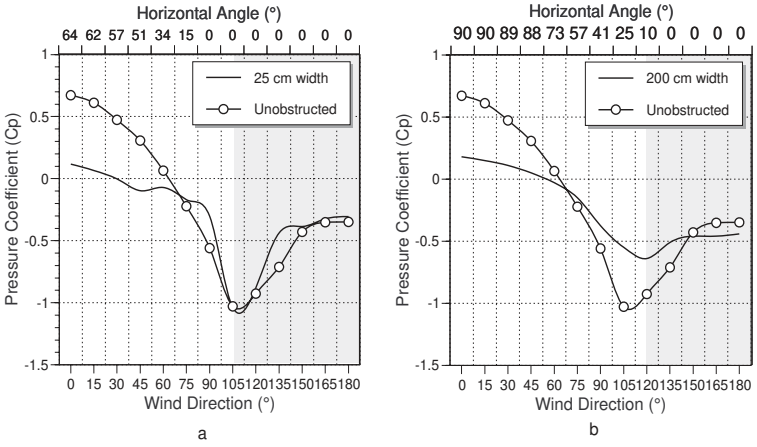

Figure 4-74 Effect of changing the wind direction on C_p for a 25 cm wide obstruction block.

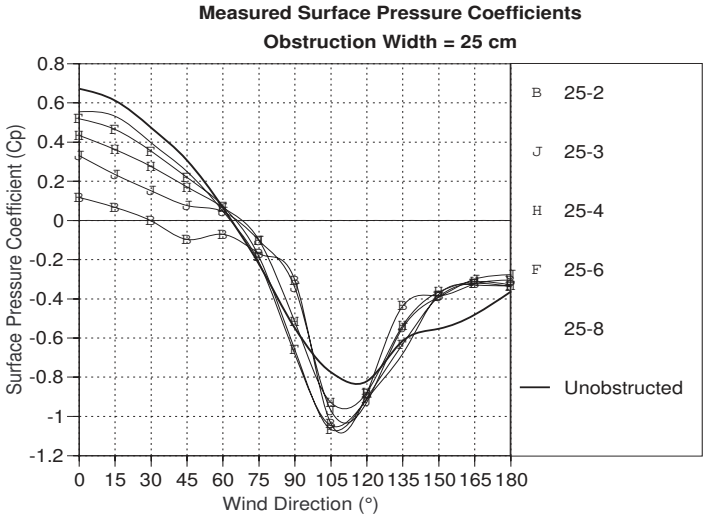

Figure 4-75 Effect of changing the wind direction on C_{pm} for a 25 cm wide obstruction block.

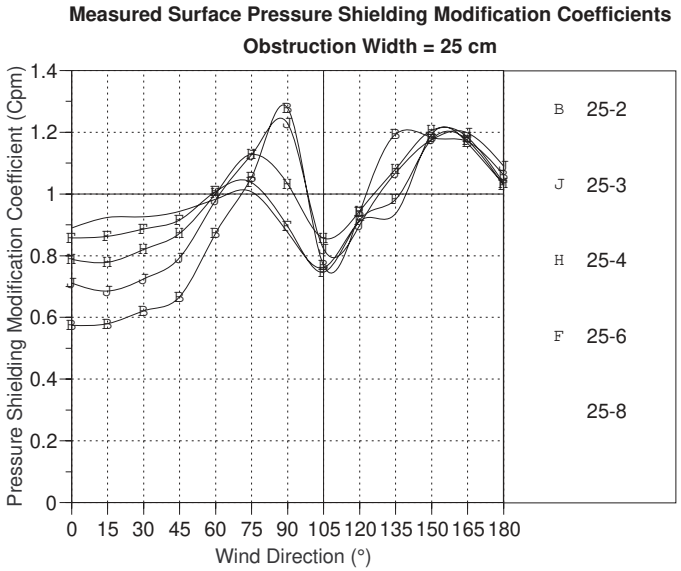

Because of the small width of the 25 cm obstruction block, variation in the spacing affects the values of the Pressure Coefficients (C_p) only between 0˚-60˚. Beyond this wind direction range, measured C_p almost coincides with the unobstructed block. However, Figure 4-75 shows that the C_{pm} graph demonstrates a need for correction at wind directions ≥ 105˚. The 105˚ wind direction corresponds to the average wind direction after which the obstruction is no longer visible.

Figure 4-76 Effect of changing the wind direction on C_p for a 61 cm wide obstruction block.

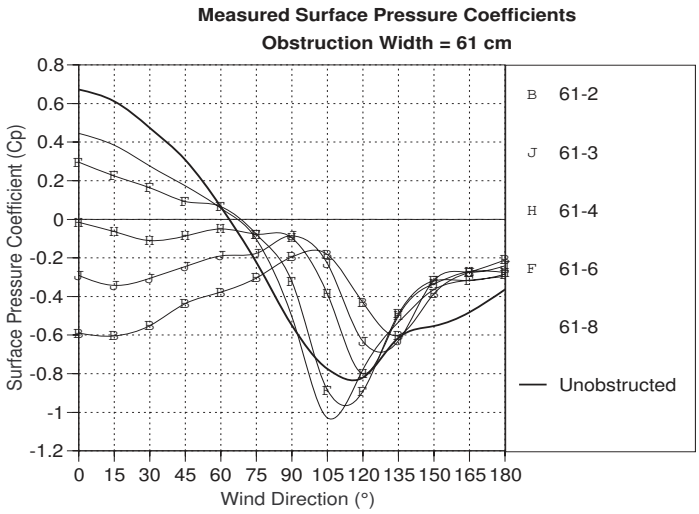

Figure 4-77 Effect of changing the wind direction on C_{pm} for a 61 cm wide obstruction block.

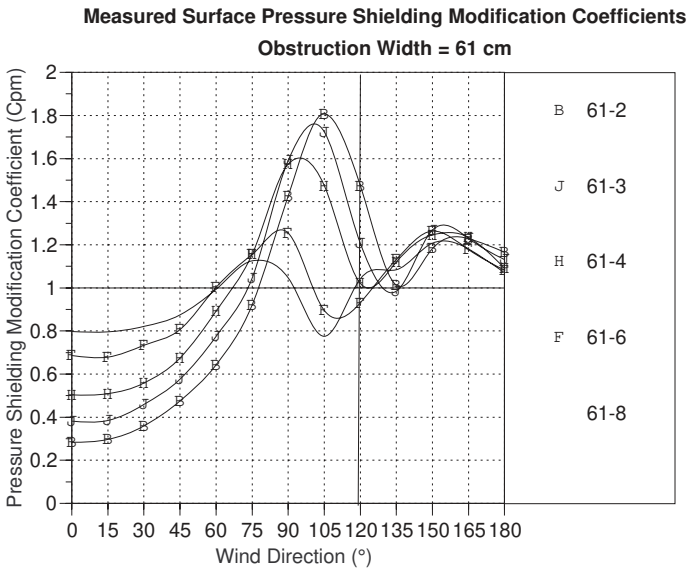

Figure 4-78 Effect of changing the wind direction on C_p for a 86 cm wide obstruction block.

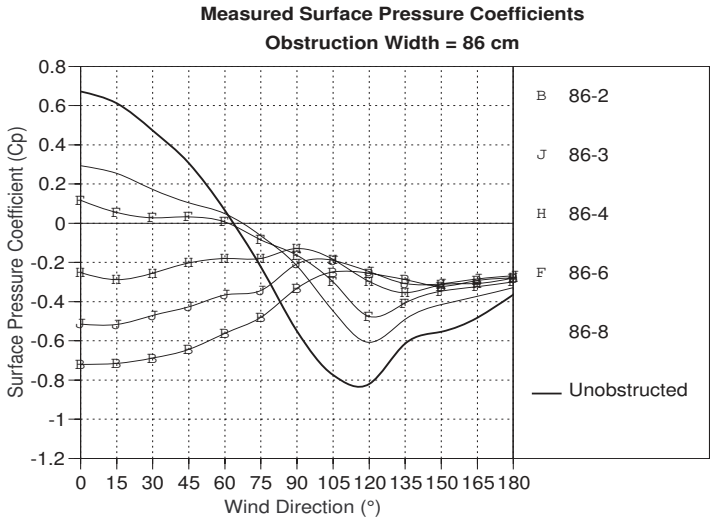

Figure 4-79 Effect of changing the wind direction on C_{pm} for a 86 cm wide obstruction block.

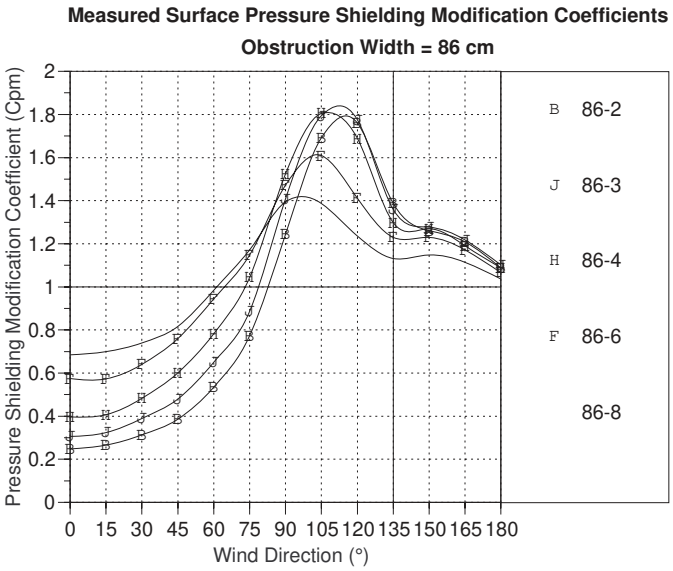

With longer obstruction widths (61 and 86 cm), the difference between the unobstructed C_p value and the shielded model in the 0˚-90˚ range can be largely explained by the orthogonal model (Figures 4-76 and 4-78). However, a slight correction was needed to account for the depressurization caused by the obstruction block (Figures 4-77 and 4-79). When compared with the unobstructed block, and to a lesser extent, the 25 cm

wide block, it is evident that the correction is dependent on the wind direction (Θ) and the visibility of the obstruction block.

Figure 4-80 Effect of changing the vertical Spacing of a 200 cm wide obstruction block.

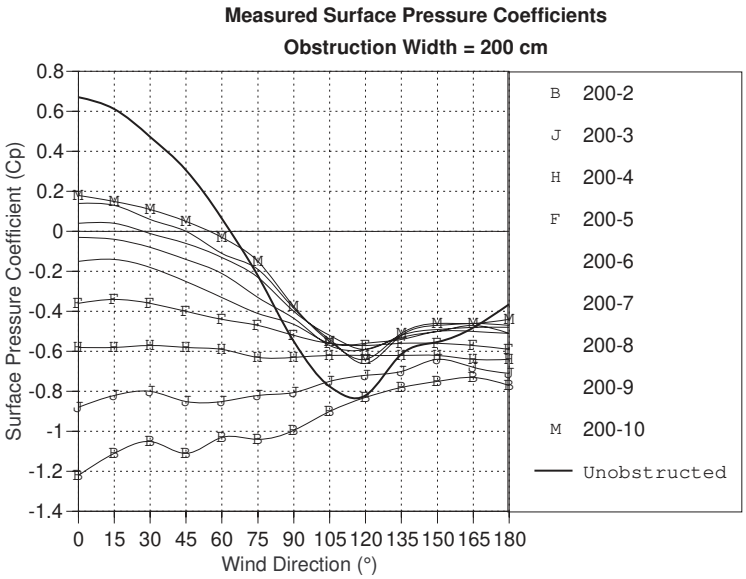

Figure 4-81 Effect of changing the wind direction on C_p for a 200 cm wide obstruction block.

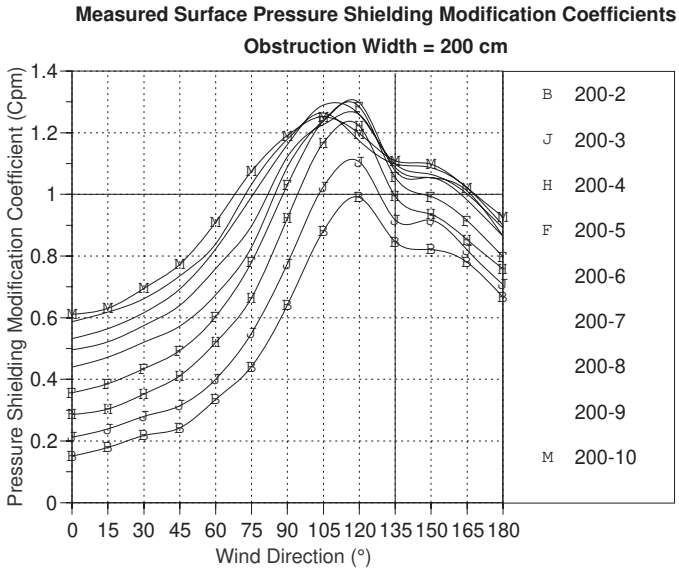

The infinitely long obstruction blocks (200 cm wide) are found to behave in a similar fashion to the smaller widths

except that the curves were much flatter because of the large wake bubble formed behind the obstruction block.

Based on the above discussion, two formulæ were derived based on the horizontal visibility of the obstruction block (α_h). The purpose of these functions is to correct the values of predicted Pressure Modification Coefficients $C_{pm_{\alpha d(corr)}}$ when the geometric relationship between the obstruction block and the instrumented model resembles those of Scenario II[33]. These relationships were organized in the following order:

TABLE 4-5 **Scenario II Functions**

Obstruction Visibility	Formula
$\alpha_h > 10°$	Equation 4-19
$\alpha_h \leq 10°$	Equation 4-20

4.14.4.3 Scenario II Functions

When;

$\alpha_h > 10^{\circ}$

Therefore;

4-33 Non-orthogonal relationship between the instrumented model and obstruction block.

$$
\begin{aligned}
C_{pm_{\Theta(corr)}} = \; & C_{pm_{\alpha d(corr)}} + C_1 \cdot (1 - \cos\Theta) + \\
& C_2 \cdot (1 - \cos\Theta) \cdot \sin\frac{\alpha_h}{2} + \\
& C_3 \cdot [(1 - \cos\Theta) \cdot \sin\alpha_v]^2 + \\
& C_4 \cdot [(1 - \cos\Theta) \cdot \sin\alpha_d]^3 + \\
& C_5 \cdot \left(\sin\Theta \cdot \sin\frac{\alpha_h}{2}\right)^3 + \\
& C_6 \cdot \left[(1 - \cos\Theta) \cdot \sin\frac{\alpha_h}{2}\right]^3 + \\
& C_7 \cdot (\sin\Theta \cdot \sin\alpha_v)^3 + \\
& C_8 \cdot \sin\frac{\alpha_h}{2} \cdot \sin\alpha_v \cdot \sin\alpha_d \cdot \sin\Theta
\end{aligned}
\qquad \textbf{(4-19)}
$$

Where

$C_1 = 0.2496$ $\quad C_2 = 0.7224$

$C_3 = 7.1652$ $\quad C_4 = -0.2397$

$C_5 = -0.8735$ $\quad C_6 = -3.5514$

$C_7 = -9.6$ $\quad C_8 = -4.618$

When;

$\alpha_h \leq 10^{\circ}$

Therefore;

$$
\begin{aligned}
C_{pm_{\Theta(corr)}} = \; & C_1 \cdot Radians(\Theta) + \\
& C_2 \cdot \sin\Theta \cdot S_o + \\
& C_3 \cdot (\sin\Theta \cdot S_o)^2
\end{aligned}
\qquad \textbf{(4-20)}
$$

Where

$$C_1 = 0.3179$$

$$C_2 = 0.113$$

$$C_3 = -0.0064$$

The result of these corrections is a data correlation fit of an adjusted $R^2 = 0.92$ for the left part of the curve while the right side function has an adjusted $R^2 = 0.98$. A comparison between the measured and predicted values of Pressure Coefficients are presented in Appendix F, Figures F-9 to F-12.

4.15 Multiple Obstructions

So far all the experiments and functions were based on a single obstruction block. In this set of tests the objective was to identify the shielding effects of multiple obstruction blocks.

4.15.1 The Premise of the Experiments

The shielding effect of a group of obstruction blocks could be estimated based on averaging the shielding of the individual component blocks of the group and the gaps between the obstruction blocks.

4.15.2 Experiment Setup

In order to test the effect of the multiple obstruction blocks, two identical and horizontally aligned obstruction blocks were located parallel to the instrumented model (Figure 4-82). The relationship between these two blocks and the instrumented was varied to analyze the effect of the variables listed in Table 4-6.

Figure 4-82 Setup of experiment. The drawing shows the studied variables.

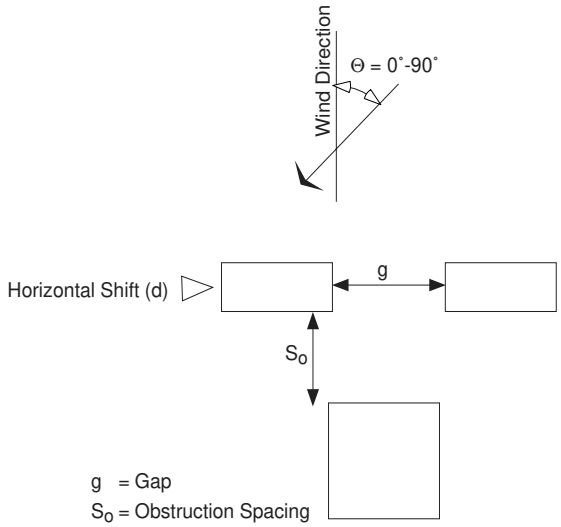

The shielding effect was analyzed based upon varying the following parameters:

TABLE 4-6 **Tested Variables in the Multiple Obstruction Block Configuration**

Description of the Variables	Variation (#)
• The gap between the obstructions blocks (g).	12.5, 25, and 37.5 cm (4).
• Spacing between the obstruction blocks and the instrumented model (S_o).	2, 3, and 4 (3).
• Horizontal shift (d). This was performed for one spacing only (2).	Three shift configurations were tested. See Figure 4-83.
• Wind Directions (Θ).	0˚-90˚ in 15˚ intervals (7).

Figure 4-83 The tested three shift positions.

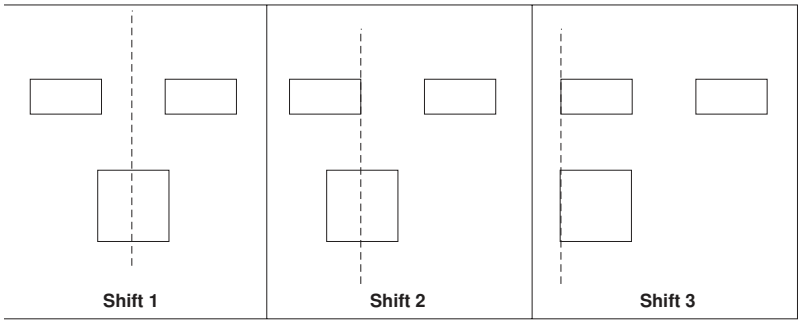

The resulting total number of conducted tests was 105.

4.15.3 The Results

Figures 4-84 to 4-87 show the various test results presented in comparative form to show the effect of each variable versus wind direction on the average surface pressure coefficients (C_p). Each figure contains three smaller figures that show a third variable. In each of the small figures, a fourth variable is represented by three curves. Data representing the Pressure Modification Coefficient (C_{pm}) are similarly presented in Appendix G (Figure G-3).

In general, the larger the gap, the higher the surface pressures. When the gap is wide enough, the airflow between the obstruction blocks causes the C_p values to equal those of the unobstructed surface. This observation agrees with the conclusion of Chand *et al* (Ref. 50). However, the gap width is not the operative factor in increasing the value of the measured C_p. In analyzing the data, it was found that with large gap widths, the obstruction blocks tend to be further apart. This, in turn, reduces the shielding effect of each obstruction block. The value of C_p for the multiple obstruction was similar to that of the block at a closer distance to the instrumented sur-

face regardless of the gap width (Figure G-4). This means that the effect of the gap is a function of its separation between the obstruction blocks. Therefore, the location of the gap relative to the instrumented surface should be the variable by which the gap effect is determined.

Figure 4-84 Effect of changing spacing (S_o) and gap width (g).

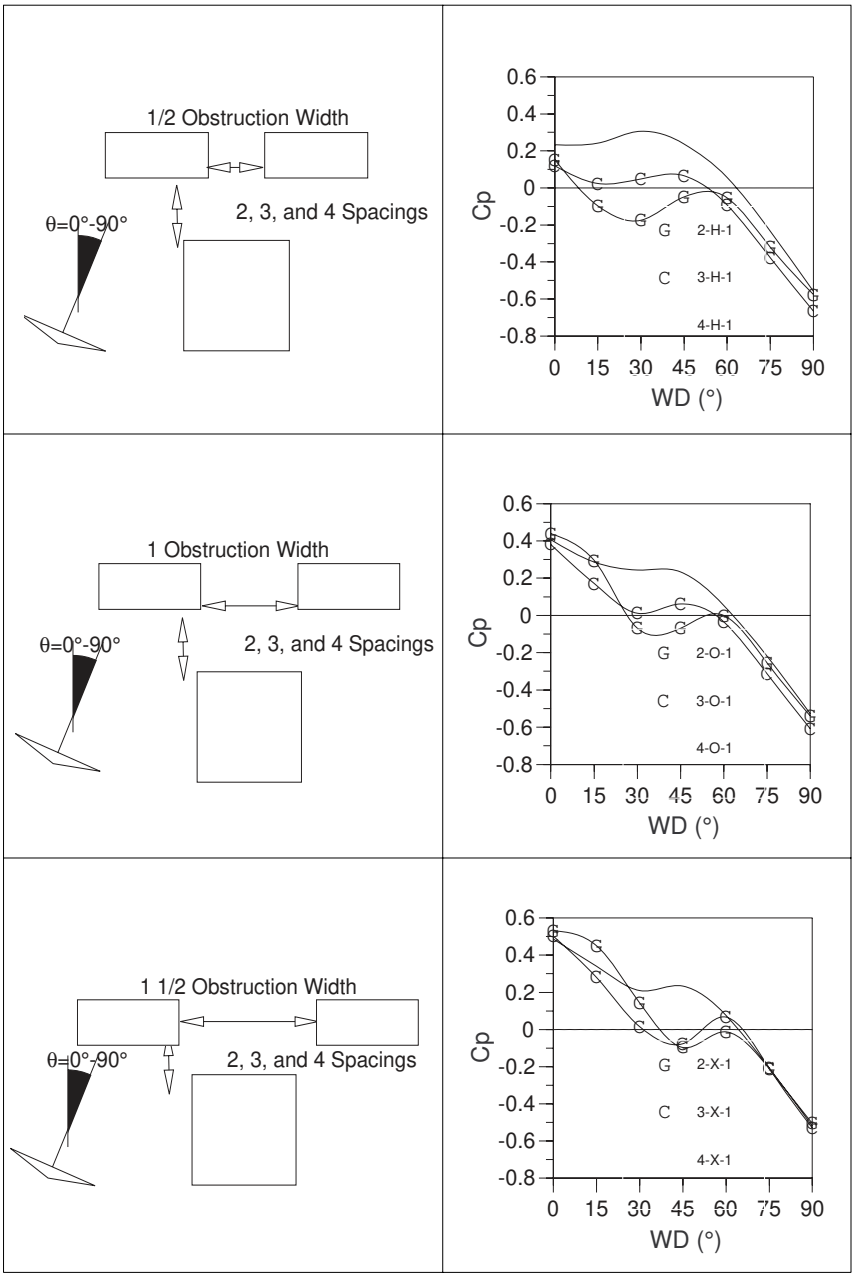

Figure 4-85 Effect of changing gap width (g) and spacing (S_o).

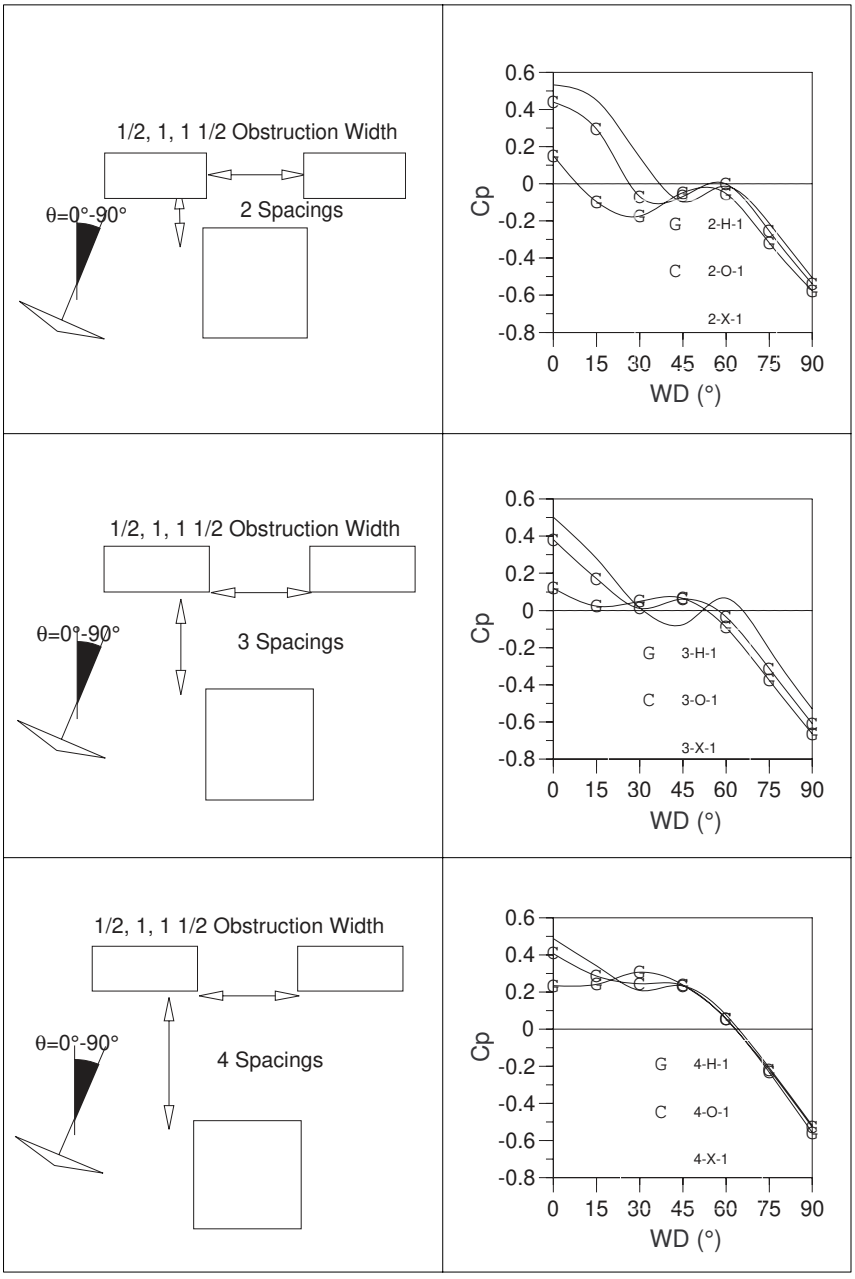

Figure 4-86 Effect of changing displacement (d) and gap width (g).

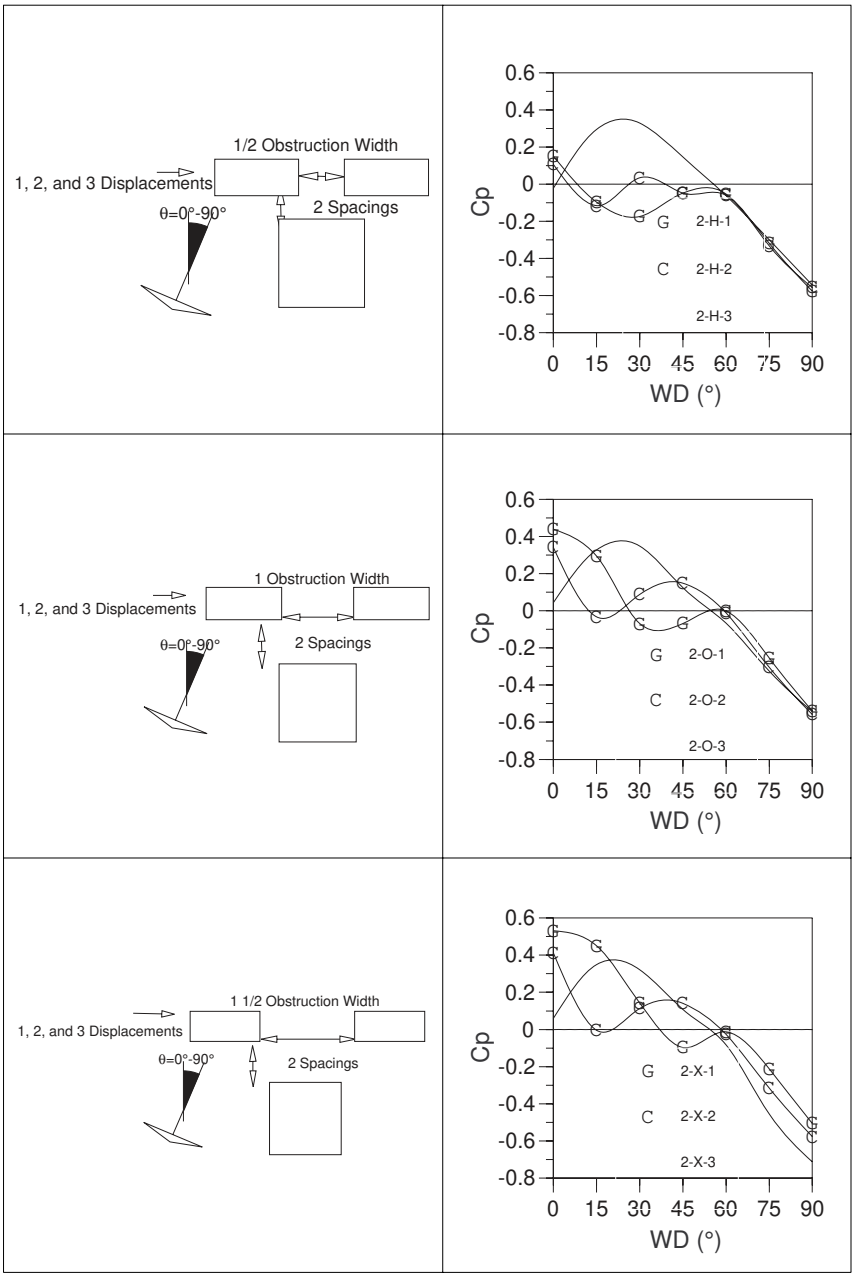

Figure 4-87 Effect of changing gap width (g) and displacement (d).

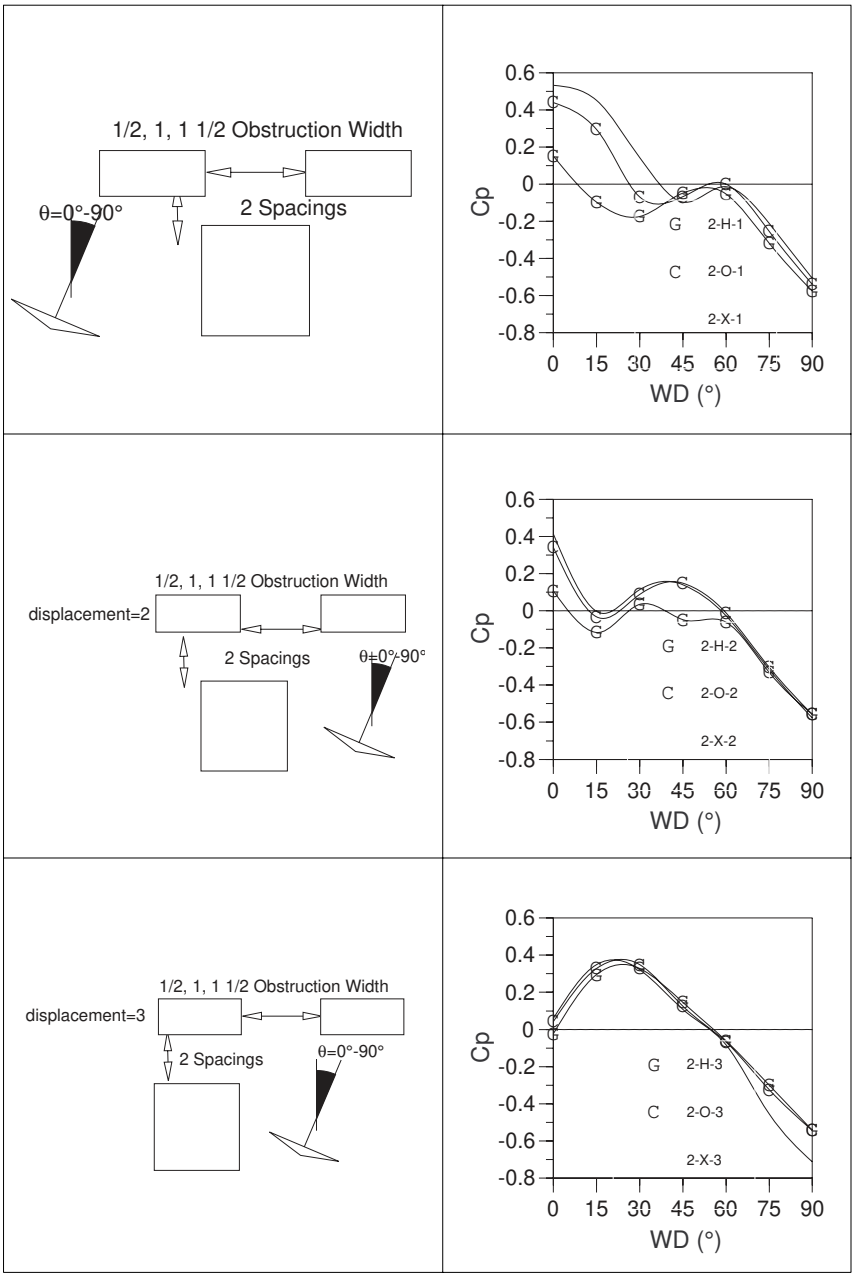

Figures G-2.1.-G-2.15 in Appendix G represent the profiles of the Pressure Modification Coefficients C_{pm} values distributed alongside the obstructed and unobstructed surfaces. The pro-

files are plotted for each wind direction for each of the 105 tested configurations.

4.15.4 Discussion of the Results

The averaging of the obstruction blocks within the Shielding Effectiveness Zone (SEZ) could be achieved by one of two methods;

The first method establishes an average shielding block representing all existing blocks within the SEZ, and then calculates the Pressure Modification Coefficients C_{pm}. The problem with this approach is that the prediction model already uses equivalent obstruction blocks in estimating individual block shielding effects with respect to changes in wind direction (see section 4.14.2). The multiple steps needed to determine the equivalent obstruction block geometry and the resulting shielding will have very little to do with the actual layout and geometry of the obstruction blocks.

The second method calculates the C_{pm} value for each individual block, and then averages the coefficients rather than the dimensions of the obstruction block. The problem with this approach is that the averaging is not linear, i.e. the obtained C_{pm} values do not correspond well to the arithmetic average of individual values of C_{pm}. However, the author found that the geometric average of the C_{pm} values might be corrected using the relative location of the gaps between the obstruction blocks. This means that a block that is located in front of the instrumented model, relative to the wind direction, has the largest effect. In addition, the more perpendicular the gap to the instrumented surface, the higher the corresponding C_{pm}.

These gaps tend to offset the shielding effect of the obstruction blocks by increasing the surface pressures. Correcting for these factors results in a prediction model that is not only sensitive to the relative location of each obstruction block to the surface but also to the gaps in between.

4.15.5 The Gap Rule

The *gap* in the mathematical model is defined as the space between and around the obstruction blocks within the Shielding Effectiveness Zone (140° windward arc). If the gap exists between two objects, but part of it lies outside the 140° arc, then only the part of the gap that lies within the SEZ is considered (Figure 4-88).

Figure G-4 in Appendix G shows a comparison between the C_{pm} measured behind the two obstruction blocks and the predicted C_{pm} value of each of the individual blocks. In all cases, the combined shielding did not equal the average[34] shielding of the individual blocks. The analysis of Figure G-4 showed that it was necessary to add an element in the function that represents the gap between the blocks. To take the gap into account in the determination of the weighted average Pressure Modification Coefficient, the gap should be dealt with as an object of zero height (Figure 4-88). This means that the displacement angle of the gap should be measured using the same definition that is used for measuring obstruction blocks.

4-34 Arithmetic or geometric.

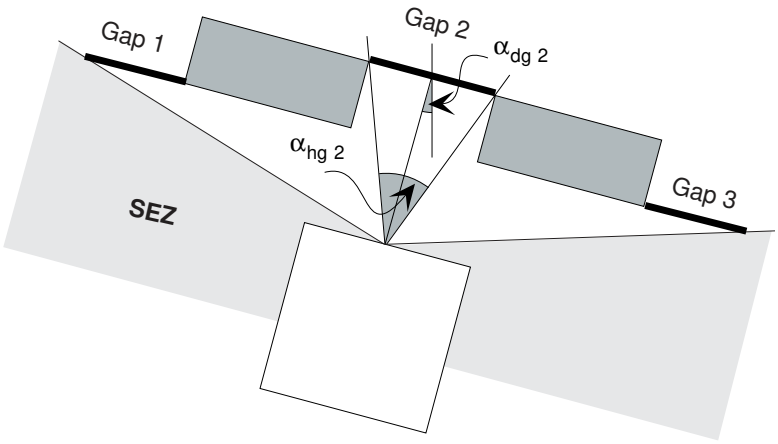

Figure 4-88 The Gaps are the spaces between the obstruction blocks and lie within the SEZ.

Since the gap is a void, the gap rule is a location function rather than a function that denotes the magnitude of an effect. This means that only the location of the gap relative to the instrumented surface is accounted for in the derived relationship.

4.15.6 Deriving the Function

The fitting function was derived using a nonlinear regression routine to determine the power to which each variable was raised (Equation 4-21). The general form of the relationship is:

$$C_{pm_{\text{multiple}}} = \prod (C_{pm_i})^{(k_1)/n} + \sum \frac{(\cos \alpha_{d(gap_i)})^{k2}}{n} \quad \textbf{(4-21)}$$

The First part of the right side of the equation deals with the averaging of the effects of the individual shielding blocks (discussed in section 4.15.3). The second part, was added to take into account the effect of the location of the gaps between obstruction blocks (section 4.15.5). The resulting formula was as follows;

$$C_{pm_{\text{multiple}}} = (C_{pm_1} \cdot C_{pm_2} \ldots)^{k_1} + C_1\left(\frac{\cos\alpha_{d_{\text{gap}_1}} + \cos\alpha_{d_{\text{gap}_2}} + \ldots}{n}\right)^{k_2} + C_2\left(\frac{\cos\alpha_{d_{\text{gap}_1}} + \cos\alpha_{d_{\text{gap}_2}} + \ldots}{m}\right)^{2 \cdot k_2} \quad \textbf{(4-22)}$$

Where;

$C_{pm_{multiple}}$ = Pressure Modification Coefficient of multiple objects

C_{pm_i} = Predicted corrected individual Pressure Modification Coefficient

= $C_{pm_{\Theta(corr)}}$

$\alpha_{d_{\text{gap}_n}}$ = Displacement angle of Gap

n = Number of adjacent blocks seen by the surface

m = Numbe of visible gaps within SEZ

i = 1, 2

and;

C_1 = 0.481

C_2 = –0.5874

k_1 = 1.0907

k_2 = 1.8738

Figure 4-89 Comparison between measured and predicted values of C_p [a]. (Figure G-5 shows the comparison between the measured and predicted values of C_{pm}) .

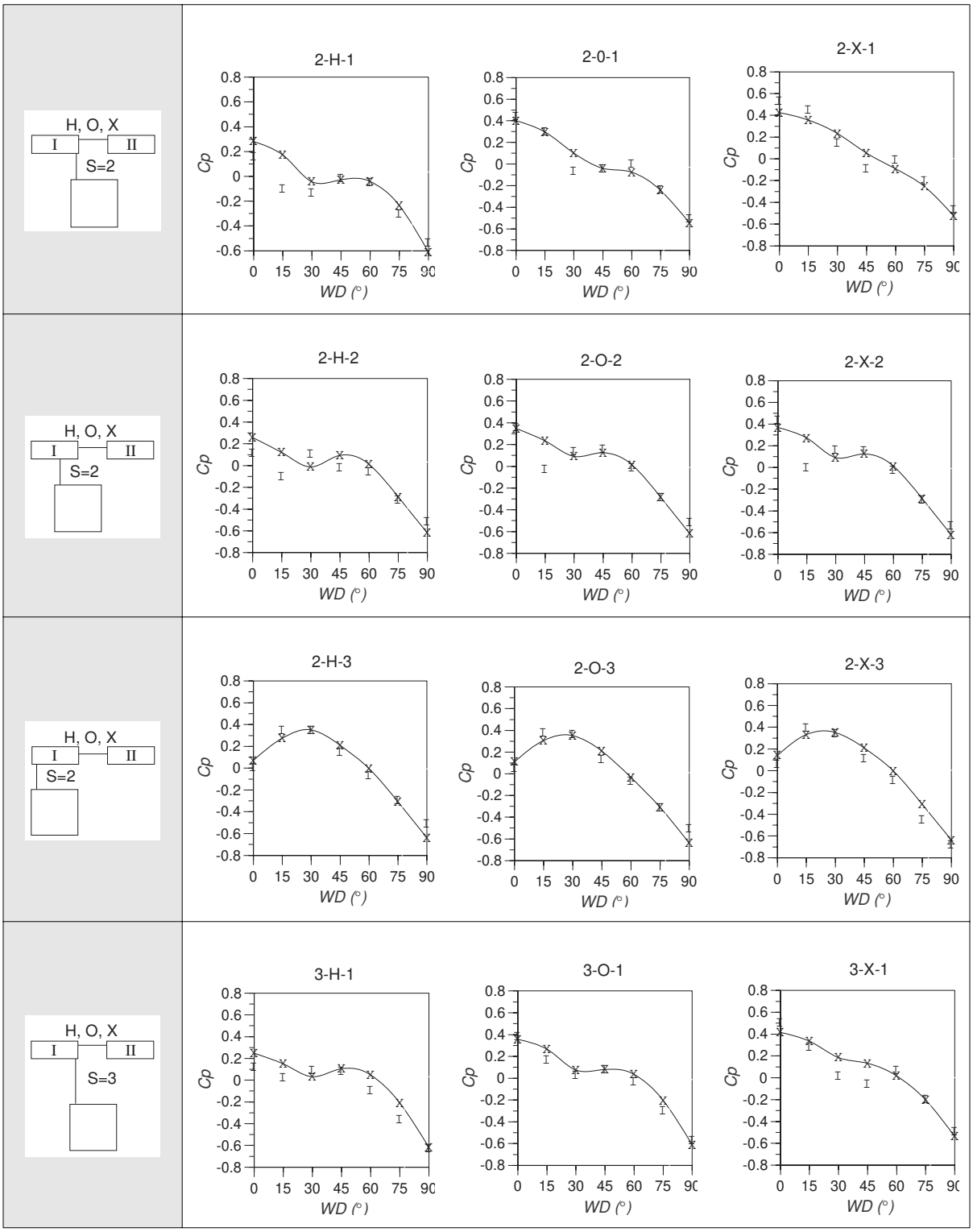

Figure 4-89 Comparison between measured and predicted values of C_p [a]. (Figure G-5 shows the comparison between the measured and predicted values of C_{pm}) (Continued).

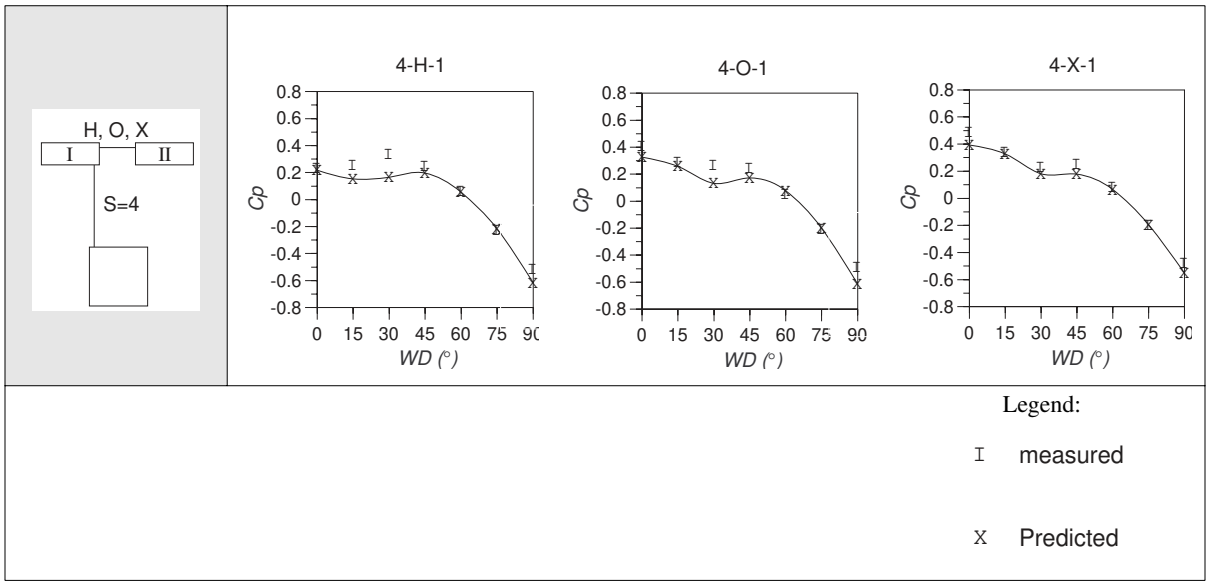

a. For the description of the variables in the left margin of the graphs, refer to TABLE 4-6 .

It should be noted that there are many visible obstruction blocks whose shielding is small or negligible, i.e. $C_{pm_{\Theta(corr)}} \approx 1.0$, the resulting $C_{pm_{\text{multiple}}}$ will be exaggerated when applying Equation (4-22). Such blocks should not be included in the equation. Similarly, on analyzing surface pressures above those obtained from unshielded surfaces when the wind direction exceeds 140˚, the value of calculated $C_{pm_{\text{multiple}}}$ was higher than 1.0. As a result, the blocks that fulfill the following condition are not to be included in the Equation (4-22):

$$0.99 < C_{pm_{\Theta(corr)}} < 1.06 \qquad \textbf{(4-23)}$$

Figure 4-89 shows the comparison between the predicted and the measured values of the multiple obstruction function

C_{pm}. In general, the prediction fits the measured data with an adjusted correlation coefficient $R^2 = 0.95$.

4.16 Complex Instrumented Models

This part deals with the estimation of C_{pm} values for complex building forms. These include L, U, Z-shaped building in which wall surfaces may be shielded from the wind by the rest of the building. In these cases, only the obstruction building blocks that are seen from the surface of interest are considered (Figure 4-90). This case is similar to situations where an obstruction block is not fully visible from the mid point of the surface of a simple rectangular model (Figure 4-91). In either case, only the obstruction blocks located within the visible portion of the shielding effectiveness zone are included in the model.

The major difference between the simple and complex model forms, however, is that each has a different value of mean unobstructed Pressure Coefficient ($C_{p\text{Unshielded}}$). As a result, the denominator in equation (4-3) for the L-shaped model, for example, will reflect the effect of the self-shielding on $C_{p\text{Unshielded}}$ values[35] (Figure 4-92).

4-35 For a full description of the sources of pressure data of unobstructed block refer to Section 5.6, page 197.

Figure 4-90 Self-shielding should be treated as an obstruction block.

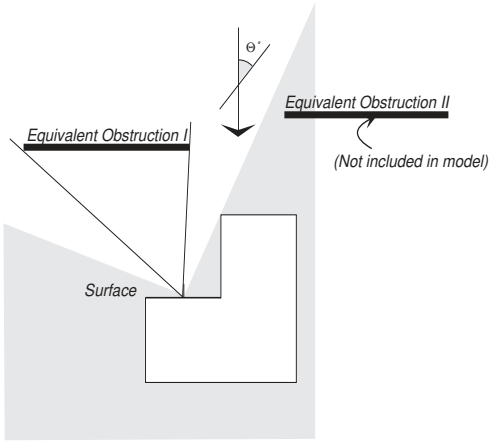

Figure 4-91 Self-shielding of the instrumented model.

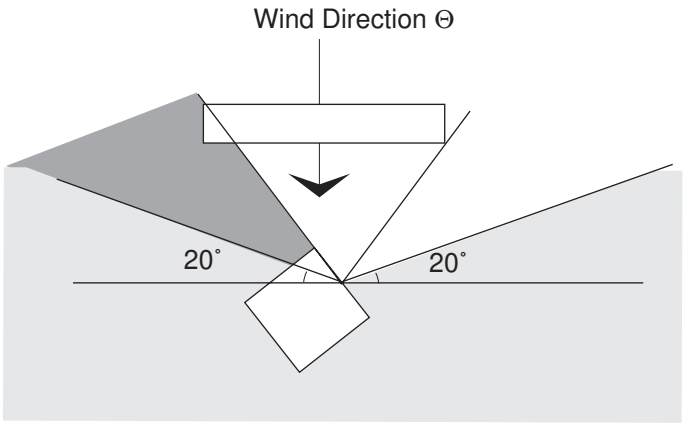

The consequence of this suggestion is that surface pressures coefficients (C_p) of a rectangular model will be different than those for an L-shaped model when identical conditions exist. This occurs despite the fact that there is no difference in the value of predicted Pressure Modification Coefficient (C_{pm}) in either configuration.

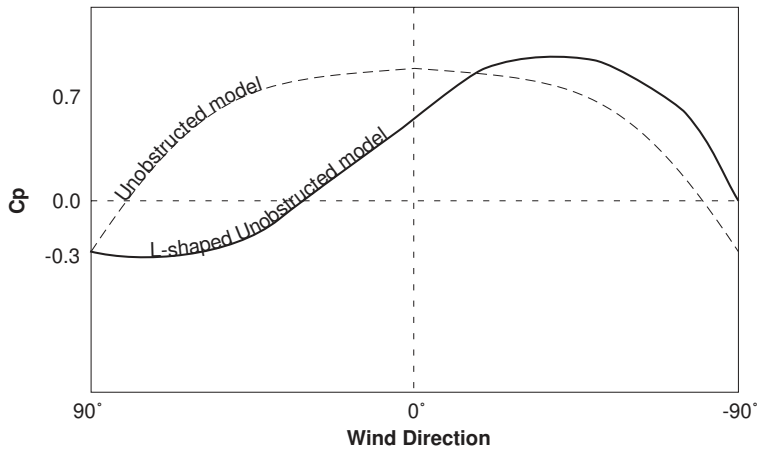

Figure 4-92 Surface pressures on L-shaped building, Sources: Ernest (Ref. 74).

4.17 Verification of the Model

In this section the Pressure Modification Coefficient (C_{pm}) model was subjected to verification in two stages. First, to compare the predicted pressure coefficients values to already-obtained values from previous research projects and; second, to verify the mathematical model with pressure modification coefficients obtained by testing a realistic model of a hypothetical urban area. This model is described fully in Section 4.17.4 and used in the example discussed in Appendix H .

4.17.1 Wiren's Experiments

Wiren's earlier experiments at the *National Swedish Institute for Building Research* (Ref. 227) were used to verify the C_{pm} model. These experiments investigated the wind pressure distribution of a model of a typical Swedish house with double-pitched (gable) roof under various shielding configurations. The studied variables were the number of surrounding building rows (1, 2, and 3), and the spacing between the surrounding buildings as well as between the surroundings blocks and the model (1, 1.5, 2, and 3 spacings). These experiments are illustrated in Figures 4-93 and 4-96.

4.17.2 Wiren's Single obstruction Experiments

The most basic configuration in Wiren's experiments was the single windward obstruction (Figure 4-93). His pressure coefficients for the four surfaces were then compared to an unobstructed model (A00). This setup was used to verify the basic orthogonal mathematical prediction model.

The variables in this set of experiments began with variation of the spacings of the windward block from the model (Table 4-7). Both model and obstruction block were centered, thus no displacement was considered. Second, seven wind directions 0˚-90˚, in 15˚ intervals were tested obtaining pressure coefficients for the four model surfaces.

4.17.2.1 Description

The mathematical model for a single obstruction (section 4.14.2) was used to estimate the average pressure coefficients on both facade and gable end walls.

Figure 4-93 Wiren's single obstruction experiments.

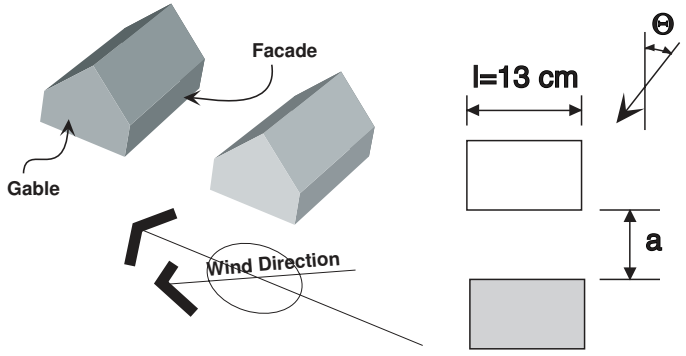

TABLE 4-7 **Wiren's Single Obstruction Configurations**

Configuration	A10	A20	A30	A40
a/l	1	1.5	2	3

4.17.2.2 Results and Discussion

The following section discusses the results of predicting the surface pressures on four model surfaces and explains the results for each of the configurations.

Figure 4-94 Comparison between the prediction model and Wiren's results.

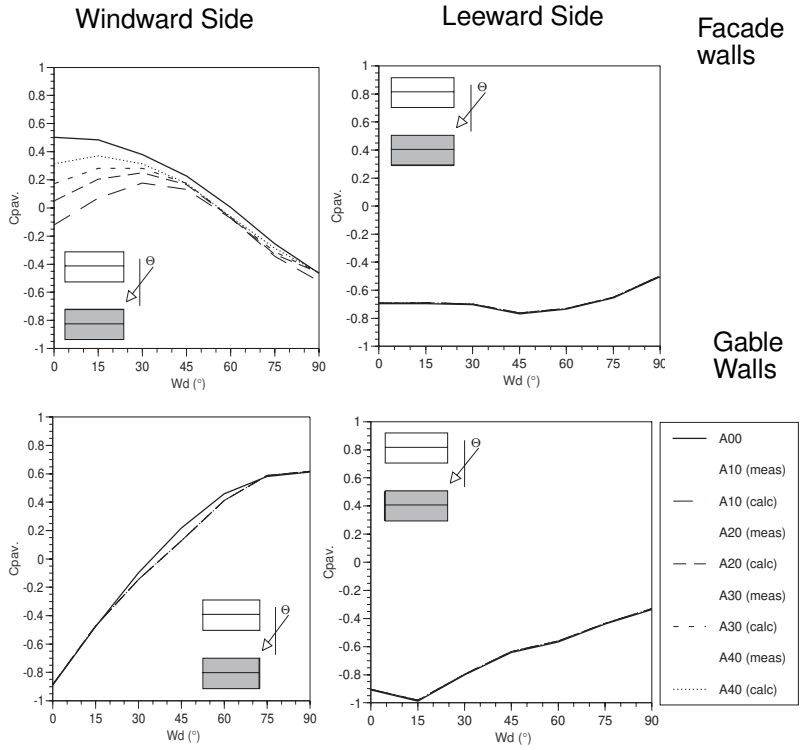

Figure 4-94 shows four graphs of the model predicting average Pressure Coefficients $C_{p_{av}}$ on the facade and gable end walls for both windward and leeward directions and compares the results with the measured data[36]. This comparison shows a good agreement on the windward facade wall (top left corner of Figure 4-94).

However, the measured values for the leeward side of the facade wall (top right corner of Figure 4-94) show an inverse

4-36 The measured data was extracted from a scanned copy of a graph in the report (Ref. 227) using dataThief© 2.0b by Kees Huyser and Jan Van der Laan.

effect between the spacing of the obstruction building block and the average surface pressures between 0˚-15˚. This result could not be predicted by the pressure shielding model as the, unobstructed side (leeward side) did not see the obstruction block at any of the relative positions at any wind direction. Thus, no effect was predicted and the resulting values coincided with those of the unobstructed model. In fact, this phenomenon was not encountered while testing the configurations in *The Effect of Changing Wind Direction* (Section 4.14.3) where very little variation occurred in the pressure coefficients on the unobstructed side between 0˚-15˚. When the wind directions is greater than 30˚, the prediction fits the measured results well. The disagreement (between 0˚ and 15˚) can be explained by the following; at wind directions normal or close to normal to the surface under consideration, the wake sizes in Wiren's experiments were larger than those generated by the this experiment's simple cubical model used for deriving the mathematical relationships. Evans' experiments (Ref. 79) on the size and extend of the wake behind various block sizes and configurations showed that double-pitched roofs tend to create longer wakes (maximum 35% longer wake[37]) than those generated behind blocks with flat roofs. As a result, Wiren's instrumented model at this wind direction was within the wake of upwind block, preventing it from fully developing its own wake, and consequently increasing the surface pressures above those of the unobstructed model.

4-37 The study that was conducted on various building geometries, roof shapes showed that the wake length of a 1:2 roof slope increased the by about 35% relative to the flat roof, however this increase was inversely correlated with building lengths

At wind directions $\Theta \geq 30°$, the instrumented model falls outside the generated wake, thus remaining virtually unshielded by the obstruction block. The result in this range is well predicted by the model and both the measured and predicted $C_{p_{av}}$ values coincide with the unobstructed block.

In the other two walls (gable walls), the prediction model falls short by overestimating the shielding effects when the wind is parallel or near parallel (0˚-15˚) to the surface under investigation[38]. The probable reason for this discrepancy is that the model assumes no shielding is taking effect since the facade cannot '*see*' the obstruction block. As a result, predicted values of $C_{p_{av}}$ equal those obtained from the unshielded configuration (Figure 4-94). Similar to the case on the leeward side, the wake generated by the windward block engulfs the sides parallel to the wind direction. Consequently, the value of $C_{p_{av}}$ is increased by the elimination of the separation zone at the windward corner of the block (Figure 4-95).

4-38 At wind direction 0˚, the gable wall is actually at 90˚ relative to the wind direction. In Chapter 5, this issue will be thoroughly discussed.

Figure 4-95 The average pressure coefficients at the gable wall is lower when unobstructed than when shielded.

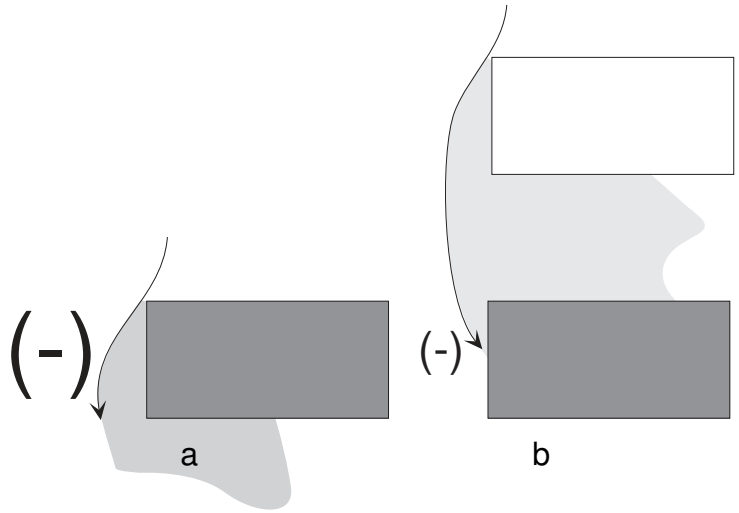

4.17.3 Wiren's Multiple Obstructions

The second part of the verification of the mathematical model was to investigate the applicability of the functions to a complex layout similar to those conducted in Wiren's Experiments (Ref. 226). In addition to the orthogonal function, the correction for displacement, wind direction, and effect of multiple obstruction blocks and gaps were also included for the determination of surface pressure coefficients of a model amidst the tested urban setting (Figure 4-96).

4.17.3.1 Description

The number of tested configurations was three corresponding to three rows of obstruction blocks (H11, H12, H13) as shown in Figure 4-97. Only one spacing (a/l = 2)[39] was compared to the prediction model (Figure 4-96).

4-39 Refer to Table 4-7 for tested configurations.

Figure 4-96 Wiren multiple blocks grid-iron configuration.

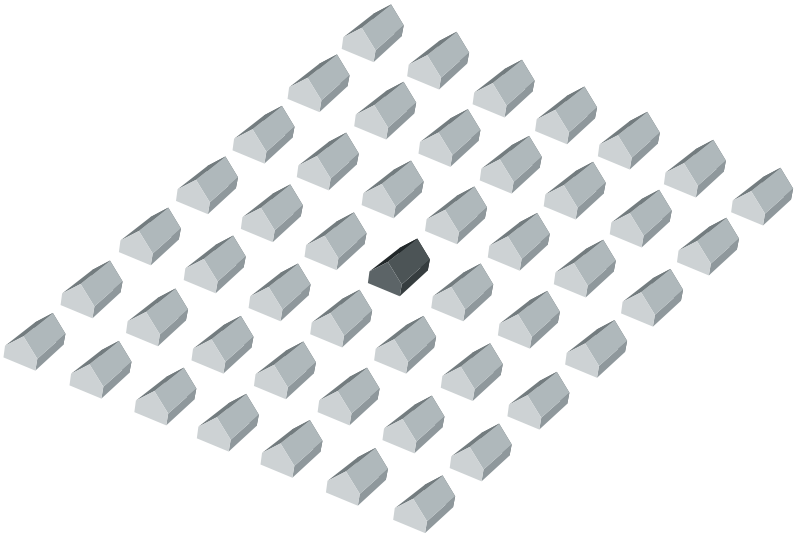

Figure 4-97 Wiren's grid-iron layout and spacing.

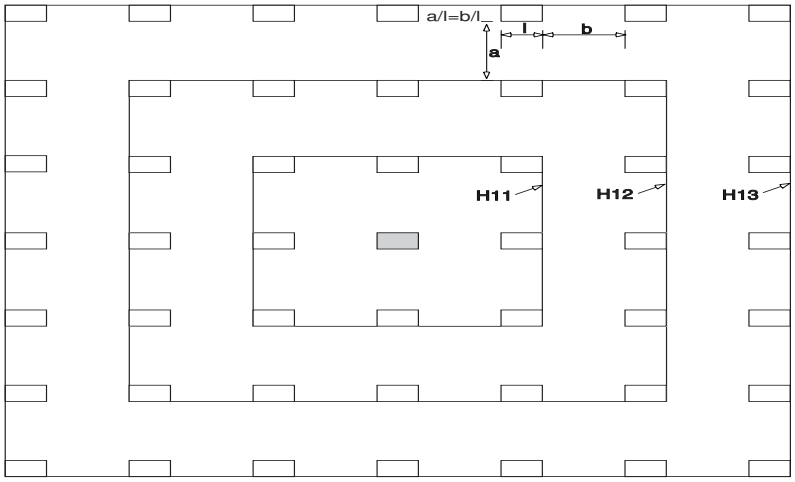

TABLE 4-8 **Wiren's Multiple Obstruction Configurations**

Configuration	H11	H12	H13
a/l=b/l	1	1.5	2

Figure 4-98 Comparison between the prediction model and Wiren's results.

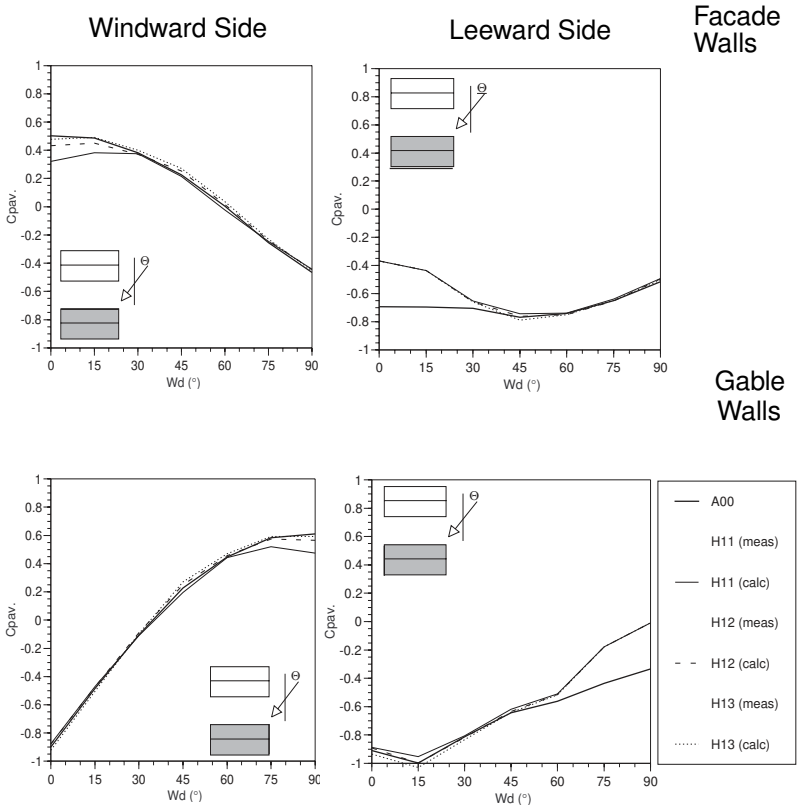

4.17.3.2 Discussion of Results

Figure 4-98 shows a comparison between the measured values of $C_{p_{av}}$ when 48 adjacent obstruction blocks surround the instrumented model. The following can be observed from the comparison:

- The predicted values of $C_{p_{av}}$ at the windward facade surface (top left corner Figure 4-98) fit the measured curve except at the 0˚-15˚ wind directions. This is true for all tested configurations except for the single row configuration (H11). The reason for the discrepancy is the inherent problem of the multiple effect function (equation 4-21) where the averaging of a large number of obstruction

blocks with high modification coefficients ($C_{pm} \approx 1.0$), tend to favor the high values and produce slightly exaggerated values of $C_{p_{av}}$.

- The predicted $C_{p_{av}}$ values for leeward side (top right corner Figure 4-98) show a good fit from 0˚-30˚ as a result of the correction for pressurization effect analyzed in Section 4.14.3. However, at wind directions ≥ 45˚, the model does not account for any shielding by obstruction blocks the surface does not see.
- The predicted values of the $C_{p_{av}}$ at the gable walls (bottom two graphs of Figure 4-98) demonstrates similar behavior to those calculated for the single obstruction, with the exception of the leeward gable side at wind direction above 60˚, where the pressurization correction reduces the shielding effect[40].

4.17.4 The Realistic Model

The intention of this section is to demonstrate the ability of the mathematical (PMC) model to predict surface pressures for buildings located at complex urban layouts. The tested layout did not represent an actual site, but attempted to include several geometric and spatial complexities that might not all occur in one site. The result was a simple rectangular model with its four wall surfaces facing different quadrants of a complex hypothetical urban layout (Figure 4-99).

The surface pressures were measured in boundary conditions similar to those of a small town or a suburban setting (Table B-1).

4-40 Increased the value of the Pressure Modification Coefficients.

4.17.4.1 Description

The instrumented model was constructed out of transparent 2mm thick plexiglass measuring $200 \times 100 \times 98$ mm (Figure 4-100). Two adjacent surfaces of the model were rigged with 24 pressure taps connected to the data acquisition system described in Section A.2 in Appendix A. In order to measure the surface pressures on the other two sides, the model was rotated 180˚. Finally, to take into account the change of wind direction, the whole layout setup (model and surroundings) was rotated from 0˚-360˚ at 10˚ intervals.

The surrounding obstructions were made of extruded polystyrene blocks of different heights and located at different distances from the instrumented model. In addition, two of the obstruction blocks were not parallel to the instrumented model and positioned on the northwestern quadrant of the site. A set of obstructions made up of three blocks of different heights and positions relative to the instrumented model was located on the east side of the site.

Figure 4-99 Plan of the complex layout model.

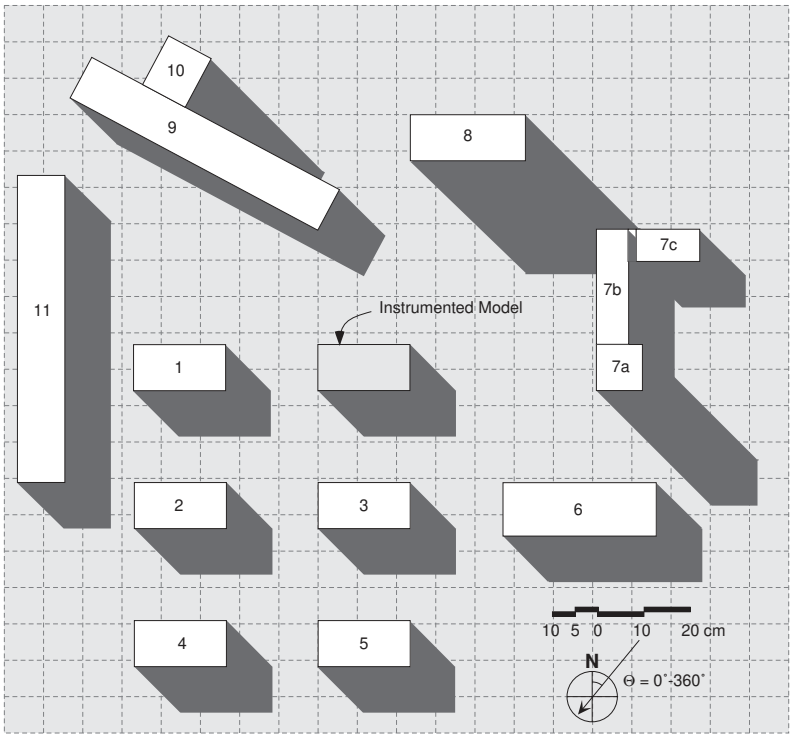

Figure 4-100 Instrumented model used in the complex layout experiments.

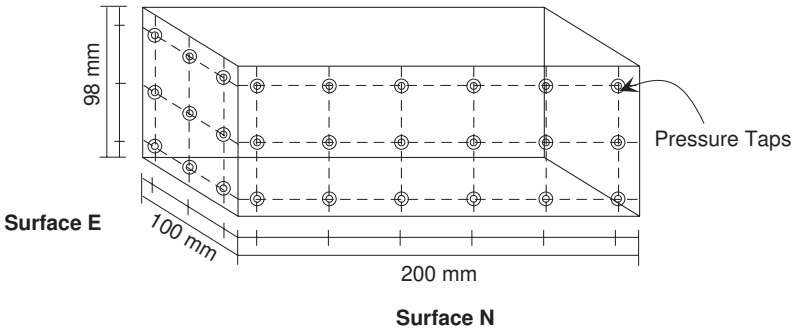

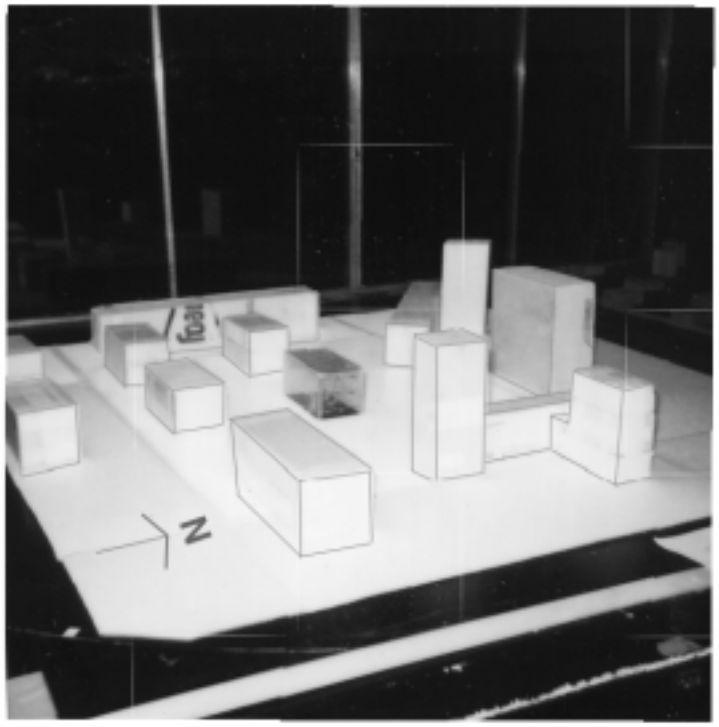

Figure 4-101 View from the southwest corner of the tested model and the surrounding blocks.

4.17.4.2 Difference from Other Physical Models

The difference between this configuration and most of the previous studies lies in the level of complexity in both the geometry of the obstruction blocks and the relationship between the instrumented and the surrounding blocks. The major four areas of difference are as follows:

4.17.4.2.1 Non-parallel Obstruction Blocks

Two blocks (9 and 10) were chosen to represent this geometric configuration. The two blocks were located to the northwest of the model site (Figure 4-99).

4.17.4.2.2 Complex Obstruction Model

An obstruction block that was made up of three simple cubic blocks (7a, b, and c) was located at the northeastern side of the model facing the east side. These three blocks varied in shape, height, and relation to the surfaces from which they could be seen.

4.17.4.2.3 Partially Hidden Obstruction Blocks

The model contained two categories of partially visible obstruction blocks. The first category was when an obstruction block could be seen over a relatively shorter block i.e. $\alpha_{v\text{back block}} > \alpha_{v\text{ front block}}$. An example of this was positioned behind the non-parallel obstruction block and the complex obstruction block (10 and 7c). The second category occurred when a long obstruction block was located behind shorter one and parts of it were still visible ($\alpha_{v\text{ back block}} > \alpha_{v\text{ front block}}$). Such conditions were included in the model on the western side of the site (11).

4.17.4.3 Results

Following the steps explained in Chapter 5, the predicted values were compared to the measured Pressure Coefficients C_p in Figures 4-102 to 4-105.

Figure 4-102 Comparison between predicted and measured values of C_p on the North side of the model.

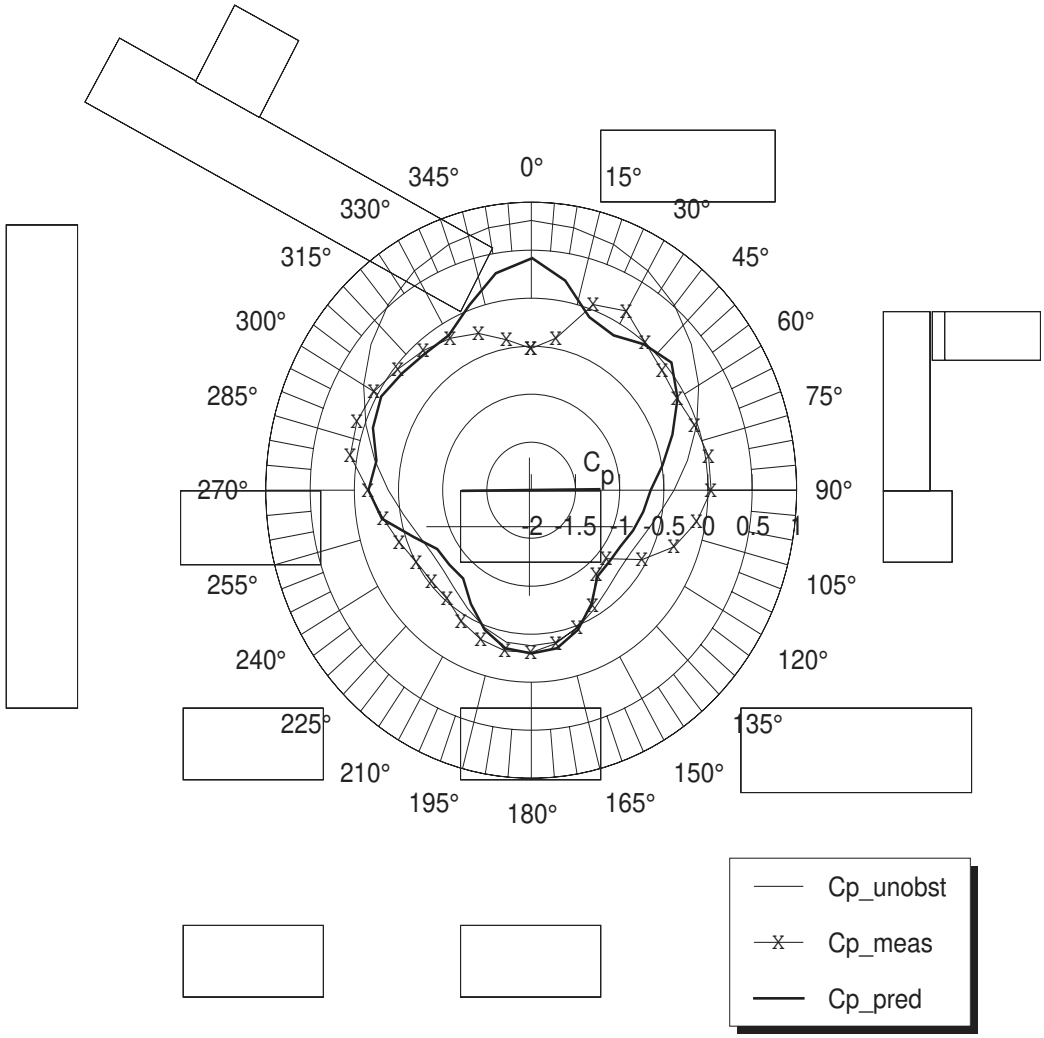

Figure 4-103 Comparison between predicted and measured values of C_p on the South side of the model

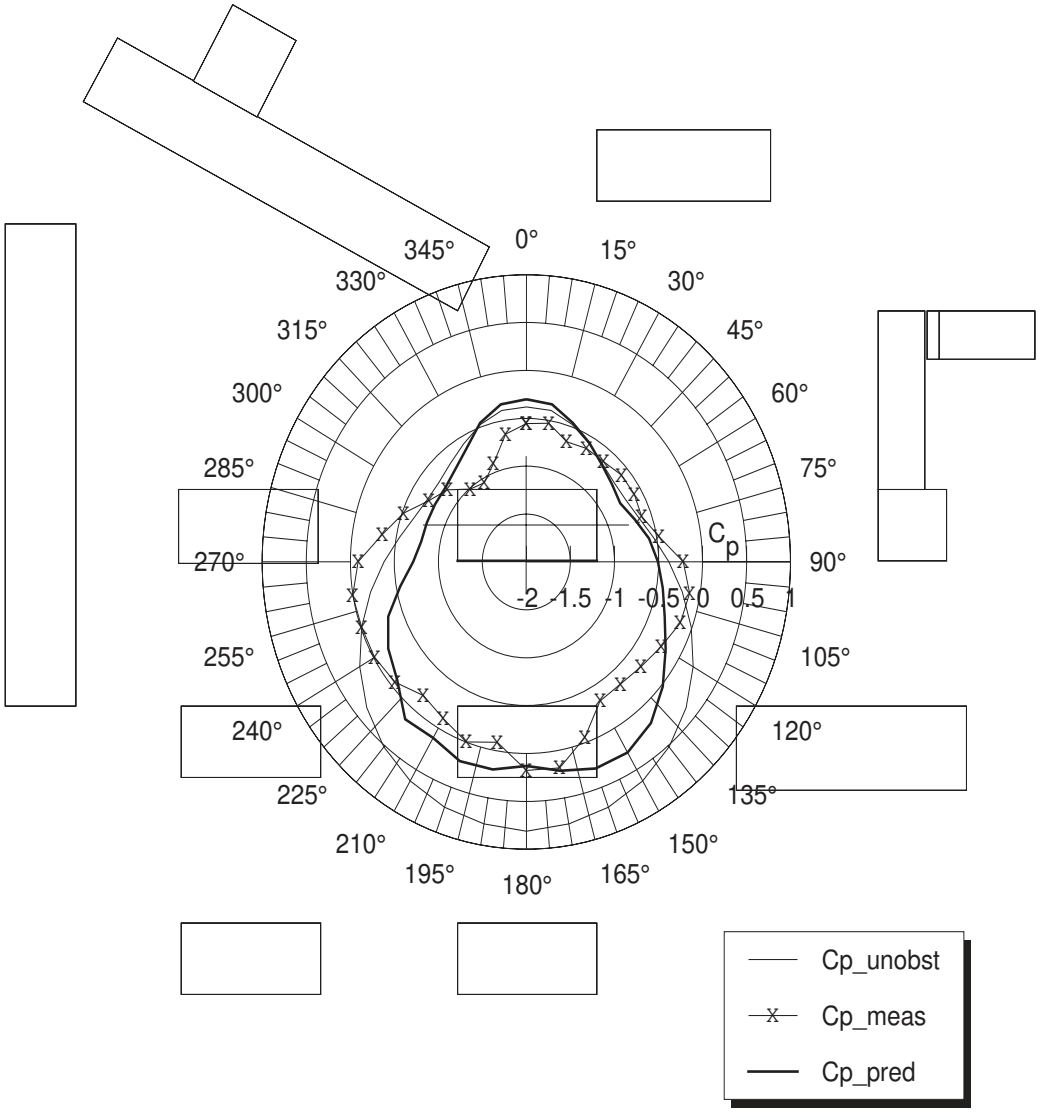

Figure 4-104 Comparison between predicted and measured values of C_p on the East side of the model.

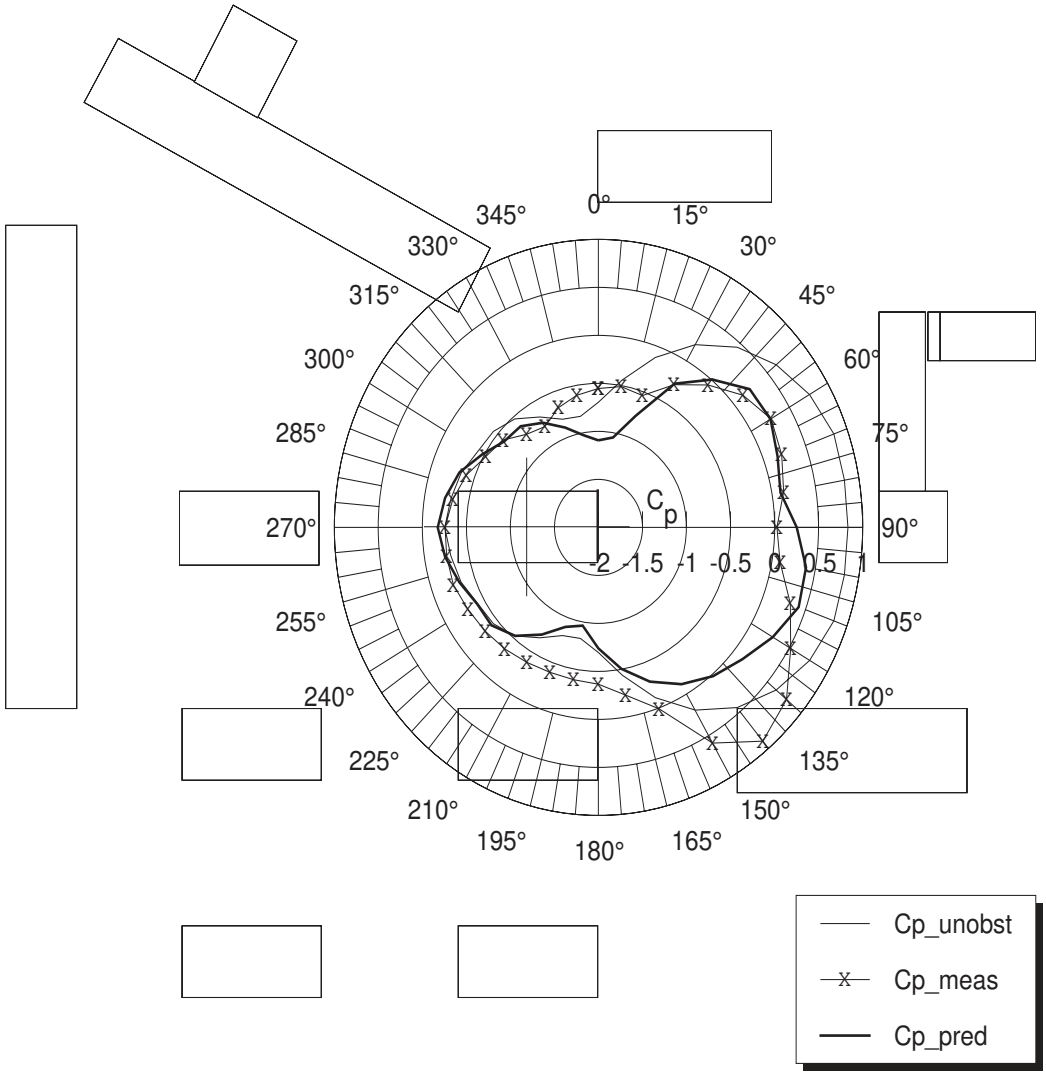

Figure 4-105 Comparison between predicted and measured values of C_p on the West side of the model.

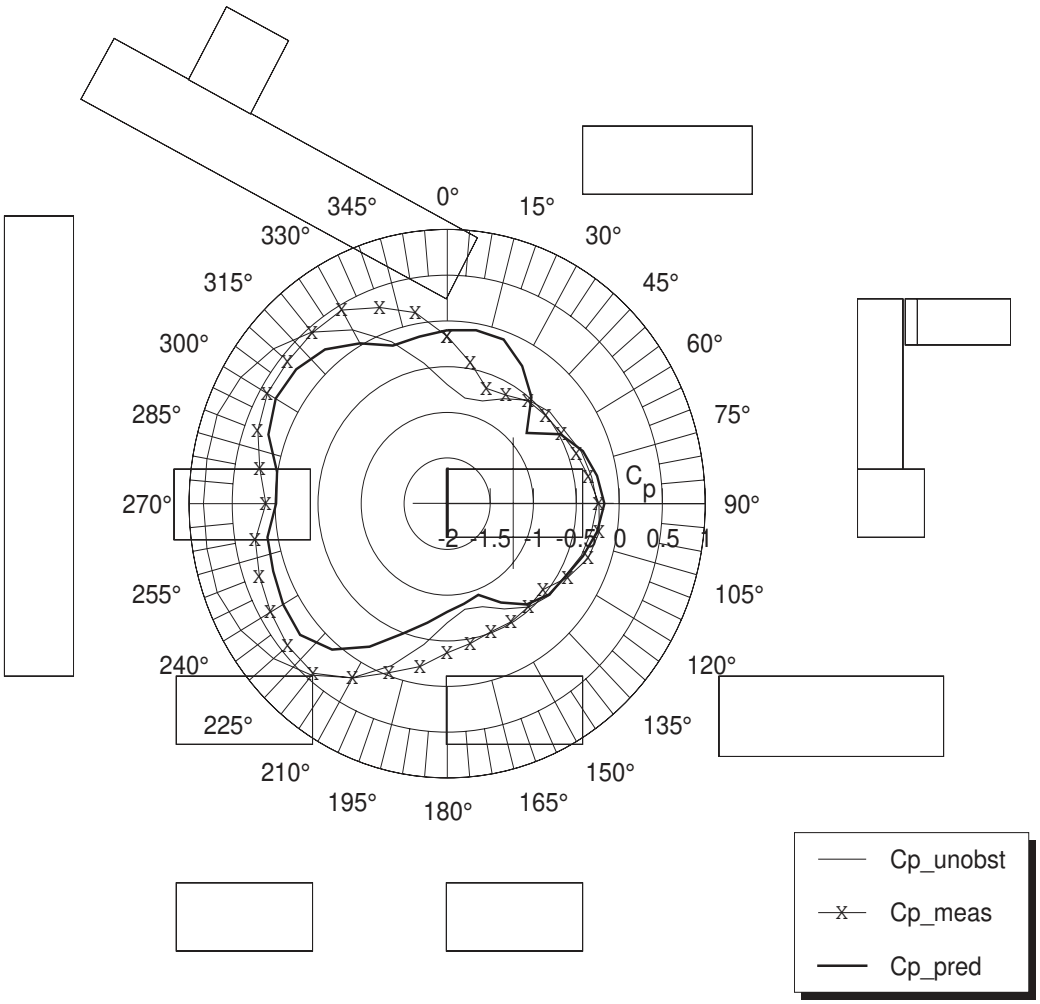

4.17.4.4 Discussion

In general, the predicted values are close to the measured data. However, there are some exceptions where the pressure prediction model fell short:

Figure 4-102 shows a comparison between the predicted, measured and unobstructed values of C_p on the north surface of

the instrumented model. In wind directions between 330˚-15˚, the prediction model overestimates the pressure coefficients. The high value of C_p could be attributed to the gap located upwind which in the mathematical model tends to increase the value of $C_{pm(\text{multiple})}$. However, the orientation of obstruction block (9) in relation to the instrumented model channels the flow and shifts the wake towards the north surface.

Figure 4-102 shows that between 70˚-125˚ the mathematical model underestimates C_p values. The same can be observed in Figure 4-104 (110˚-150˚). In both cases, the pressurization is caused by airflow through gaps that could not be seen from the surface under investigation.

4.18 Conclusions

A mathematical model has been developed for the prediction of surface pressure coefficients in a shielded environment. The model uses three angles of description for the individual obstruction blocks relative to surface for which pressure is to be estimated. A number of corrections were added to the function to account for building geometric relationships other than orthogonal symmetrical configurations.

Wind direction affects airflow around buildings in such a way that the generated wakes are shifted either towards or away from the surface in question. These effects are found to be influenced by the relationship between the obstruction block and the model, wind direction, and whether the obstruction block could be visible to the surface under consideration. Leeward blocks affect the surface pressures of the surfaces facing

them by increasing the pressures as a result of airflow diversion into the wake of the instrumented model.

The effect of multiple obstructions is estimated based on the geometric averaging of the shielding effect of the individual blocks. Passageways or gaps between the obstruction blocks increase the surface pressures as a function of their location relative to the instrumented surface.

An arc of 140° around the axis formed by the wind direction striking the surface is found to be the limit beyond which most obstruction blocks do not affect the surface pressures.

The verification of the model using Wiren's experimental results shows that the proposed procedure produces a good fit to data obtained from some of his experiments. This despite of Wiren's use of gable-roof models for both instrumented and surrounding blocks instead of the flat-roof models used in deriving the mathematical model.

When the mathematical model was tested against a model of a hypothetical urban setting that contained complex building configurations, multiple gaps and building relationships, and various block heights, a reasonable fit was produced. This was true except for wind directions where the gaps between the surrounding blocks channeled the air causing pressure increases even on surfaces from which these gaps could not be seen. Another effect, a shifting of wake could not be fully described or predicted by the mathematical model, resulting in predicted surface pressure values higher than those obtained from the tests.

In many ways the gap effects in the verification are more extreme than would normally be encountered in urban layouts, where there are more obstructions beyond the gaps.

In general, the proposed model was found to predict most of the possible relationships between the instrumented surface and the obstruction blocks. This meant that the model was flexible enough to predict surface pressures in urban settings unrestricted by a pre-tested layout.

Chapter 5

5

Implementations of the Prediction Model

5.1 Introduction

This Chapter deals with developing the tools for predicting the surface pressures of shielded buildings. This determination follows the mathematical relationships discussed in Chapter 4. The tools include methods for describing obstruction blocks in the form needed by the mathematical model. In addition, a method for predicting local wind speeds from weather station data is described.

The second part of the chapter deals with the integration of the Pressure Prediction Model (PPM) with the Indoor Ventilation Coefficient (IVC) Model developed by Ernest (Ref. 74). The IVC model uses pressure coefficient values and local wind speeds to predict indoor air velocities, turbulence, as well as other descriptives of indoor airflow.

Figure 5-1 shows how the PPM, IVC, and SITECLIMATE are combined in this chapter to produce a method for predicting indoor air velocities of shielded buildings using wind data obtained at remote stations. This model is called the Indoor Velocity Model (IVM).

Figure 5-1 The Different phases of the Indoor Velocity Model (IVM).

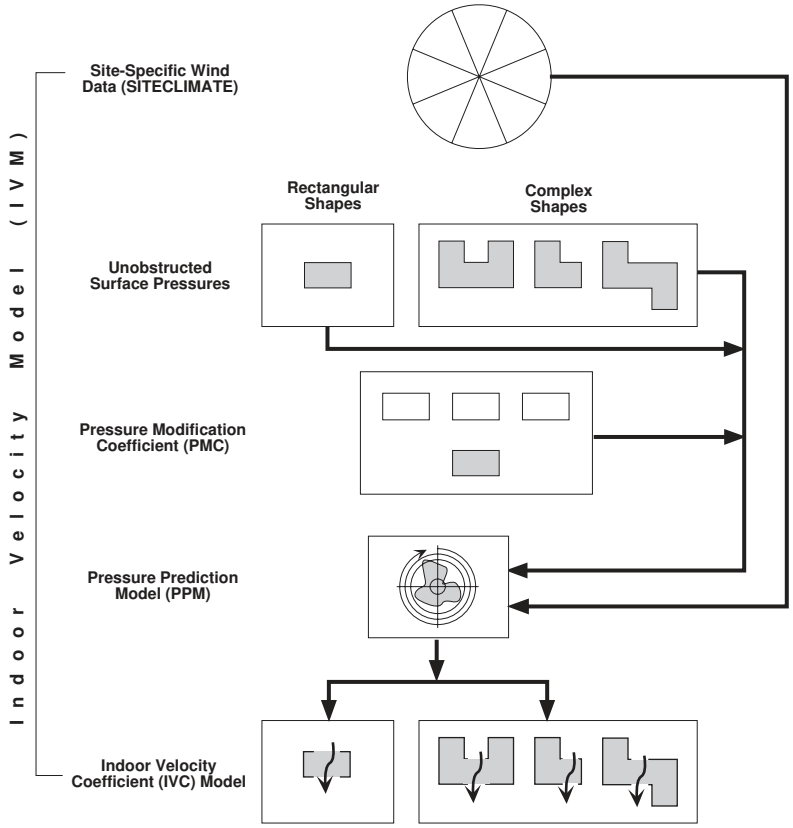

5.2 Application of Pressure Modification Coefficient Method

Natural ventilation is predicted by the Pressure Modification Coefficient Method (PMC) through the following steps:

- Obtain Surface pressure data for an unobstructed surface.
- Calculate the pressures for wind directions other than perpendicular to the surface.
- Determine the angles describing the individual obstruction blocks visible to the surface under consideration.
- For the surface under consideration, calculate the pressure modification coefficients of the visible individual obstruction blocks.

- Calculate surface pressures using the pressure modification coefficients and the pressure coefficients of the wind-direction-coincident unobstructed surfaces.
- Use the calculated pressure values at the different surfaces to predict indoor air velocities using the IVC model developed by Ernest (briefly discussed in Section 5.8).

5.3 Inputting Model Description Variables

The research thus far has concentrated on the geometric variables from which the mathematical functions were derived (i.e. α_h, α_v, α_d, and α_{d_g}). These angles represent a static description of the relationship between the obstruction block and the surface for which the pressure is calculated. On changing the wind direction, these angles have to be re-measured or recalculated to account for the newly created geometric relationships between the blocks and the model. This process seriously complicates implementation of the mathematical model. To simplify the input to the mathematical model, a universal system of obstruction description was developed that uses polar coordinates to describe the individual obstruction blocks and the gaps in between them. A similar system was used by Taylor *et al* (Ref. 208) to describe windward obstruction blocks. The advantages of using polar coordinates over the using cartesian angles of description were as follows:

- The polar coordinates are measured once. The changes of the geometric relationships caused by the wind direction changes are calculated from the same coordinates.
- The polar coordinates of the visible corners of the obstruction blocks are easier to measure, whether from plans or on site specially when large number of wind directions are involved.

5.3.1 Conventions

In order to use a single function for calculating the angles of description, a standard convention for measuring the polar coordinates was established (Figure 5-2).

Figure 5-2 Using the polar coordinates as basis for describing obstruction blocks.

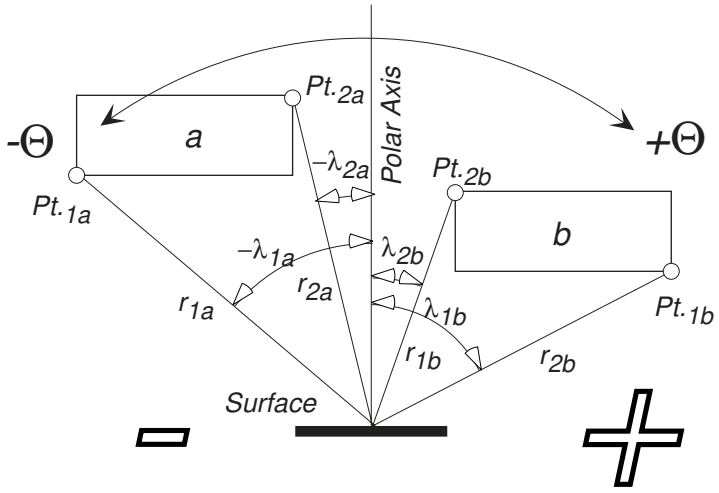

In the proposed polar coordinate system, the radial distance *(r)* is measured in terms of the obstruction spacings[1] (S_o) from the center of the surface to the outermost visible corner of the obstruction block. If a corner of is obscured by another obstruction block, the furthest visible point of the surface can be used instead (Figure 5-3). The polar angular coordinate *(λ)* is measured from a line perpendicular to the surface of the model *(polar axis)*. As a convention, any angle left of the axis is negative while on the right is positive (Figure 5-2).

5-1 Distance of obstruction block expressed in terms of its height, for more details, refer to the definition in Section 4.6.2.4, page 66.

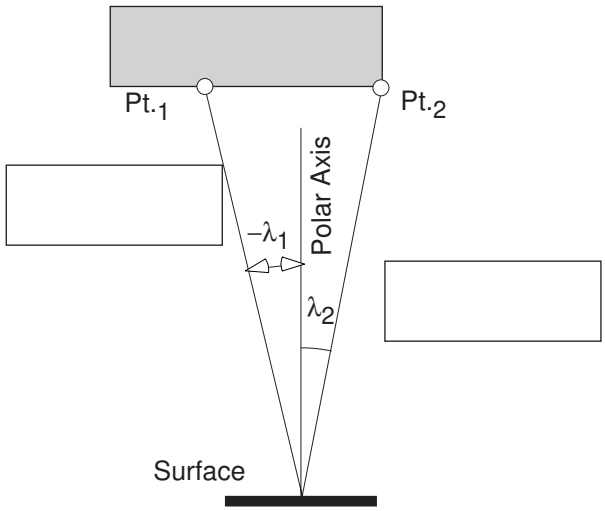

Figure 5-3 Polar coordinates for an obstruction block with one corner not visible from surface in question.

5.3.2 Graphically Determining Angles of Obstruction Blocks

A special protractor was devised to measure the polar coordinates of the visible corners of obstructing buildings. This protractor can either be used directly for measuring the coordinates, as will be shown in this section, or for the mathematical derivation of the obstruction angles (equations 5-7 to 5-20).

The protractor consists of two layers and a cursor for measuring both the angular and radial coordinates of the obstruction block and the wind direction acting on the building surface under considerations (Figure 5-6).

The first layer (Figure 5-4) is used to measure the polar coordinates of obstruction blocks and gaps, seen from the surface for which the pressure coefficient to be determined. This layer is composed of two concentric circles. The inner circle is marked 0˚-180˚ on the right side and 0˚-(-180˚) on the left, corresponding to the convention established in Section 5.3.3 and illustrated in Figure 5-2. At the center of the circle, a hori-

zontal bar representing the surface under investigation is used to align the transparent protractor over a plan of the model. The (F) and (B) letters denote the Front and Back sides of the building relative to the wind direction. Sides F and B can stand for surfaces N and S (Figure 5-8) when the wind direction Θ equals 0˚ respectively. The same is true for surfaces E and W when Θ equals 90˚.

When measuring the coordinates of the visible corners of each obstruction block, the F/B bar should be positioned such that it coincides with the surface under consideration. The cursor should then be rotated to intersect with the corner or the furthest visible point on the obstruction block. The inner circle (Figure 5-4) is used to measure the angular coordinate of that corner while the cursor is used to measure the radial coordinate from the markings on the cursor itself.

The outer circle (Figure 5-4) represents the wind direction relative to the surface under investigation. Both circles work in unison so that when the wind is perpendicular to surface N (Figure 5-5) surfaces, E, S, and W, experience wind directions -90˚, 180˚, and -90˚ respectively.

Figure 5-4 The base layer of the protractor

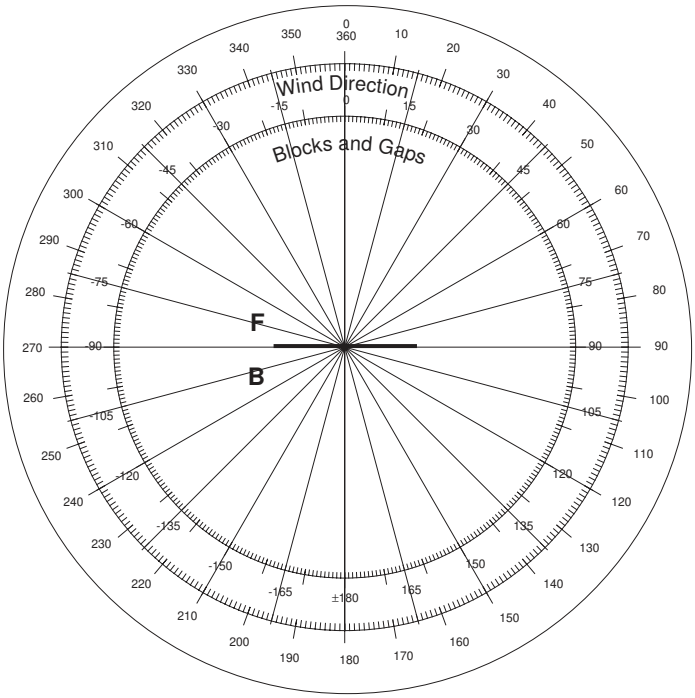

Figure 5-5 Wind directions relative to model surfaces.

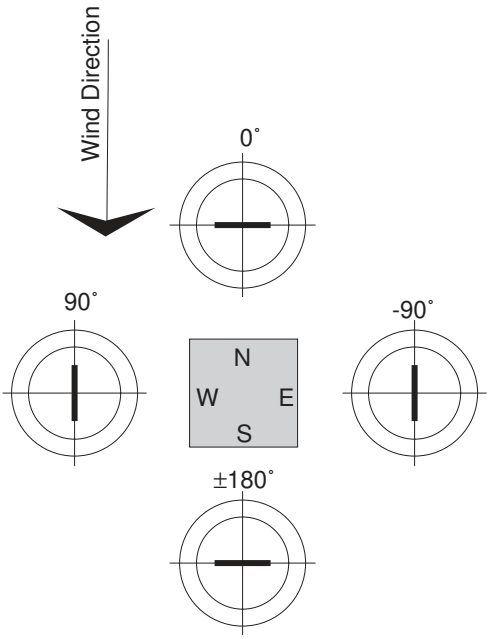

The second layer (Figure 5-6) is used in determining the Shielding Effectiveness Zone component of the mathematical model. This layer contains a line indicating the wind direction

in the middle of a transparent sector covering an arc of 140° representing the shielding effectiveness zone (SEZ). This zone of the protractor is used to determine what the surface '*sees*' at a certain wind direction. Obstruction blocks that show under the transparent SEZ are the ones to be used in the estimation of the shielding effect. Any block lying in the shaded sector Pressure Prediction Model (PPM).

Figure 5-6 The wind direction layer and cursor.

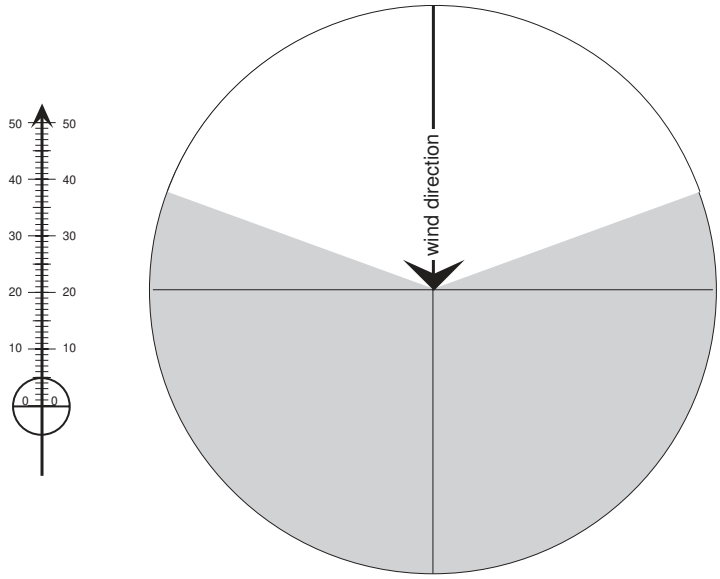

The cursor (Figure 5-6 left) is the pointing, marking, and measuring scale of the protractor from the center of the surface of the building. It is designed for two purposes. The first is to mark the polar angles of the visible edges of an obstruction block. The second, is to measure the distance to these edges.

Figure 5-7 shows an example of using the protractor. First, the user aligns the first layer on top of the model plan so that the F/B bar coincides with the surface of interest. In the example, two obstruction blocks appear in view of surface N. However,

when the second layer is positioned to match the wind direction (Θ°), the left block is no longer visible. The polar coordinates (r_1,$-\lambda_1$) and (r_2,λ_2) of the remaining block are then taken off using the inner circle of the first layer and the cursor.

Figure 5-7 An example of protractor use.

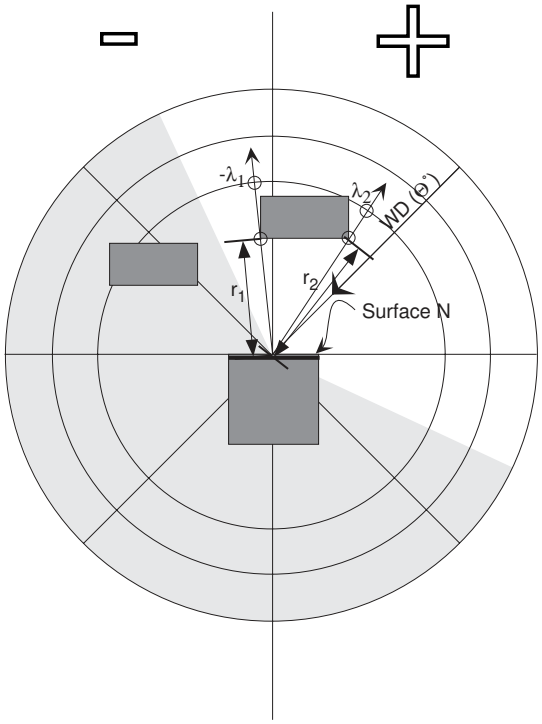

5.3.3 Calculating the Angles to Obstruction Blocks

Repeating such measurements for all wind directions using the protractor (Section 5.3.2) would be difficult for any large number of obstructions. Instead, a number of mathematical equations can be used to calculate the angles of description for the polar coordinates (r_n,λ_n) of all the visible corners of obstruction blocks. The equations are expanded to determine the visibility of obstruction blocks within the Shielding Effectiveness Zone.

5.3.3.1 Wind Direction

The discussion in Section 5.3.2 shows that for a wind direction (Θ=0˚), the four surfaces of the model experience different relative wind directions. Therefore, the conventional[2] definition of the wind direction has to be expanded. Three definitions are proposed in this section. The first definition is the conventional weather station wind direction, while the other two are relative to the surface under investigation. Even though the three definitions refer to the same actual wind, each definition is used differently in the equations for the calculations of the angles of obstruction.

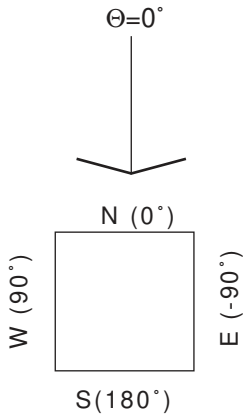

Figure 5-8 For the same wind direction, each surface experiences a different view of the wind.

5.3.3.1.1 Weather Station Wind Direction (Θ_{ws})

This definition is based on the reported wind directions from weather stations expressed in angles from 0˚-360˚ (Figure 5-9). It is the base from which other wind direction definitions are computed.

5-2 Wind direction measured at weather stations indexed to North (0°) and expressed as $0° \le \Theta \le 360°$ following a clock-wise direction.

Figure 5-9 Weather station wind direction.

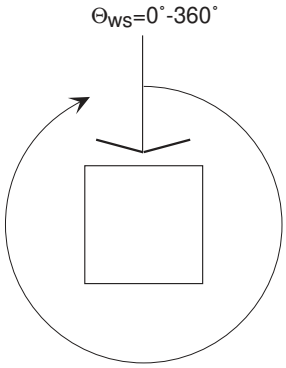

5.3.3.1.2 Model Wind Direction (Θ_{mod})

This definition is used in the calculation of all Pressure Modification Coefficients[3]. The range of this angle is defined as $0° \leq \Theta_{mod} \leq 180°$ (Figure 5-10). Hence, for surface N, the wind direction 340˚ is handled in the prediction model the same as 20˚. The only difference is the relative position of the surrounding obstruction blocks seen from the vantage point of that surface.

Figure 5-10 Wind direction as used in the prediction model.

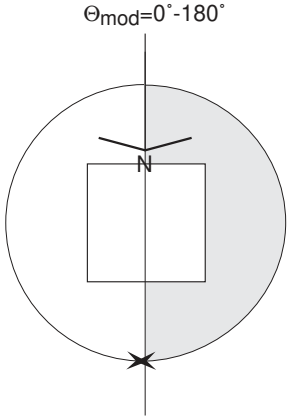

5-3 Used in all the surface pressure calculations in Chapter 4.

5.3.3.1.3 Relative Wind Direction (Θ_{rel})

The relative wind direction is used in the determination of the position of the obstruction blocks relative to the surface of interest. The relative wind direction range is 0˚-±180˚ (Figure 5-11).

Figure 5-11 Wind direction as used in the determination of the relative location of the obstruction blocks.

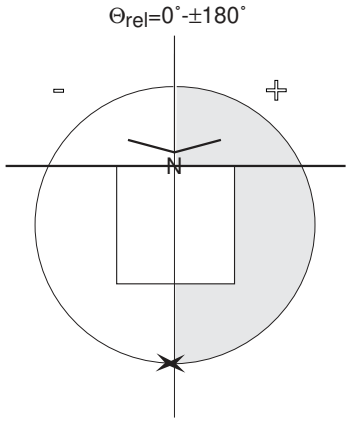

Figure 5-11 shows that for surface N, the wind direction on the right side of the line perpendicular to the surface is designated a positive sign while the left of the line is negative. At wind direction $\Theta_{ws} = 0°$, Figure 5-8 shows that the relative wind direction Θ_{rel} depends on the relative position of the surface to the wind direction. The sign of Θ_{rel} at the four sides correspond to the previously discussed convention. The following is the values of Θ_{rel} for all the surfaces at $\Theta_{ws} = 0°$:

$$\begin{aligned} &\text{Surface N, } \Theta_{rel} @ \Theta_{ws = 0°} = 0° \\ &\text{Surface S, } \Theta_{rel} @ \Theta_{ws = 0°} = 180° \\ &\text{Surface E, } \Theta_{rel} @ \Theta_{ws = 0°} = -90° \\ &\text{Surface W, } \Theta_{rel} @ \Theta_{ws = 0°} = 90° \end{aligned} \quad \textbf{(5-1)}$$

5.3.3.2 The Mathematical Definition of the Angles

In order to mathematically determine the value of the two derivative wind direction angles (Θ_{mod} and Θ_{rel}), the following algorithms have been derived;

5.3.3.2.1 Model Wind Direction (Θ_{mod})

if $(\Theta_{rel} @ \Theta_{ws = 0^\circ} + \Theta_{ws}) \geq 180^\circ$

then, $\Theta_{mod} = \left|\Theta_{rel} @ \Theta_{ws = 0^\circ} + \Theta_{ws} - 360^\circ\right|$ **(5-2)**

else, $\Theta_{mod} = \left|\Theta_{rel} @ \Theta_{ws = 0^\circ} + \Theta_{ws}\right|$ **(5-3)**

5.3.3.2.2 Relative Wind Direction (Θ_{rel})

if $(\Theta_{rel} @ \Theta_{ws = 0^\circ} + \Theta_{ws}) \geq 180^\circ$

then, $\Theta_{rel} = \Theta_{rel} @ \Theta_{ws = 0^\circ} + \Theta_{ws} - 360^\circ$ **(5-4)**

else, $\Theta_{rel} = \Theta_{rel} @ \Theta_{ws = 0^\circ} + \Theta_{ws}$ **(5-5)**

5.3.3.3 The Equivalent Obstruction Block (EOB)

In Section 4.14.2, the concept of *equivalent obstruction* was introduced. The objective then was to accommodate the orthogonal model to wind directions that were not perpendicular to the obstruction block. The same equivalency scheme is extended to encompass all non-orthogonal configurations including those created by changing the wind direction.

The polar coordinate system is used determine the four basic variables[4] for both *real* and *equivalent* obstructions. Figure 5-12 shows that the polar coordinates of two equivalent obstruction blocks are based on those of the actual blocks (a and b). The choice whether the EOB is located on the near side of the block [block (a) in Figure 5-12] or on the far side [block (b) in

5-4 α_h, α_v, α_d, and spacing.

Figure 5-12] depends on the selection of the first point from which the equivalent would be calculated ($Pt_{1\ a\&b}$).

It is therefore, essential to define which point is to be designated as Point 1 ($Pt._1$), since the mathematical description of the equivalent depends on it. Figure 5-12 shows that point 1 was chosen in such a way that the obstruction block with large windward depth (block b in Figure 5-12) will have an equivalent block of a spacing larger than the one with a shallower depth (block a). Since the vertical and displacement angles are measured from the EOB, the shielding effect of block (a) is larger than that of block (b)[5]. This selection of points order takes into account the relatively shorter wake length of block (b) in accordance with the results of Evans (Ref. 79). The slightly wider equivalent width does not lead to the over estimation of the shielding effect since the large displacement angle will guarantee the insignificance of this extension to the obstruction width.

Figure 5-12 Equivalent obstruction widths.

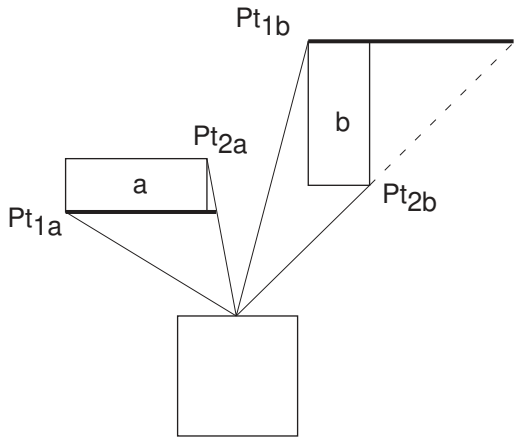

5-5 Refer to Section 4.14.2.2, page 114.

In general, the rule of thumb is that the Point 1 is always located at the edge of the longer visible surface (Figure 5-12). The following is a description of a mathematical algorithm that checks the selection of the points. The purpose of the geometric relation presented in Equation (5-6) is to eliminate the need for the user of the mathematical model to predetermine the order of each visible corners of each block.

After randomly choosing the polar coordinates of the two corners of the obstruction building (r_x,λ_x and r_y,λ_y), the following function will determine whether the order is correct or needs to be changed;

$$\text{if } \left| \frac{r_x \cdot \sin\lambda_x - r_y \cdot \sin\lambda_y}{r_y \cdot \cos\lambda_y - r_x \cdot \cos\lambda_x} \right| \leq 1 \qquad \textbf{(5-6)}$$

Therefore, choose point with higher absolute value of λ to be Point 1.

Else, choose point with lower absolute value of λ to be point 1.

5.3.3.4 Calculating the Angles of Description of Real Obstruction Blocks

This section is limited to the special case when both obstruction and equivalent obstruction block are parallel to the instrumented surface[6]. It occurs when the obstruction is parallel to the surface and the wind direction is 0˚. This special case is used as a base for general equations involving non-orthogonal configurations and wind directions other than 0˚. Figure 5-13 illustrates the input of polar coordinates of the two outer most

5-6 This means that the geometric function described in this section can not be used in the derivation of the four variables in either Scenario II or Scenario III or when $\Theta \neq o^\circ$.

visible corners of the block (pt.$_1$ and pt.$_2$) as well as the derived variables used to calculate the angles of obstruction α_h, α_v, and α_d.

Figure 5-13 Calculating the obstruction angles based on the polar coordinates when wind direction=0°.

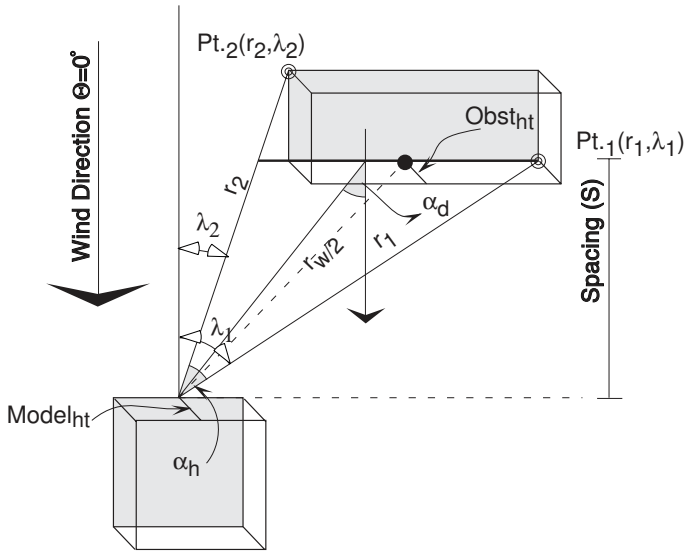

When the wind direction $\Theta = 0°$ (for orthogonal configurations), the angles of description for the *real* obstruction block are calculated as follows:

$$\alpha_h = \left|\lambda_1 - \lambda_2\right| \quad \textbf{(5-7)}$$

$$\text{Spacing } (S_o) = \cos\lambda_1 \cdot r_1 \quad \textbf{(5-8)}$$

$$r_{\text{calc}} = \frac{S_o}{\cos\lambda_2} \quad \textbf{(5-9)}$$

$$r_{w/2} = \sqrt{\left(\frac{\sin\lambda_1 \cdot r_1 + \sin\lambda_2 \cdot r_{\text{calc}}}{2}\right)^2 + {S_o}^2} \quad \textbf{(5-10)}$$

$$\alpha_v = \text{atan}\left(\frac{ht_o}{r_{w/2}}\right) \quad \textbf{(5-11)}$$

$$\alpha_d = \frac{|\lambda_1 + \lambda_2|}{2} \quad \textbf{(5-12)}$$

Where

λ_n = Polar angular coordinate of visible obstruction corner

$S_o = \dfrac{\text{Distance of obstruction block from surface}}{ht_o}$

r_n = Radial distance coordinate in Spacings (S_o)

ht_o = Obstruction height

However, it should be noted that when the obstruction block falls outside the SEZ, C_{pm} should be equals to 1.0 (Equations 4-11 and 4-13). In order to obtain $C_{pm} = 1.0$, the following values of the angles should be used:

$$\alpha_h = 0°$$
$$\alpha_v = 0° \quad \textbf{(5-13)}$$
$$\text{and } \alpha_d = 90°$$

5.3.3.5 Calculating the Angles of Description of Equivalent Obstruction Block (General Form)

For the likely occasions when the wind direction is not perpendicular to the obstruction block, a group of modified geometric functions are needed to describe the equivalent obstruction block. To avoid complicating the data input, the new derived coordinates are based on the measured polar coordinates of the visible corners (Equations 5-14 to 5-17).

In order to calculate the polar coordinates of the equivalent obstruction plane, the polar coordinates of point $Pt._{calc}$ have to be determined (Figure 5-14). This involves calculating the radial distance of the intercept to the equivalent plane and the line of vision (r_{calc}).

Figure 5-14 Polar coordinates of the EOB.

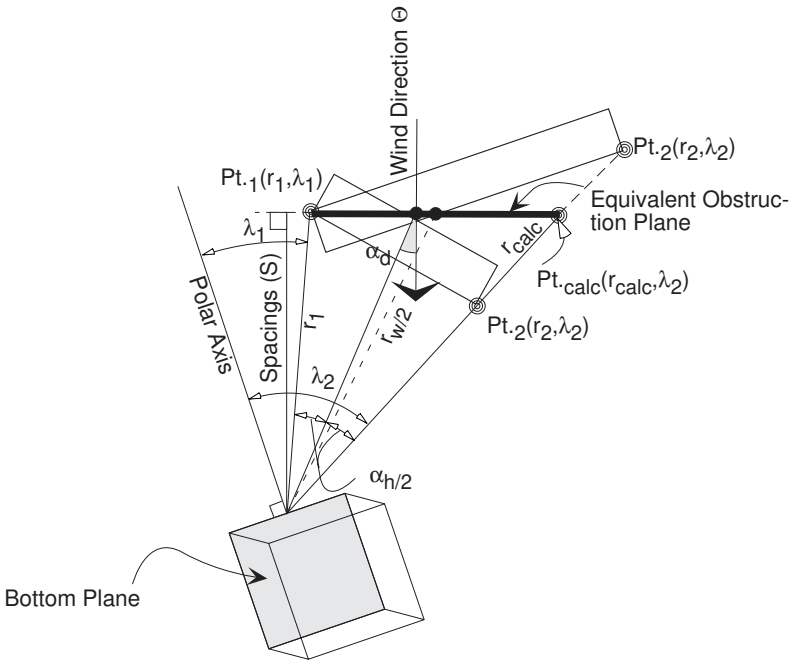

α_h (use Equation 5-7).

$$\text{Spacing}(S_o) = \cos\left|\Theta_{rel} - \lambda_1\right| \cdot r_1 \quad \textbf{(5-14)}$$

$$r_{\text{calc}} = \frac{\cos\left|\Theta_{rel} - \lambda_1\right| \cdot r_1}{\cos\left|\Theta_{rel} - \lambda_2\right|} \quad \textbf{(5-15)}$$

$\therefore$ polar coordinates are $(r_{\text{calc}}, \lambda_2)$ -Figure 5-14

$$r_{w/2} = \sqrt{\left(\frac{\sin\left|\Theta_{rel} - \lambda_1\right| \cdot r_1 + \sin\left|\Theta_{rel} - \lambda_2\right| \cdot r_{\text{calc}}}{2}\right)^2 + S_o^2} \quad \textbf{(5-16)}$$

α_v use equation 5-11[7].

5-7 It should be noted that the above calculation of the value of α_v is an approximation since the value $r_{w/2}$ of the equivalent obstruction is large than that of the original. Thus, the result will always be smaller than the actual value of α_v.

$$\alpha_d = \frac{|\lambda_1 + \lambda_2|}{2} - \Theta_{rel} \quad \textbf{(5-17)}$$

5.3.3.6 Defining the 140˚ Shielding Effectiveness Zone (SEZ)

The 140˚ limit of the shielding effectiveness zone of the obstruction block[8] is measured relative to the wind direction (Figure 5-16a). The limits of this zone always supersede those of the outer most visible angles that define the obstruction block (Figure 5-16b). However, since the 140˚ limit is based on the wind direction, while the polar coordinates are measured from the polar axis (Figure 5-15), the following relationships is developed to reconcile the two:

$$\lambda_{70} = 70° - (\Theta_{ws} - \Theta_{rel\,=\,0}) \quad \textbf{(5-18)}$$

and

$$\lambda_{-70} = (-70)° - (\Theta_{ws} - \Theta_{rel\,=\,0}) \quad \textbf{(5-19)}$$

Figure 5-15 The determination of the values of the SEZ relative to polar coordinates

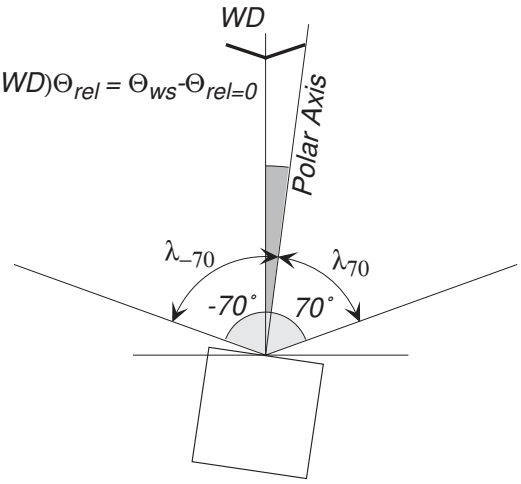

5-8 The 140˚ Shielding Effectiveness Zone is discussed in Section 4.12.2.2.2 on page 89 and illustrated in Figure 5-16a.

Consequently, the horizontal angle α_h can be defined as the visible portion of the obstruction block that lies within the 140˚ zone of shielding effectiveness (Figure 5-16a to 5-16c)[9].

As a result of this definition, Equation (5-20) represents are the polar coordinates of the point where the shielding effectiveness arc intercepts the equivalent obstruction block:

if $\lambda_n \geq 70°$, or $\lambda_m \leq (-70)°$;

$$\therefore\ [Pt_{\text{calc}} r_{\text{calc}}, ((\pm 70°) - (\Theta_{ws} - \Theta_{rel\,=\,0}))] \qquad \textbf{(5-20)}$$

5-9 The model self-shielding is also treated in the same way (Figures 5-16b and 5-16c).

Figure 5-16 Defining the 140˚ limit of the obstruction block.

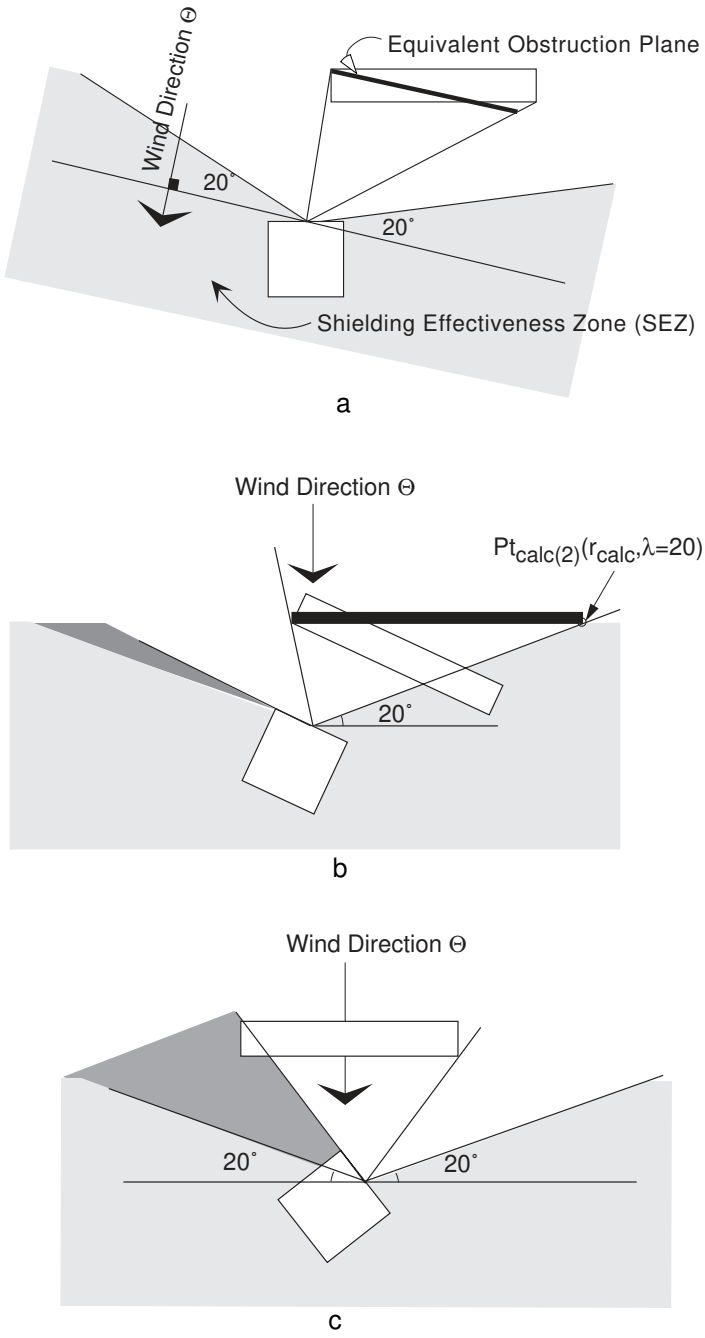

Figures 5-16c demonstrates an instance when the surface of the model under consideration obstructs the full view of the shielding block. In such cases, the self-obstruction of the

model surface should be taken into account in determining the horizontal angle of view. This should take place when measuring the polar coordinates of the visible corners of the obstruction block.

The self-shielding of the model surface reduces the viewable area of the obstruction block and consequently reduces the horizontal angle of obstruction. Similar to the 140˚ shielding effectiveness zone, this reduction supersedes the visible corners of the obstruction block.

In the example shown in Figure 5-17, *Pt.1* is determined by the self-shielding of the model surface. As a result, the polar coordinate of point *Pt.1* is (r_1,λ_1).

Figure 5-17 Self-shielding reduces the horizontal angle of view and consequently reduces the shielding effect of the obstruction block.

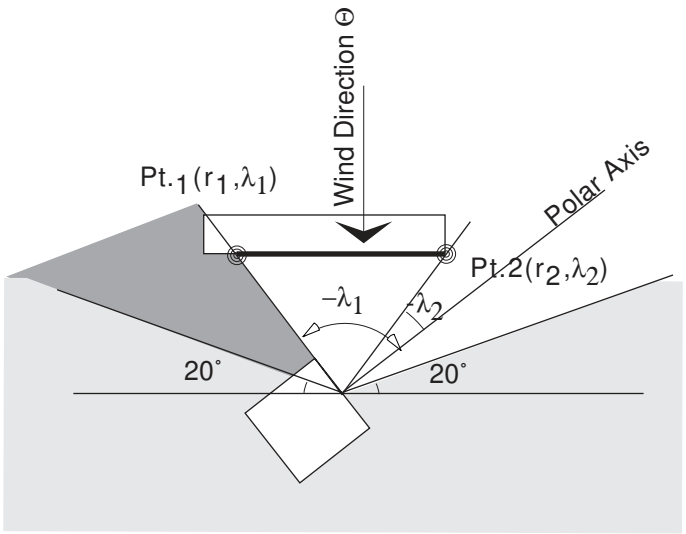

5.3.3.7 Defining a Gap

The angle that describes a gap[10] can be calculated using the polar coordinates of the points encompassing the gap

5-10 The gap is defined in Section 4.15.5, page 144.

(Figure 5-18). These coordinates are then plugged into equation 5-17 to determine the displacement angle α_{dg} of an equivalent gap whose horizontal angle of obstruction is identical to that of the original gap.

Figure 5-18 The Gap should be treated as a solid object.

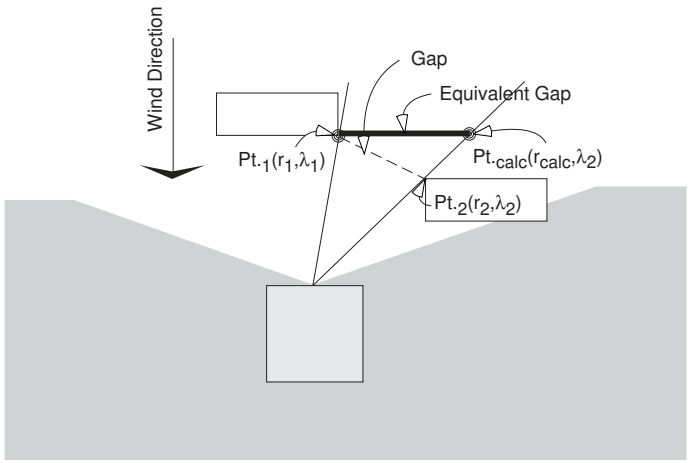

5.3.4 Complex Obstruction Blocks

The obstruction angles discussed in sections 5.3.2 and 5.3.3 are for simple obstruction block configurations. More complex obstruction configurations can include:

- Multiple obstruction blocks surrounding the surface under consideration. This level of complexity is addressed in Section 4.15 where the weighted average of the shielding effect of individual blocks and gaps was determined[11]. That approach allows the angle determination functions of individual blocks to be used in describing complex surroundings. An example of this concept is demonstrated in the verification of the model using Wiren's multiple grid-iron setup (Section 4.17.3).

5-11 See Equation 4-22.

- Complex individual obstruction blocks such as the juxtaposition of building blocks with different heights and forms. The determination of the shielding effect of the these complex forms can be obtained by breaking the complex building block into simpler components (Figure 5-19). The shielding effect of the whole complex is then determined using the multiple obstruction formula derived in Section 4.15.
- *Hidden buildings* are encountered either horizontally or vertically[12]. Figure 5-20 demonstrates the concept of the partially hidden adjacent block where only a part of an obstruction block is visible from the surface. The horizontally hidden block (left model in Figure 5-20) causes the longer block to be divided into two blocks. The higher block on the other hand, is measured as if it were fully visible despite the fact that the lower part is hidden behind the shorter and closer block (top side of the model).
- When a non-uniform layout of surrounding buildings is being considered, the method for determining the total shielding effect is not different from that of a uniform layout. The reason for this is that the non-uniform layout can be broken into individual blocks each of which can be related to the surface of concern.

5-12 Explained in Section 4.17.4.2.3.

Figure 5-19 Complex obstruction blocks.

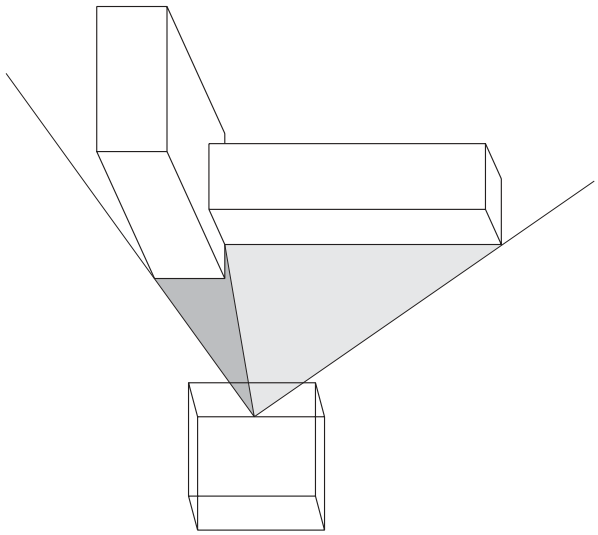

Figure 5-20 Partially. hidden obstruction blocks

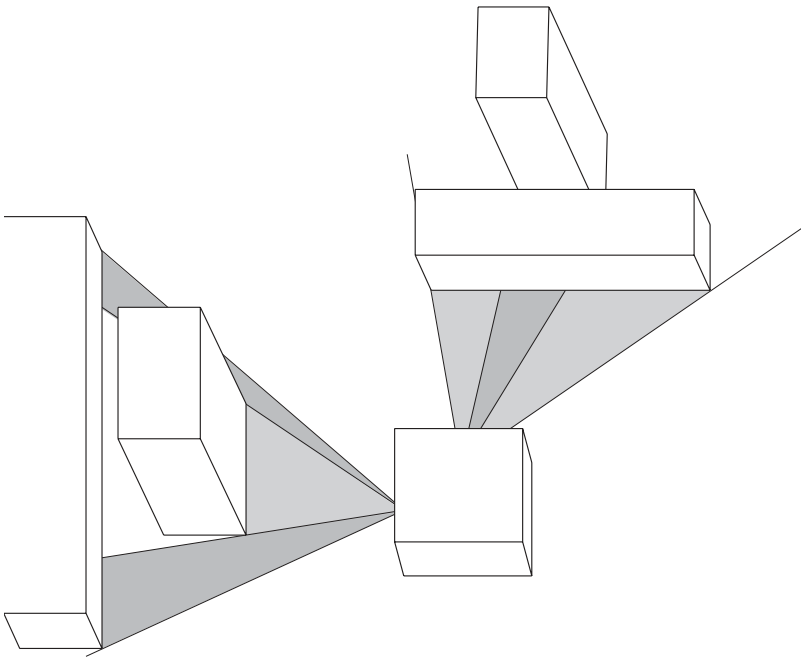

5.4 Predicting Indoor Air Velocity

The following sections describe a model to predict the indoor velocity using the pressure prediction model (PPM) discussed in Chapter 4, a model for predicting indoor velocity coefficients (IVC) developed by Ernest (Ref. 74), and a site-specific

weather data conversion procedure (SITECLIMATE) developed by Arens *et al* (Ref. 10). The combination of the three models constitutes the prediction algorithm that will be referred to as the Indoor Velocity Model (IVM).

5.5 Weather Data

Wind data come from a variety of sources. In applying them in the proposed model, one should consider the following (Ref. 10):

- Location of the station.
- Terrain and geographic features affecting climatic conditions at the location of the station.
- Height at which wind measurements were taken.
- Distance from site under consideration and a general understanding of the nature of the terrain between the site and the weather station.
- Location and setting of the sensors and the relationship with the buildings or structures in their immediate vicinity.

5.6 Pressure Data

Building surface pressure data have long been available for the structural design community (Ref. 7). Data exclusively collected for infiltration and ventilation studies have been rare until recently. Most data are for unshielded buildings. Some included the effects of surroundings in arrays of obstruction blocks (Section 4.4). The problem with these studies is that their geometries are quite specific making their results hard to generalize. Despite these limitations, researchers have developed a large body of pressure data that describe specific surface pressure for simple building blocks under numerous

conditions (Ref. 27). The proposed algorithm modifies the available pressure data for use in the IVM model by correcting for the terrain effects, the location of data sources, and the effects of immediate surrounding buildings.

5.7 Wind Speeds at Site

Available weather data are most likely to be measured at locations remote from the sites of concern such as weather stations located at airport and atop of high-rise buildings. These data as are of little use in the design of buildings located amid surrounding terrains different from those where the weather data were collected. Since the conditions at the sites may significantly differ from those at the weather station, design decisions based on the data collected at the latter can be erroneous. This section uses a method developed by Arens *et al* (Ref. 10) in 1985 to create *site-specific* weather data.

The SITECLIMAE routine corrects the weather station wind data to account for the factors affecting wind characteristics at the site. The factors include the terrain roughness, hills and escarpments, and wakes behind upwind obstructions. The first two factors will be incorporated directly in the IVM while the wake effect of obstruction blocks is accounted for by the pressure prediction part of the model (PPM) developed in this thesis.

5.7.1 Terrain Roughness and Height above the Ground

In order to account for the roughness of the terrain and the difference in height between the weather station and the site for which the wind speed is determined, the logarithmic wind profile equation (A-1) in Appendix A is used. If the distance

between the weather station and the site of concern is less than 500 m, the routine assumes that no significant change in wind characteristic takes place. However, when the distance between the weather station and building site exceeds 500 m, the procedure assumes a fully developed boundary layer profile downstream of the site. To modify the weather station data to account for the site roughness, the following equation is used to calculate the roughness factor[13] (ROGRAT).

$$\text{ROGRAT} = \left(\frac{u_f}{u_{f1}}\right) \cdot \left[\frac{\ln\left(\frac{z}{z_0}\right)}{\ln\left(\frac{z1}{z1_0}\right)}\right] \qquad \textbf{(5-21)}$$

Where

u_f = friction velocity characteristic of the site

u_{f1} = friction velocity characteristic of the weather sation

z_0 = site roughness length (see Appendix A.1.2)

$z1_0$ = weather station roughness length

According to Bietry *et al* (Ref. 36), all roughness factors are defined in terms of a particular reference height and roughness length. The reference height is 10 meters above the ground in open terrain ($z_0 = 0.07$) to match typical airport weather station conditions. With these values and using the notation:

$$p = \left(\frac{u_f}{u_{f1}}\right) \qquad \textbf{(5-22)}$$

Equation (5-21) can be written as:

5-13 The roughness factor is defined as a non-dimensional ratio that describes the modification level of wind speed downstream of a surface roughness (Ref. 10).

$$\text{ROGRAT} = 0.2p \cdot \ln\left(\frac{z}{z1_0}\right) \quad \textbf{(5-23)}$$

When multiplied by the measured wind velocity at the reference weather data location, the roughness factor (ROGRAT) predicts the velocity at height z downwind of a change in roughness from open terrain having a characteristic roughness length of z_0. Note that when z is not equal to 10 meters, Equation (5-23) also accounts for changes in height between the measurement and site locations. Table H-7 in Appendix H lists typical values of z_0 and the ratio p to apply in Equaion (5-23).

5.7.2 Hills and Escarpments

The SITECLIMATE routine also accounts for the acceleration effect of wind flowing up moderately-sloped hills. The changes in velocity at any height above a hill can be estimated using a slope factor (SLPFAC) that is defined as;

$$\text{SLPFAC}\,(\text{x},\Delta z) = \frac{U(x,\Delta z)}{U_0(\Delta z)} \quad \textbf{(5-24)}$$

Where (refer to Figure 5-21);

x = upwind distance from the top of the slope
Δz = vertical height above the local terrain
$U(x, \Delta z)$ = mean wind speed at any point
$U_0(\Delta z)$ = undisturbed upstream wind profile

Figure 5-21 Aerodynamic acceleration over a low hill without separation (Source: Arens et al (Ref. 10)

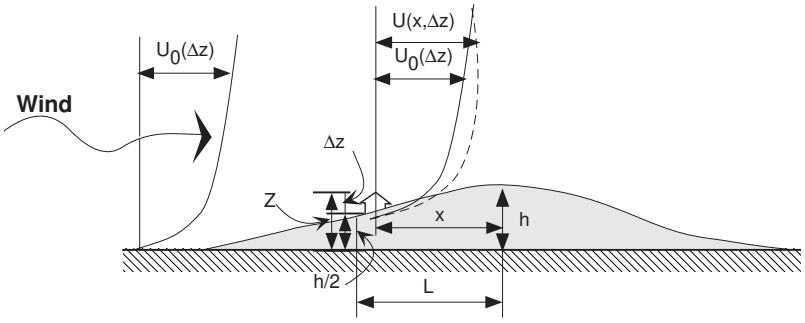

Since the *velocity perturbation* is defined as:

$$\Delta U = U(x, \Delta z) - U_0(\Delta z) \quad \textbf{(5-25)}$$

Which, in its normalized form, is defined as *fractional speed-up ratio*:, or;

$$\Delta S(x, \Delta z) = \frac{U(x, \Delta z)}{U_0(\Delta z)} = \text{SLPFAC} - 1.0 \quad \textbf{(5-26)}$$

This algorithm is applicable to moderately-sloped ($h/L < 0.5$), approaching wind ($U_0 > 3$ m/s), and constricted to windward side of the hill, and wind directions within ±45° of normal.

In order to calculate the SLPFAC, the *fractional speed-up* is estimated to be -25% of ΔS_{max} which occurs at the ground level at the top of the hill (TABLE 5-1). A linear interpolation is then used to determine the *fractional speed-up* ratio at the ground level at the building site (ΔS_{max}, site). An exponential reduction factor (RF) is calculated to account for the reduction with height of ΔS from its maximum value at the surface. The slope factor in Equation (5-26) can be rewritten as:

$$\text{SLPFAC} = 1.0 + (\text{RF}) \times \Delta S_{\max}, \text{ site} \quad \textbf{(5-27)}$$

Where[14]*:*

$$\text{RF} = e^{-\phi \Delta z / L}$$

$\Delta S_{\max}$, site = maximum fractional speed-up ratio at ground level at building site

and;

ϕ = 4.0 for the three-dimensional hills, and;
= 3.0 for the two-dimensional hills
= 2.5 for two-dimensional escarpment

TABLE 5-1 **Maximum Fractional Speed-up Ratios ($\Delta S_{\max}$) for Different Hill Shapes**[a]

Hill Description	$S_{\max}$
Two-dimensional ridge.	$2.0(h/L)$
Two-dimensional escarpment.	$0.8(h/L)$
Combination two-dimensional ridge and escarpment.	$1.4(h/L)$
Three-dimensional axisymmetric hill.	$1.6(h/L)$
Combination two-dimensional ridge and three-dimensional axisymmetric hill.	$1.8(h/L)$

a. Arens *et al* (Ref. 10).

5.7.3 Application of SITECLIMATE Factors

By applying the following equation, the designer would get reference wind speed values that approximate those at window level at the site of concern:

$$V_o = V_w \times \text{ROGRAT} \times \text{SLPFAC} \quad \textbf{(5-28)}$$

5-14 Taylor and Lee (Ref. 207).

where

V_o = reference site velocity m/s

V_w = weather station velocity m/s

5.8 Predicting Indoor Ventilation Coefficients

Ernest (Ref. 74) developed a set of empirical functions that predict the interior velocity coefficients, coefficient of spatial variation, and turbulence coefficients of interior wind flows. The mathematical relationships take into account several building configurations such as relation to wind direction, pressure on external surfaces, number, location and size[15] of openings as well as inlet-outlet relationship. Other configurations included wing walls, roof shapes, and interior partitions. This model is referred to in this study as the Indoor Velocity Coefficients (IVC) prediction model.

5.8.1 Advantages of IVC Model

- Ease of use as it is designed to be used by non-technical users.
- The model requires only few input environmental variables[16] in addition to the ones that can be taken off directly from architectural drawings.
- The broad spectrum of predicted outputs, such as velocity coefficients, turbulence levels, velocity distribution is useful for analyzing indoor thermal comfort analysis programs.

5-15 Wall porosity $(0.06 \leq \varphi \leq 0.25)$ of floor area.

5-16 These variables include pressure data, boundary layer conditions, wind directions.

- The ventilation coefficients (IVC) and shielding modification (PPM) prediction models are compatible because both studies were conducted in the same facility, using the same instrumentations, boundary layer, and pressure model.

5.8.2 Limitations of the IVC Model

- The pressure difference coefficients ΔC_p in the IVC model were derived from models with openings on the opposite sides of the instrumented model at the same height from ground surface. Thus, the functions do not apply to airflows through windows located at wall surfaces perpendicular to each other.
- The model does not account for multiple openings on a single surface.

5.9 The IVM Calculation Algorithm

The following is a summary of the steps required in the implementation of the model:

- STEP1: Determine the reference site velocity using the routine described in Section 5.7. Using the SITECLIMATE routine, correct for the effects of boundary layer differences and terrain.
- STEP 2: Determine the unobstructed surface pressures from available pressure data. This study's Pressure Modification Coefficients (PMC) model can be used to correct for the shielding effects of visible obstruction blocks on the surface pressures.

- STEP 3: Determine the average indoor velocity coefficient (C_v) using Ernest's IVC model (Ref. 74). This step is computed in four stages using four different functions accounting for wind direction (f_1), window size (f_2), interior partitions (f_3), and window accessories[17] (f_4).

$$C_v = f_1(C_p, \Theta) \cdot f_2(\varphi) \cdot f_3(p_n, \Theta) \cdot f_4 \quad \textbf{(5-29)}$$

Where

C_v = average indoor velocity coefficient

C_p = pressure coefficient

Θ = wind direction

φ = building porosity

p_n = interior partition type

- STEP 4: Determine indoor turbulence levels. The outcome of this step is to produce an average turbulence coefficient, a dimensionless indicator of the indoor turbulence intensity levels in the space under investigation.
- STEP 5: Determine indoor velocity distribution. This distribution describes the percentage floor area in which wind exceeds a specified speed. It is determined in three substeps: First, the determination of the coefficient of spatial distribution (C_{sv}). Second, calculated the velocity exceeded for a certain percentage of the space. Third, calculate the percentage of the space in which a certain speed is exceeded. It is important to note that the second and third substeps are interchangeable, i.e. if the percentage of space is given, the velocity can be estimated, and vice versa.

5-17 Window accessories in this context are referred to window type and in terms of presence and porosity of screens.

5.10 Example of IVM use

Appendix H demonstrates the use of the IVM to predict indoor air velocities in the single-space flat-roofed rectangular building located in a complex urban setting described in Section 4.17.4. The tested building has two large openings in opposite sides (north and south) and shielded by obstruction blocks on all sides. The example shows how the IVM uses the three prediction models (SITECLIMATE, PPM, and IVC) to calculate the indoor air velocity for all wind directions.

The wind rose in Figure H-22 shows the sensitivity of the mathematical model (IVM) to the surrounding obstruction blocks and their relative positions to the openings. The lowest indoor air speeds correspond to a wind direction facing the windowless sides of the instrumented model. However, the wind direction facing the window did not produce the highest predicted indoor velocities. Instead, these coincided with the wind directions flowing through the gaps between the obstruction blocks.

5.11 Conclusion

This chapter is devoted to the implementation of the Pressure Prediction Model (PPM) developed in Chapter 4. A set of functions has been developed in the first part of the chapter to calculate the obstruction angles for visible blocks at any wind direction. These functions were formulated so that the 140˚ shielding effectiveness zone, self-shielding, and obstruction visibility in relation to wind direction, are all taken into consideration.

The study sets the rules governing the treatment of multiple and complex obstruction blocks by breaking them into individual units of simple rectangular geometries. Partially visible objects are also handled by rules set in the chapter. If the obstruction block is seen above a closer and shorter one, the model deals with it as a completely visible block. On the other hand, parts of a model that can be seen behind the sides of a shorter and closer model are considered as separate obstruction blocks.

The second part of the chapter deals with the combination of the PPM with an indoor velocity coefficient prediction model developed by David Ernest (Ref. 74). A third routine is added to convert weather station data to outdoor air velocities at the site. This routine is developed by Arens *et al* (Ref. 10) to determine the wind speeds at the site from measurements at the weather station considering the differences in the terrain at the two locations and the topography at the site. The combination of the three models is referred to as the Indoor Velocity Model (IVM) and its use is demonstrated in Appendix H .

Chapter 6

6

Conclusions and Recommendations

6.1 Summary of Findings

Thermal comfort issues in designed spaces should not be tackled as fixes to environmental problems rising form the specific design solution. Instead, early consideration of climatic impact on space and form should be an integral part of the design process.

Airflow is among the climatic elements that a designer may manipulate to achieve thermal comfort for occupants of architectural spaces. This study aims at providing designers with the ability to predict indoor air velocity of buildings located in an urban setting.

In developing a tool for predicting building pressure and airflows, the traditional measure of spacing between obstruction blocks and the test building was not the only variable to predict pressure coefficients. For the same spacing, one would find substantially different wind pressure coefficients, resulting from factors such as size, shape, and number of obstruction blocks and their relative position to the wall surface of concern.

On the other hand, the proposed angular description of visible surrounding buildings was found to successfully describe the shielding effect of the tested building. The reason is that these angles include in their definition the spatial description of the obstruction blocks and their locations and heights relative to the tested surfaces. The obstruction and gap visibility criterion was true in most tested situations, except in instances when air is channeled to surfaces that cannot see the gaps. When this happens, the result is always underestimating the wind pressures.

The study showed that a three dimensional block can be represented (geometrically) by a two dimensional equivalent plane. This plane has the same horizontal angle of obstruction of the 3-D object it replaces. The advantage of using an equivalent plane is that, for wind directions other than 0˚, the model assumes that the obstruction block is always perpendicular to the wind direction. The resulting 2-D obstruction is easier to describe mathematically and does not sacrifice accuracy of the model.

The shielding effect of multiple obstruction blocks can be computed or estimated by averaging[1] the shielding effect of individual blocks. However, averaging alone produces a weighted value that does not take into account the effect of the gaps between the surrounding buildings. The effect of gaps can be added to the average shielding effect of windward

6-1 Using geometric averaging of Pressure Modification Coefficients of individual obstruction blocks. (See Section 4.15.6).

obstruction blocks. Thus providing a complete description of the obstruction field of view as seen by the surface of interest.

Analysis shows that neither the gap width nor its distance from the surface influences the gap effect. Instead, the effect is directly correlated to the position of the gap relative to the building surface.

Since the product of this mathematical model is an estimate of surface pressures, any of the ventilation prediction algorithms that use these values can be used to predict the ventilation rates within a space. Accurately predicted surface pressure coefficients will allow these existing ventilation models to respond well to the urban setting in which the building is situated.

6.2 Impact of Study

The proposed Indoor Velocity Model (IVM) is aimed at providing the designer with a tool to predict natural ventilation in indoor environments based on the knowledge of the surrounding buildings. With this knowledge, the designer would be able to incorporate natural ventilation into the design of residential and other comparable low-rise buildings in the context of a built-up area. The benefits of this incorporation can be categorized in the following;

The IVM developed in this study can be used to help the designers to predict energy uses of a space. The pressure prediction component of the model provides a key step towards predicting energy uses resulting from infiltration-driven thermal loads. Indoor velocity estimation derived from C_p can be

used to predict thermal comfort and nighttime structural cooling.

If indoor thermal comfort in ventilated buildings could be accurately predicted, one would expect energy efficiency to benefit from such knowledge. The designer has an accessible tool for studying the effect of changing window location, size, building orientation on the overall energy usage of a space. By considering the surrounding buildings and gaps, the designer can obtain more realistic predictions of natural ventilation in urban settings.

Infiltration-driven thermal loads depend in part on the difference between the exterior and interior surface pressures. The infiltration algorithms in energy analysis programs can benefit from the input of this model. Through such programs, energy standards may better account for ventilation and infiltration. Thus, by rewarding the designer for her/his application of various ventilation strategies, reliance on air-conditioning may be reduced.

With the IVM, operable windows for ventilation can be better incorporated in the architectural design. Since surrounding buildings affect airflow in or around the building wall surfaces, this model could play a role in the selection of window location and sizing.

The ability to accurately and reliably predict natural ventilation, can help reduce air-conditioning use as a supplement to the overall cooling system. As a result of the partial reduction in cooling loads, smaller air-conditioning units would be used.

In addition, by accounting for the effects of the surrounding buildings, the resulting surface pressures which are usually lower than those of published data (*for isolated buildings*) may further reduce the air-conditioning component sizes as a result of the lower expected infiltration rates.

6.3 The Model as a Design Tool

The model can be used as a tool that allows the designer to evaluate different ventilation-promoting design solutions early in the design process. The variation may include the location of windows, spacing and location of walls relative to neighboring buildings.

The example demonstrated in Appendix H shows how the model can also be used to predict natural ventilation knowing the surrounding buildings, and some design elements of the building. This usage represents a post-design evaluation of a proposed or even an existing structure.

Window sizing is another way the proposed model can be used as design tool. Arens and Watanabe (Ref. 13) have published a method for designing naturally ventilated buildings using bin climate data in which the window sizing procedure requires surface pressures[2]. A component of IVM model (Pressure Prediction Model) can produce site-specific pressure values that replace the tabulated data[3] and surrounding building correction factors[4] suggested by the authors.

6-2 Steps 8 and 9 in the window sizing procedure (Ref. 13).

6-3 Tables A-1 and A-2 (ibid).

6-4 Table A-3 (ibid).

6.4 Unique Features of the IVM Model

The following is a summary of the of advantages of the proposed mathematical model and prediction method;

- The prediction model takes into account the effect of both the spacing between the obstruction buildings and the gaps between individual blocks.
- It links between the effect of the individual obstruction building and the effect of multiple obstructions.
- It can be used to predict indoor airflows in most urban layouts.
- The pressure prediction component of the model can be used as source of input data for many ventilation prediction methods that use pressure coefficients in their calculation.
- The IVM model may be used as source of input data for various energy estimation and thermal comfort prediction algorithms.

6.5 Limitation of the IVM Model

As in any model based on empirical studies, the application of the suggested coefficients is limited by the range of variables included in the determination of those coefficients. The following is an itemization of the limitations of the proposed procedure:

- Only simple single-space models were used in the derivation of the functions.
- Average coefficients do not help in identifying the pressure distribution across the surface which may vary drastically in the same surface.
- The model allows velocity prediction only for rectangular buildings with sharp edges, since the model is based on wake shapes of rectangular blocks.

- No vegetation or permeable obstruction were studied.
- The model overestimates the shielding effect of the displaced wake configurations.
- The model does not predict pressures on the roof surfaces, or the effect of roof pitch on the surface pressures.
- The model does not predict the effect of any gaps that cannot be seen from the surface. These gaps can affect the pressure if the gap redirects the wind.
- No model spacing ($S_m < 1$) was tested.

6.6 Future Work

the follwing is a list of items and topics for future work:

- The development of a simplified manual method for quickly and roughly estimating the impact of surrounding buildings on specific building wall. This method should be developed to help the designer during the early design stages.
- Expand the model to include high-rise buildings.
- Include roof form, pitch, and eaves in the model.
- Develop functions to predict surface pressure distribution on shielded building surfaces.
- Expand the model to predict pressure at any point of the surface and where windows are located rather than the mean for the whole surface.
- Correct for, and take into account the effect of displaced wakes.
- Consider gaps that can not be seen from the surface but act as channels for the wind to reach the site and the surface of concern.
- Test model spacings $S_m < 1$.

- Include functions to determine the shielding effects of permeable object such as trees, wind screens or fences.

7

Bibliography

7.1 Ventilation:

1. Air Infiltration and Ventilation Centre (AIVC). 1987. Natural Ventilation of School Buildings, Research Report, Second Consortium of Local Authorities, Air Infiltration and Ventilation Centre, Great Britain.

2. Akbari, H., Y.J. Huang, and H. Taha. Date Unknown, The Wind-shielding and Shading Effects of Trees on Residential Heating and Cooling Requirements, Technical Report: LBL-24131.

3. Akins, R. E., J.A. Peterka, and J.E. Cermak. 1977. "Mean Force and Moment Coefficients for Building Turbulent Boundary Layers." Journal of Industrial Aerodynamics,Vol.2, pp. 195-209.

4. Allard, F., E. Dascalaki, K. Limam, and M. Santamouris. September 1996. "Natural Ventilation Studies within the EC PASCOOL Joule II Project." Air Infiltration Review, The World Wide Web Edition,Vol.17, no. 4,.

5. Allard, F., and M. Herrlin. 1989. "Wind-induced Ventilation." ASHRAE Transactions,Vol.95, no. 2,

6. Alp, Ahmet Vefik. 1991. "Vernacular Climate Control in Desert Architecture." Energy and Buildings,Vol.16, pp. 809-815.

7. American Society of Civil Engineers. 1987. Wind Tunnel Model Studies of Buildings and Structures, New York,

American Society of Civil Engineers, ASCE Manuals and Reports on Engineering Practice No. 67.

8. Anton, Howard, Calculus with Analytic Geometry. John Wiley and Sons, New York, 1980.

9. Arens, Edward A. 1976. Aerodynamic Effects of terrain, Vegetation, and Wind Screens, [Transcript].

10. Arens, E. A., E. Lee, F. Bauman, and Flynn L. 1985. "SITECLIMATE: a Program to Create Hourly Site-specific Weather Data." Proceedings of the ASHRAE/DOE/ BETCC Conference on Thermal Performance of the Exterior Envelopes of Buildings III, Clearwater Beach, FL, pp. 91-108.

11. Arens, E. A., A. G. Blyholder and G. E. Schiller. 1984. "Predicting Thermal Comfort of People in Naturally Ventilated Buildings." ASHRAE Transactions, Vol. 90, Part 1B:.

12. Arens. E.A, and J. Peterka. 1986 1. "Controlling the Wind Climate around Buildings", in Civil Engineering Practice, Vol. 1, No. 1, Boston, MA.

13. Arens, E. A. and N. Watanabe. 1986 2. "A Method for Designing Naturally Cooled Buildings using Bin Climate Data." ASHRAE Transactions, Vol. 92, Part 2B:.

14. Arens, Edward A., and Phillip B. Williams. 1977. "The effect of Wind on Energy Consumption in Buildings." Energy and Buildings,Vol.1, pp. 77-84.

15. Ashley, Sophia, and Max Sherman. 1984. "The Calculation of Natural Ventilation and Comfort." ASHRAE Transactions,Vol.90, no. 1B, pp. 253-271.

16. ASHRAE. 1989 1. ASHRAE Standard 62-1989, Atlanta, GA, American Society of Heating, Refrigerating and Air-conditioning Engineers.

17. _____. 1989 2. ASHRAE Standard AHRAE/IES 90.1–198, Atlanta, GA, American Society of Heating, Refrigerating and Air-conditioning Engineers.

18. _____. 1989 3. “Chapter 14: Air Flow Around Buildings.” ASHRAE Handbook of Fundamentals, Atlanta: American Society of Heating, Refrigerating and Air-conditioning Engineers, Inc.

19. _____. 1989 4. “Chapter 23: Infiltration and Ventilation.” ASHRAE Handbook of Fundamentals, Atlanta: American Society of Heating, Refrigerating and Air-conditioning Engineers Inc.

20. _____. 1989 5. “Chapter 24: Weather Data.” ASHRAE Handbook of Fundamentals, Atlanta: American Society of Heating, Refrigerating and Air-conditioning Engineers Inc.

21. _____. 1981 1. Standard 55-81 - Thermal environment conditions for human occupancy. Atlanta: American Society of Heating, Refrigerating and Air-conditioning Engineers, Inc.

22. _____. 1981 2. Cooling and Heating Calculation Manual, Atlanta, GA: American Society of Heating and Refrigerating and Air-conditioning Engineers, Inc.

23. Awbi, H. B. 1991. Ventilation of Buildings. London: E & FN Spon.

24. Aynsley, Richard M. 1989. “The Estimation of Wind Pressures at Ventilation Inlets and Outlets of Buildings.” ASHRAE Transactions, Vol. 95, Part 2:.

25. _____. 1982. “Natural Ventilation Model Studies.” in Proceedings of the International Workshop on Wind Tunnel Modeling Criteria and Techniques for Civil Engineering Applications, ed. A. Reinhold Timothy. Gaithersburg, Maryland, USA, April. Cambridge University Press, pp. 465-485.

26. _____. 1985. “Modeling Parameters for Boundary Layer Wind Tunnel Studies of Natural Ventilation.” ASHRAE Transactions,Vol.91, no. 2A,

27. _____,1982. “Natural Ventilation Model Studies.” Proceedings of the International Workshop on Wind

Tunnel Modeling Criteria and techniques for Civil Engineering Applications, Timothy A. Reinhold. Cambridge, New York: Cambridge University Press, pp 465-485.

28. _____. 1988. "A Resistance Approach to Estimating Natural Airflow through Buildings with Large Openings due to Wind." ASHRAE Transactions,Vol.94, part 2,

29. Aynsley, Richard M., and Marcus Spruill. Date Unknown. "Thermal Comfort Models for Outdoor Thermal Comfort in Warm Humid Climates and the Probabilities of Low Wind Speeds." [Transcript]

30. Aynsley, R. M., Melbourne W., Vickery B. 1977. Architectural Aerodynamics. London: Applied Science Publishers.

31. Baechlin, Wolfgang. 1987. "Pressure inside Buildings – A Dominant Parameter for Calculating Effective Natural Ventilation." Indoor Air '87, Proceedings of the 4th. International Conference on Indoor Air Quality and Climate, Vol. 3, pp. 337-341.

32. Baker, P. H., R.D. Heap, and S. Sharples. 1986. "Airflow though Perforated Screens at Small Pressure Difference." Building Services Engineering Research & Technology, Vol. 7, no. 2, pp. 96-97.

33. Balazs, K. 1989. "A Wind Pressure Database from Hungary for Ventilation and Infiltration Calculations." Air Infiltration Review, Vol. 10, No. 4:.

34. Bauman, F., D. Ernest and E. Arens. 1988. ASEAN Natural Ventilation Study: Wind Pressure Distributions on Long Building Rows in Urban Surroundings. Final Report, CEDR-03-88. Berkeley, CA: Center of Environmental Design Research, University of California Berkeley.

35. _____. 1988. "The Effects of Surrounding Buildings on Wind Pressure Distributions and Natural Ventilation in Long Building Rows." ASHRAE Transactions, Vol. 94, Part 2:pp. 1670-1695.

36. Bietry, J., C. Sacre, and E. Simu. 1978. “Mean Wind Profiles and Change of Terrain Roughness”. Journal of the Structural Division, ASCE 104, No ST10, pp. 1585-1593.

37. Blomsterberg, A. 1992. “Improved Ventilation Combined with Energy Efficiency in Naturally Ventilated Houses.” Ventilation for Energy Efficiency and Optimum Indoor Air Quality, 13th. AIVC Conference, Nice, France, pp. 166-174.

38. Bloomfield, D. P., K. J. Lomas, and J.C. Martin. April 1992. Assessing Programs which Predict the Thermal Performance of Buildings. BRE Information Paper.

39. Borges, A. R. Janeiro, and J.A. Gil Saraiva. 1983. “Ventilation Rates of Two Communication Low Rise Buildings as Affected by Terrain Roughness.” Journal of Wind Engineering and Industrial Aerodynamics,Vol.15, pp. 39-46.

40. Bowen, Arthur J. 1976. A Wind Tunnel Investigation using Simple Building Models to Obtain Mean Surface Wind Pressure Coefficients for Air Infiltration Estimates, Report LTR-LA-209, National Research Council Canada.

41. _____. 1983. “Design Guidelines on Lateral Airflow through and around Buildings.” Second International PLEA Conference, Oxford, Pergamon Publishers, pp. 517-533.

42. _____. December 1976. A Wind Tunnel Investigation using Simple Building Models to Obtain Mean Surface Wind Pressure Coefficients for Air Infiltration Estimates, National Research Council Canada, Report LTR-LA-209.

43. _____. 1981. ““Historical Responses to Cooling Needs in Shelter and Settlement, Proceedings of the International Passive and Hybrid Cooling Conference, American Section of the International Solar Energy Society.

44. Busch, John F. 1992. "A Tale of Two Populations: Thermal Comfort in Air-conditioned and Naturally Ventilated Offices in Thailand." Energy and Building,Vol.18, pp. 235-249.

45. Byrne, S. J., Y. J. Huang, R. L. Ritschard and D. M. Foley. 1986. "The Impact of Wind Induced Ventilation on Residential Cooling Load and Human Comfort." ASHRAE Transactions, Vol. 92, Part 2:pp. 793-803.

46. California Energy Commission. 1988. Energy Conservation Manual for New Residential Buildings. Sacramento, CA.

47. Caudill, William W, Sharman E. Crites, and Elmer G. Smith. 1951. Some General Considerations in the Natural Ventilation of Buildings. Research Report, Texas Engineering Experiment Station, College Station, TX.

48. Cermak, J. E., M. Poreh, J. A. Peterka and S. Ayad. 1982. Wind Tunnel Investigation of Natural Ventilation American Society of Civil Engineers Convention and Exhibit Preprint. New Orleans: LA., Preprint 82-519.

49. Chand, I. and Krishak N.L.V. 1969. "Effect of Window Size, Location, and Orientation on Indoor Air Motion." Journal of the Institute of Engineers (India), CI Vol. 49:pp. 375-378.

50. Chand, I., N. L. V. Krishak and V. K. Sharma. 1975. "Studies of Air Motion in Shielded Buildings." The Indian Engineer Vol. 19, pp. 23-29.

51. Chand, Ishwar, V.K. Sharma, and N.L.V. Krishak. 1989. "Ventilation Survey of Typical Airy Buildings – A Few Case Studies in Hot Dry and Hot Humid Zones of India." Building and Energy, Vol.24, no. 3, pp. 229-238.

52. Chand, Ishwar. Date Unknown. "Wind Induced Ventilation in Shielded Buildings." Report, Central Building Research Institute, Roorkee, India.

53. Chandra, Subrato, Philip W. Fairey, and Michael M. Houston. 1986. Cooling with Ventilation, Golden Colo-

rado: Solar Energy Research Institute, Report no. SERI/SP-273-2966.

54. Chandra, Subarto, and Philip W. Fairey. 1982. Passive Cooling by Natural Ventilation, Florida Solar Energy Center.

55. Chandra, Subarto, and Philip W. Fairly. 1981. Passive Cooling by Natural Ventilation: a Literature Review, Draft Final Report Task 1, Florida Solar Energy Center, Report number FSEC-CR-81-27 (TT), Caper Canevral, Florida.

56. Chien, Ning et. al. 1951. Wind-tunnel Studies of Pressure Distribution on Elementary Building Forms, Iowa Institute of Hydraulic Research, State University of Iowa.

57. Choinière, Y., H. Tanaka, J.A. Munroe, and A. Suchorski-Tremblay. 1991. "Prediction of Wind-Induced Ventilation for Livestock Housing." 8th. Annual ICWE (Draft).

58. Choinière, Y., J.A. Munroe, and A.S. -Tremblay. 1992. "NATVENT Software Predictions versus Full-scale Estimates of Wind Induced Natural Ventilation in a Swine Barn." Agricultural Institute of Canada Annual Conference.

59. Chow, W. K., and W.Y. Fung. 1994. "Investigation of the Subject Response to Elevated Air Velocities: Climate Chamber Experiments in Hong Kong." Energy and Building,Vol.20, pp. 187-192.

60. Clifford, M. J., P.J. Everitt, R. Clarke, and S.B. Riffat. 1997. "Using Computational Fluid Dynamics as a Design Tool for Naturally Ventilated Buildings." Building and Environment,Vol.32, no. 4, pp. 305-312.

61. Cook, Jeffrey. 1989. Passive Cooling, Cambridge, Massachusetts: The MIT Press.

62. Cook, N. 1982. "Simulation Techniques for Short Test-section Wind Tunnels: Roughness, Barrier, and Mixing-device Methods." Proceedings of the International

Workshop on Wind Tunnel Modeling Criteria and Techniques for Civil Engineering Applications, pp. 126-136.

63. _____. 1977. "Determination of the Model Scale Factor in Wind-tunnel Simulations of the Adiabatic Atmospheric Boundary Layer." Journal of Industrial Aerodynamics,Vol.2, pp. 311-321.

64. Cooper, Alison. March 1993. "Using CFD Techniques to Evaluate Wind Pressure Distribution for Air Infiltration Analysis." Air Infiltration Review,Vol.14, no. 2.

65. Cowan, H. 1980. Solar Energy Applications in the Design of Buildings, Applied Science Publishers Ltd. London.

66. Degelman, L. O. 1986. Bin and Degree Hour Weather Data for Simplified Energy Calculations. Atlanta: American Society for Heating Refrigerating, and Air-conditioning Engineers, Inc.

67. Department of the Air Force, the Army, and the Navy. 1978. Engineering Weather Data. Publication AFM 88-29, Washington D.C.

68. Dick J.B. October 1951. "Ventilation Research in Occupied Houses." Vol.19, pp. 306-326.

69. _____. June 1950. "The Fundamentals of Natural Ventilation of Houses." Journal of the Institute of Heating and Ventilating Engineers,Vol.18, pp. 123-134.

70. _____. December 1949. "Experimental Studies in Natural Ventilation of Houses." Vol.17, pp. 429-466.

71. Dubin, Fred S and Chalmers G. Long Jr. 1978. Energy Conservation Standards for Building Design, Construction, and Operation. McGraw-Hill Co. New York.

72. Engineering Sciences Data Units,1983. Strong Winds in the Atmospheric Boundary Layer, London: ESDU International Ltd.Item No. 83045.

73. Engineering Sciences Data Units,1984. Longitudinal Turbulence Intensities over Terrain with Roughness

Changes for Flat or Hilly Sites, London: ESDU International Ltd.Item No. 84030.

74. Ernest, D. R. 1991. Predicting Wind-Induced Indoor Air Motion, Occupant Comfort, and Cooling Loads in Naturally Ventilated Buildings. Doctoral Dissertation. Berkeley: Department of Architecture, University of California, Berkeley.

75. Ernest, D. R., F. Bauman and E. Arens. 1991. "The Prediction of Indoor Air Motion for Occupant Cooling in Naturally Ventilated Buildings." ASHRAE Transactions, Vol. 97, Part 1.

76. _____. 1991 2. "The Prediction of External Wind Pressure on Wind-induced Air Motion inside Buildings." Proceedings of the 8th. International Conference on Wind Engineering, July 8. London, Ontario.

77. Etheridge, D. W., and J.A. Nolan. 1979. "Ventilation Measurements at Model Scale in a Turbulent Flow." Building and Environment,Vol.14, pp. 53-64.

78. Evans, Benjamin H. 1979. "Energy Conservation with Natural Airflow through Windows." ASHRAE Transactions,Vol.85 Part 2, pp. 641-650.

79. _____. 1975. Natural Airflow around Buildings. Research report No. 50, Texas Engineering Experiment Station, College Station, TX.

80. Fanger, P.O. 1992. "Efficient Ventilation for Human Comfort." International Symposium on Room Air Convection and Ventilation Effectiveness, University of Tokyo Japan.

81. Fanger, P.O. 1990. "New Principles for a Future Ventilation Standards." The Fifth International Conference on Indoor Air Quality and Climate, July 29-August 3, Toronto, Canada, pp. 353-363.

82. Fanger, P. O., A.K. Melikov, H. Hanzawa, and J. Ring. 1988. "Air Turbulence and Sensation of Drought." Energy and Buildings,Vol.12, pp. 21-39.

83. Fanger, P.O., and C.J.K. Pedersen,1977. "Discomfort due to Air Velocities in Space." Proceedings of Meeting of Commission B1, B2, E1 of the International Institute of Refrigeration, Vol. 4, pp 289-296.

84. Farrel, Cesar and M. Sitheeq. 1993, "Wind Pressure Distribution on Sheltered Buildings: An Analysis of Existing Data for Application to Infiltration Loss Estimates." Conference Proceedings: The 7th. U.S. National Conference on Wind Engineering. Vol.1, June 27-30, UCLA, pp. 223-232.

85. Fernandez, A., S. de Schiller, and J.M. Evans. 1991. "Wind in Urban Spaces: Development and Application of an Evaluation Method." Architecture and Urban Space, Sept.1991 Seville, Spain, Kluwer Academic Publishers, pp. 35-40.

86. Fleury, B., and C.Nicolas. 1992. "Occupant's Behaviour with Respect to Window Opening: A Technical and Sociological Study." Ventilation for Energy Efficiency and Optimum Indoor Air Quality, 13th. AIVC Conference, Sept.92, Nice, France, pp. 198-206.

87. Fountain, Mark. December 1993. Laboratory Studies of the Effect of Air Movement on Thermal Comfort: A comparison and Discussion of Methods. Draft Report, Center for Environmental Design, University of California, Berkeley.

88. Fontaine, J. R., F. Biolley, R. Rapp, and J.C. Sérieys.Sept. 1991. "Ventilation Flow Analysis - Flow Visualization and LDA Measurements in Water Scale Models, Validation of Numerical Results." Air Movement and Ventilation Control within Buildings, 12th AIVC Conference, Ottawa, Canada, pp. 47-75.

89. Fürbringer, Jean-Marie, and Hacobus Van Der Maas. 1995. "Suitable Algorithms for Calculating Air Renewal Rate by Pulsating Air Flow Through a Single Large Opening." Building and Envrionemnt,Vol.30, no. 4, pp. 493-503.

90. Gadilhe, A., L. Janvier, and G. Barnaud. 1993. "Numerical and Experimental Modeling of the Three-dimensional Turbulent Wind Flow through an Urban Square." Journal of Wind Engineering and Industrial Aerodynamics,Vol.46 & 47, pp. 755-763.

91. Gadilhe, Agnès, and Camille Solliece. December 1990. Coefficients de Pression: Faisabilité d' un détermination numérique, CSTB Paris, France Centre Scientifique et Technique du Batiment 315.

92. Gandemer, Jacques, and Guy Barnaud. 1989. Ventilation Naturelle en Climat Tropical Humide: Prise end Compte du Vent dans l'Habitat. CIB, pp. 227-236.

93. Gandemer, Jacques, and Alain Guyot. 1981. La Protection Contre le Ven: Aérodynamique des Brise-vent et Conseils Partiques. Paris, France: Centre Scientifque et Technique du Batiment (CSTB),

94. Gandemer, J. 1975. "Wind Environment around Buildings: Aerodynamic Concepts." Proceedings of the 4th. International Conference on Wind Effects on Buildings, pp 423-432.

95. Gaze, A. I.,1986. Natural Ventilation of Buildings – A Review, with an Annotated Bibliography, Research Report 11/86: Timber Research and Development Association.

96. Geiger, Rudolf,1975. The Climate near the Ground, 5th. ed. Cambridge, Massachusetts: Harvard University Press.

97. Givoni, Baruch. 1998. Climate Considerations in Building and Urban Design. New York: Van Nostrand Reinhold.

98. Givoni, Baruch. 1994. Passive and Low Energy Cooling of Buildings. New York: Van Nostrand Reinhold.

99. Givoni, Baruch. 1992. "Comfort, Climate Analysis and Building Design Guidelines." Building and Environment,Vol.18, pp. 11-23.

100. _____. 1991. "Urban Design for Humid and Hot Dry Regions." Architecture and Urban Space, Seville, Spain, Kluwer Academic Publishers, pp. 19-31.

101. _____. 1984. "Options and Applications of Passive Cooling." Energy and Buildings,Vol.7, pp. 297-300.

102. _____. 1981. Man, Climate, and Architecture. New York: Van Nostrand Reinhold.

103. _____. June 1965. "Laboratory Study of the Effect of Window Size and Location on Indoor Air Motion." Architectural Science Review, pp. 42-45.

104. _____. 1964. "Physiological and Architectural Aspects of Ventilation in a Hot Climate." Natural Ventilation of Rooms,Vol.4, pp. 31-34.

105. Glaumann, Mauritz. Date Unknown. Wind Environment in Housing Areas in Sweden. The National Swedish Institute for Building Research.

106. Glaumann, Mauritz, and Ulla Westerberg. Date Unknown. Climatic Planning-Wind. The National Swedish Institute for Building Research.

107. _____.Date Unknown. Estimation of Local Windiness. The National Swedish Institute for Building Research.

108. Gowda, B.H. Lakshmana and M. Sitheeq. 1990. "Effect of Interference on the Pressure Distribution on the Ground Plane around two Low-rise Prismatic Bodies in Tandem Arrangement." Applied Scientific Research, Vol. 47, pp. 129-149.

109. Grimsrud, D. T. 1990. "Future Directions for Ventilation Standards." The Fifth International Conference on Indoor Air Quality and Climate, July 29-August 1990, Toronto, Canada, pp. 365-369.

110. Grosso Mario. 10 September 1989. "Pressure Distribution." COMIS Fundamentals, TG VII Draft.

111. _____. 1992. "Wind Pressure Distribution around Buildings: A Parametrical Model." Energy and Buildings, Vol. 18, pp. 101-131.

112. Gustén, Jan,1989. Wind Pressures on Low-rise Buildings: An Air Infiltration Analysis Based on Full-scale Measurements, Gothenburg: Division of Structural Design, Chalmers University of Technology

113. Hanafi, Zulkifi. 1994. "Housing Design in relation to Environmental Comfort – A Comparison of the Traditional Malay House and Modern Housing."

114. Hanby, V. I. 1978. "The use of Models to Represent Trees on Wind Tunnel Experiments." Journal of Industrial Aerodynamics,Vol.3, pp. 379-386.

115. Handa, Kamal. 1979. Wind Induced Natural Ventilation, Swedish Council for Building Research, Report D10.

116. Hanzawa, H., A.K. Melikov, and P.O. Fanger. 1987. "Airflow Characteristics in the Occupied Zone of Ventilated Spaces." ASHRAE Transactions,Vol.93, no. 1, pp. 524-538.

117. Holford, Lord. 1971. Problems for the Architect and Town Planner caused by Air in Motion. Philosophy Transactions Royal Society, Vol.269, pp. 335-341.

118. Holleman, Theo R. 1951. Air Flow through Conventional Window Openings, Research report No. 33, Texas Engineering Experiment Station, College Station, TX.

119. Holmes, M. J., and F. Cousins. 1992. "Optimization of the Thermal and Ventilation Performance of Naturally Ventilated Building Facades." Ventilation for Energy Efficiency and Optimum Indoor Air Quality, 13th. AIVC Conference, Sept. 1992, Nice, France.

120. Holmes, J. D. 1983. Wind loads on low Rise Buildings: a Review, Commonwealth Scientific and Industrial Research Organization. Melbourne, Australia: Printed by BUIDREASEARCH.

121. _____. 1980. “Discussion: In response to: Comparative Measurements of Wind Pressure on a Model of the Full-scale Experimental House at Aylesbury, England.” Journal of Industrial Aerodynamics, Vol.6, pp. 181-182.

122. Holmes, J. D. and R. J. Best. 1979. A Wind Tunnel Study of Wind Pressures on Grouped Tropical Houses, James Cook University. Wind Engineering Report 5/79.

123. Hosker, R.P. Jr. 1985. “Flow around Isolated Structures and Building Clusters: A Review.” ASHRAE Transactions,Vol.91, no. 2.

124. Hussain, M. and B. E. Lee. 1980. “A Wind Tunnel Study of the Mean pressure Forces acting on a Large Groups of Low-rise Buildings.” Journal of Wind Engineering and Industrial Aerodynamics, Vol. 6:pp. 207-225.

125. Iversen, D. James, Wen-Ping Wang, Keld R. Rasmussen, Harald E. Mikkelsen, Jan F. Hasiuk, and Rod N. Leach. 1990. “The Effect of a Roughness Element on Local Station Transport.” Journal of Wind Engineering and Industrial Aerodynamics,Vol.36, pp. 845-854.

126. Iversen, James D., and Wen-Ping Wang. “Wind Tunnel Modeling of Time-Dependent Drift Topography.”

127. Jackson, P. and J.R.C. Hunt. 1975. “Turbulent Wind Flow over a Low Hill.” in Quarterly Journal of the Royal Meteorological Society, Vol. No. 101, pp. 929–955.

128. Janssen, John. 1984. “The ASHRAE Ventilation Standard 62-1981.” 3rd. International Conference on Indoor Air Quality and Climate, Vol.5, August 20-24 1984, Stockholm, Sweden, Swedish Council for Building Research, pp. 199-206.

129. Jensen, Martin. November 1958. “The Model-Law for the Phenomena in Natural Wind.” Ingeniøren,Vol.2, no. 4, pp. 121-128.

130. Jensen, M. and N. Franck. 1965. Model-scale Tests in Turbulent Wind, Part II: Phenomena Dependent of the

Velocity Pressure. Wind Loads on Buildings, Danish Technical Press, Copenhagen.

131. Jones, P. J., and G.E. Whittle. 1992. "Computational Fluid Dynamics for Building Air Flow Prediction–Current Status and Capabilities." Building and Environment,Vol.27, no. 3, pp. 321-338.

132. Kammerud, R., E. Ceballos, B. Curtis, W. Place and B. Anderson. 1984. "Ventilation Cooling of Residential Buildings." ASHRAE Transactions, Vol. 90, Part 1B:pp. 226-252.

133. Katayama, T., J. Tsutsumi, and A. Ishii,1991. "Full-scale Measurements and Wind Tunnel Tests on Cross-ventilation." Proceedings of the 8th. International Conference on Wind Engineering,

134. Kato, Shinsuke, Shuzo Murakami, Akashi Mochida, Shin-ichi Akabayashi, and Yoshihide Tominaga. 1992. "Velocity–Pressure Field of Cross Ventilation with Open Windows Analyzed by Wind Tunnel and Numerical Simulation." Journal of Wind Engineering and Industrial Aerodynamics, no. 2575-2586.

135. Kenworthy, A. T. 1985. "Wind as an Influential Factor in the Orientation of the Orthogonal Street Grid." Building and Environment, Vol.20, no. 1, pp. 33-38.

136. Kimura, Ken-ichi. 1992. "Effect of Ventilative Cooling on Indoor Thermal Environment." International Symposium on Room Air Convection and Ventilation Effectiveness, July 1992, University of Tokyo, Tokyo, Japan.

137. Kindangen, J., G. Krauss, and P. Depecker. 1997. "Effects of Roof Shapes on Wind-Induced Air Motion Inside Buildings." Building and Environment,Vol.32, no. 1, pp. 1-11.

138. Kishore, V. V. N. 1988. "Assessment of Natural Cooling Potential for Buildings in Different Climatic Conditions." ASHRAE Transactions, Vol.23, no. 3, pp. 215-223.

139. Knoll, B., J.C. Phaff, and W.F. de Gids. June 1996. "Pressure Coefficient Simulation Program." Air Infiltration Review, Vol.17, no. 3.

140. Knoll, B., and W. Kornaat. 1991. "Controlled Natural Ventilation." Air Movement and Ventilation Control within Buildings, 12th AIVC Conference, Sept. 1991, Ottawa, Canada, pp. 193-217.

141. Koenigsberger, OH., T.G. Ingersoll, A. Mathews, and S.V. Szoklay. 1973. Manual of Tropical Housing and Building, London, Longman.

142. Krauss, G., J. I. Kindangen, and P. Depecker. 1997. "Using Artificial Neural Networks to Predict Interior Velocity Coefficients." Building and Environment,Vol.32, no. 4, pp. 295-303.

143. Krüger, Ulf. "Laboratory Tests and Field Measurements of a Air Velocities and Temperature Gradients in Residential Buildings." pp. 325-339.

144. Kukreja, C. P. 1978. Tropical Architecture. TATA McGraw-Hill Publishing Company Ltd, New Delhi.

145. Kwok, K. C. S., and H.A. Bridgman. September 1980. "Wind Tunnel Model Study of Environmental Wind Conditions around Building." Architectural Science Review, Vol.23, pp. 57-63.

146. Lawson, T. V. 1980 1. Wind Effects on Buildings, Vol.1. London: Applied Science Publishers Ltd.

147. _____. 1980 2. Wind Effects on Buildings, Vol.2. London: Applied Science Publishers Ltd.

148. Lebrun, J., and V. Goedseels. 1989. Air Flow Patterns in Ventilated Spaces, Technical Report, The National Fund for Scientific Research in Belgium, Liege, Belgium.

149. Lee, B. E., M. Hussain and B. F. Soliman. 1980, February. "Predicting Natural Ventilation Forces Upon Low-rise Buildings." ASHRAE Journal, pp. 35-39.

150. Lee, B. E. 1977. "The Susceptibility of Tests on Two-dimensional Bluff Bodies to Incident Flow Variations." Journal of Industrial Aerodynamics,Vol.2, pp. 133-148.

151. Linden, P. F., G.F. Lane-Serff, and D.A. Smeed. 1990. "Emptying Filling Boxes: the Fluid Mechanics of Natural Ventilation." Journal of Fluid Mechanics, Reprint,Vol.212, pp. 309-335.

152. Lord, D. 1986. "Air Quality in Western Culture: A Short History." IQ'86: Managing Indoor Air for Health and Energy Conservation, April 20-23, 1986 Atlanta, GA American Society of heating, Refrigerating, and Air Conditioning Engineers, pp. 106-118.

153. Mair, W. A., and D.J. Maul. 1971. "Aerodynamic Behaviour of Bodies in the Wakes of Other Bodies." Phil. Trans. Roy. Soc., Vol.269, pp. 425-437.

154. Mathews, E. H. 1987. "Prediction of the Wind-generated Pressure Distribution around Buildings." Journal of Wind Engineering and Industrial Aerodynamics, Vol.25, pp. 219-228.

155. Mathews, E. H., and P. G. Rousseau. 1994. "A New Integrated Design Tool for Naturally Ventilated Buildings Part 1: Ventilation Model." Building and Environment, Vol.29, no. 4, pp. 461-471.

156. Mathews, E. M., Y. Etzion, E. Erell, P.G. Richards, and P.G. Rousseau. October 1992. "Simplified Analysis of Naturally Ventilated Desert Buildings." Building and Environment, Vol.27, no. 4, pp. 423-432.

157. Mattingly, George E., David T. Harrje, and Gordon M. Heisler. 1979. "The Effectiveness of an Evergreen Windbreak for Reducing Residential Energy Consumption." ASHRAE Transactions, Vol.85, no. 2.

158. Mattingly, George E., and Eugene F. Peters. 1977. "Wind and Trees: Air Infiltration Effects on Energy in Housing." Journal of Industrial Aerodynamics,Vol.2, pp. 1-19.

159. Mayer, Erhard. "New Measurements of the Convective Heat Transfer Coefficient: Influences of Turbulence, Mean Air Velocity and Geometry of the Human Body." pp. 263-276.

160. McNall, P. E. 1983. "The Impact of Building Codes and Regulations on Indoor Air Quality." An Engineering Foundation Conference on Management of Atmospheres in Tightly Enclosed Spaces, Oct. 17-21, 1983, Santa Barbara, California Atlanta, GA American Society of Heating, Refrigerating and Air Conditioning, Inc., pp. 57-61.

161. Melaragno, M. G. 1982. Wind in Architectural and Environmental Design. New York: Van Nostrand Reinhold Co.

162. Melbourne, W. H. 1987. "Criteria for Environmental Wind Conditions." Journal of Industrial Aerodynamics, Vol.3, pp. 241-249.

163. Milbank, Neal. February 1978. "Principles of Natural Ventilation." BRE Digest, pp. 1-7.

164. Milica, Jovanovic Popovic. 1991. "Residential Densities and Application of Passive Solar Systems." Architecture and Urban Space, Sept. 1991 Seville, Spain Kluwer Academic Publishers, pp. 263-267.

165. Moser, Alfred. March 1993. "Annex 26: Energy Efficient Ventilation of Large Enclosures - Large is Beautiful." Air Infiltration, Vol.14, no. 2.

166. _____. "Scaling for Air Flow Patterns in Room Ventilation." Air Movement and Ventilation Control within Buildings, 12th. AIVC Conference, Ottawa, Canada, pp. 77-89.

167. Murakami, S., S. Kato, S. Akabayashi, K. Mizutani and Y. -D Kim. 1991. "Wind Tunnel Test on Velocity-Pressure Field of Cross-Ventilation with Open Windows." ASHRAE Transactions, Vol. 97, Part 1.

168. Murakami, Shuzo, and Hiromi Komine. 1983. "Prediction Method for Surface Wind Velocity Distribution by Means of Regression Analysis of Topographic Effects on Local Wind Speeds." Journal of Wind Engineering and Industrial Aerodynamics, Vol.15, pp. 217-230.

169. Nielsen, Peter V.,1989. "Airflow Simulation Techniques -Progress and Trends." Progress and Trends in Air Infiltration and Ventilation Research, 10th. AIVC Conference, pp 165-184.

170. _____,October 1988. "Simplified Models for Room Air Distribution." Air Flow Pattern within Buildings, Institute for Building Technology and Structural Engineering. International Energy Agency ed. Denmark.

171. Ohba, M., and S. Murakami N. Kobayashi. 1988. "Study on the Assessment of Environmental Wind Conditions at Ground Level in a Built-up Area." Journal of Wind Engineering and Industrial Aerodynamics, Vol.28, pp. 129-138.

172. Pederson, C. O., J. D. Spitler, C. E. Fisher, P. F. Menne and J. Cantillo. "Standard Hourly Energy Calculation Methods for Predicting Performance of Ventilative Cooling." Final Report, ASHRAE 529-RP. University of Illinois at Urbana Champaign.

173. Peterka, J. A. and J. E. Cermak. 1975. "Turbulence in Building Wakes." Pp. 447-463 in the Proceedings of the 4th. International Conference on Wind Effects on Buildings and Structures, London: Cambridge University Press.

174. Poreh, M., J. E. Cermak and J. A. Peterka. 1982. "Wind Tunnel Research of Flow fields within Naturally Ventilated Rooms of Simple Geometry", Fluid Dynamics and Diffusion Laboratory. Report CER82-83MP-JEC-JAP17. Fort Collins, CO.: Colorado State University.

175. Raine, J. K., and D.C. Stevenson. 1977. "Wind Protection by Model Fences in a Simulated Atmospheric Boundary Layer." Journal of Industrial Aerodynamics, Vol.2, pp. 159-180.

176. Rao, Jiwu, and Fariborz Haghighat. "Wind Induced Fluctuating Airflow in Buildings." Air Movement and Ventilation Control within Buildings, 12th AIVC Conference, Ottawa, Canada, pp. 111-121.

177. Richalet, V., and F. Neirac. 1992. "Influence of Windows Openings on Building Thermal Characterization using Identification Techniques." International Symposium on Air Convention and Ventilation Effectiveness, July 1992, University of Tokyo, Japan, pp. 612-617.

178. Ring, J. W., Richard de Dear, and Arsen Melikof. 1993. "Human Thermal Sensation: Frequency Response to Sinusoidal Stimuli at the Surface of the Skin." Energy and Buildings,Vol.20, pp. 159-165.

179. Rousseau, P. G., and E.H. Mathews. 1994. "A New Integrated Design Tool for Naturally Ventilated Buildings Part 2: Integration and Application." Building and Environment, Vol.29, no. 4, pp. 473-484.

180. Schiller, Gail. 1991. Architecture 243: Natural Cooling and Ventilation, a class reader. University of California, Berkeley, Vol. 2.

181. Selvam, R. Panneer, and Phani B. Konduru. 1993. "Computational and Experimental Roof Corner Pressures on the texas Tech Building." Journal of Wind Engineering and Industrial Aerodynamics, Vol.46 & 47, pp. 449-454.

182. Shao, L., S. Sharples, and I.C. Ward. 1992. "Building Pressure Coefficients: Application of three-dimensional CFD Methods to Prediction." Building Service Engineering Research Technology, Vol.13, no. 2, pp. 107-111.

183. Sharag-Eldin, Adil and T. Xu. 1998. "Fan Generated Air Frequencies and Potential Effects on Comfort", (in progress).

184. Sherman M.H., and D.T. Grimsrud. 1982. "Wind and Infiltration Interaction for Small Buildings." Technical Report LBL-13949: Annual Meeting of American Soci-

ety of Civil Engineers, 23-29 October 1982, New Orleans, LA.

185. Simu, E., R. Scanlan. 1978. Wind Effects on Structures: An Introduction to Wind Engineering. New York: John Wiley and Sons.

186. Smith, M. G., R.R. Walker, and M.D.A.E.S. Petera. Prediction of Natural Ventilation Air Flow in a Non-urban Office. Building Research Establishment, [Report transcript], Watford, UK, pp. 463-478.

187. Smith, Elmer G. 1951. The Feasibility of using Models for Predetermining Natural Ventilation. Research Report, Texas Engineering Experiment Station, College Station, TX.

188. Sobin, H. 1981. "Window Design for Passive Ventilative Cooling: An Experimental Model-Scale Study", Proceedings of the 1981 International Passive/Hybrid Cooling Conference, pp. 191-195.

189. Sobin, H. 1983. Analysis of Wind Tunnel Data on Naturally Ventilated Models. Tuscon: Harris Sobin Assoc.

190. Soliman, Baher F.,December 1973. Effect of Building Grouping on Wind Induced Natural Ventilation, Report No. BS 14.

191. Soliman, B. F. 1976. Effect of Building Group Geometry on Wind Pressure and Properties of Flow. Report No. B.S. 29.

192. Soliman, Baher F., and Brian E. Lee. 1974. "Some Aspects of Density and Form relevant to Air Flow in Urban Areas." Build Inrternational,Vol.7, pp. 451-473.

193. Souster, C. G., and B.E. Lee. July 1975. The Measurement of Airflow Patterns Upstream of Some Simple Building Shapes, BS 26.

194. Spitler, Jeffry David. 1990. An Experimental Investigation of Air Flow and Convective Heat Transfer in Enclo-

sures having Large Ventilative Flow Rates. Doctoral Dissertation. Urbana-Champaign: University of Illinois.

195. Stathopoulos, T., and Y.S. Zhou. April 1995. "Numerical Evaluation of Wind Pressures on Flat Roofs with the k–ε Model." Building and Environment,Vol.30, no. 2, pp. 267-276.

196. Stathopoulos, T., Dominic Chiovitti, and Luisa Dodaro. 1994. "Wind Shielding Effects of Trees on Low Buildings." Building and Environment, Vol.29, no. 2, pp. 141-150.

197. Stathopoulos, Theodore, and Horia D. Luchian. July 1989. "Transient Wind-induced Internal Pressures." Journal of Engineering Mechanics, Vol.115, no. 7, pp. 1501-1515.

198. Stathopoulos, T., and R. Storms. 1986. "Wind Environmental Conditions in Passage Between Buildings." Journal of Wind Engineering and Industrial Aerodynamics, Vol.24, pp. 19-31.

199. Steemers, K. A. 1991. "Low Energy Design in an Urban Context." Architecture and Urban Space, Sept. 1991, Seville, Spain, Kluwer Academic Publishers, pp. 275-280.

200. Straaten (van), J. F.,1967. Thermal Performance of Buildings, Amsterdam: Elsevier Publishing Company. pp 228-283.

201. Suchorski-Tremblay, A., Y. Choinière, J.A. Munroe, and A.S. Tremblay. 1992. "NATVENT: A Natural Ventilation Software Package for Livestock Buildings and Greenhouses."paper no. 92-203, Agricultural Institute of Canada Annual Conference, July 1992, Brandon, Manitoba.

202. Sundaram, T. R., G. A. Ludwig, and G. T. Skinner,1971. "Modeling of the Turbulence Structure of the Atmospheric Surface Layer." Paper 71-136, 9th. Atmospheric Sciences Meeting, New York: AIAA.

203. Swami, M. V. and S. Chandra. 1988. "Correlation for Pressure Distribution on Buildings and Calculation of Natural-ventilation air Flow." ASHRAE Transactions, Vol. 94, Part 1:pp. 243-266.

204. Swami, Muthusamy V., and Subrato Chandra, March 1987. Procedures for Calculating Natural Ventilation Airflow Rates in Buildings, Cape Canaveral, Florida: Florida Solar Energy Center.

205. Tacken, M. 1989. "A Comfortable Wind Climate for Outdoor Relaxation in Urban Areas." Building and Environment, Vol.24, pp. 321-324.

206. Takakura, S., Y. Syama, and M. Aoyama. 1993. "Numerical Simulation of Flow field around Buildings in an Urban Area." Journal of Wind Engineering and Industrial Aerodynamics, Vol.46, pp. 765-771.

207. Taylor, P. and R.J. Lee. 1984. "Simple Guidelines for Estimating Wind Speed Variations due to Small scale Topographical Features", Climatological Bulletin of the Canadian Meteorological and Oceanographic Bulletin.

208. Taylor, P. and J. Salmon, November 1993. "A Model for the Correction of Surface Wind Data for Sheltering by Upwind Obstacles", Journal of Applied Meteorology, American Meteorological Society: pp. 1683-1694.

209. Teichman, K. Y., and J.E. Wood. "Ventilation and Indoor Air Quality: Regulations, Codes, and Voluntary Consensus Standards." in the Proceedings of the ASHRAE Conference: IAQ 87, May 18-20, 1987, Arlington, Virginia, pp. 3-13.

210. Telbany, M. M. M., M.R. Mokhtarzadeh-Dehghan, and A.J. Reynolds. 1985. "Single-sided Ventilation–Part I. The Flow between a Cavity and External Air Stream." Building and Environment, Vol.20, no. 1, pp. 15-24.

211. _____. 1985. "Single-sided Ventilation–Part II. Further Considerations." Building and Environment, Vol.20, no. 1, pp. 25-32.

212. Tsutsumi, J., T. Katayama, and M. Nishida. 1991. "Wind Tunnel Tests of Wind Pressure on Regularly Aligned Buildings." International Conference of Wind Engineering, July 1991, University of Western Ontario.

213. Tsutsumi, Jun-ichiro, Tadahisa Katayama, Tetsuo Hayashi, and Ping He. 1992. "Numerical Simulation of Cross-ventilation in a Single Unit House." International Symposium on Air Convention and Ventilation Effectiveness, July 1992, University of Tokyo, Japan, pp. 632-637.

214. Tucker, W. Gene. "ASHRAE Standard 62: Ventilation for Acceptable Indoor Air Quality." pp. 211-219.

215. Vickery, B. J. and C. Karakatsanis. 1987. "External Wind Pressure Distributions and Induced Internal Ventilation Flow in Low-rise Industrial and Domestic Structures." ASHRAE Transactions, Vol. 93, Part 2:pp. 2198-2213.

216. Vitruvius,1960. The Ten Books of Architecture. Translated by Morris Hicky Morgan. New York: Dover Publications, Inc.

217. Walker, Iain S. September 1992. "Pressure Coefficients on Sheltered Buildings." Air Infiltration Review,Vol.13, no. 4.

218. Walker, Iain S., and David J. Wilson. December 1994. "Practical Methods for Improving Estimates of Natural Ventilation Rates." Air Infiltration Review.

219. Watson, Donald, and Kenneth Labs. 1983. Climatic Design. Energy-efficient Buildings: Principles and Practices. New York: McGraw-Hill Book Co.,

220. Warren, P. R., and L.M. Parkins. 1984. "Single-sided Ventilation through Open Windows." Windows in Building Design and Maintenance, Proceedings Appendix Part 2; 13-15, June 1984, Goteberg, Sweden, pp. 209-228.

221. White, Robert F. 1954. Effects of Landscape Development on the Natural Ventilation of Buildings and their Adjacent Areas. Research Report No. 45, Texas Engineering Experiment Station, College Station, TX.

222. Whittle, Geoff. December 1996. "Flow Simulation using Computational Fluid Dynamics -a Cost Effective Tool for Flow Simulation." Air Infiltration Review,Vol.18, no. 1, pp. 5-7.

223. Wilson, A. Grant. 1990. "A Canadian Standard for Residential Ventilation Systems." The Fifth International Conference on Indoor Air Quality and Climate, July 29-August 3, 1990, Toronto, Canada Ottawa, pp. 371-377.

224. Wilson, D. J., and I.S. Walker. 1991. "Wind Shelter Effects on Air Infiltration for Row of Houses." Air Movement and Ventilation Control within Buildings, 12th AIVC Conference, Sept. 1991, Ottawa, Canada, pp. 335-345.

225. Wirén, B. G. 1985. Effects of Surrounding Buildings on Wind Pressure Distributions and Ventilation Losses for Single-family Houses; Part 1: 1 1/2 Storey Detached Houses. Report No. M85:19. The National swedish Institute for Building Research.

226. _____. 1987. Effects of Surrounding Buildings on Wind Pressure Distributions and Ventilation Losses for Single-family Houses; Part 2: 2 Storey Terrace Houses. The National swedish Institute for Building Research.

227. _____. 1984. Wind Pressure Distribution and Ventilation Losses for a Single-family House as Influenced by Surrounding Buildings - a Wind Tunnel Study. Wind Pressure Workshop, Sweden: Air Infiltration Centre.

228. Wise, A. F. E. 1971. Effects due to Groups of Buildings. Philosophic transactions of the Royal Society, London, no. 269, pp. 469-485.

229. Wood, C. J. 1983. "Building Orientation and Environmental Wind-comfort (an Epitaph to the Green Giant)."

Journal of Wind Engineering and Industrial Aerodynamics, Vol.12, pp. 237-244.

230. Yamamoto, T., D.S. Ensor, L.E.Sparks, M.Inokushi, M. Koganei, and M. Lee. "Ventilation Model: Comparison of PC and Work Station." pp. 326-333.

231. Yamanaka, Toshio, Masaya Narasaki, and Masaaki Higuchi. October 1992. "Design Method of Wind-forced Ventilation including Effect of Turbulence of Wind on Ventilation: Part 3–The Air Flow Rate and Ventilation Efficiency in the Case of one-opening Ventilation." (Japanese with English Abstract), Transactions of the Heating, Refrigerating, Air-conditioning and Sanitary Engineers of Japan, no. 50, pp. 1-13

232. Zhang, J. S., G.J. Wu, and L.L Christianson. February 1992. "Full-scale Experimental Results on the Mean Turbulent Behaviour of Room Ventilation Flows." ASHREA Transactions, Vol.98, no. 2.

233. Zhu, Dan, Srinivasa Reddy Mallidi, and Paul Fazio. 1995. "Approach for Urban Driving Rain Index by using Climatological Data Recorded at Suburban Meteorological Station." Building and Environment, Vol.30, no. 2, pp. 229-236.

7.2 Climate and Culture

234. Al-Khuli, Muhammad Badr al-Din. 1978. Al-Mu'ath-thirat al-munakhiyah wa-al-'imarah al-'Arabiyah, Dar al-Ma'arif, Al-Qahirah.

235. Allen, Edward, J. A. Moore, D. E. Mahone. 1981. Beginning Exercises In Energy-conscious Design: A Resource Book In Building Climatology, Association of Collegiate, Schools of Architecture, Series title: Teaching passive design in architecture, Washington, DC.

236. Alvarez Servando (ed.). 1991. International PLEA Conference Architecture and urban space: proceedings of the Ninth International PLEA Conference, Seville, Spain, September 24-27, 1991, sponsors, Commission of the European Communities, Published on behalf of

the International PLEA Organisation by Kluwer Academic Publishers, Boston.

237. Bahadori, Mehdi N. 1979. "Natural Cooling in Hot Arid Regions." Pp. 195-225 in Solar Energy Application in Building, ed. Sayigh. New York: Academic Press.

238. Beazley, Elisabeth and M. Harverson. 1982. Living With The Desert: Working Buildings Of The Iranian Plateau, Aris & Phillips, Warminster, Wilts, England.

239. Bourdier, J.P, and N. AlSayyad (eds.) 1989. Dwelling, Settlements and Tradition: Cross-cultural Perspectives, International Association for the Study of Traditional Environments, Berkeley, CA, University Press of America, Lanham.

240. Campbell, Robin McKellar. 1965. Designing for Comfort in Tropical Climate, Melbourne University Department of Architecture, Tropical building studies, v. 2, no. 2. Melbourne, Australia.

241. Carter, George Francis. 1964. Man and the Land, a Cultural Geography, Holt, Rinehart and Winston, New York.

242. Coles, Anne and Peter Jackson. 1975. A Wind Tower House in Dubai, Art and Archaeology Research Papers, Series title: AARP (Series), London.

243. Crouch, Dora P., A. Petruccioli, I. Boolaky. 1989. Physical Determinants of Settlement Form, Center for Environmental Design Research, University of California at Berkeley, Series title: Traditional dwellings and settlements working paper series;

244. Eliade, Mircea. 1959. The Sacred and the Profane: the Nature of Religion, R. Trask (trans), New York.

245. Evans, Martin. 1980. Housing, Climate, and Comfort, J. Wiley, New York.

246. Fathi, H. 1986. Natural Energy and Vernacular Architecture: Principles and Examples with Reference to Hot

Arid Climates, Shearer, W. and A. Sultan (eds.), Published by the University of Chicago Press, Chicago.

247. Fathi, Hassan. 1969. Gourna: A Tale of Two Villages, by the Ministry of Culture, Cairo

248. Fernandes, E. et. al. 1989. Energy And buildings For Temperate Climates: A Mediterranean Regional Approach: proceedings of the Sixth International PLEA Conference, 27-31 July 1988, Porto, Portugal, Published on behalf of the International PLEA, Organisation by Pergamon Press, New York.

249. De Figueroa C.A. 1980. Architecture for the Tropics: A Bibliographical Synthesis (from the Beginning to 1972), Editorial Universitaria, University de Puerto Rico, Rio Piedras, Puerto Rico.

250. Fry, Maxwell and Jane Drew. 1982. Tropical Architecture in the Dry and Humid Zones, 2d ed., R.E. Krieger Pub. Co., Malabar, Fla.

251. Gabriel, P. and D. Garda. 1988. "Climatic Response in a Traditional Settlement: Bastakia of Dubai", in Traditional Dwellings and Settlements in a Comparative Perspective, International Symposium- University of California, Berkeley, Bourdier, J.P., and N.

252. Gabriel, Paul et. al. 1989. Form, Energy and Climate, Center for Environmental Design Research, University of California at Berkeley, Series title: Traditional dwellings and settlements working paper series, vol. 18, Berkeley, CA.

253. Gideon S. Golany, (ed.). 1983. Design For Arid Regions, Van Nostrand Reinhold, New York.

254. Golany, G. (ed.). 1982. Desert Planning: International Issues, The Architectural Press, London.

255. Hough, Michael. 1984. City form and natural process: towards a new urban vernacular, Van Nostrand Reinhold, New York.

256. Jackson, W. A. Douglas. 1985. The Shaping of Our World: A Human and Cultural Geography, Wiley, New York.

257. Jordan, Terry G., and Lester Rowntree. 1986. The Human Mosaic: A Thematic Introduction to Cultural Geography, 4th ed., Harper & Row, New York.

258. Kenneth N. Clark and Patricia Paylore, (eds.). 1980. Desert Housing: Balancing Experience and Technology for Dwelling in Hot Arid Zones, sponsored by the University of Arizona Arid Lands Natural Resources Committee, University of Arizona, Office of Arid Lands Studies, Tucson, Ariz.

259. Koenigsberger, et. al. 1973. Manual Tropical Housing and Building: Part 1, Climatic Design, Longman, London.

260. Konya, Allan. 1980. Design Primer for Hot Climates, The Architectural Press Ltd. London.

261. Lynch, Kevin. 1984. Good City Form, The MIT Press, Cambridge, MA

262. Lynch, Kevin. 1985 (17th. ed.). The Image of the City, The MIT Press, Cambridge, MA.

263. Manzoor, Shokrollah. 1989. Tradition and Development: an Approach to Vernacular Architectural Patterns in Iran, Chalmers University of Technology, School of Architecture, Division for Housing Design, Gothenburg.

264. Markus, T. A., and E. N. Morris. 1980. Buildings, Climate, and Energy, Pitman Pub., Marshfield, Mass.

265. McIntyre, D. A. 1980. Indoor Climate, Applied Science Publishers, Series title: Architectural science series, London.

266. Meffert, Erich F. 1980. Hygrothermal Comfort in Lamu Town: A Building-climatological Investigation into a High-density Settlement in the Warm-humid Climate of the Kenyan Coast, University of Nairobi, Dept. of

Architecture, Environmental Science Section, Series title: Environmental science; paper no. 6, Nairobi.

267. Ministry of Public Works, and Electric Power and the Building Research Institute. DATE UNKNOWN. Traditional Buildings of Indonesia: volume 1, Batak Toba, Bandung, Indonesia.

268. Ministry of Public Works, and Electric Power and the Building Research Institute. DATE UNKNOWN. Traditional Buildings of Indonesia: volume 2, Batak Karo, Bandung, Indonesia.

269. Ministry of Information. 1990. Jakarta: Overview, Pemerintah Daerah Khusus Ibukota Jakarta, Jakarta, Indonesia.

270. Mousalli, M. S., F. A. Shaker and O. A. Mandily. 1977. An Introduction to Urban Patterns in Saudi Arabia: The Central Region, Art and Archaeology Research Papers, Series title: AARPs, London.

271. National Buildings Organisation. 1961. Climatic Data For Design Of Buildings (Jaipur Region), National Buildings Organization. The Organization, Series title: National Buildings Organisation (India) Technical bulletin No. 17, New Delhi.

272. Nilsson, Sten Ake. 1968. European Architecture in India, 1750-1850, [1st American ed.], Taplinger Pub. Co. New York.

273. Norberg-Shultz, C. 1980. Genius Loci: towards a Phenomenology of Architecture, Rizzoli International Publications, Inc., New York.

274. Olgyay, Aladar, and V. Olgyay. 1957. Solar Control and Shading Devices, Princeton University Press, Series title: Princeton paperbacks, Princeton.

275. Olgyay, V. 1963. Design With Climate: Bioclimatic Approach to Architectural Regionalism. Some chapters based on cooperative research with Aladar Olgyay. Princeton, N.J., Princeton University Press.

276. Powell, Robert, and Ken Yeang. 1989. Rethinking The Environmental Filter, Landmark Books, Singapore.

277. Prasad, Dharmendra. 1986. Social and Cultural Geography of Hyderabad City: A Historical Perspective, Inter-India Publications, New Delhi, India.

278. Prijotomo, J. 1984. Ideas and Forms of Javanese Architecture, Gadjah Mada University Press, Yokyacarta, Indonesia.

279. Rapoport, Amos. 1969. House Form and Culture, Foundations of Cultural Geography Series, Prentice-Hall, Inc., Englewood Cliffs, NJ.

280. Saini, B. S. and G.C. Borrack. 1960. Control of Windblown Sand and Dust by Building Design and Town Planning in the Arid Zone, University of Melbourne, Department of Architecture, Melbourne.

281. Sehgal, J. L. 1964. Control of Sunlight Penetration in Buildings at Stations between Latitude 17030' N to 20030' N, National Buildings Organisation, Ministry of Works & Housing & Regional Housing Centre, ECAFE, Series title: Technical information series, New Delhi, India.

282. Sharag-Eldin, Adil. 1988 The Architectural Implications of Passive Solar Energy in Hot Arid Climates, Master of Science in Architectural Studies, Massachusetts Institute of Technology, Cambridge, MA.

283. _____. 1994. "The Direction Sensitivity of Wind Catchers" from the Proceedings of the 19th. Passive Cooling Conference, ASES, San Jose, CA.

284. Singh, R. L. (ed.). 1973. IGU Symposium on Urban Geography in Developing Countries, proceedings of I.G.U. Symposium no. 15, Varanasi, November 22-29, 1968, National Geographical Society of India, Varanasi.

285. Taha, Haider Ghani Hasoon. 1984. Energy and Climatic Performance versus Design and Form: A Comparative

Analysis of Urban Patterns in Hot-arid Climates. DISSERTATION, University of California, Los Angles, CA.

286. Tappuni, R. and A. Rassam. 1981. "Analysis and Development of Two Vernacular Passive Cooling Systems for Use in the Design of Modern Buildings". in Solar Heating, Cooling, and Desalination, Veziroglu, T. (ed.), Alternative Energy Sources IV, Vol. 2, Ann Arbor, MI.

287. Taylor, Brian Brace, 1985. "University, Qatar". in Mimar: Architecture in Development. Concept Media Pte Ltd. Singapore, pp. 20-27.

288. Williams, J.F., S. Brunn, and J. Datden. 1983. "Chapter 1; World Urban Development" in Cities of the World: World Urban Regional Development, Brunn and Williams (eds.), Harper and Row, Publishers, New York.

289. Yeang, K. 1987. Tropical Urban Regionalism: Building in a Southeast Asian City, Concept Media Pte Ltd. Singapore.

Appendix A

Appendix A

Boundary Layer, tested Model, and Instrumentation

A.1 General Setup of the Experiments

This Appendix includes a description of the general setup of the experiments, the boundary layer, instrumentation, and the measurement procedures.

A.1.1 The Boundary Layer Wind Tunnel

The systematic parametric study discussed in the text was conducted in a Boundary Layer Wind Tunnel (BLWT)[1] in which only small number of variables were tested at a time. The BLWT is of an open circuit design with interior dimensions of 1.5 m high, 2.1 m wide, and 19.5 m in length. As shown in Figure A-1, the flow processing section occupies the first 12.8 m of the wind tunnel. This processing section contains a combination of turbulence-generating devices and roughness blocks that cover the floor to simulate flow characteristics of the wind approaching the instrumented model[2]. Immediately downwind of the processing section there is a 3.5 m testing section in which the scale models are placed on a 2.0 m diameter rotating turntable. The pressure and velocity data processing instrumentation are located under the turntable. A PC-based data acquisition system is located at an adjacent room and is used for data collection and analysis of obtained data.

A-1. The facility is located in the Building Science Laboratory, Department of Architecture at the University of California, Berkeley.

A-2. For a break down of the processing section, refer to TABLE A-1 .

Figure A-1 Boundary layer wind tunnel.

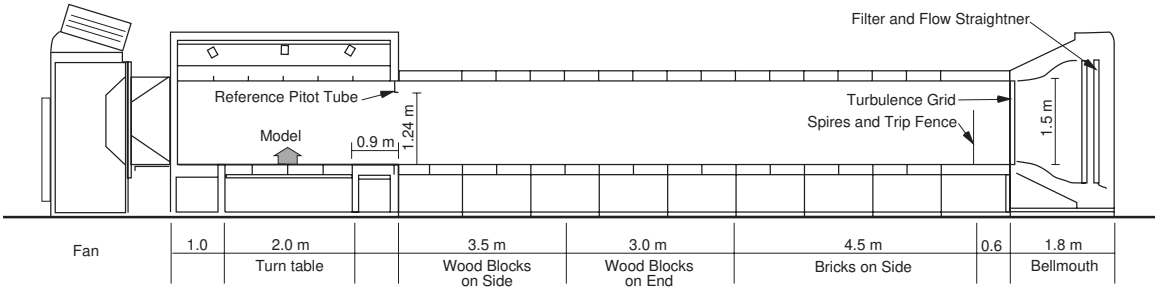

Figure A-2 Model and boundary layer growth acceleration roughness blocks -inside view of the BLWT.

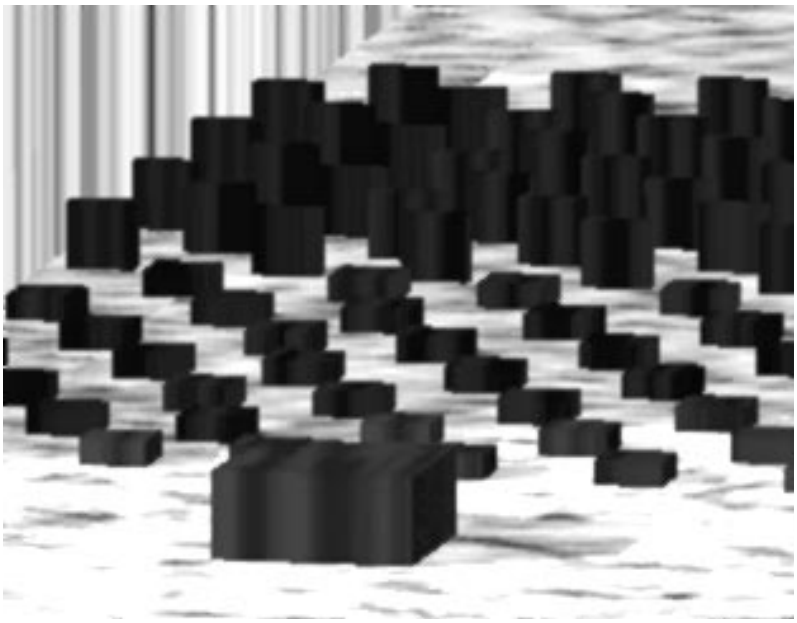

A.1.2 Boundary Layer

The variation of wind velocity with height in the lower level of the atmospheric boundary layer can be represented by the following relationship (Ref 202):

$$V_z = \left(\frac{U_f}{k}\right) \cdot \ln\left[\frac{(z-d)}{z_0}\right] \qquad \textbf{(A-1)}$$

Where

V_z = mean velocity at height z (m/s)

U_f = friction velocity (m/s)

k = von Karmans constant

= 0.4

z = height above ground level (m)

d = zero plane displacement height (m)

z_0 = roughness length (m)

For this study, the roughness length was maintained at 0.079 m (full scale), corresponding to a relatively smooth terrain typical of a village or outskirts of small towns. The model roughness was purposefully kept low to increase wind speeds near the ground, thus maintaining a high Reynold number while still simulating realistic flow conditions. Methods to artificially accelerate the development of a boundary layer of a sufficient depth in a short wind tunnel were used [Cook (Ref 62)]. The following wind tunnel devices and roughness elements were used to produce the desired boundary layer for a model of 1:30 scale (Figure 1):

TABLE A-1 **Boundary Layer Description**

	Description	Distance from Trip Fence (m)	Length of Section (m)	Element Geometry (mm)	Density (%)
1	a filter and a square mesh turbulence grid at entrance to wind tunnel	-0.6	_____	_____	_____
2	four spires 0.9 m high spaced 0.42 m c/c with a 0.34 m high sawtooth (0.2 m high teeth) and a trip fence 0.6 m downwind of grid	0.0	_____	_____	_____
3	Bricks placed on side	0.6	4.5	100 high 210 wide 60 deep	16.5

TABLE A-1 **Boundary Layer Description (Continued)**

	Description	Distance from Trip Fence (m)	Length of Section (m)	Element Geometry (mm)	Density (%)
4	wood blocks placed on end	5.1	3.0	88 high 88 wide 38 deep	5.5
5	wood blocks placed on side	8.1	3.5	38 high 88 wide 88 deep	12.8

With a reference mean velocity of 9.4 m/s, velocity and turbulence intensity profiles were measured in the wind tunnel immediately upwind of the model location to document the approaching wind conditions. These measured profiles are presented in Figure A-3. The solid line represents the regression fit ($R^2 = 0.984$) of the measured to predicted data. The fit produced a full-scale roughness length (z_0) of 0.079 m for a displacement height (d) of 0.0 m, in reasonable agreement with the expected range of values described by ESDU (Refs. 72 and 73). The measured turbulence intensities are also seen to correspond well to ESDU values for the lower region of the atmospheric boundary layer (Ref 73).

Figure A-3 Mean velocity and turbulence intensity profiles.

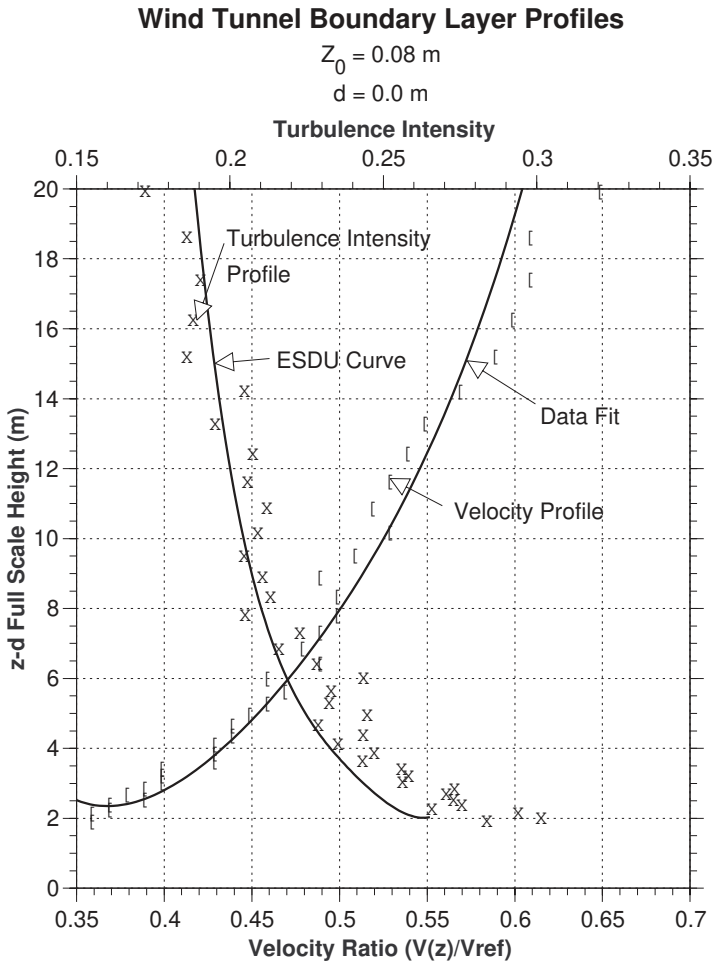

A.2 Measurement Instrumentation

Two Validyne Model DP103 differential pressure transducers (TRANS#1 & 2) were connected to Validyne Model CD15 sine wave carrier demodulator (SIG COND), which generates the analog signals to be read by the data acquisition system (Figure A-4). The voltage read by the computer was then converted into a pressure reading based on the calibration curve of the transducer. Each pressure tap on the model surface was connected by 0.60 m long 1.6 mm vinyl tubing to a rotary valve that allowed each tap to be sequentially connected

through a 4-meter long 1.6 mm O.D. tubing to a single pressure transducer. The rotary valve consists of three 24-port Scanivalve Corp. Model W0602/1P-24T fluid switch wafer (FSW) allowing up to 72 ports to be sequentially scanned by a single transducer. Computer-controlled switching between each pressure port was made possible by Scanivalve Model WS5-24 solenoid stepper drive (DRIVE) and a Model CTRL2 solenoid controller (CTLR). The Dwyer Model 166-12 reference Pitot tube was mounted at 0.25 m below the wind tunnel ceiling and 0.90 m upwind the front end of the turntable. This location, away from the building models, was chosen to eliminate potential flow interference with the building model configurations.

Figure A-4 Pressure measurement setup.

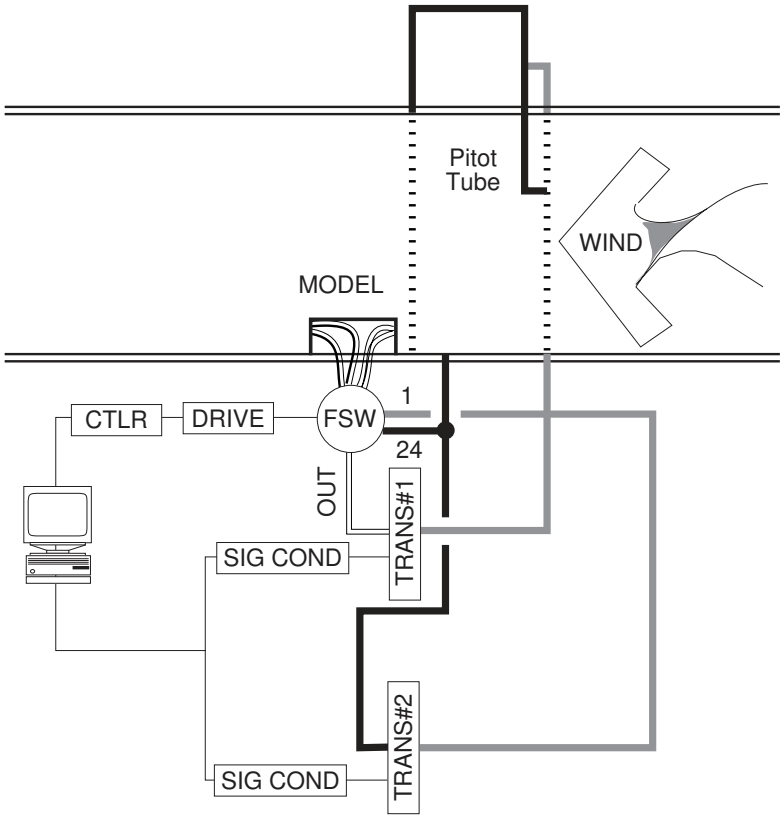

A.3 The Instrumented Model

A single-room model square in plan was fabricated out of 3 mm thick transparent acrylic sheet $25 \times 25 \times 10$ cm in dimensions (scale 1:30). Fifty four (54) pressure taps were mounted on two opposite wall surfaces of the model (Figure A-5). The model is positioned at the center of the wind tunnel's turn table and connected to the pressure transducer through an opening in the wind tunnel floor.

The setup where the model is tested without any surrounding blocks formed the basic configuration upon which all the shielded configurations throughout the research were referenced.

Figure A-5 Instrumented model.

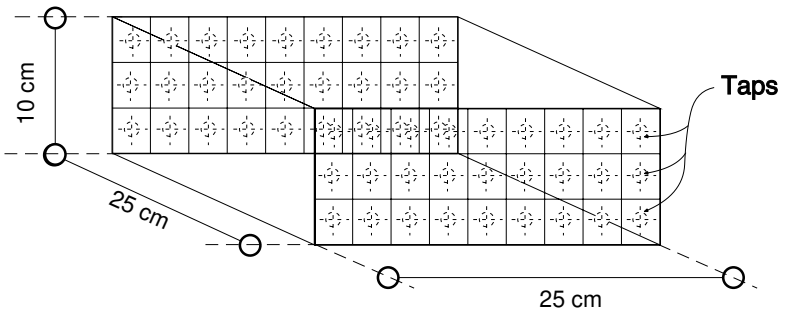

A.4 The Obstruction Blocks

Several Styrofoam blocks of different sizes were used to simulate obstruction blocks (Figure A-6). Both the size of the blocks and their relative position to the instrumented model were varied to analyze the specific variables described in the various sections in this study.

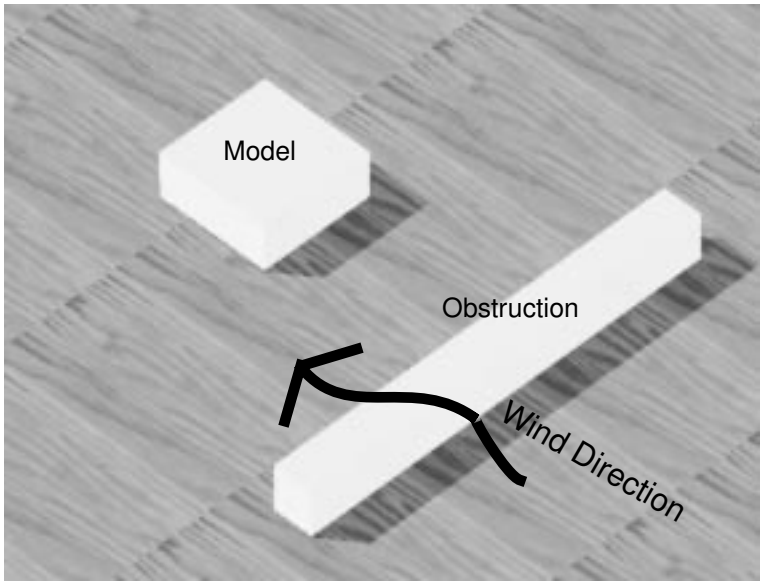

Figure A-6 Upwind obstruction and instrumented model configurations.

A.5 Measurement

The instrumented model (Section A.3) was located the center of the turn table (Figure A-3) while a single or multiple obstruction blocks were positioned at specified locations. The pressure was then measured using the data acquisition system described in Section A.2.

Each measured location point (tap–Figure A-5) was sampled at 15 scans per second for 30 seconds. The mathematical average of the 450 scans was then used to represent the pressure at that point. From previous analyses of the wind tunnel performance, the data collected for the same point tend to be normally distributed, thus the average represents an unbiased and robust measure for the central tendency of the data obtained.

Twenty seven (27) surface wind pressure readings were averaged to determine the mean pressure on each of the two opposite surfaces of the instrumented model. The average pressure

was then used in equations (3-3) and (4-1) to determine the pressure coefficient values[3].

In all tests, an unobstructed instrumented model was tested in the beginning of the experiments. The pressure coefficients of the obstructed and unobstructed were then used to determine the Pressure Modification Coefficient (C_{pm})[4].

A-3. Defined in Section 4.10.

A-4. Refer to Section 4.10 for the definition of the Pressure Modification Coefficient (C_{pm}).

Appendix B

Appendix B

Boundary Layer Conversion

B.1 Derivation of the Conversion Factor

Because all the tests needed to determine C_{pm} values were conducted under a single boundary layer condition (Section A.1.2), a correction factor would be applied when other boundary layer characteristics are encountered. This section explains the algebraic derivation of the boundary layer conversion factors. These factors should be used to correct for boundary layer conditions not used in the derivation of the mathematical model for the prediction of the Pressure Modification Coefficient.

Since;

$$C_p = \frac{(P_m - P_s)}{(0.5 \cdot \rho \cdot V_e^2)} \quad \textbf{(B-1)}$$

and from equation 4-3 in text of report;

$$C_{pm} = e^{[C_{p(Shielded)} - C_{p(Unshielded)}]} \quad \textbf{(B-2)}$$

$$C_{pm_i} = e^{\left[\frac{(P_{m_i} - P_s)}{0.5 \cdot \rho \cdot v_{e_i}^2} - \frac{(P_{un_i} - P_s)}{0.5 \cdot \rho \cdot v_{un_i}^2}\right]} \quad \textbf{(B-3)}$$

and;

$$\frac{C_{pm_1}}{C_{pm_2}} = \frac{e^{(C_{p(\mathrm{ob1})} - C_{p(\mathrm{unob1})})}}{e^{(C_{p(\mathrm{ob2})} - C_{p(\mathrm{unob2})})}} \quad \textbf{(B-4)}$$

From equations A-3 and A-4

$$\frac{C_{pm_1}}{C_{pm_2}} = e^{\left[\frac{2\cdot(P_{m_1}-P_s)}{\rho\cdot v_{e_1}^2}-\frac{2\cdot(P_{m_2}-P_s)}{\rho\cdot v_{e_2}^2}\right]} \quad \textbf{(B-5)}$$

Since;

$$P_{\text{dynamic}} = P_{m_i} - P_s \quad \textbf{(B-6)}$$

and;

$$P = 0.5\cdot\rho\cdot v^2 \quad \textbf{(B-7)}$$

Therefore;

$$P_{m_i} - P_s = 0.5\cdot\rho\cdot v^2 \quad \textbf{(B-8)}$$

Therefore by substituting value of $P_{m_i} - P_s$ from equation A-8 in A-5;

$$\frac{C_{pm_1}}{C_{pm_2}} = e^{\left\{\left[\frac{2\cdot(0.5\cdot\rho\cdot v_1^2)}{\rho\cdot v_{e_1}^2}\right]-\left[\frac{2\cdot(0.5\cdot\rho\cdot v_2^2)}{\rho\cdot v_{e_2}^2}\right]\right\}} \quad \textbf{(B-9)}$$

$$= e^{\left(\frac{v_1^2}{v_{e_1}^2}-\frac{v_2^2}{v_{e_2}^2}\right)}$$

From the exponential function that describes the decrease in mean wind speeds due to terrain roughness (Ref 18):

$$V_z = V_g\cdot\left(\frac{Z_i}{Z_g}\right)^{\alpha} \quad \textbf{(B-10)}$$

Where

V_z = Mean wind speed at height$(Z_i + Z_0)$

V_g = Mean wind speed at gradient height

Z_i = Height at point i

Z_g = Gradient height

α = Velocity profile exponent

Substituting V_i from A-10 into A-9, therefore;

$$\frac{C_{pm_1}}{C_{pm_2}} = e^{\left\{\frac{\left[V_{g_1}\cdot\left(\frac{Z_1}{Z_{g_1}}\right)^{\alpha_1}\right]^2}{\left[V_{g_1}\cdot\left(\frac{Z_{e_1}}{Z_{g_1}}\right)^{\alpha_1}\right]^2} - \frac{\left[V_{g_2}\cdot\left(\frac{Z_2}{Z_{g_2}}\right)^{\alpha_2}\right]^2}{\left[V_{g_2}\cdot\left(\frac{Z_{e_2}}{Z_{g_2}}\right)^{\alpha_2}\right]^2}\right\}} \quad \textbf{(B-11)}$$

$$\frac{C_{pm_1}}{C_{pm_2}} = e^{\left\{\left[\frac{\left(\frac{Z_1}{Z_{g_1}}\right)}{\left(\frac{Z_{e_1}}{Z_{g_1}}\right)}\right]^{2\cdot\alpha_1} - \left[\frac{\left(\frac{Z_2}{Z_{g_2}}\right)}{\left(\frac{Z_{e_2}}{Z_{g_2}}\right)}\right]^{2\cdot\alpha_2}\right\}} \quad \textbf{(B-12)}$$

or;

$$\frac{C_{pm_1}}{C_{pm_2}} = \frac{e^{\left[\left(\frac{Z_1}{Z_{e_1}}\right)^{2\alpha_1}\right]}}{e^{\left[\left(\frac{Z_2}{Z_{e_2}}\right)^{2\alpha_2}\right]}} \quad \textbf{(B-13)}$$

FIGURE A-1. **Boundary Layer Conversion Pressure Shielding Modification Coefficient C_{pm}**

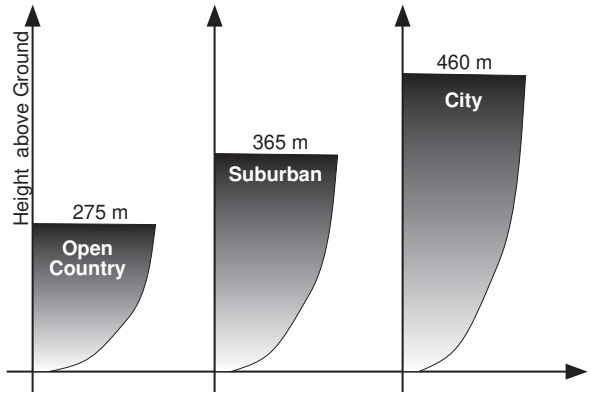

Assuming a Z_i to be equal to half the height of the model or 5 cm (1.67 m) and eave height to be 10 cm (3.33 m) -Figure A-1- and since all the tests are conducted under a boundary layer with a full-scale roughness height (Z_0) value of 0.08 and a velocity profile exponent of about 0.2, therefore;

$$\frac{C_{pm_1}}{C_{pm_2}} = \frac{e^{\left[\left(\frac{Z_1}{Z_{e_1}}\right)^{2\alpha_1}\right]}}{e^{\left[\left(\frac{1.67-0.08}{3.33-0.08}\right)^{2\times 0.2}\right]}} \quad \text{or;} \qquad \textbf{(B-14)}$$

$$\frac{C_{pm_1}}{C_{pm_2}} = \frac{e^{\left[\left(\frac{Z_1}{Z_{e_1}}\right)^{2\alpha_1}\right]}}{e^{0.75}} = \frac{e^{\left[\left(\frac{Z_1}{Z_{e_1}}\right)^{2\alpha_1}\right]}}{2.12} \qquad \textbf{(B-15)}$$

B.2 Boundary Layer Conversion

The following table shows the conversion factors for various boundary layer conditions.

***TABLE B-1* Boundary Layer Pressure Modification Coefficient C_{pm} Conversion Table**

Description of Roughness Terrain[a]	$Z_0(m)$	$Z_g(m)$	α	Conversion factor
City Center and Forest	0.7	600	0.36	0.77
Small Towns and Suburbs	0.3	450	0.25	0.92
Outskirts of small Towns	0.1	350	0.20[b]	1[c]
Open Level Country	0.03	300	0.15	1.06
Grass Plains and Some Trees	0.01	280	–	1.10
Airport (Runways)	0.003	260	0.11	1.11
Flat Deserts or Arid Areas	0.001	250		1.11

a. ESDU Ref. 72

b. Value of α is interpolated

c. Reference Boundary Layer

Figure A-2 shows the effect of boundary layer (BL) characteristics on the value of C_{pm}. The difference between the reference BL (velocity profile exponent $\alpha = 0.20$) and another e.g. $\alpha = 0.25$ can be summarized in the following. Because at the same height, wind speed in the $\alpha = 0.25$ profile is lower than that of the reference profile, the Pressure Modification Coefficient (C_{pm}) should be multiplied by 0.92 (TABLE B-1) to account for the rougher terrain.

***FIGURE A-2.* Boundary Layer differences**

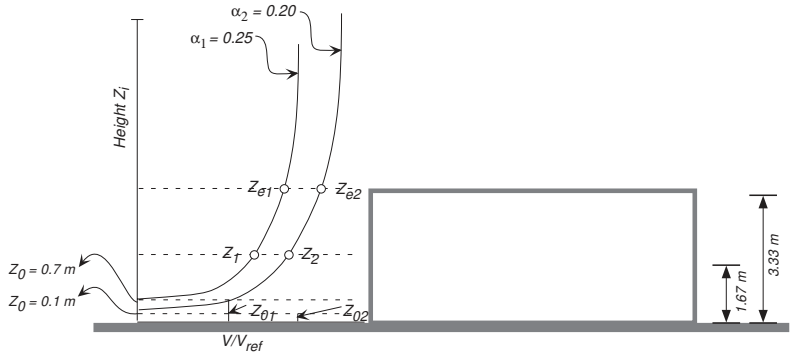

Appendix C

Appendix C

The Unshielded Model

Figure C-1. **A Contour showing C_p values plotted against bott Aspect Ratio and wind direction as Predicted by Swami and Chandra's Model**

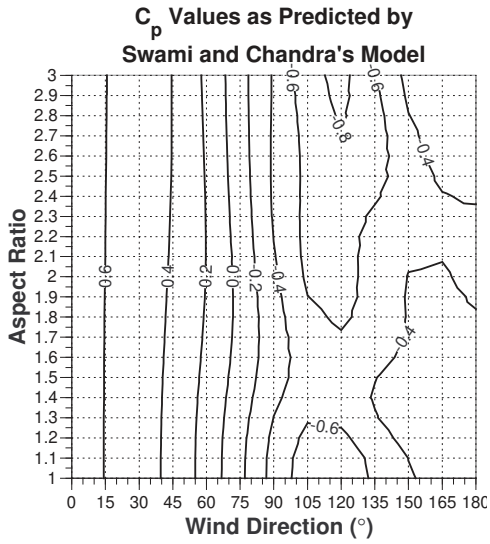

Figure C-2. **Normalized Pressure Coefficients NC_p**

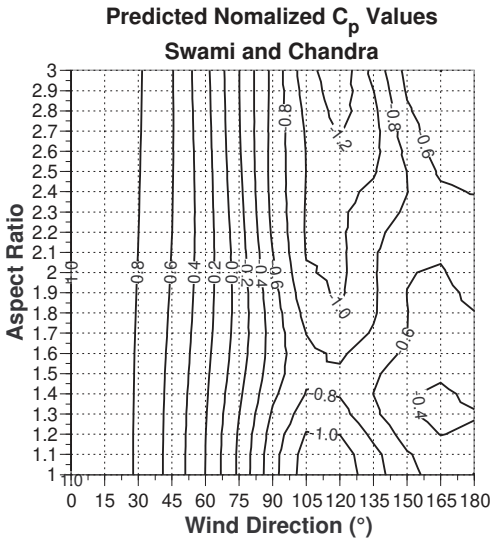

Figure C-3. **Contour plot showing the measured surface pressure coefficients C_p**

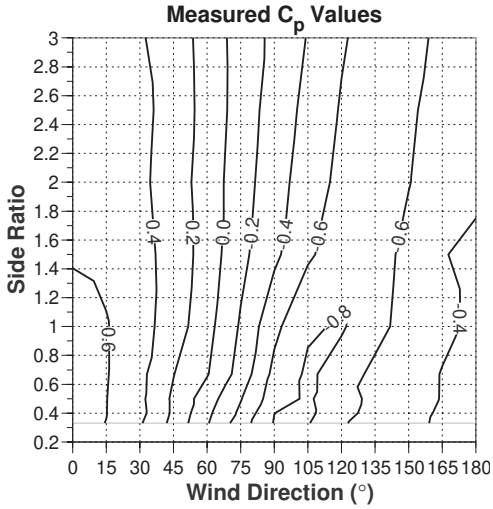

Figure C-4. **Measured NC_p values plotted against Aspect Ratio (A_s) and wind direction (Θ)**

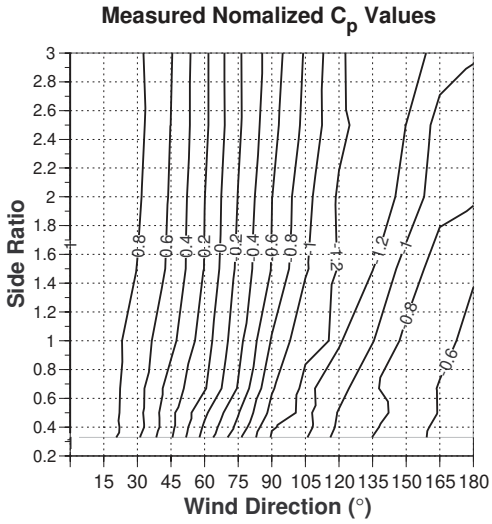

Figure C-5 **Surface Pressures**
A_s=1.00, Wind Direction=*noted in front of surface*

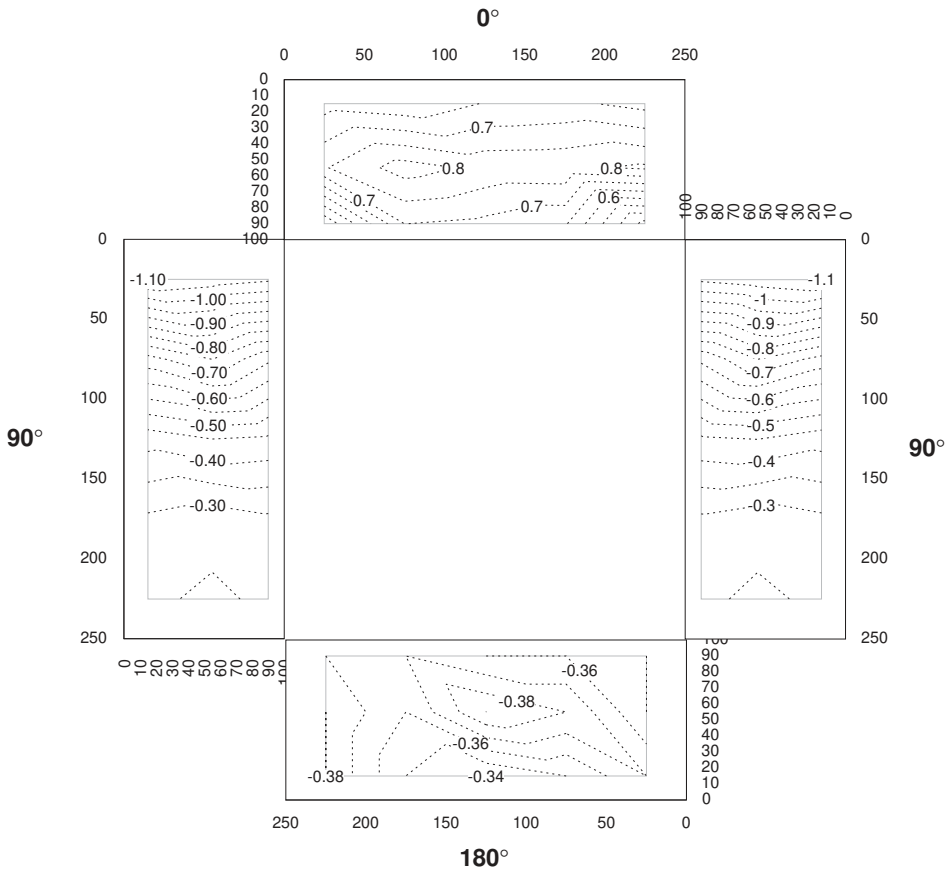

Figure C-6 **Surface Pressures**
A_s=1.00, Wind Direction=*noted in front of surface*

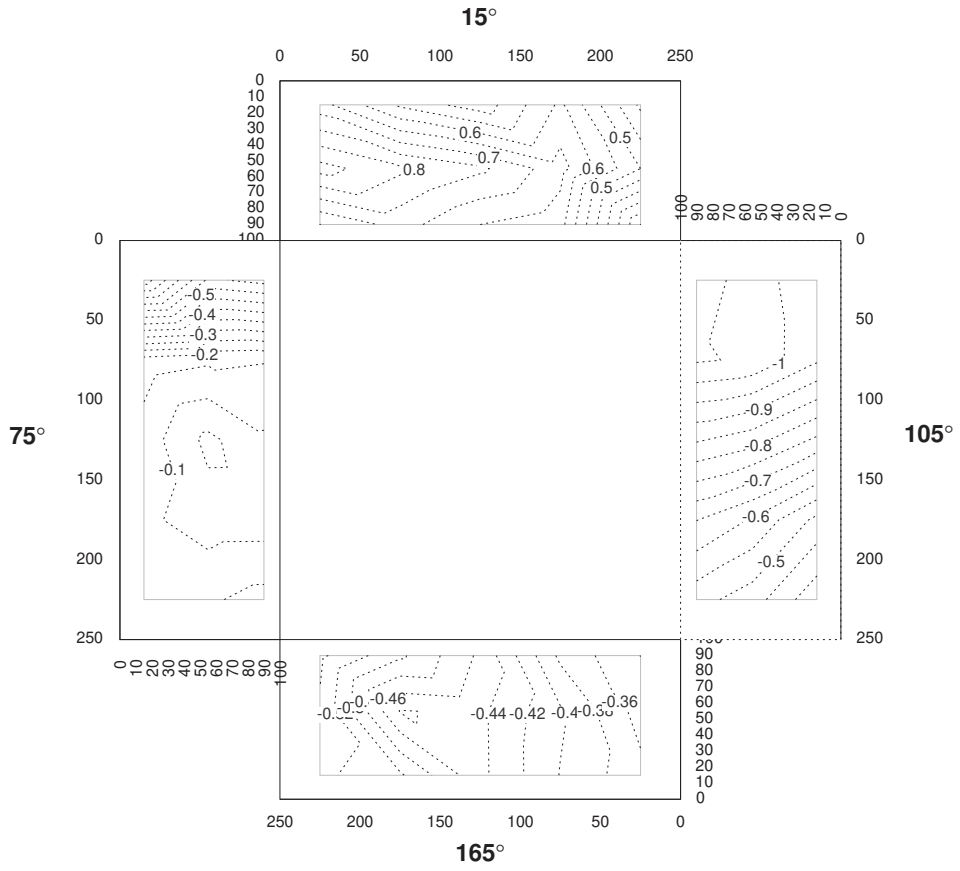

Figure C-7 **Surface Pressures**
A_s=1.00, Wind Direction=*noted in front of surface*

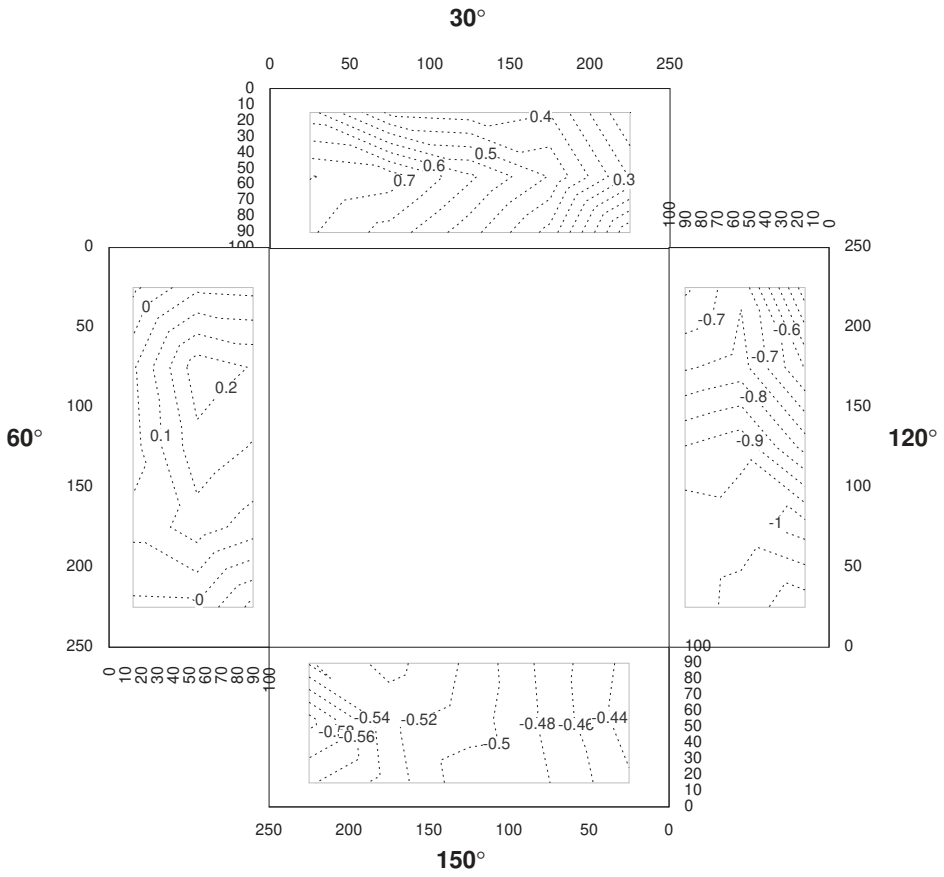

Figure C-8 **Surface Pressures**
A_s=1.00, Wind Direction=*noted in front of surface*

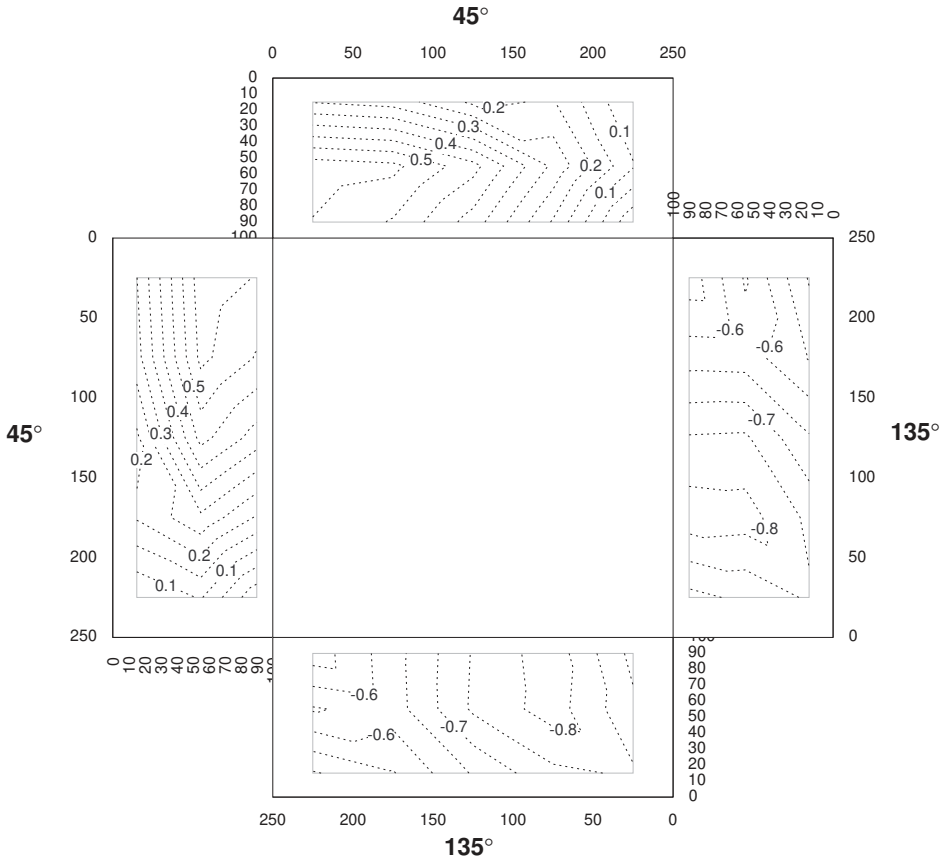

Figure C-9 **Surface Pressures**
A_s=2 and 0.5, Wind Direction=*noted in front of surface*

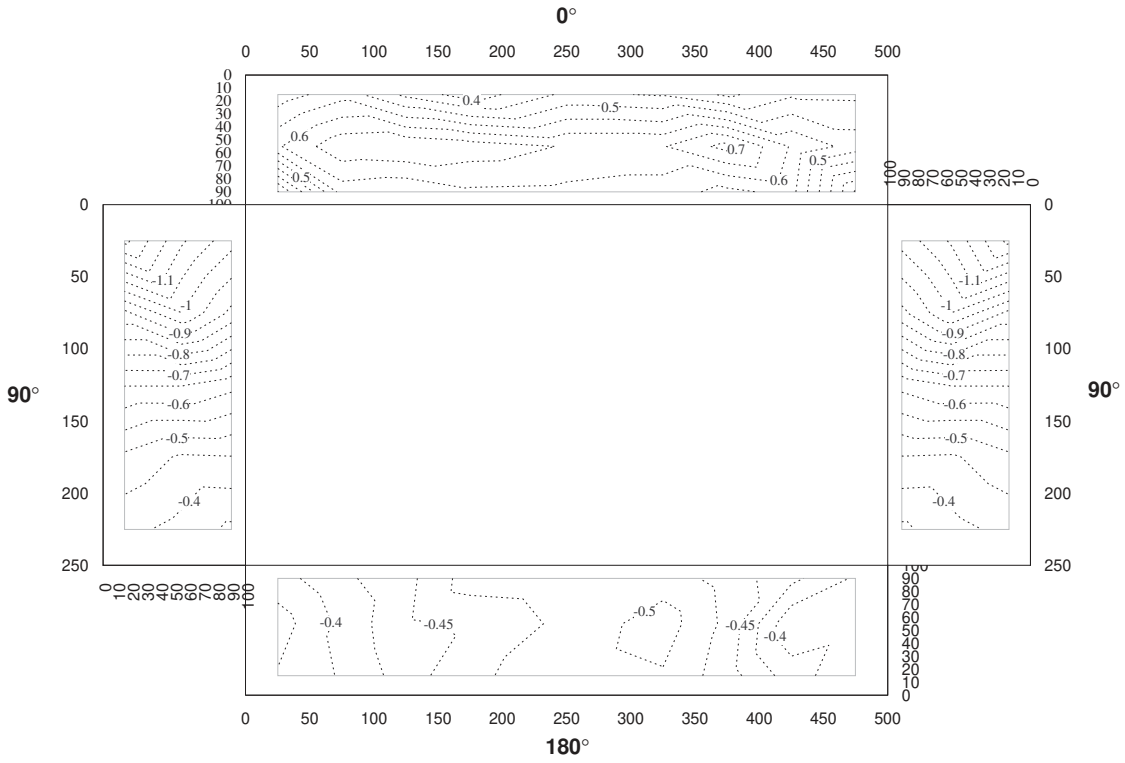

Figure C-10 **Surface Pressures**
A_s=2 and 0.5, Wind Direction=*noted in front of surface*

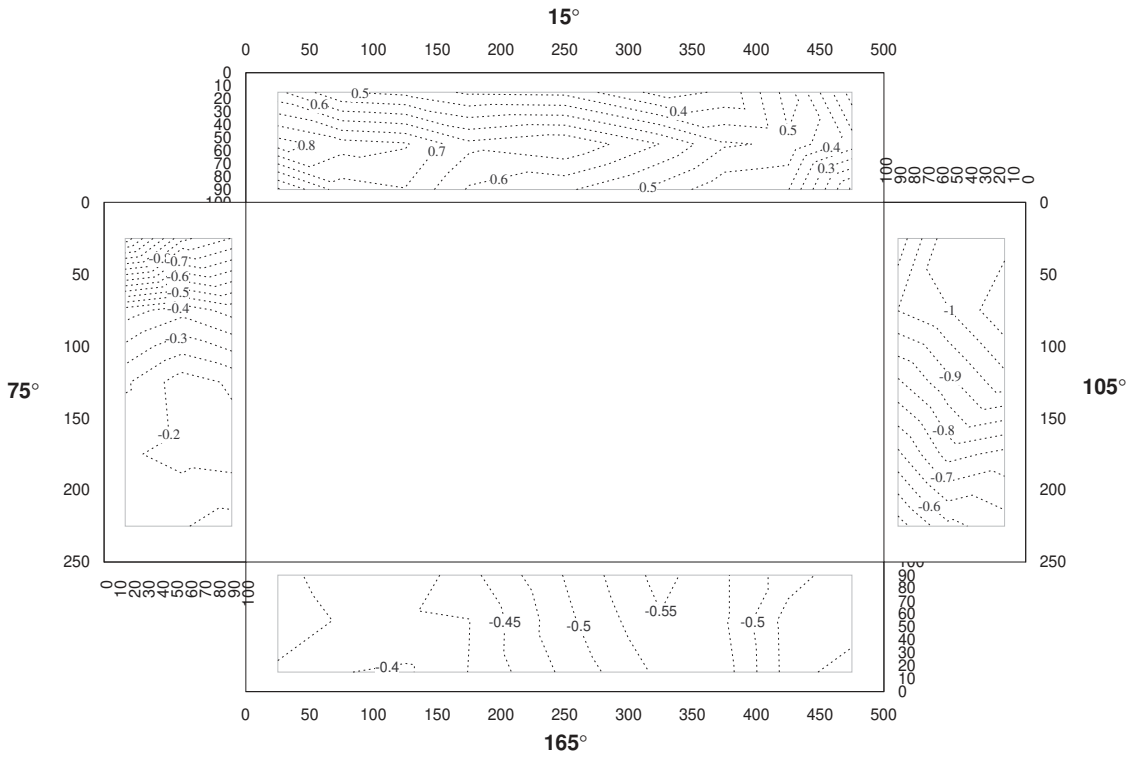

Figure C-11 **Surface Pressures**
A_s=2 and 0.5, Wind Direction=*noted in front of surface*

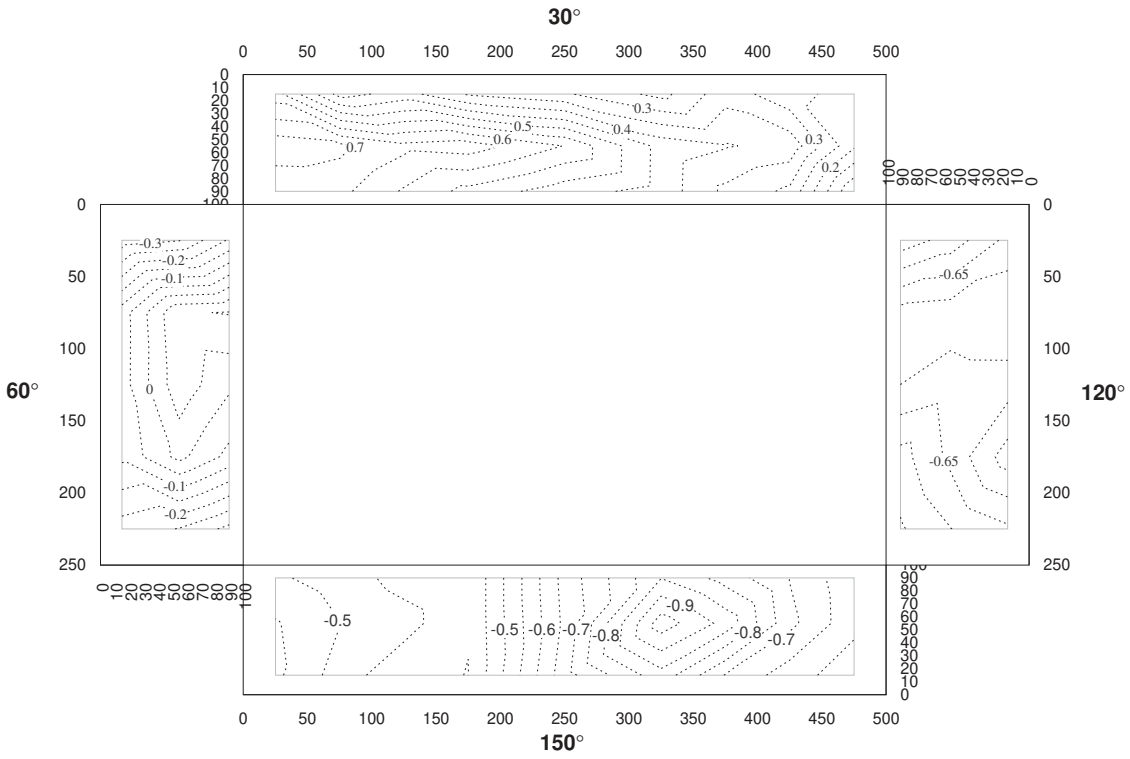

Figure C-12 **Surface Pressures**
A_s=2 and 0.5, Wind Direction=*noted in front of surface*

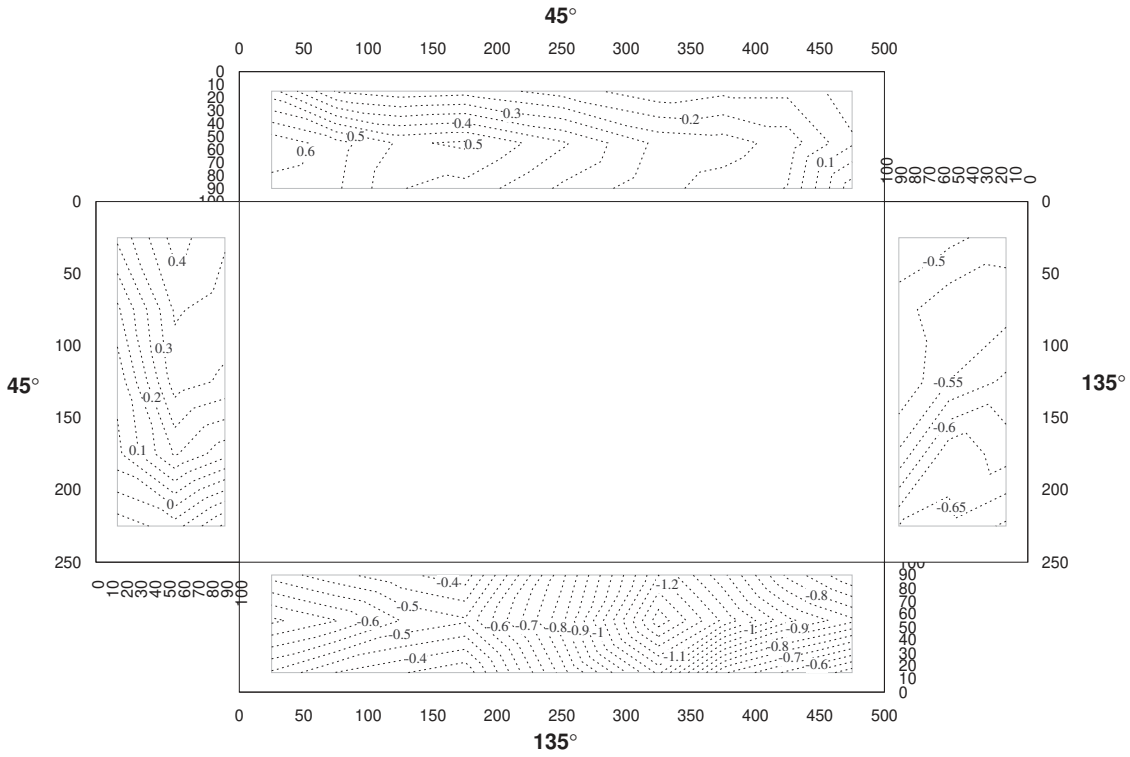

Figure C-13 **Surface Pressures**
A_s=2 and 0.5, Wind Direction=*noted in front of surface*

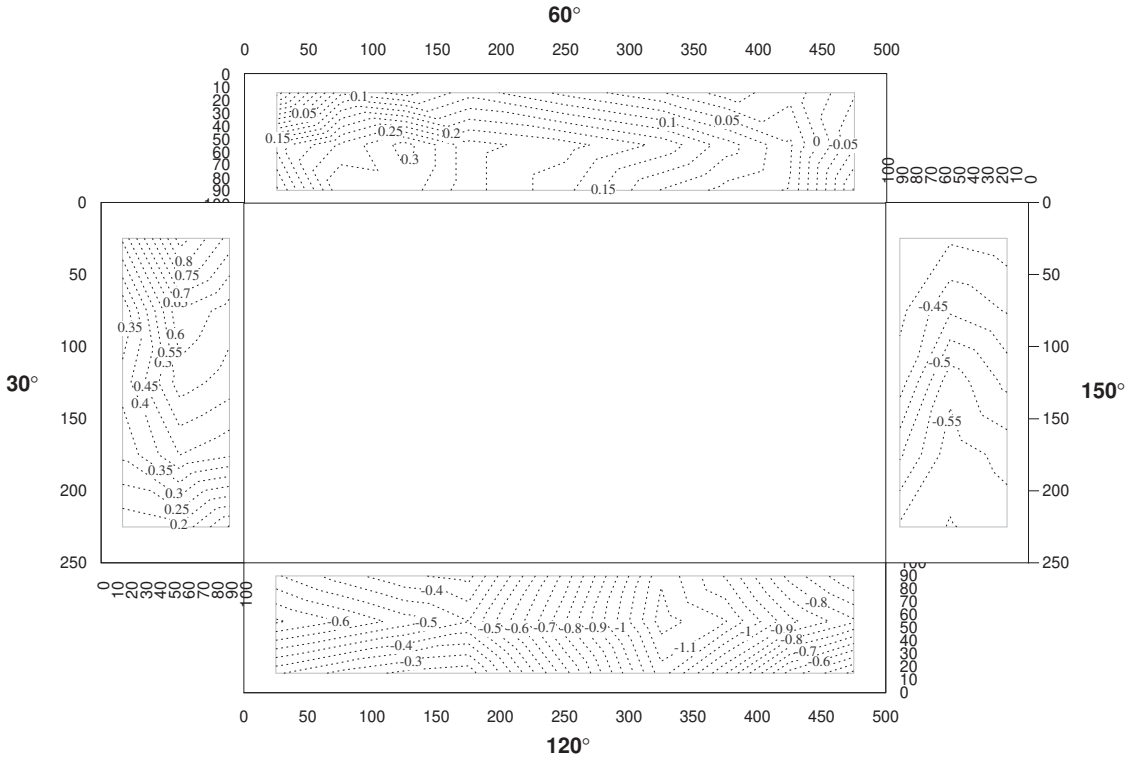

Figure C-14 **Surface Pressures**
A_s=2 and 0.5, Wind Direction=*noted in front of surface*

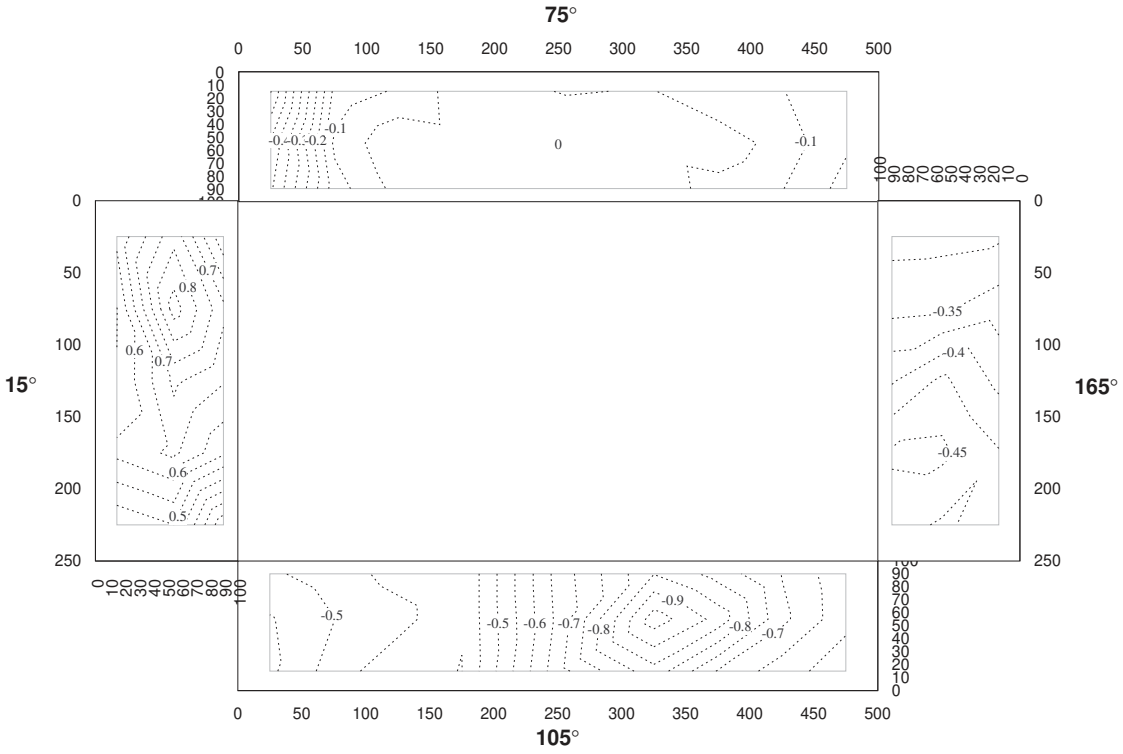

Figure C-15 **Surface Pressures**
A_s=2 and 0.5, Wind Direction=*noted in front of surface*

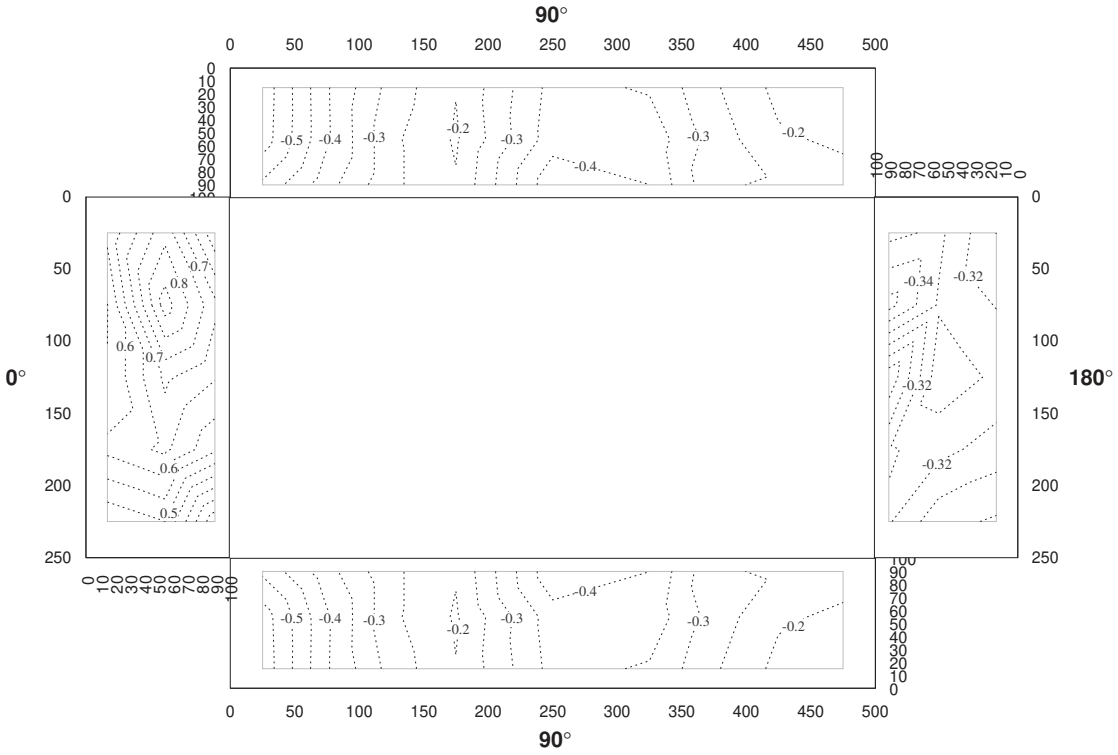

Figure C-16 **Surface Pressures**
A_s=3 and 0.33, Wind Direction=*noted in front of surface*

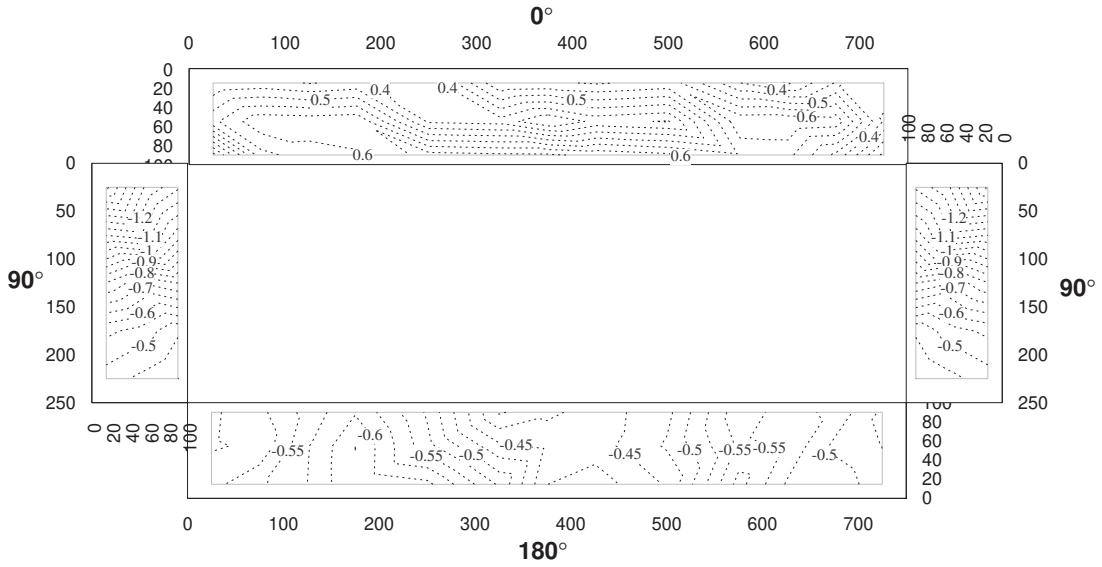

Figure C-17 **Surface Pressures**
A_s=3 and 0.33, Wind Direction=*noted in front of surface*

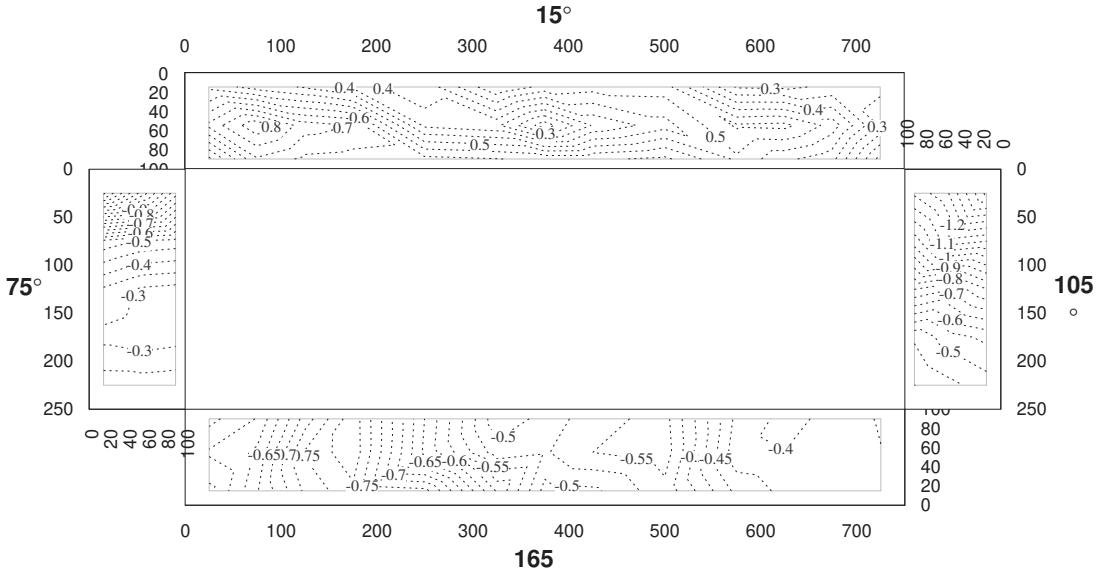

Figure C-18 **Surface Pressures**
A_s=3 and 0.33, Wind Direction=*noted in front of surface*

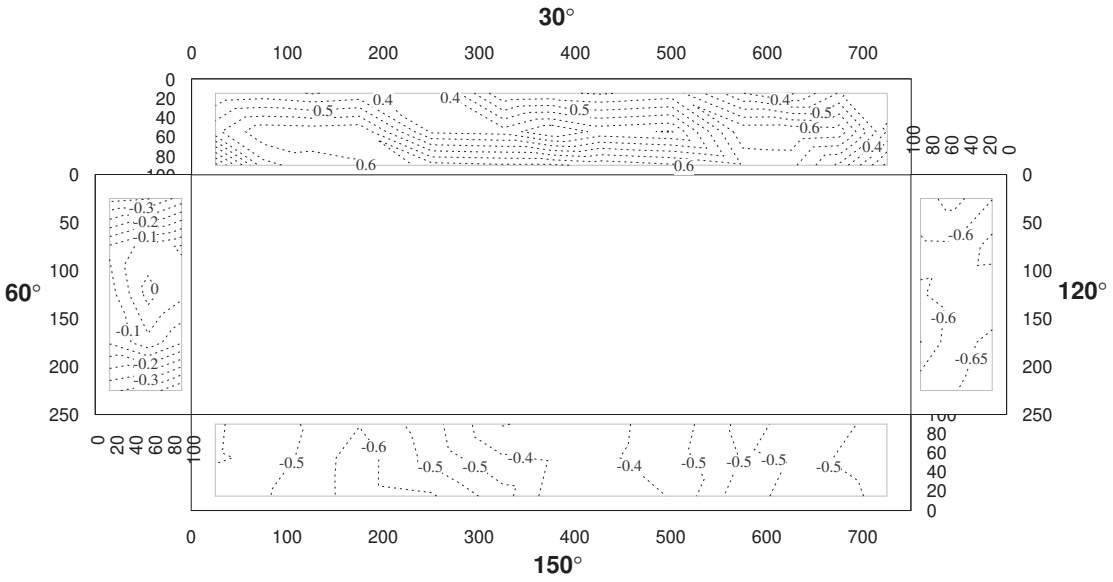

Figure C-19 **Surface Pressures**
A_s=3 and 0.33, Wind Direction=*noted in front of surface*

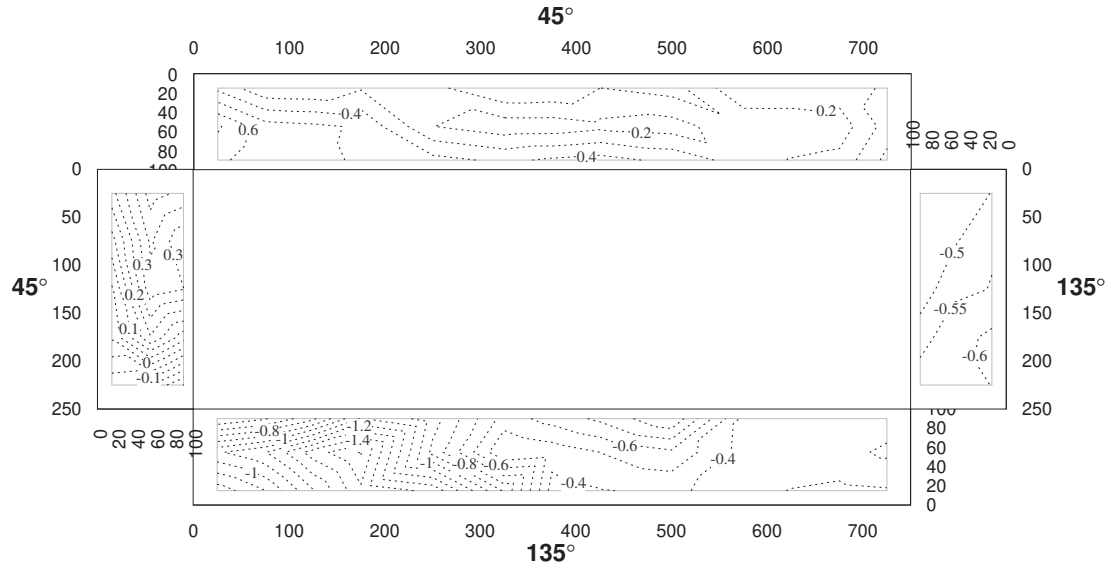

Figure C-20 **Surface Pressures**
A_s=3 and 0.33, Wind Direction=*noted in front of surface*

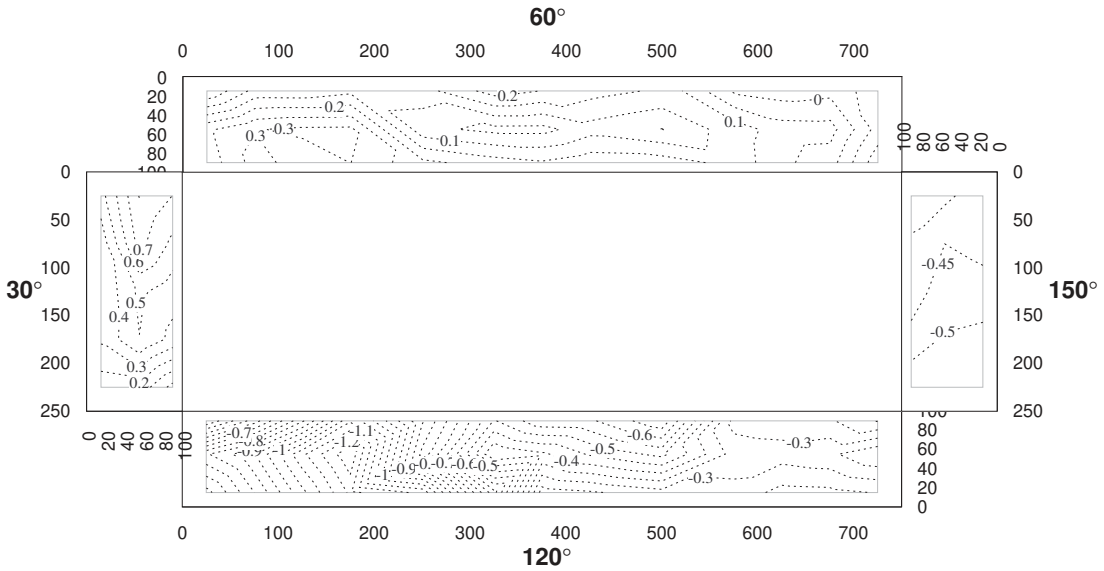

Figure C-21 **Surface Pressures**
A_s=3 and 0.33, Wind Direction=*noted in front of surface*

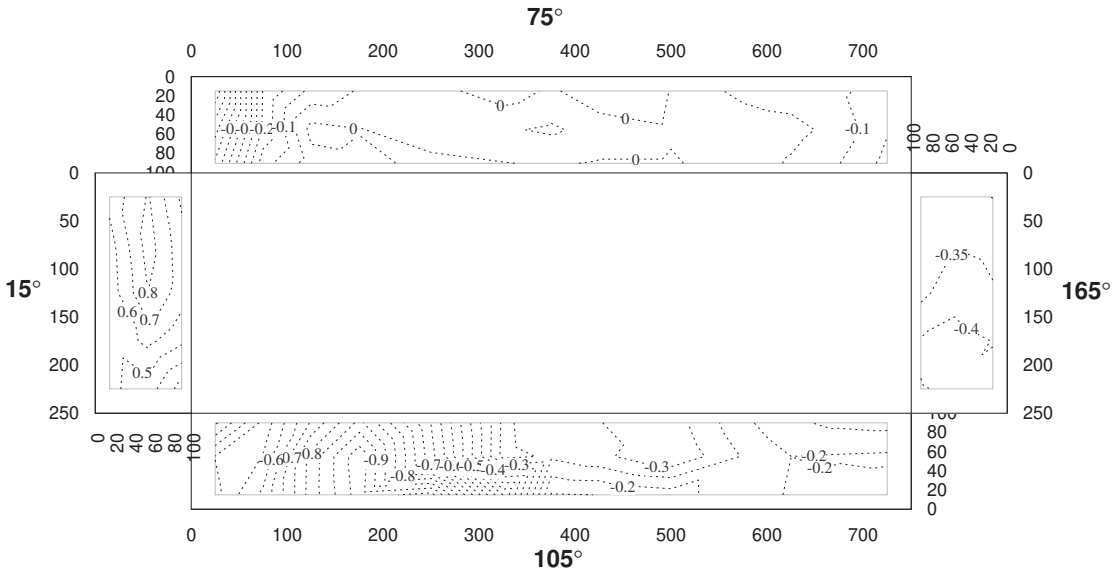

Figure C-22 **Surface Pressures**
A_s=3 and 0.33, Wind Direction=*noted in front of surface*

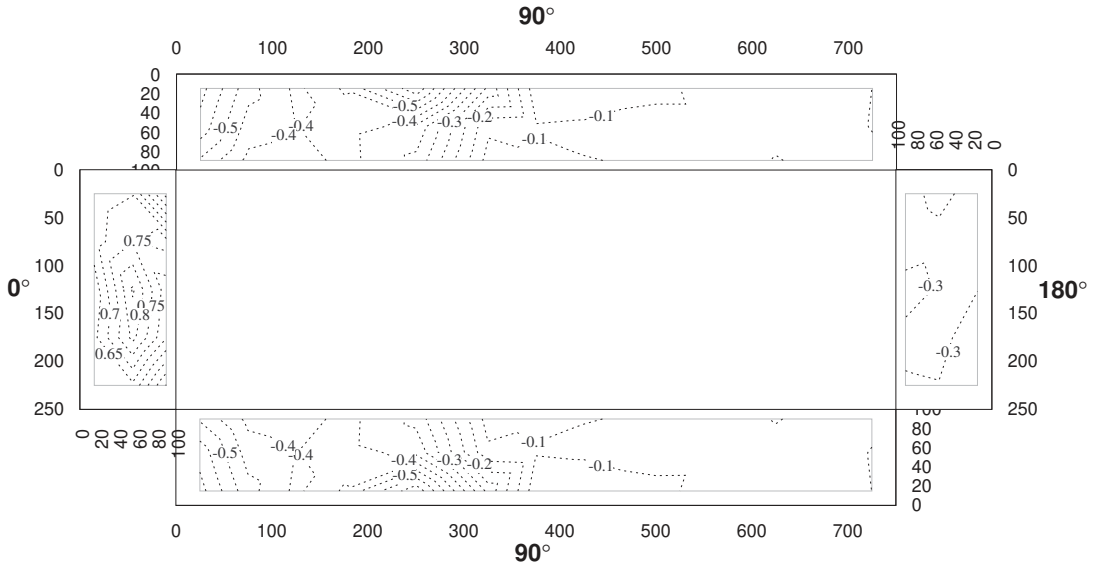

Figure C-23 **Surface Pressures**
A_s=1.5 and 0.67, Wind Direction=*noted in front of surface*

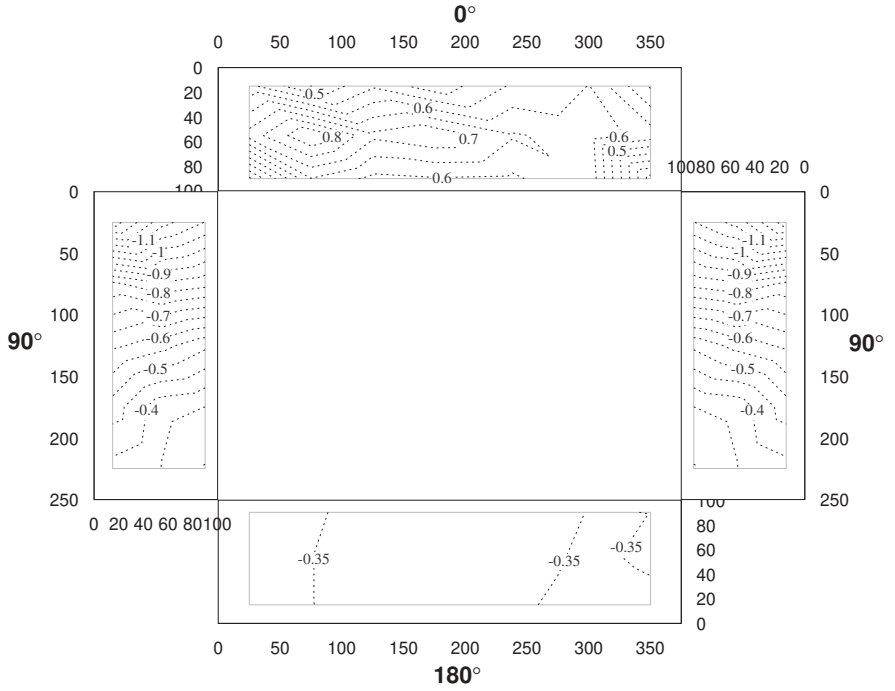

Figure C-24 **Surface Pressures**
A_s=1.5 and 0.67, Wind Direction=*noted in front of surface*

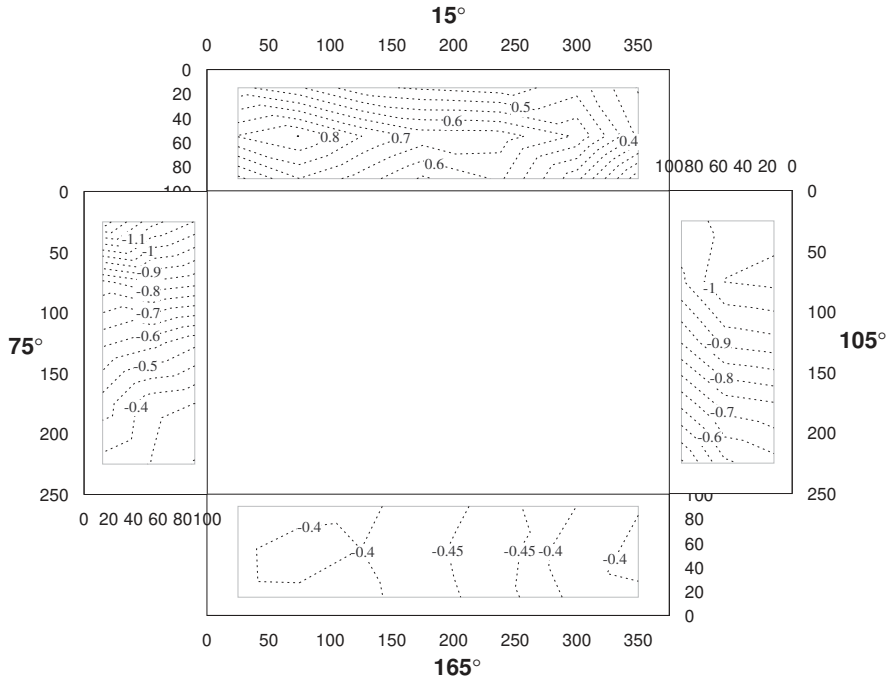

Figure C-25 **Surface Pressures**
A_s=1.5 and 0.67, Wind Direction=*noted in front of surface*

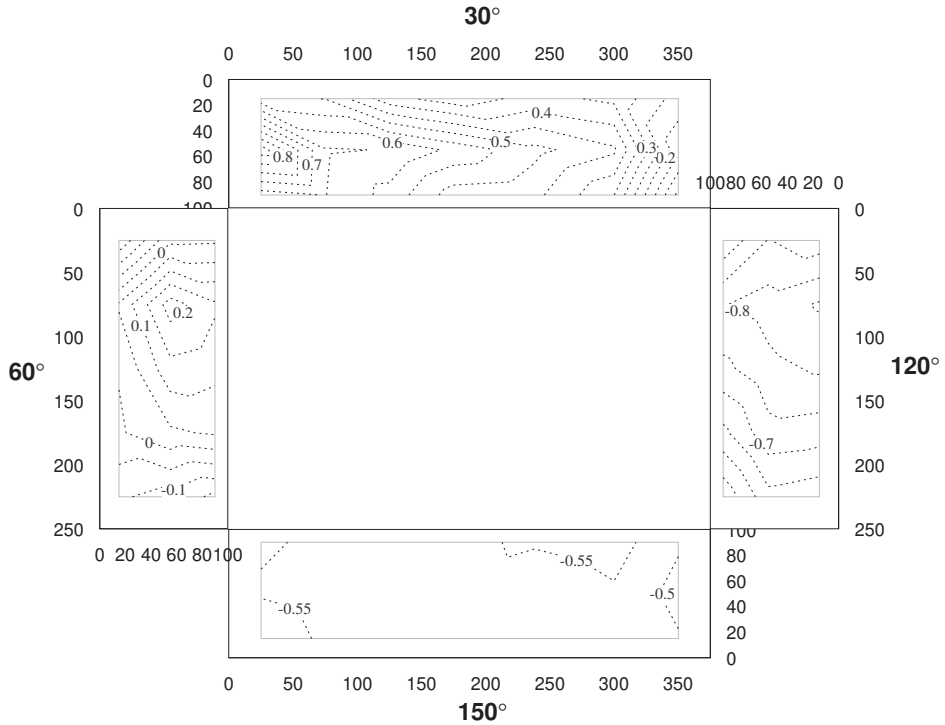

Figure C-26 **Surface Pressures**
A_s=1.5 and 0.67, Wind Direction=*noted in front of surface*

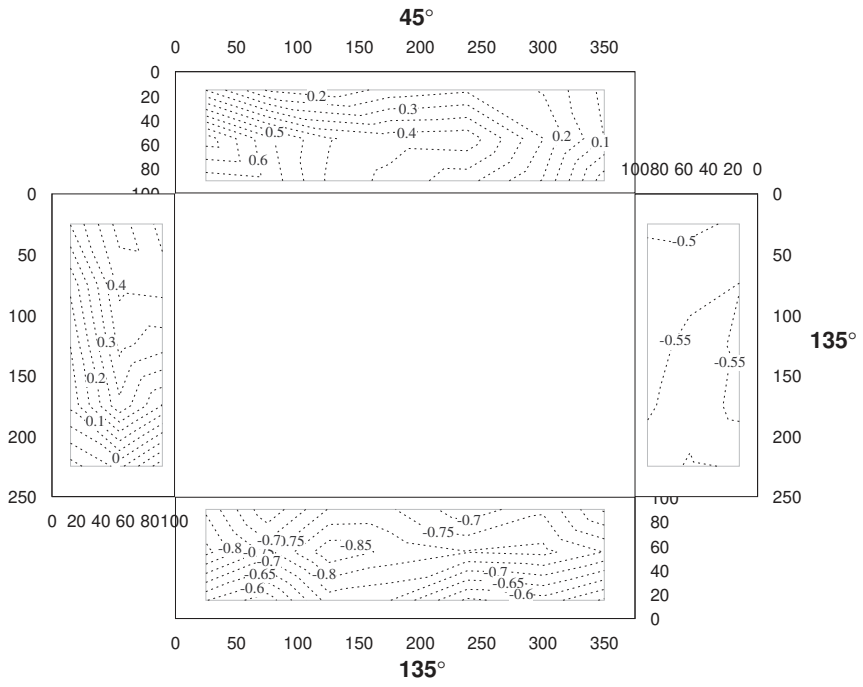

Figure C-27 **Surface Pressures**
A_s=1.5 and 0.67, Wind Direction=*noted in front of surface*

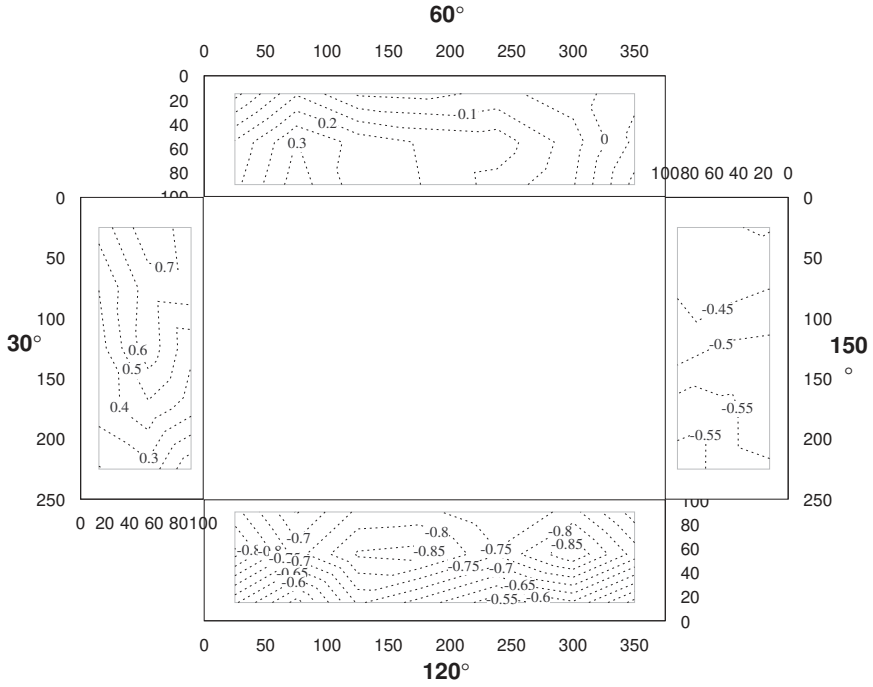

Figure C-28 **Surface Pressures**
A_s=1.5 and 0.67, Wind Direction=*noted in front of surface*

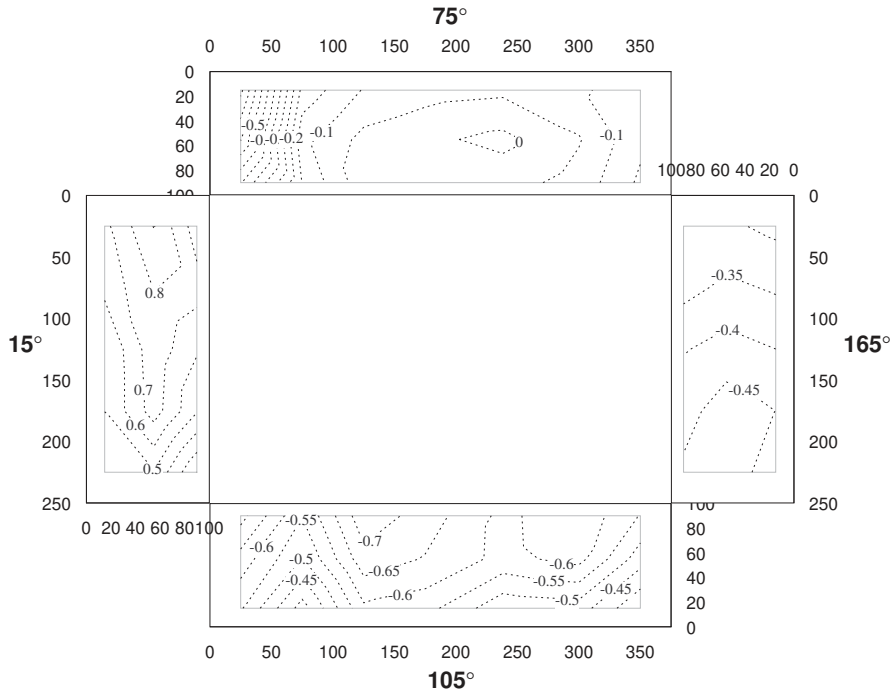

Figure C-29 **Surface Pressures**
A_s=1.5 and 0.67, Wind Direction=*noted in front of surface*

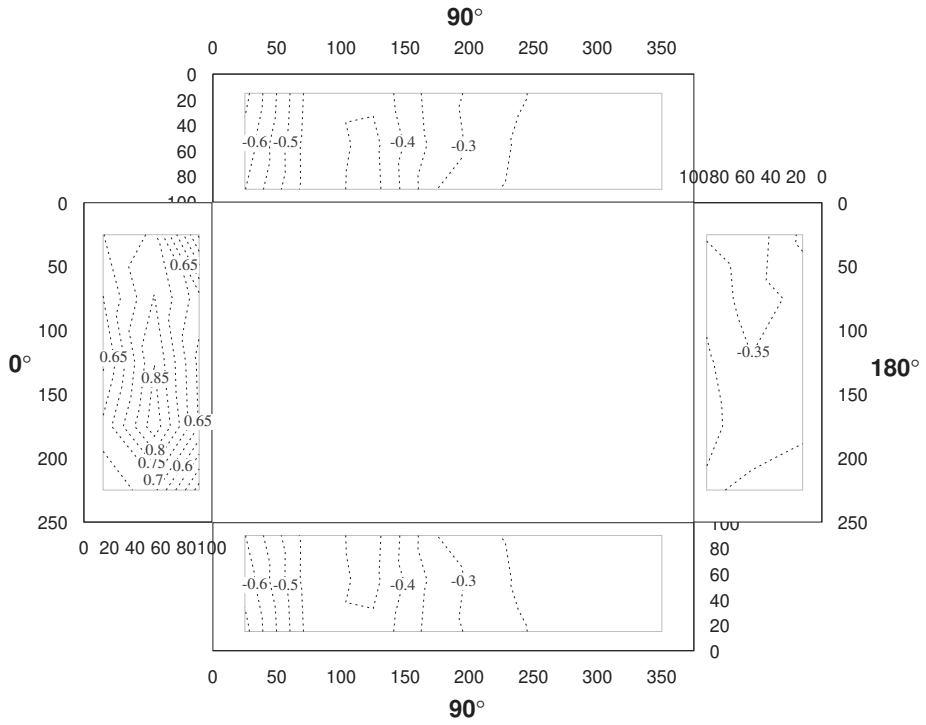

Figure C-30 **Surface Pressures**
A_s=2.5 and 0.4, Wind Direction=*noted in front of surface*

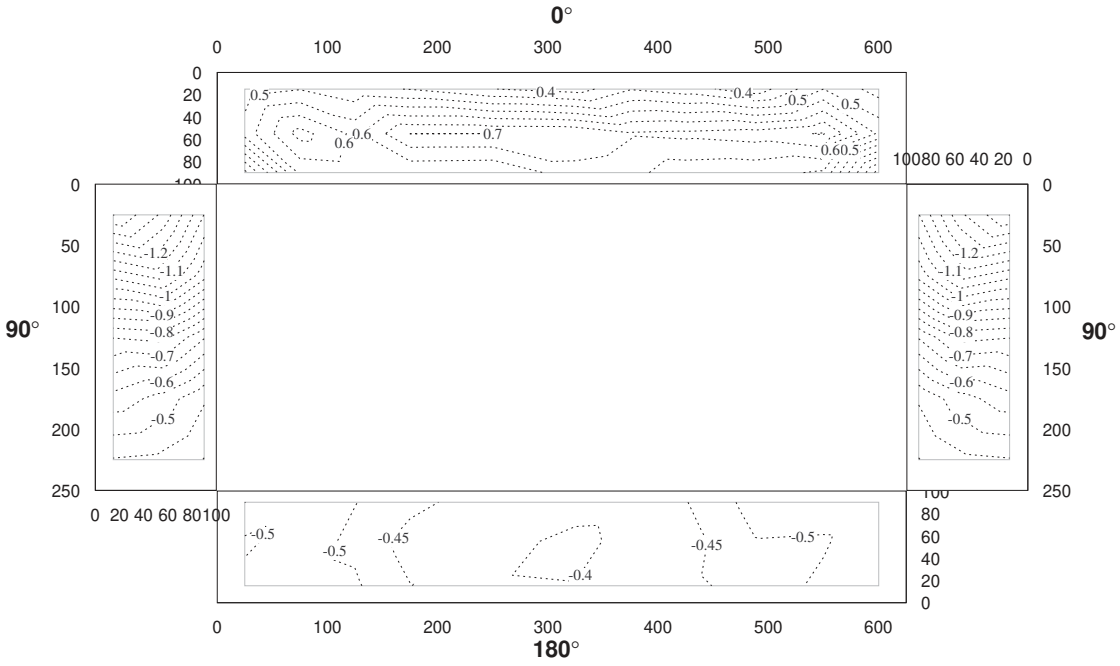

Figure C-31 **surface Pressures**
A_s=2.5 and 0.4, Wind Direction=*noted in front of surface*

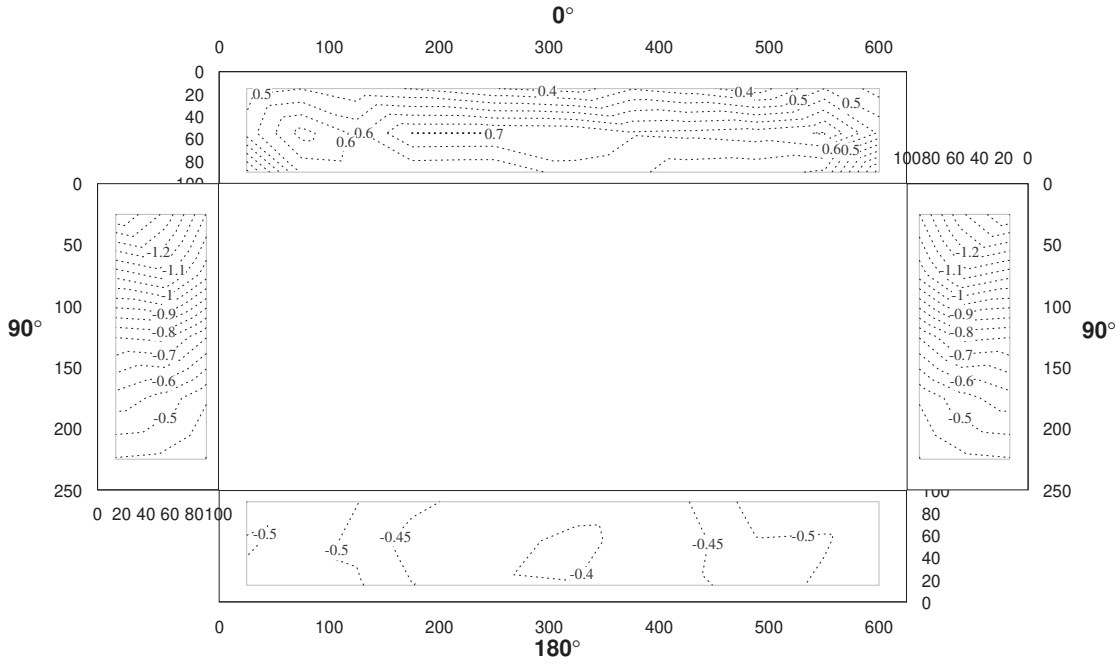

Figure C-32 **surface Pressures**
A_s=2.5 and 0.4, Wind Direction=*noted in front of surface*

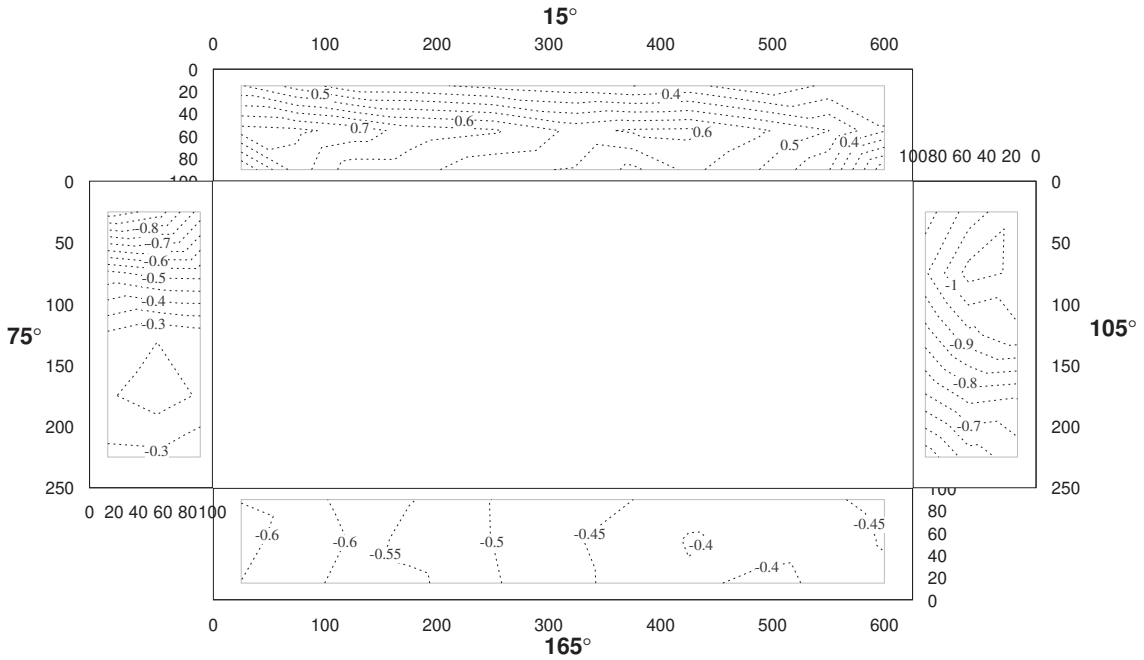

Figure C-33 **surface Pressures**
A_s=2.5 and 0.4, Wind Direction=*noted in front of surface*

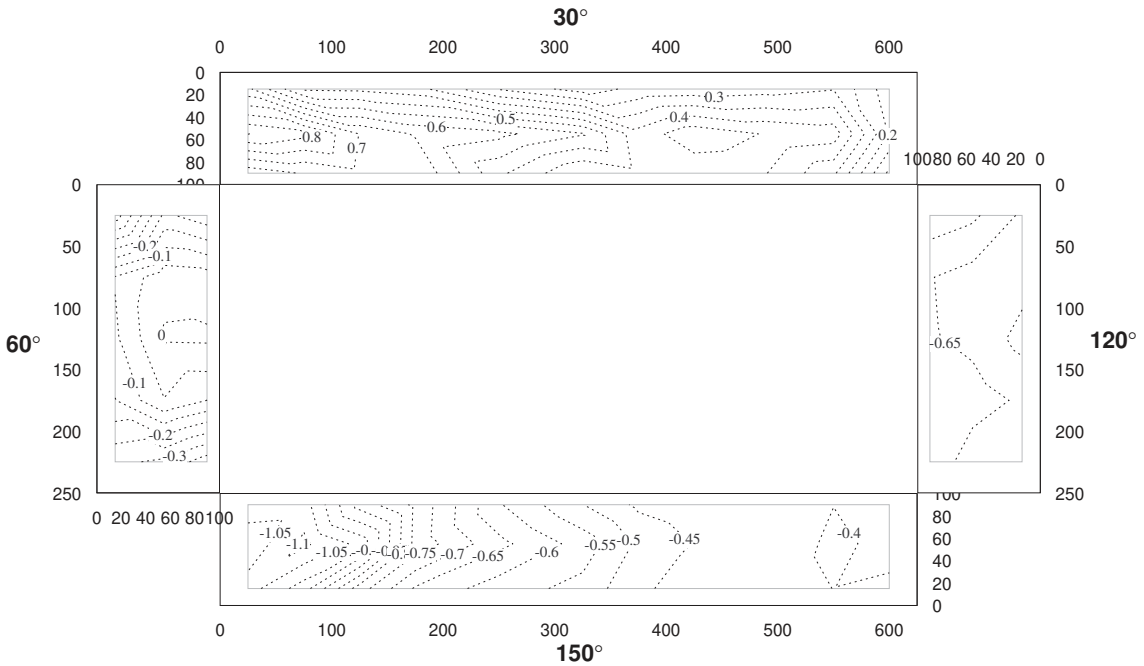

Figure C-34 **surface Pressures**
A_s=2.5 and 0.4, Wind Direction=*noted in front of surface*

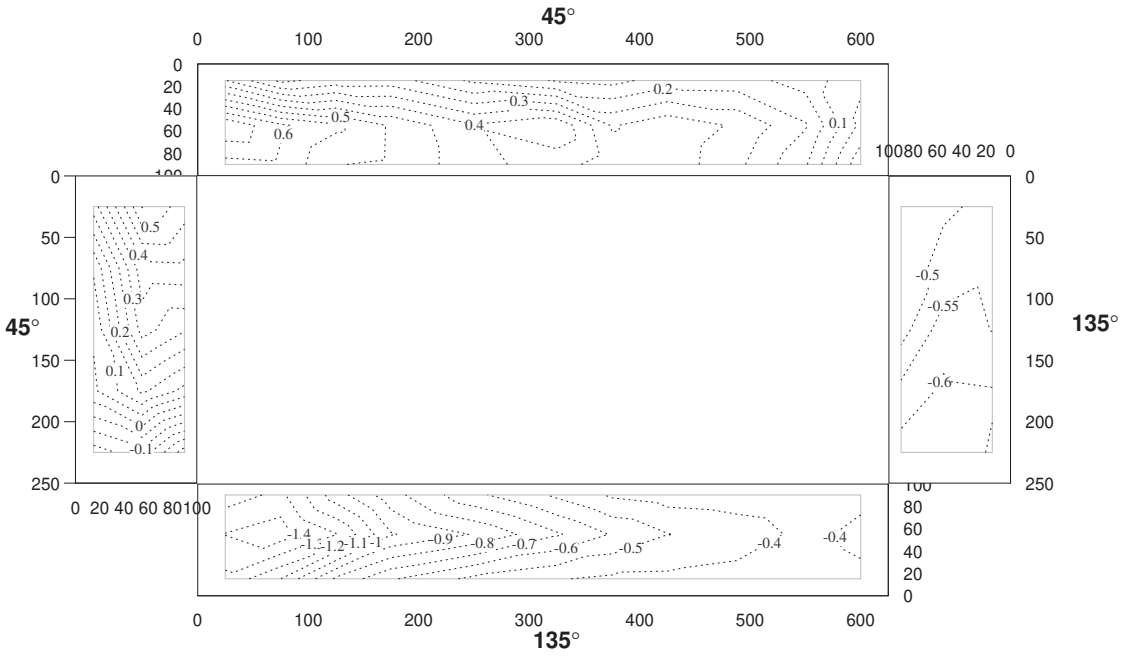

Figure C-35 **surface Pressures**
A_s=2.5 and 0.4, Wind Direction=*noted in front of surface*

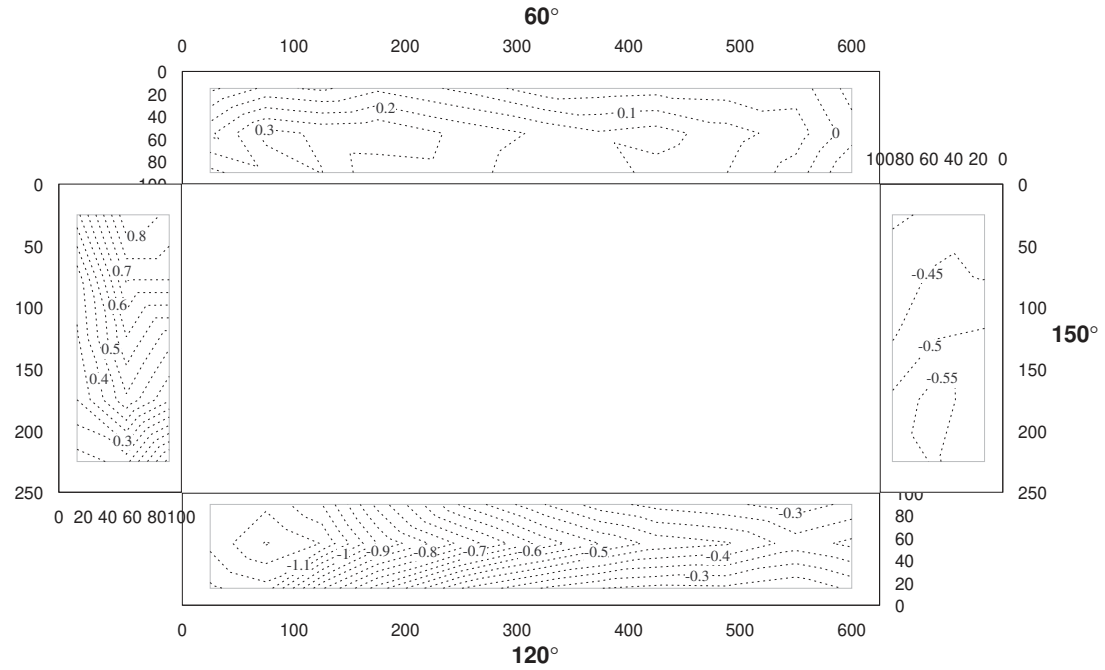

Figure C-36 **surface Pressures**
A_s=2.5 and 0.4, Wind Direction=*noted in front of surface*

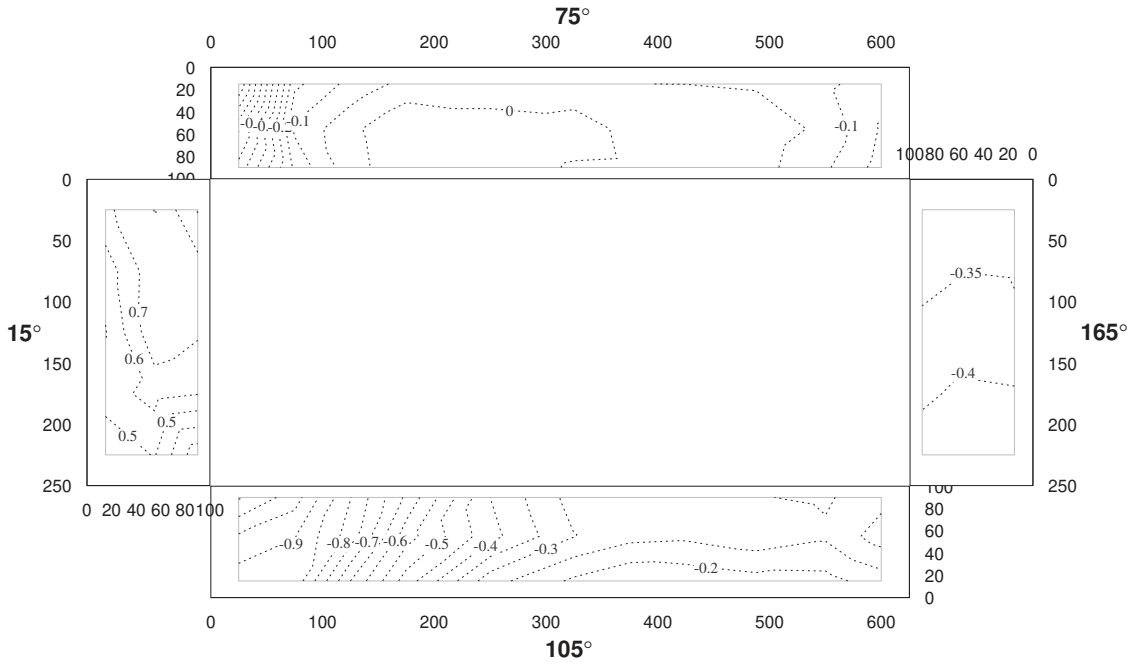

Figure C-37 **surface Pressures**
A_s=2.5 and 0.4, Wind Direction=*noted in front of surface*

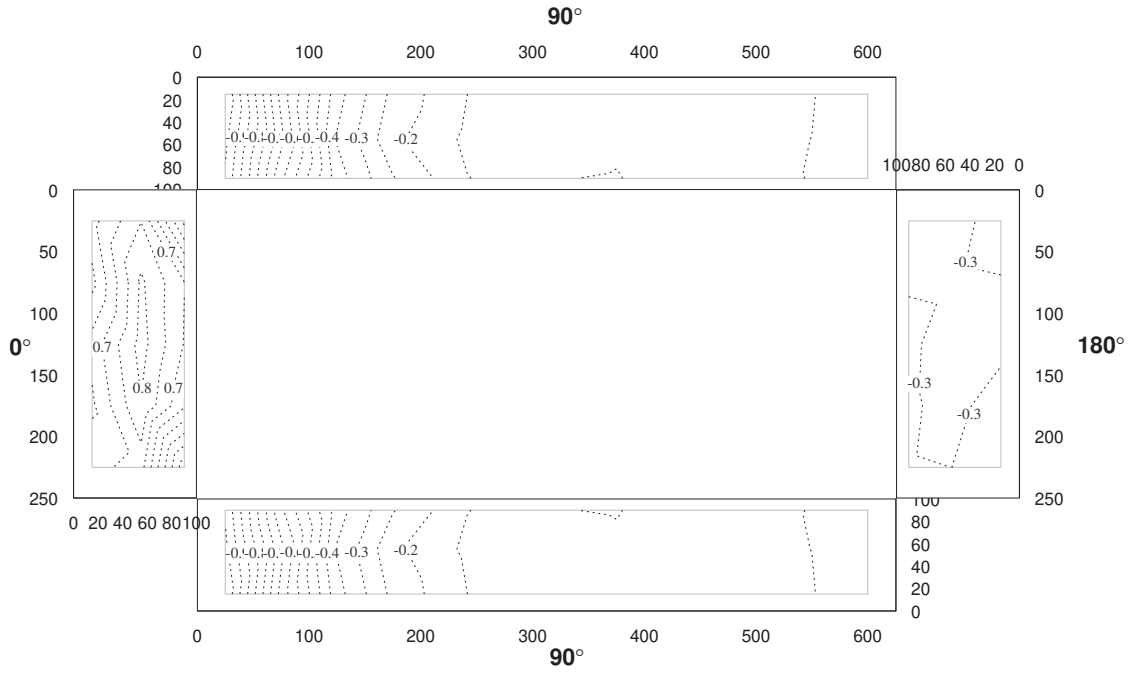

Appendix D

Appendix D

Orthogonal Configurations

D.1 Experiments Results

The following are the results of the orthogonal configurations experiments (refer to Section 4.9, page 70).

D.1.1 Spacing

Figures D-1 to D-18 represent the measured Pressure Coefficients (C_p) and Pressure Modification Coefficients (C_{pm}) expressed as a function of the obstruction spacing between the instruemented model and the obstrcution block[1]. The graphs in figures D-15 to D-18 represent a summary of the collected data and are used for comparison purposes.

D-1. Expressed in obstruction heights.

Figure D-1 **Measured pressure coefficients on windward[2] and leeward[3] surfaces (200×10) obstruction block**

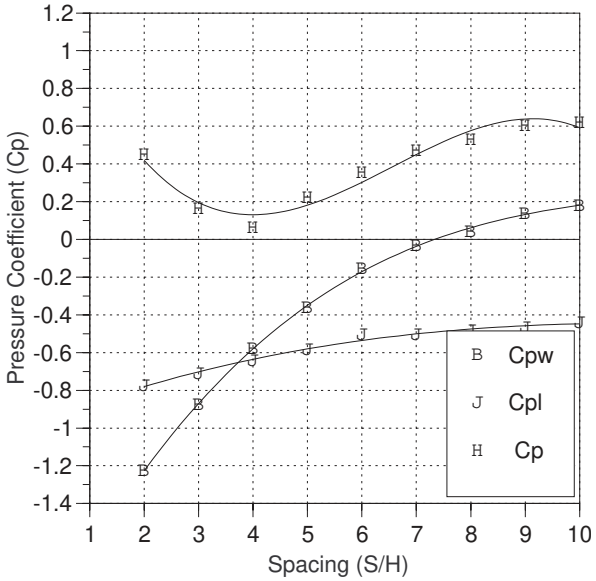

Figure D-2 **Measured pressure coefficients on windward and leeward surfaces (150×10) obstruction block**

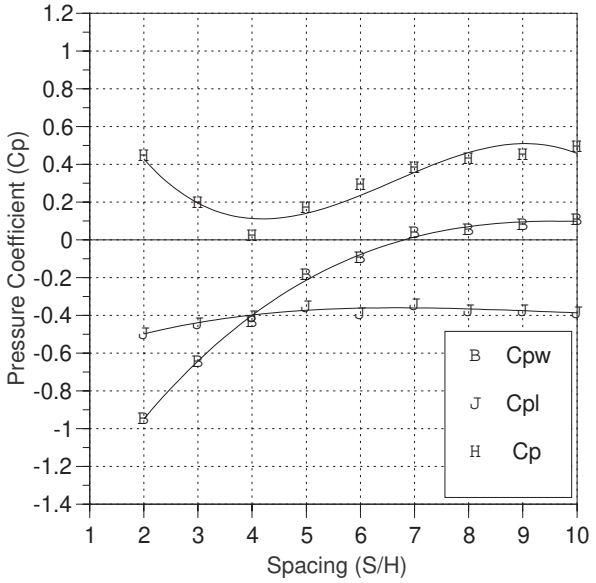

D-2.Obstruction-facing surface

D-3.Unobstructed surface

Figure D-3 **Measured cressure Coefficients on windward and leeward surfaces (89×10) obstruction block**

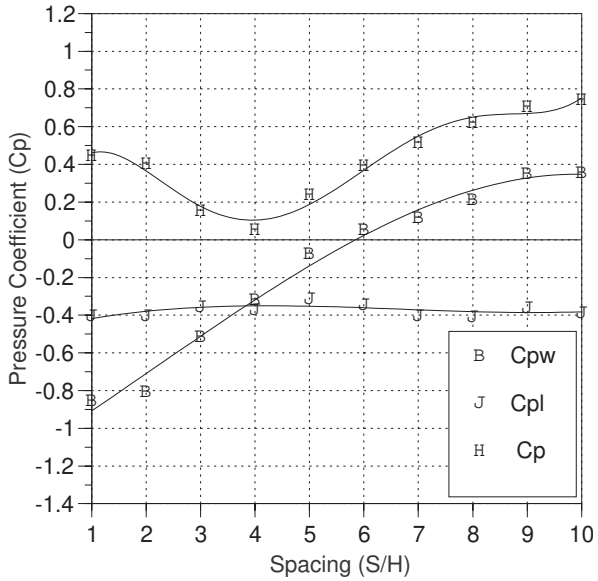

Figure D-4 **Measured pressure coefficients on windward and leeward surfaces (25×10) obstruction block**

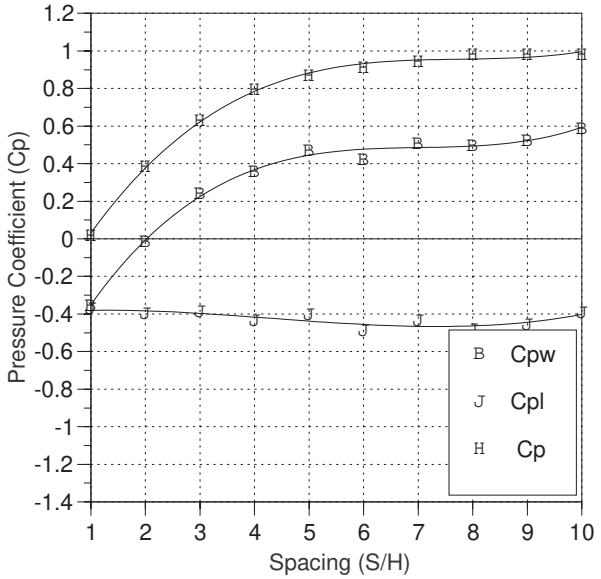

Figure D-5 **Measured pressure coefficients on windward and leeward surfaces (25×17) obstruction block**

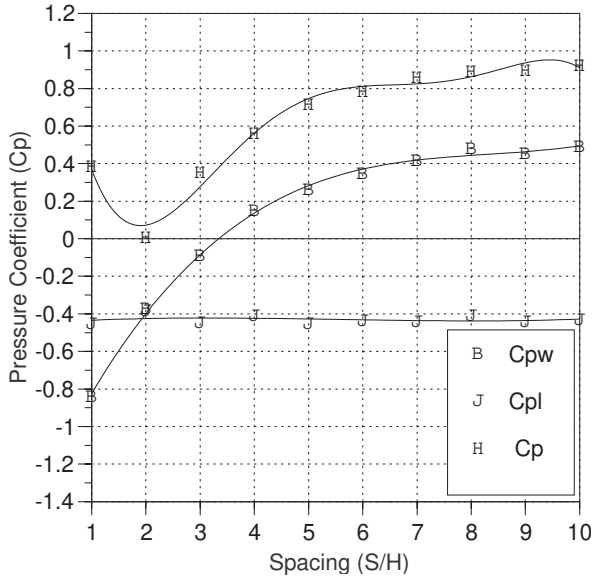

Figure D-6 **Measured pressure coefficients on windward and leeward surfaces (25×7) obstruction block**

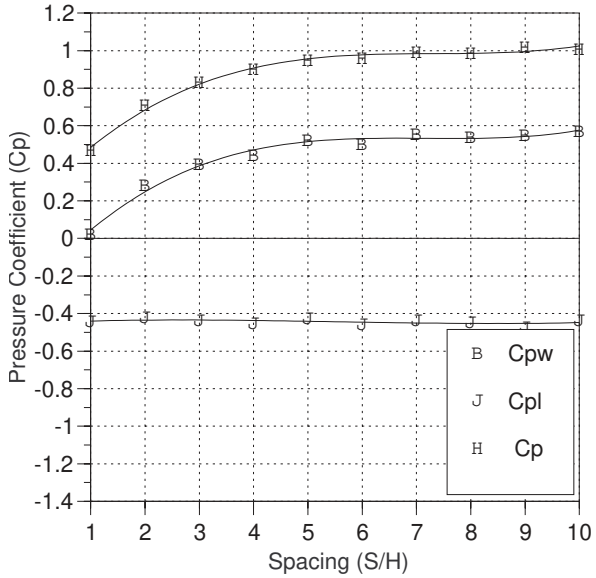

Figure D-7 **Measured pressure coefficients on windward and leeward surfaces (25×25) obstruction block**

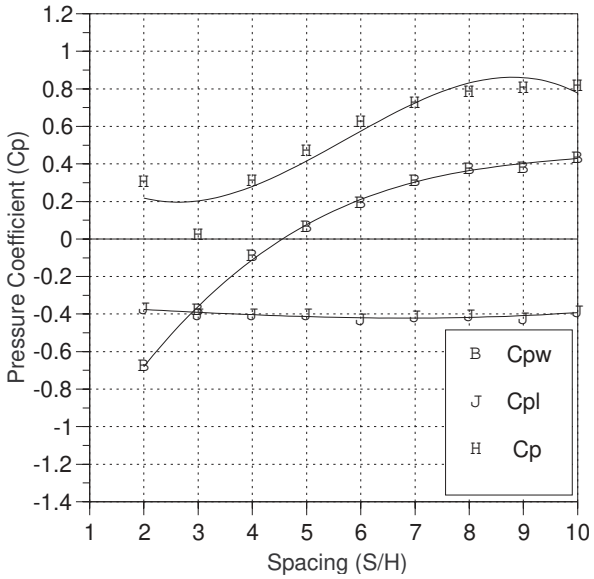

Figure D-8 **Measured pressure modification coefficients on windward and leeward surfaces (200×10) obstruction block**

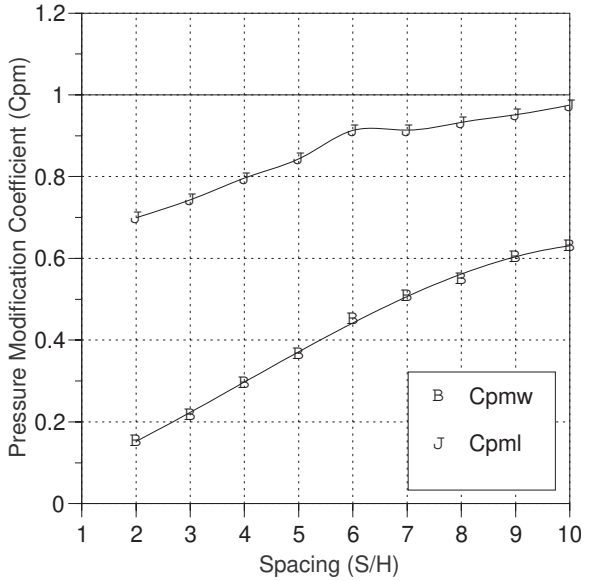

Figure D-9 **Measured pressure modification coefficients on windward and leeward surfaces (** 150×10 **) obstruction block**

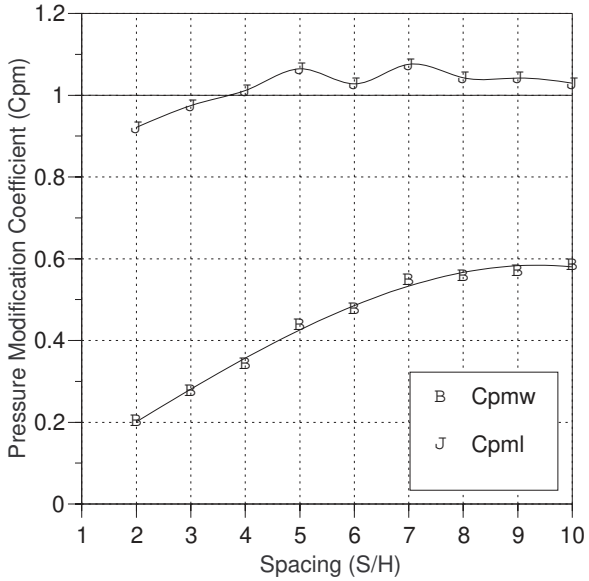

Figure D-10 **Measured pressure modification coefficients on windward and leeward surfaces (** 89×10 **) obstruction block**

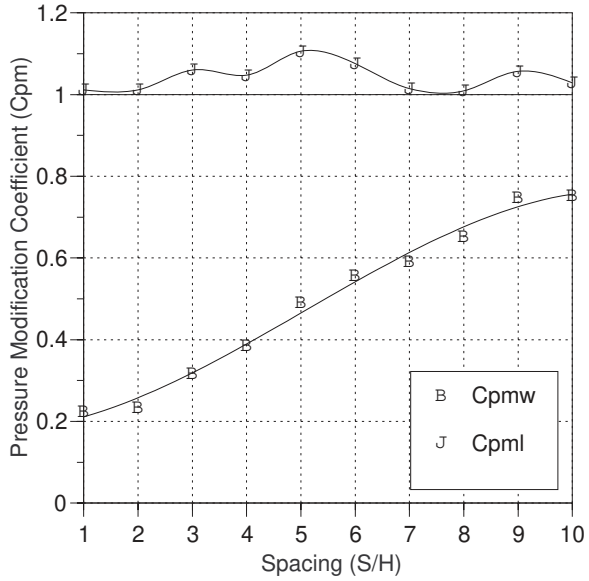

Figure D-11 **Measured pressure modification coefficients on windward and leeward surfaces (25×10) obstruction block**

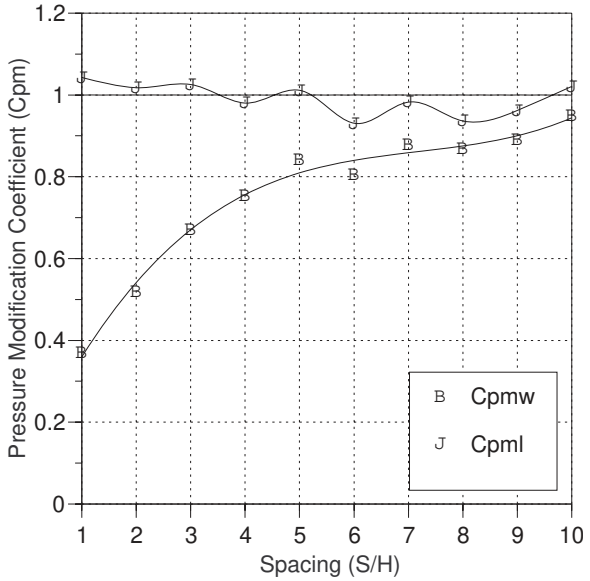

Figure D-12 **Measured pressure modification coefficients on windward and leeward surfaces (25×17) obstruction block**

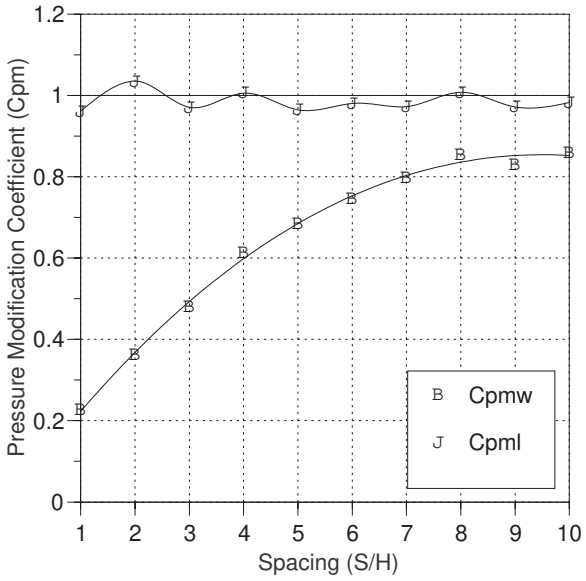

Figure D-13 **Measured pressure modification coefficients on windward and leeward surfaces (25×7) obstruction block**

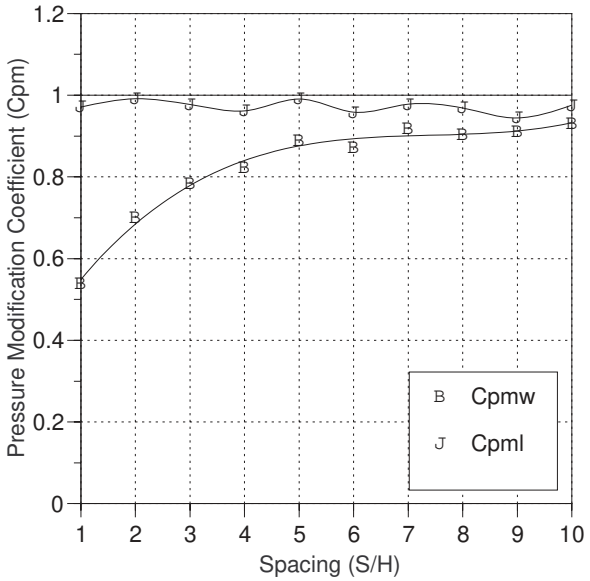

Figure D-14 **Measured pressure modification coefficients on windward and leeward surfaces (25×25) obstruction block**

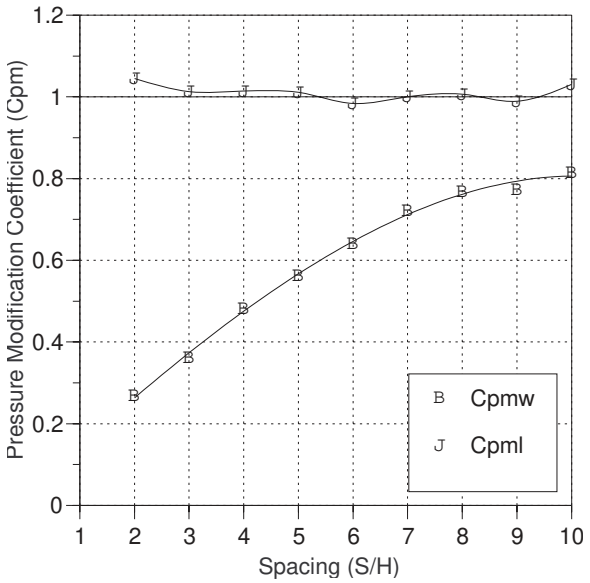

Figure D-15 **Effect of spacing on pressure coefficients (C_p) on windward (ww) and leeward (lw) sides**

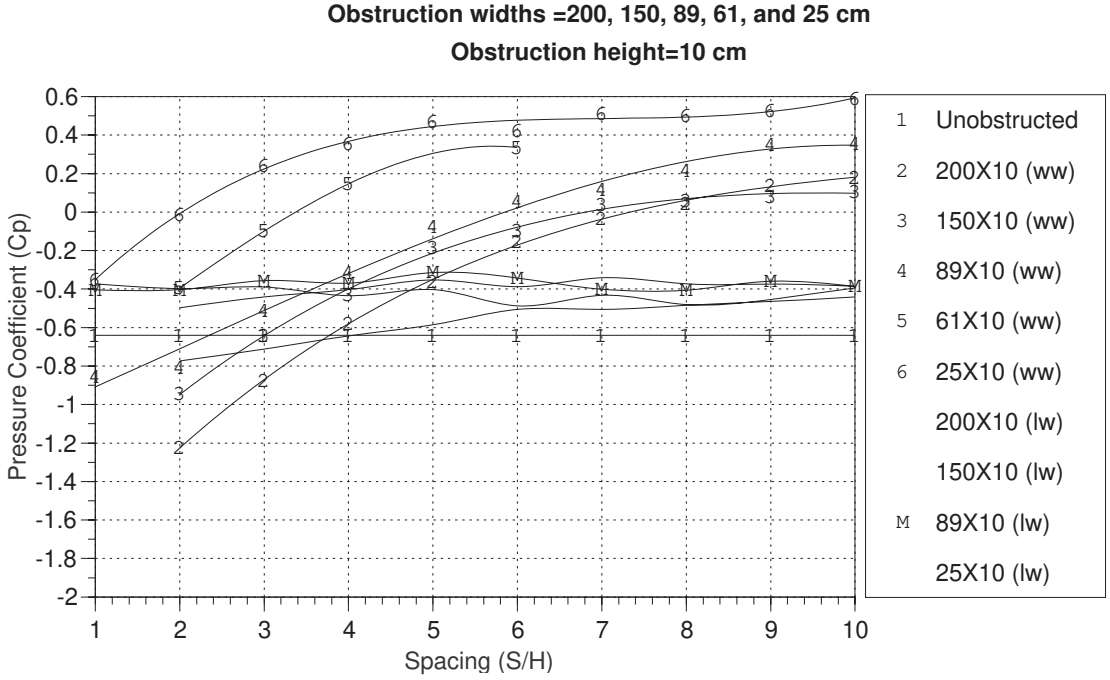

Figure D-16 **Effect of spacing on pressure coefficients (C_p) on windward (ww) and leeward (lw) sides**

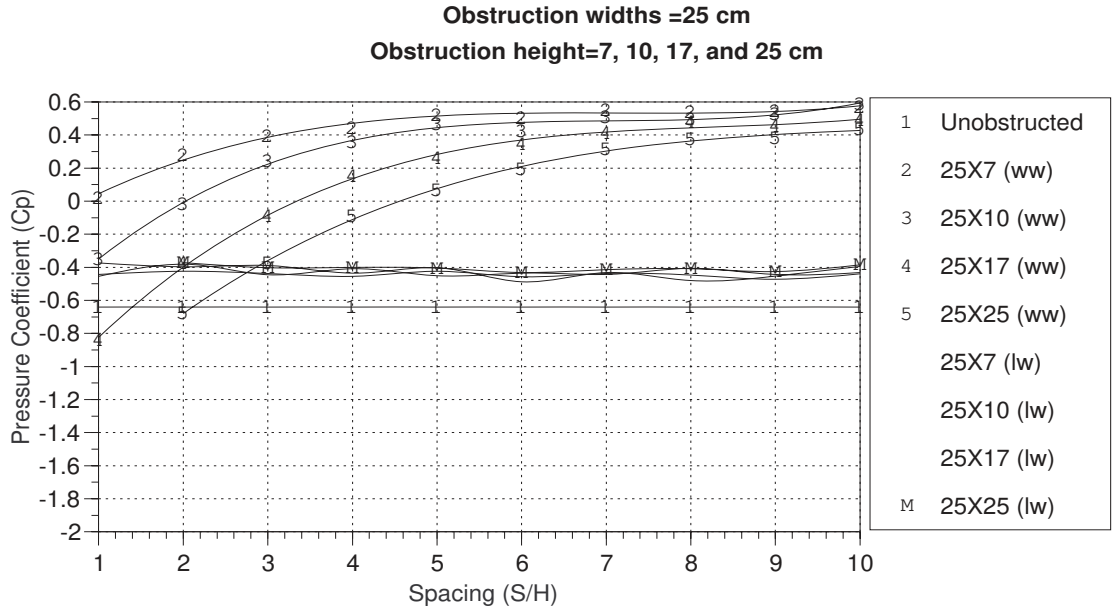

Figure D-17 **Effect of spacing on pressure modification coefficients (C_{pm}) on windward (ww) and leeward (lw) sides**

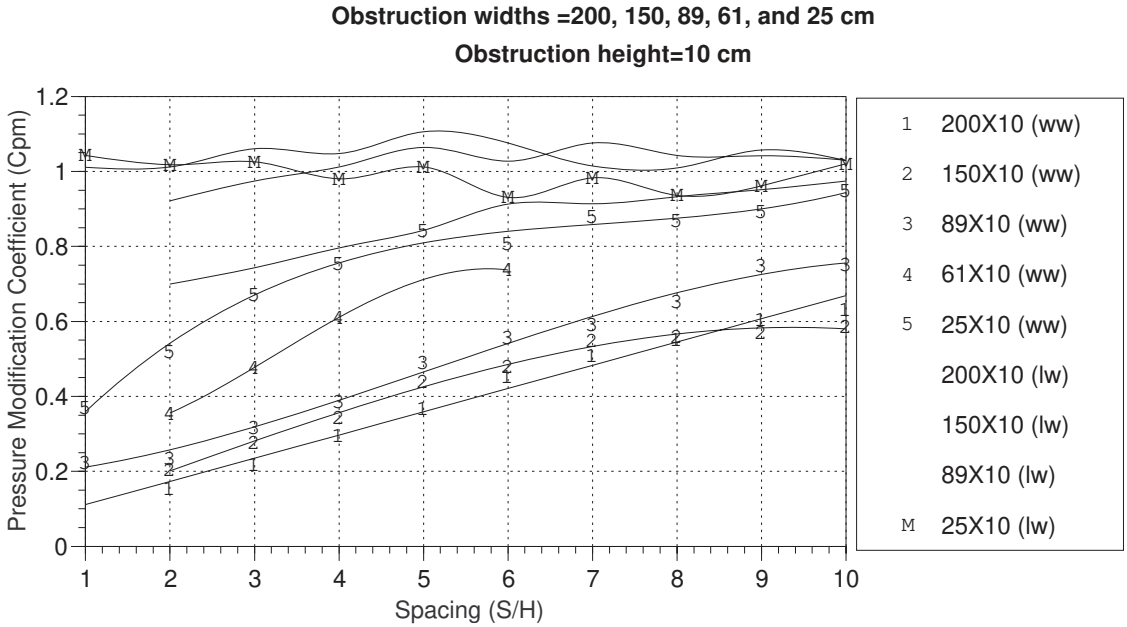

Figure D-18 **Effect of spacing on pressure modification coefficients (C_{pm}) on windward (ww) and leeward (lw) sides**

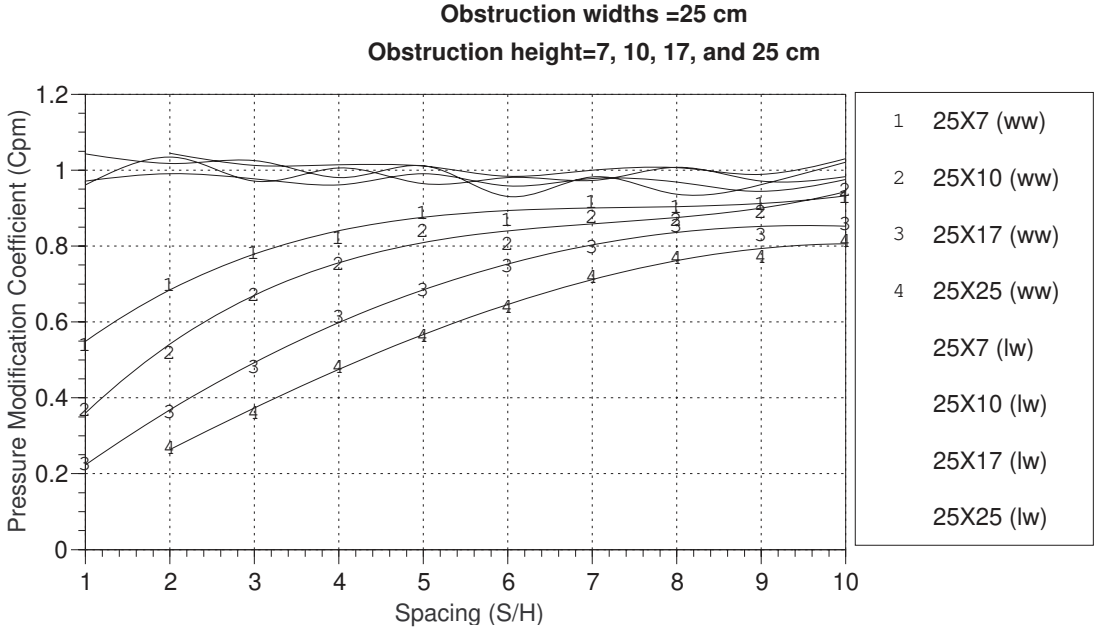

D.1.2 Horizontal Angle

Figures D-19 to D-22 represent the measured Pressure Coefficients (C_p) and Pressure Modification Coefficients (C_{pm}) expressed as a function of the horizontal angle[4] (α_h).

Figure D-19 **Effect of horizontal angle (α_h) on pressure coefficients (C_p) on the obstruction facing side**

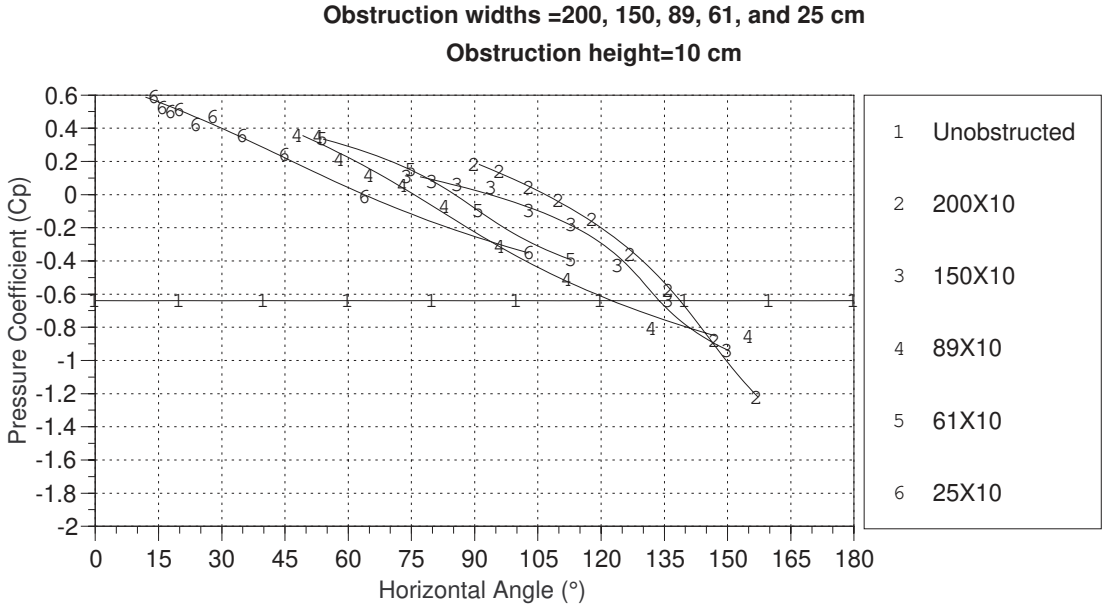

D-4. For the definition of the obstruction angles, refer to Section 4.6, page 64

Figure D-20 **Effect of horizontal angle (α_h) on pressure coefficients (C_p) on the obstruction facing side**

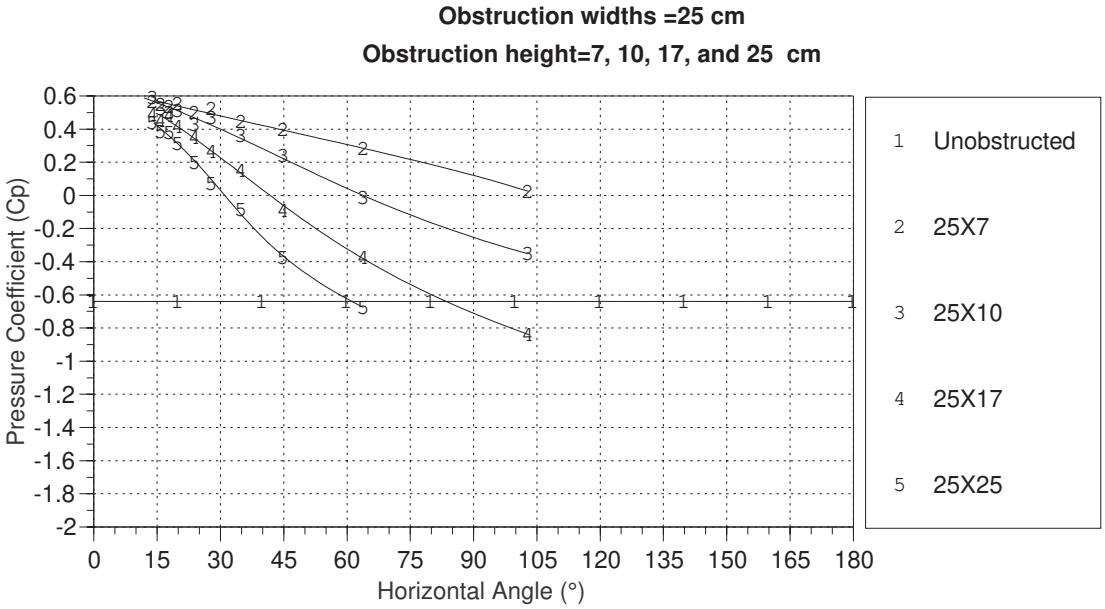

Figure D-21 **Effect of horizontal angle (α_h) on pressure modification coefficients (C_{pm}) on the obstruction facing side**

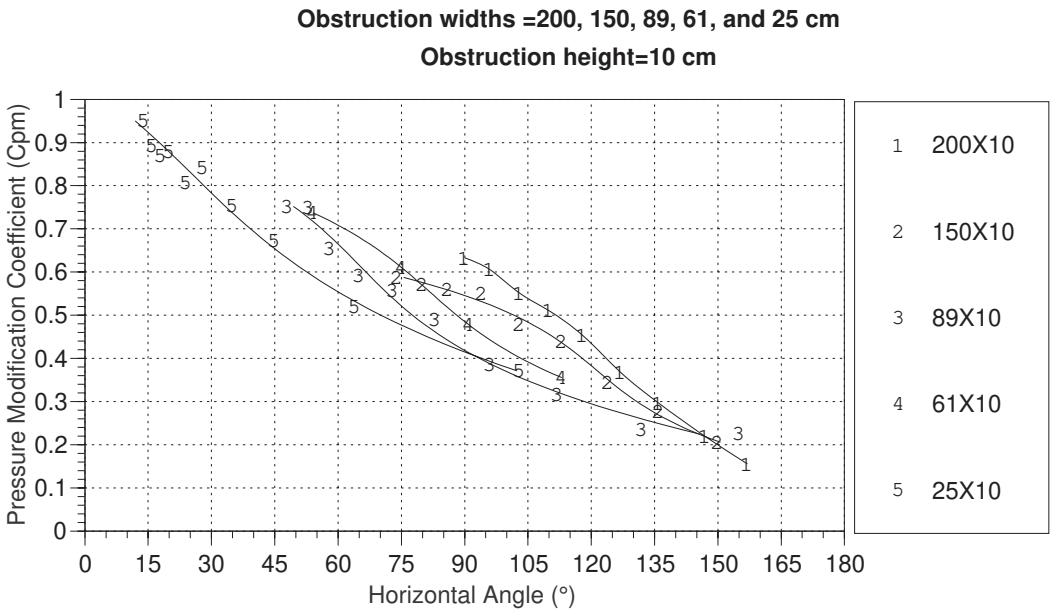

Figure D-22 **Effect of horizontal angle (α_h) on pressure modification coefficients (C_{pm}) on the obstruction facing side**

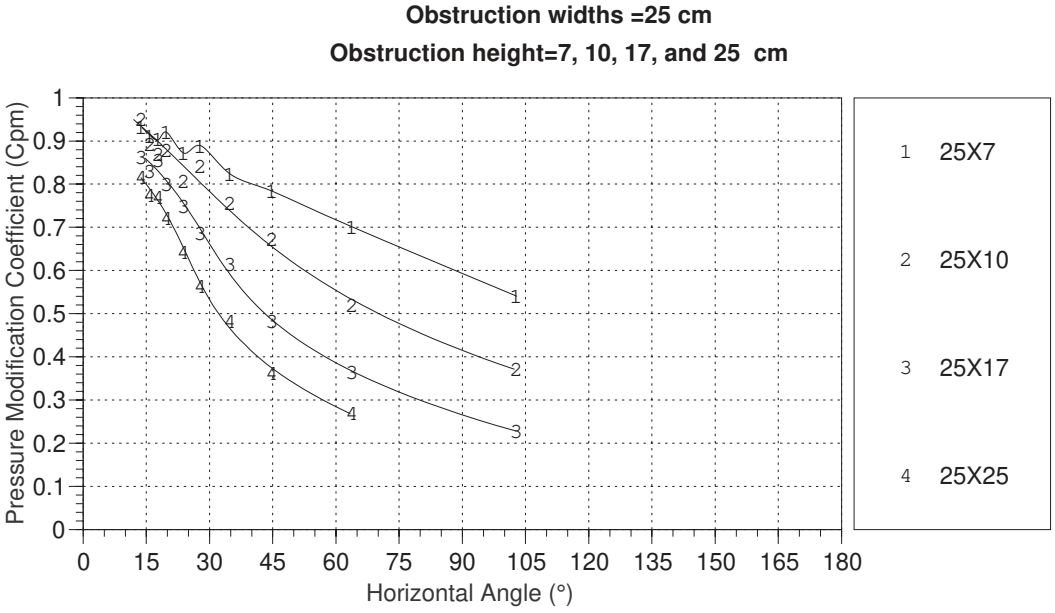

D.1.3 Vertical Angle

Figures D-23 to D-26 represent the measured Pressure Coefficients (C_p) and Pressure Modification Coefficients (C_{pm}) expressed as a function of the Vertical Angle (α_v).

Figure D-23 **Effect of vertical angle (α_v) on pressure coefficients (C_p) on the obstruction facing side**

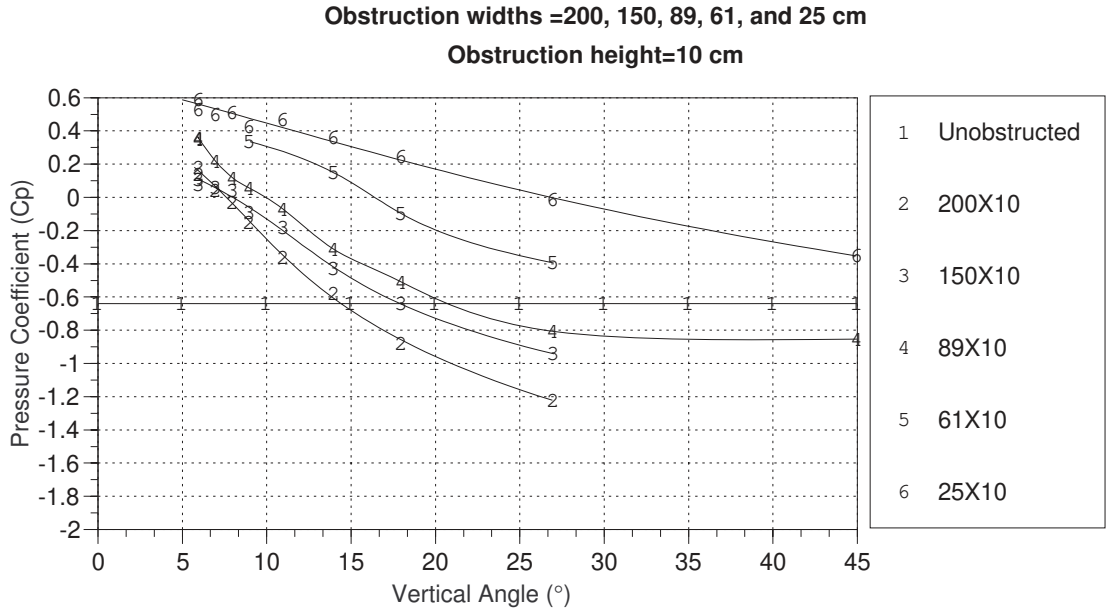

Figure D-24 **Effect of vertical Angle (α_v) on pressure coefficients (C_p) on the obstruction facing side**

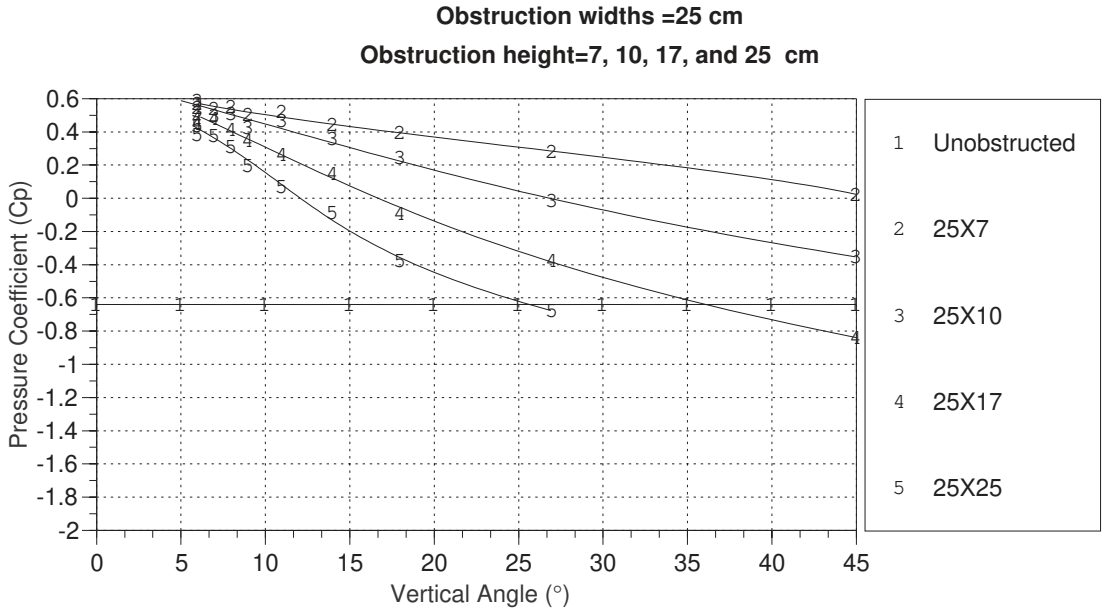

Figure D-25 **Effect of vertical angle (α_v) on pressure modification coefficients (C_{pm}) on the obstruction facing side**

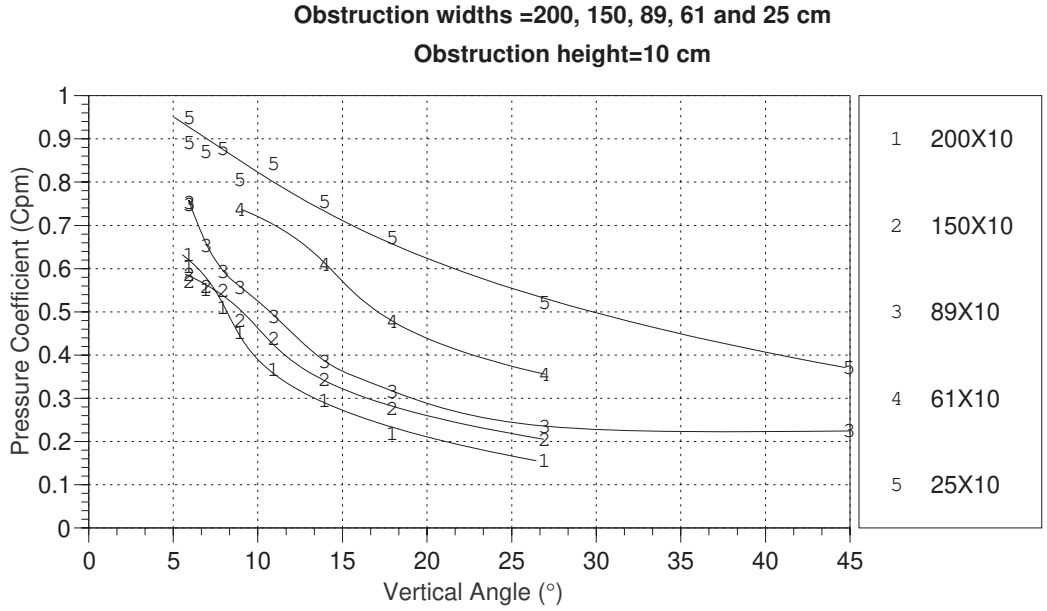

Figure D-26 **Effect of vertical angle (α_v) on pressure modification coefficients (C_{pm}) on the obstruction facing side**

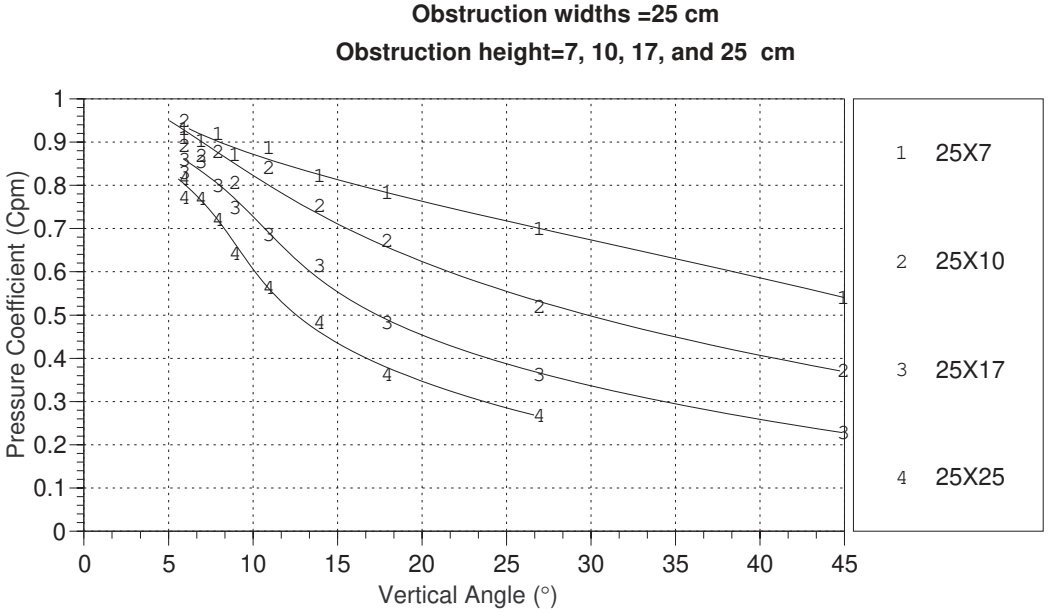

D.2 Complex Function

Section 4.12.3 in Chapter 4 describes the derivation of the orthogonal model. Two functions were developed: the first for ease of use[5], and the second for accuracy. For increased accuracy[6], the following function i.e. Equation D-1 represents the long version of the Orthogonal function used in determining the Pressure Modification Coefficient C_{pm} values shown in Figure 4-45[7]. This function is also intended to be used in the algorithm described in Chapter 5 and Appendix H .

D-5.Equation 4-11, page 96.

D-6.Increase the sensitivity of the function to predict minute variations in C_{pm} values relative to the simple function described above.

D-7. page 98.

$$C_{pm(\text{ortho})} = C_0 \cdot \sin\left(\frac{\alpha_h}{2}\right) \cdot \sin(\alpha_v) + C_1 \cdot \cos\left(\frac{\alpha_h}{2}\right)^{\sin(\alpha_v)} \quad \textbf{(D-1)}$$

$$+ C_2 \cdot \left[\cos\left(\frac{\alpha_h}{2}\right)^{\sin(\alpha_v)}\right]^2 + C_3 \cdot \cos(\alpha_v)^{\sin\left(\frac{\alpha_h}{2}\right)}$$

$$+ C_4 \cdot \left[\cos(\alpha_v)^{\sin\left(\frac{\alpha_h}{2}\right)}\right]^2 + C_5 \cdot \cos\left(\frac{\alpha_h}{2}\right)^{\sin(\alpha_v)} \cdot \cos(\alpha_v)^{\sin\left(\frac{\alpha_h}{2}\right)}$$

$$+ C_6 \cdot \left[\cos\left(\frac{\alpha_h}{2}\right)^{\sin(\alpha_v)}\right]^2 \cdot \left[\cos(\alpha_v)^{\sin\left(\frac{\alpha_h}{2}\right)}\right]^2$$

$$+ C_7 \cdot \left[\cos(\alpha_v)^{\sin\left(\frac{\alpha_h}{2}\right)}\right]^3 + C_8 \cdot \left[\cos\left(\frac{\alpha_h}{2}\right)^{\sin(\alpha_v)}\right]^3$$

$$+ C_9 \cdot \ln\left[\cos(\alpha_v)^{\sin\left(\frac{\alpha_h}{2}\right)}\right] + C_{10} \cdot \left[\cos\left(\frac{\alpha_h}{2}\right)\right]^{\left[\sin\left(\frac{\alpha_h}{2}\right) \cdot \sin(\alpha_v)\right]}$$

$$+ C_{11} \cdot [\cos(\alpha_v)]^{\left[\sin\left(\frac{\alpha_h}{2}\right) \cdot \sin(\alpha_v)\right]}$$

$$+ C_{12} \cdot \left[\cos\left(\frac{\alpha_h}{2}\right)\right]^{\left[\sin\left(\frac{\alpha_h}{2}\right) \cdot \sin(\alpha_v)\right]} \cdot [\cos(\alpha_v)]^{\left[\sin\left(\frac{\alpha_h}{2}\right) \cdot \sin(\alpha_v)\right]}$$

where

$C_1 = -10.4352$ $\quad$ $C_7 = -16.7205$

$C_2 = -72.0518$ $\quad$ $C_8 = 60.1141$

$C_3 = -12.5624$ $\quad$ $C_9 = 11.7711$

$C_4 = -41.4130$ $\quad$ $C_{10} = -4.4688$

$C_5 = -107.5238$ $C_{11} = 54.1139$

$C_6 = 72.5058$ $C_{12} = 85.4555$

$C_{13} = -32.6831$

Appendix E

Appendix E

Displacement Effects

This appendix was created to document the displacement effects of the obstruction model on the pressure coefficient C_p profile across the shielded model surface. The objective of this set of experiments was to locate the effects of horizontal obstruction model displacement. Three variables were tested; 1) obstruction width, 2) displacement, and 3) the horizontal spacing. The specifics of the tested configurations were listed in Table 4-4. A full discussion of the displacement effect is presented in Section 4.13.1, page 99.

Figure E-1. **Displacement Shielding.**

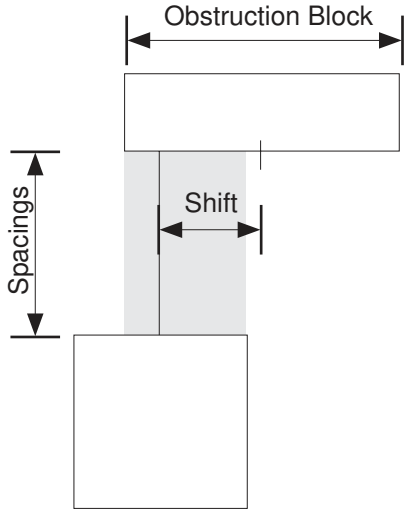

All data in the following figures were based on the Normalized Pressure Coefficients (see definition below).

$$C_{p(Norm)} = \text{Normalized Pressure Coefficient} = C_{p(Shielded)} / C_{p(Unshielded)} \quad \textbf{(E-1)}$$

Figure E-2 **Displacement profiles for obstruction width=25 cm and spacing =20 cm (shaded area = shielded area).**

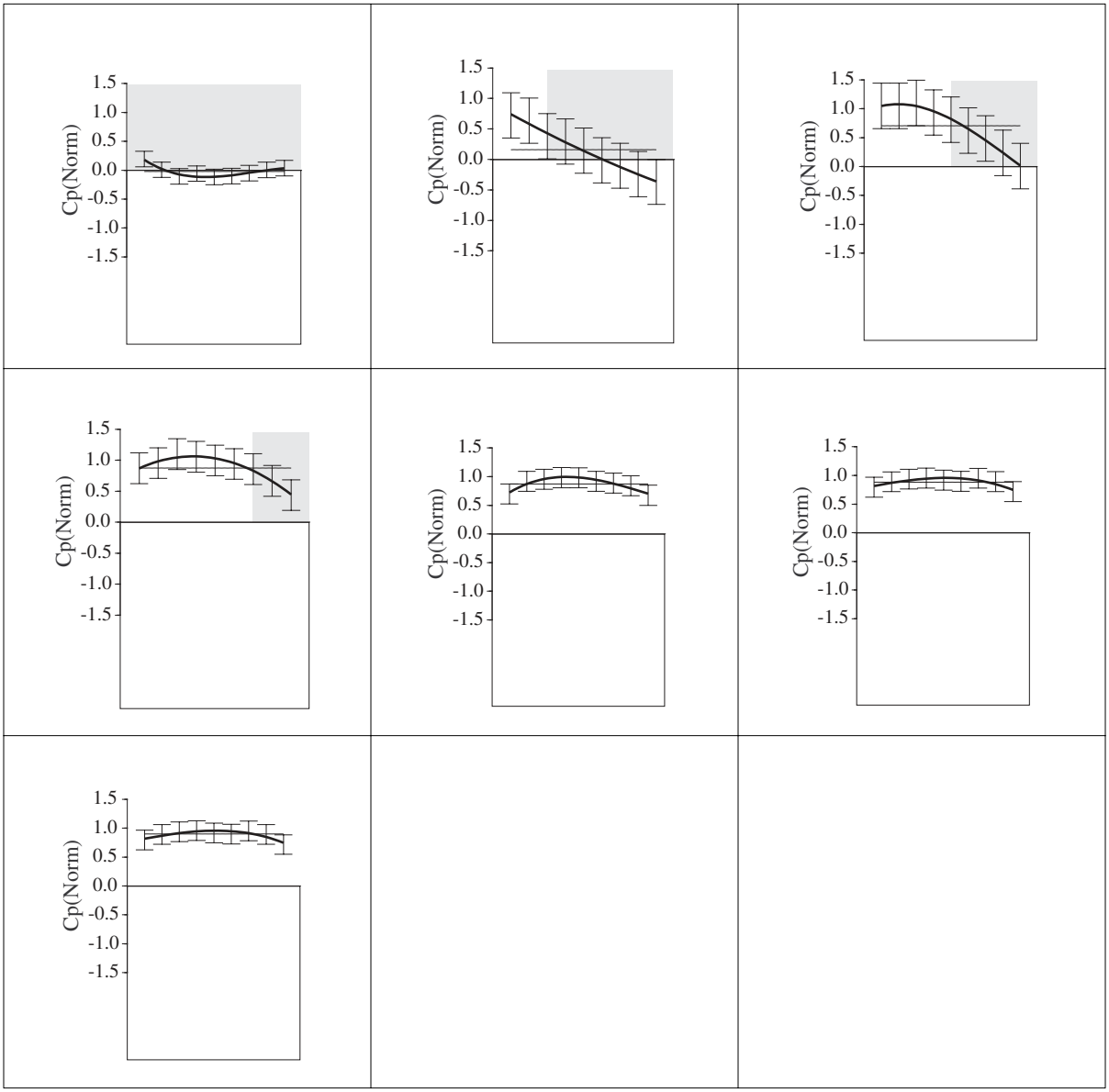

Figure E-3 **Displacement profile for obstruction width=25 cm and spacing =40 cm.**

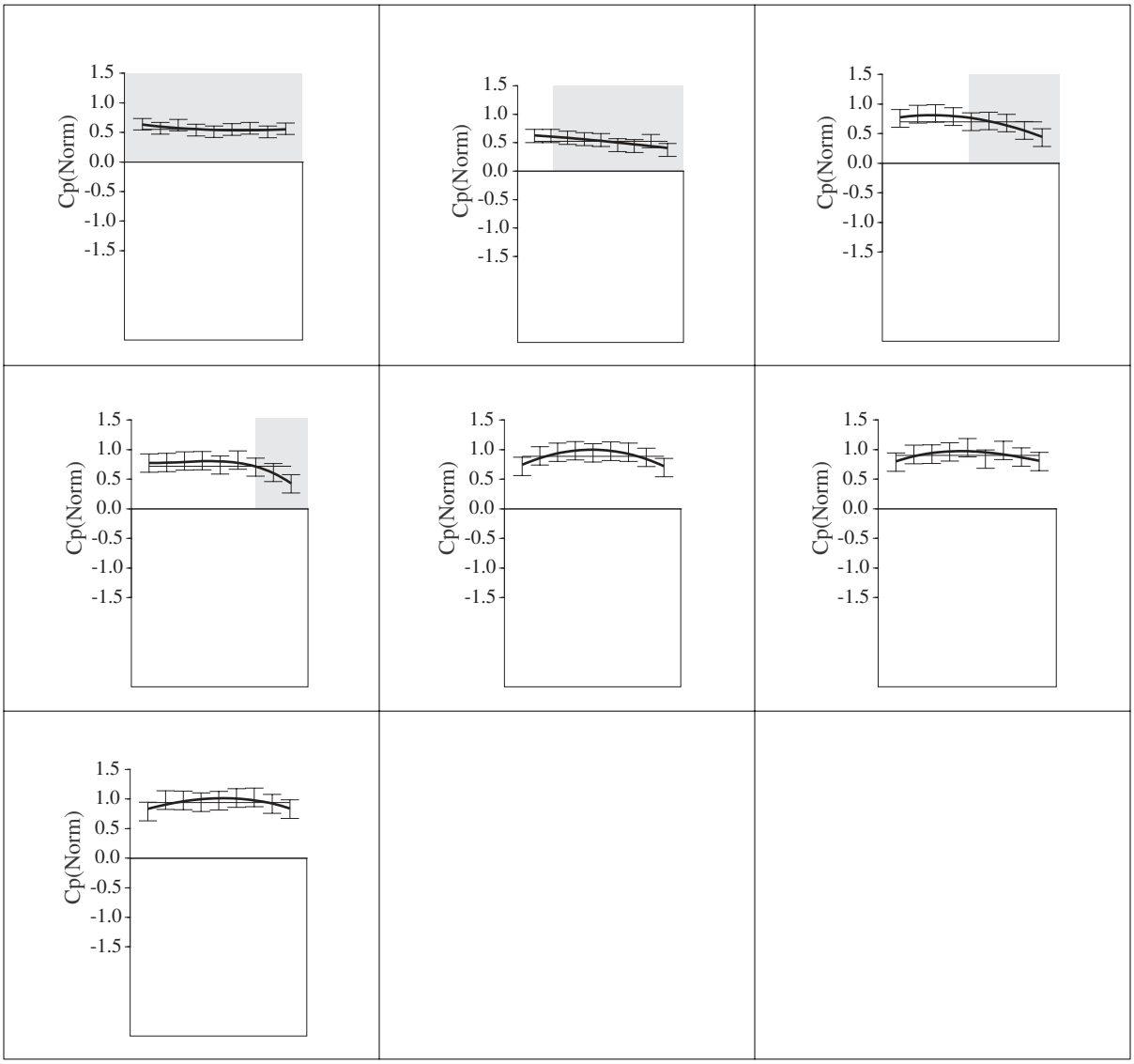

Figure E-4 **Displacement profile for obstruction width=25 cm and spacing =60 cm.**

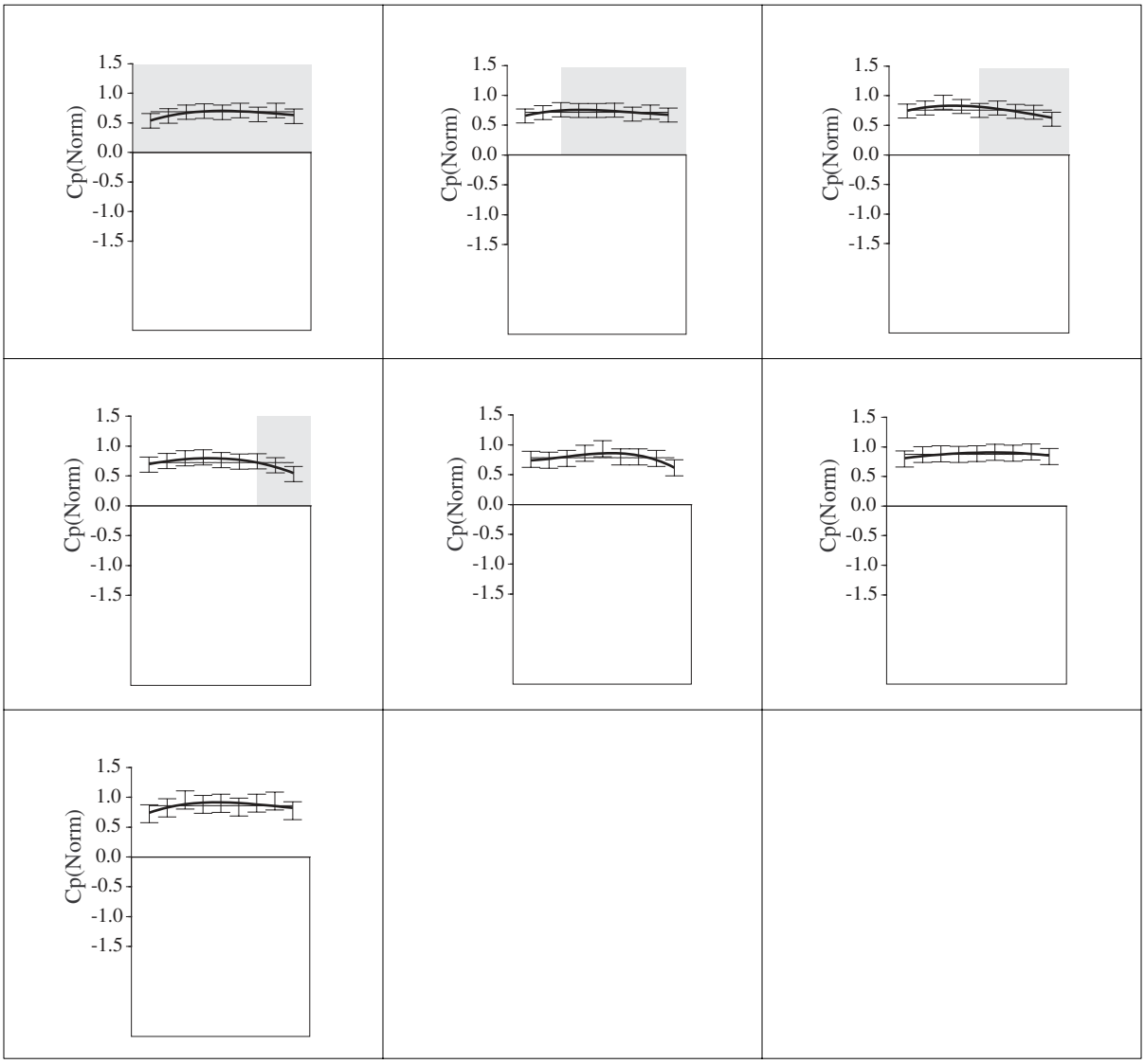

Figure E-5 **Displacement profile for obstruction width=61 cm and spacing =20 cm.**

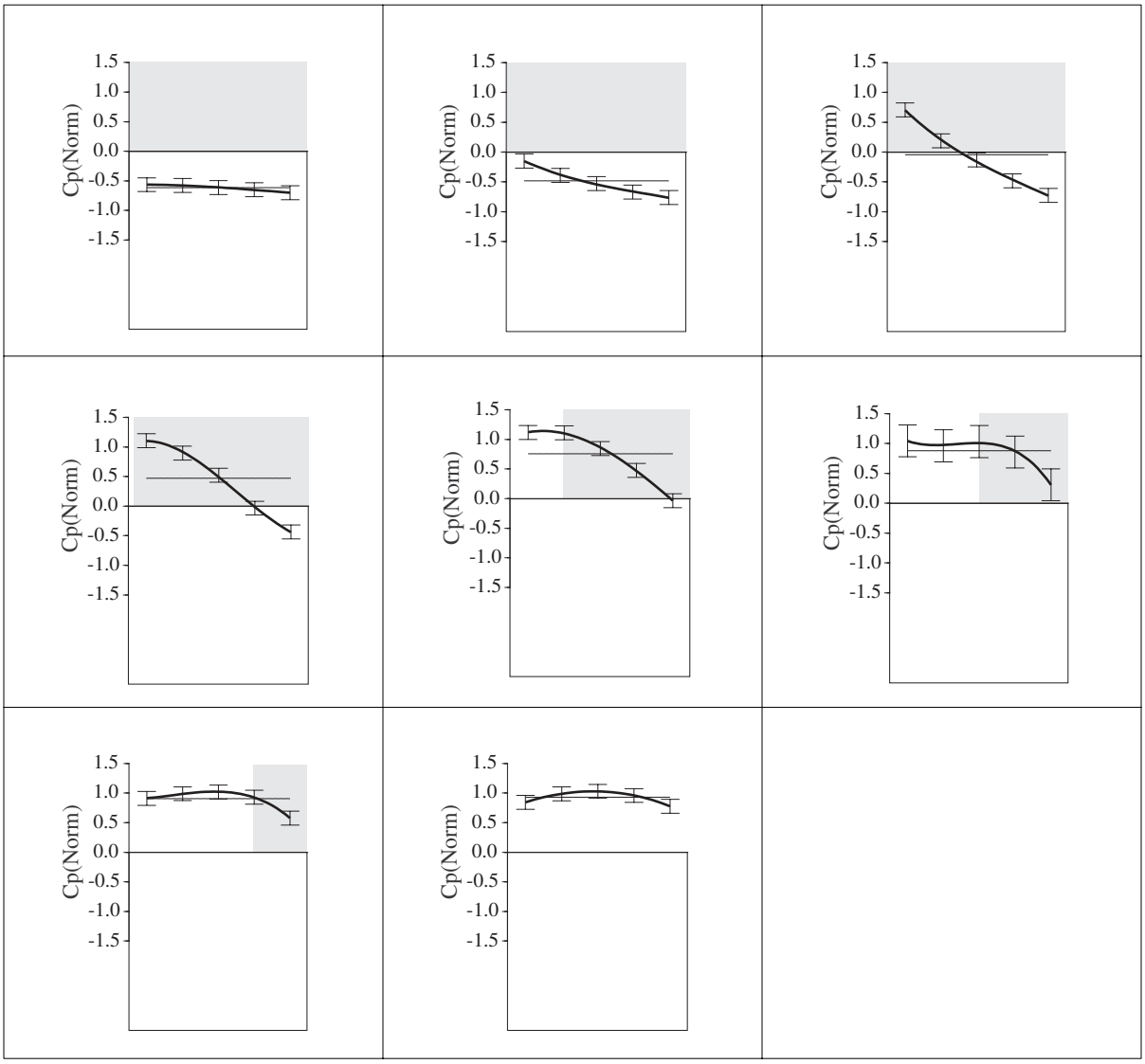

Figure E-6 **Displacement profile for obstruction width=61 cm and spacing =30 cm.**

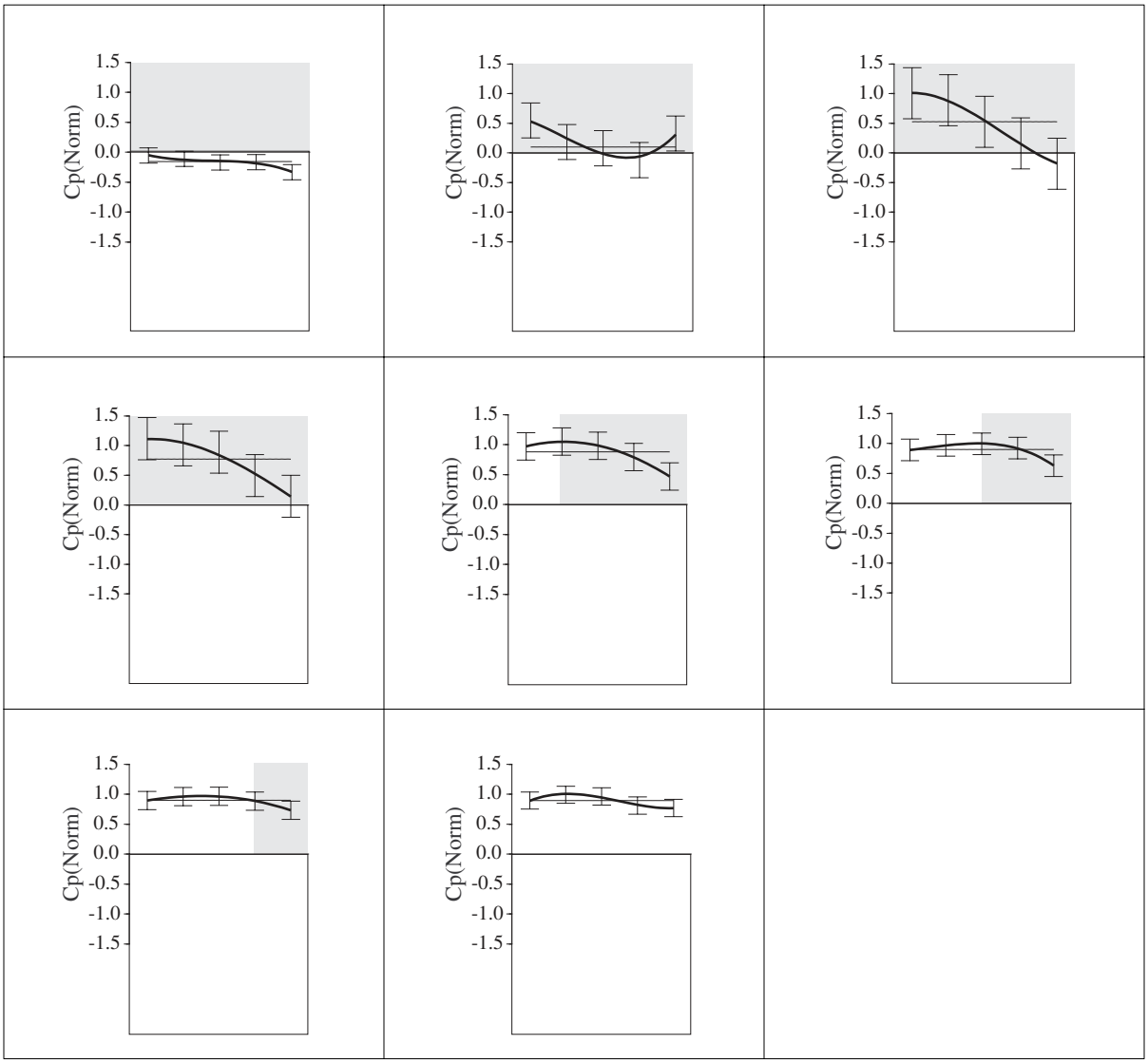

Figure E-7 **Displacement profile for obstruction width=61 cm and spacing =40 cm.**

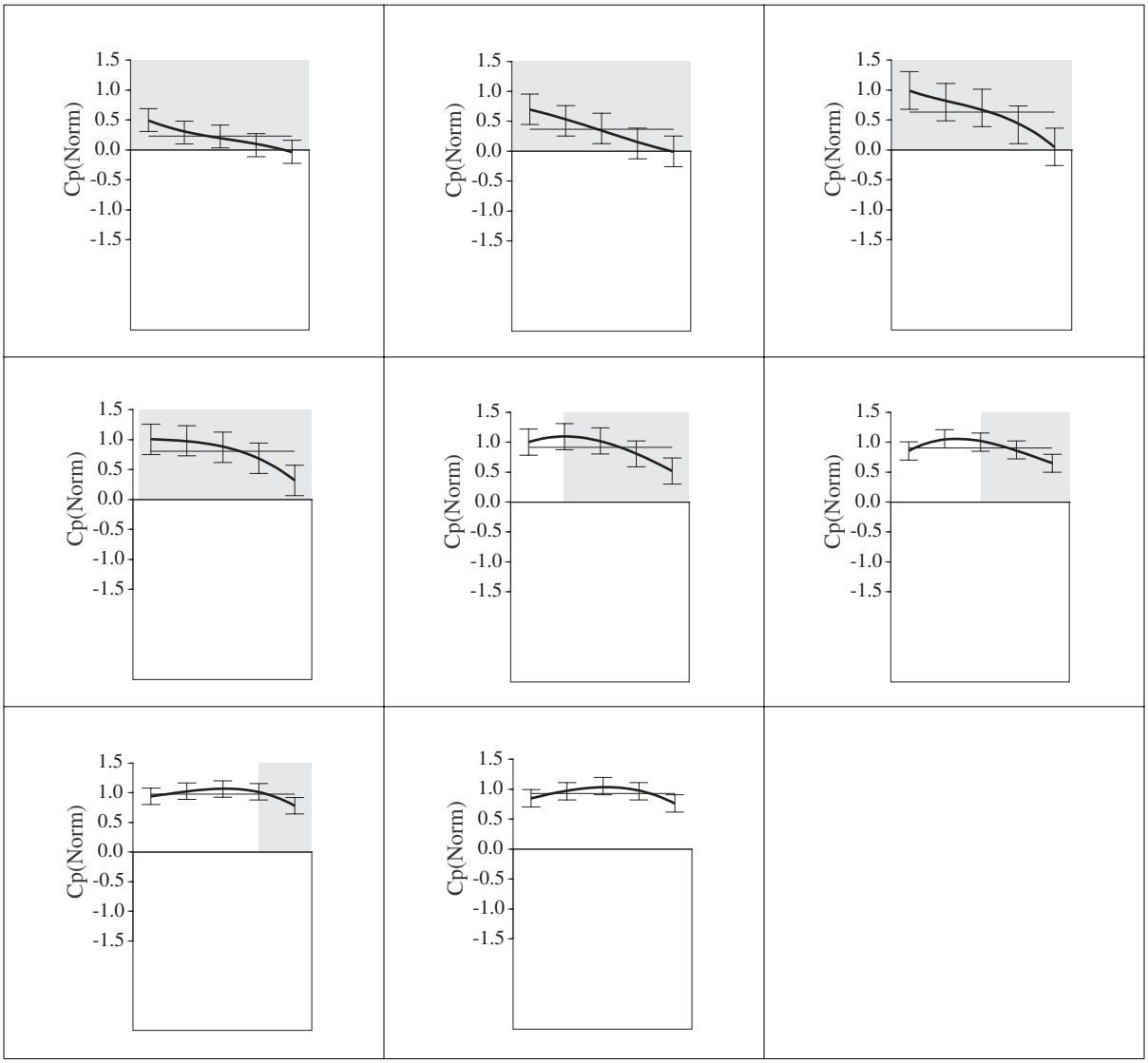

Figure E-8 **Displacement profile for obstruction width=61 cm and spacing =60 cm.**

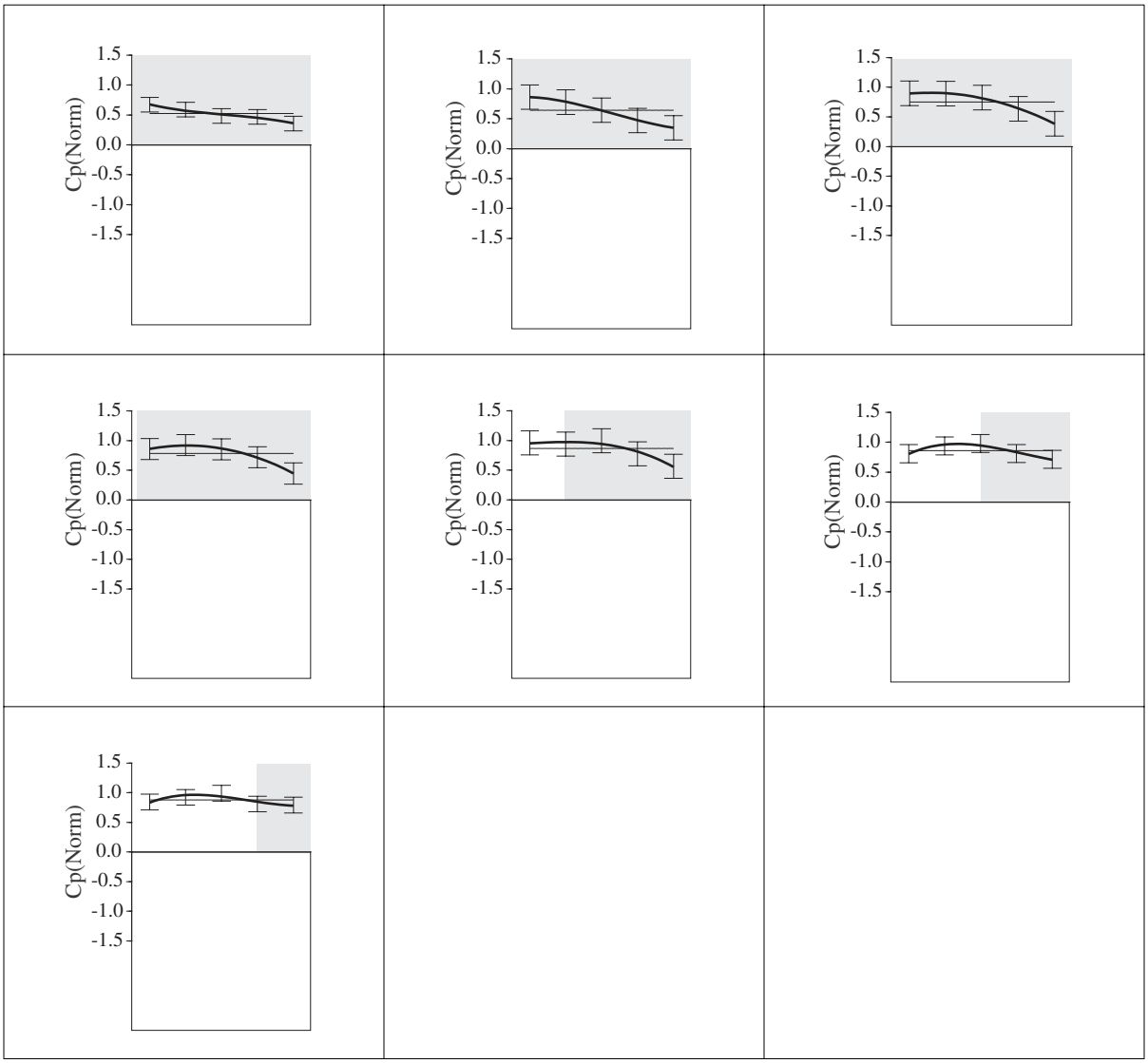

Appendix F

Appendix F

Effect of Changing Wind Direction

Model and Obstruction are always parallel:

Figure F-1 **Setup of experiment and variables (Scenario I)**

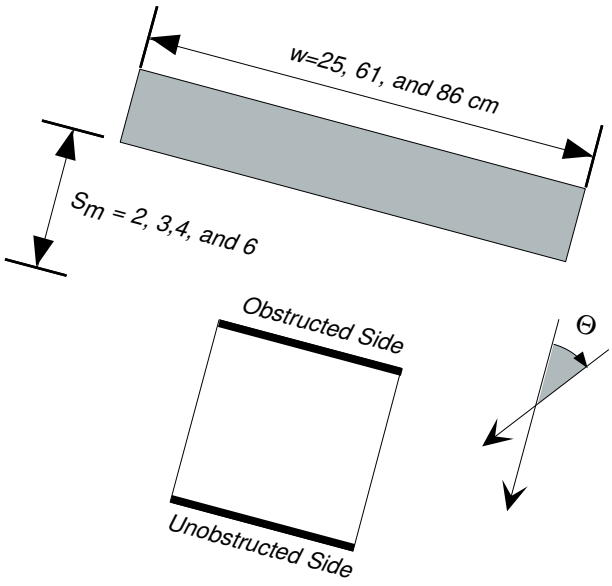

Figure F-2 **Effect of changing wind direction-measured data**

a.Effect of changing the wind direction on pressure coefficients *(C_p)*

(Obstruction-facing side)

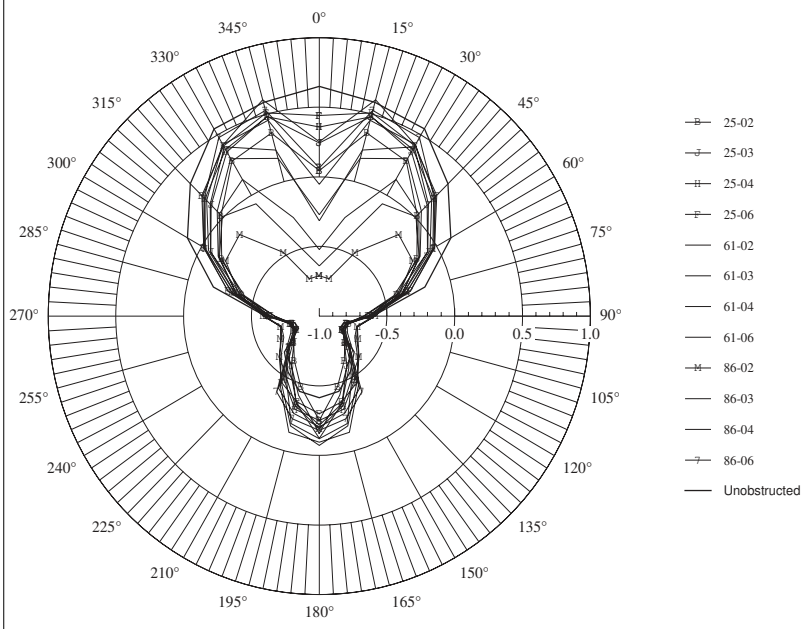

b.Effect of changing the wind direction on pressure modification coefficients *($C_{p.m}$)*

(Obstruction-facing side)

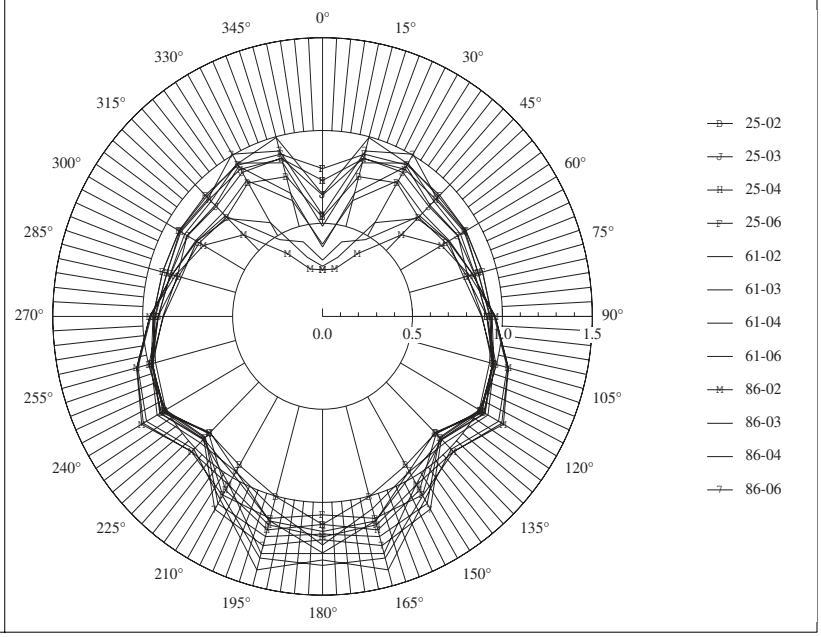

Figure F-2 **Effect of changing wind direction-measured data (Continued)**

c.Effect of changing the wind direction on pressure coefficients *(C_p)*

(Unobstructed side)

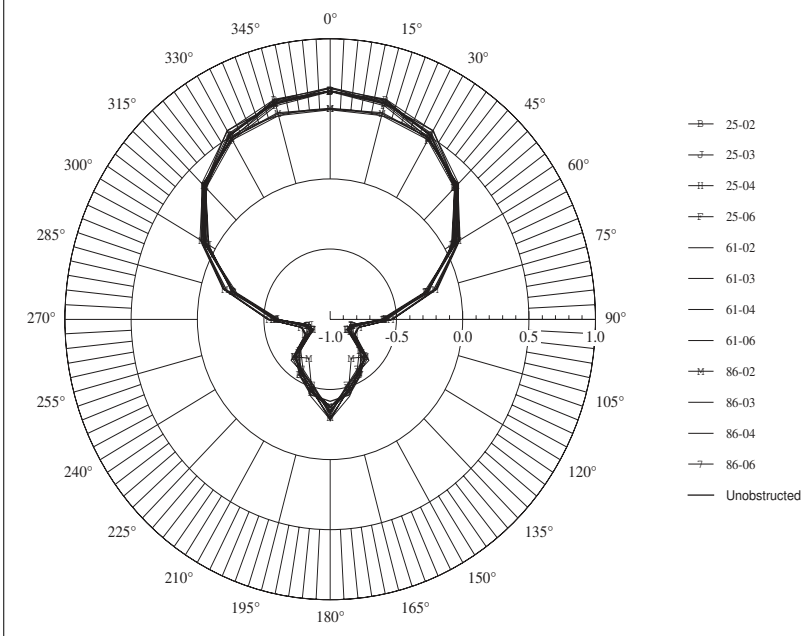

d.Effect of changing the wind direction on pressure modification coefficients *($C_{p.m}$)*

(Unobstructed side)

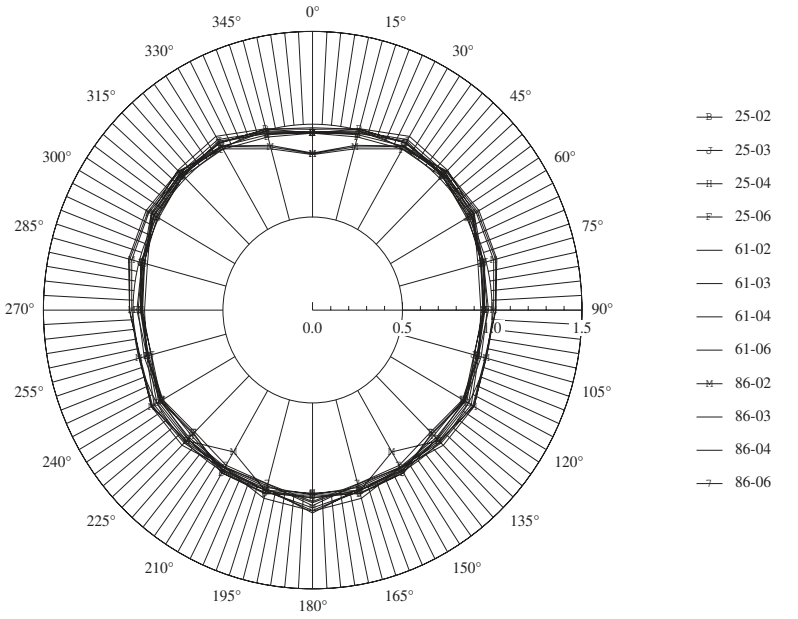

Figure F-3 **Comparison between measured and predicted values of C_p on the obstructed side. (obstruction width=25 cm)**

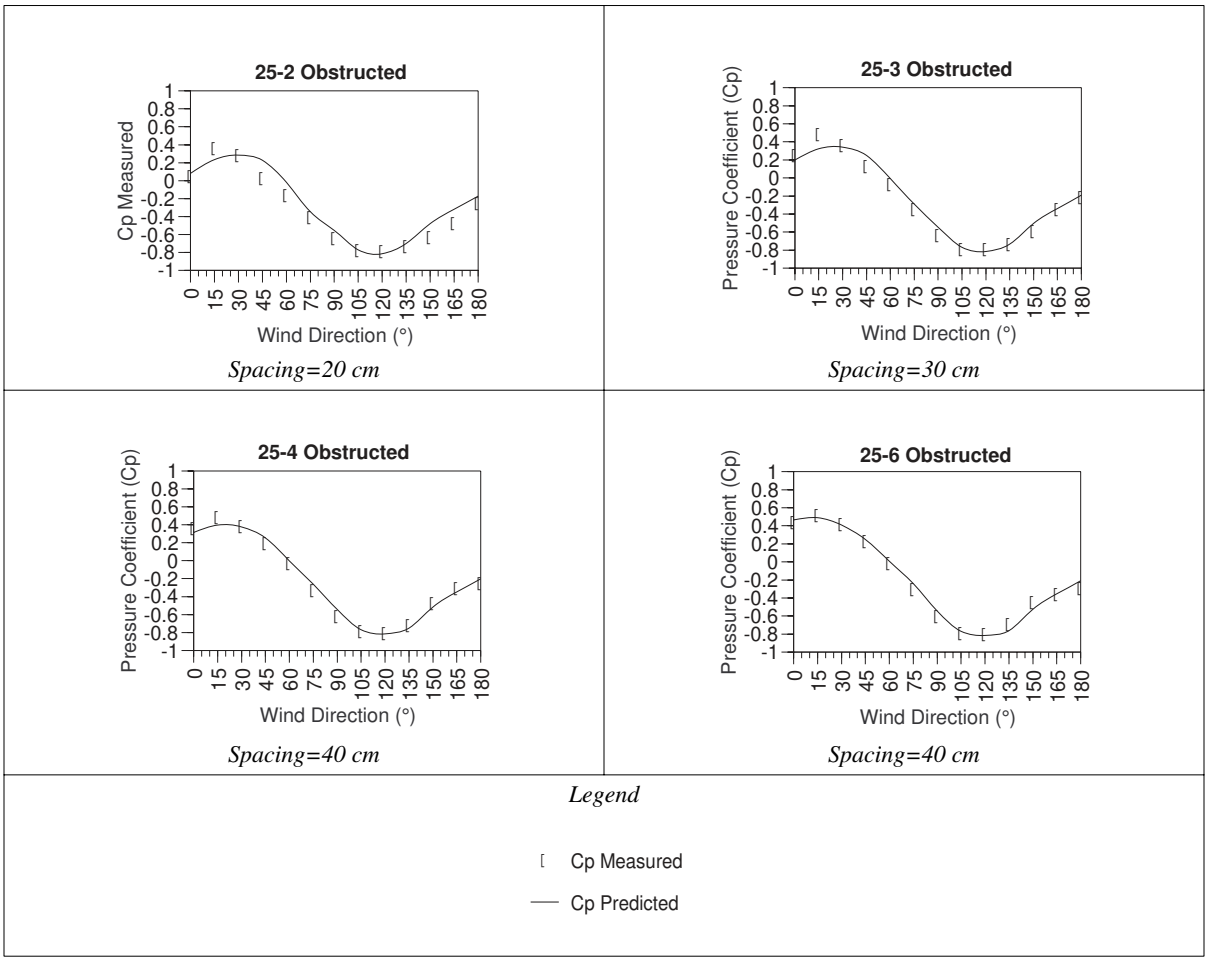

Figure F-4 **Comparison between measured and predicted values of C_p on the obstructed side. (obstruction width=61 cm)**

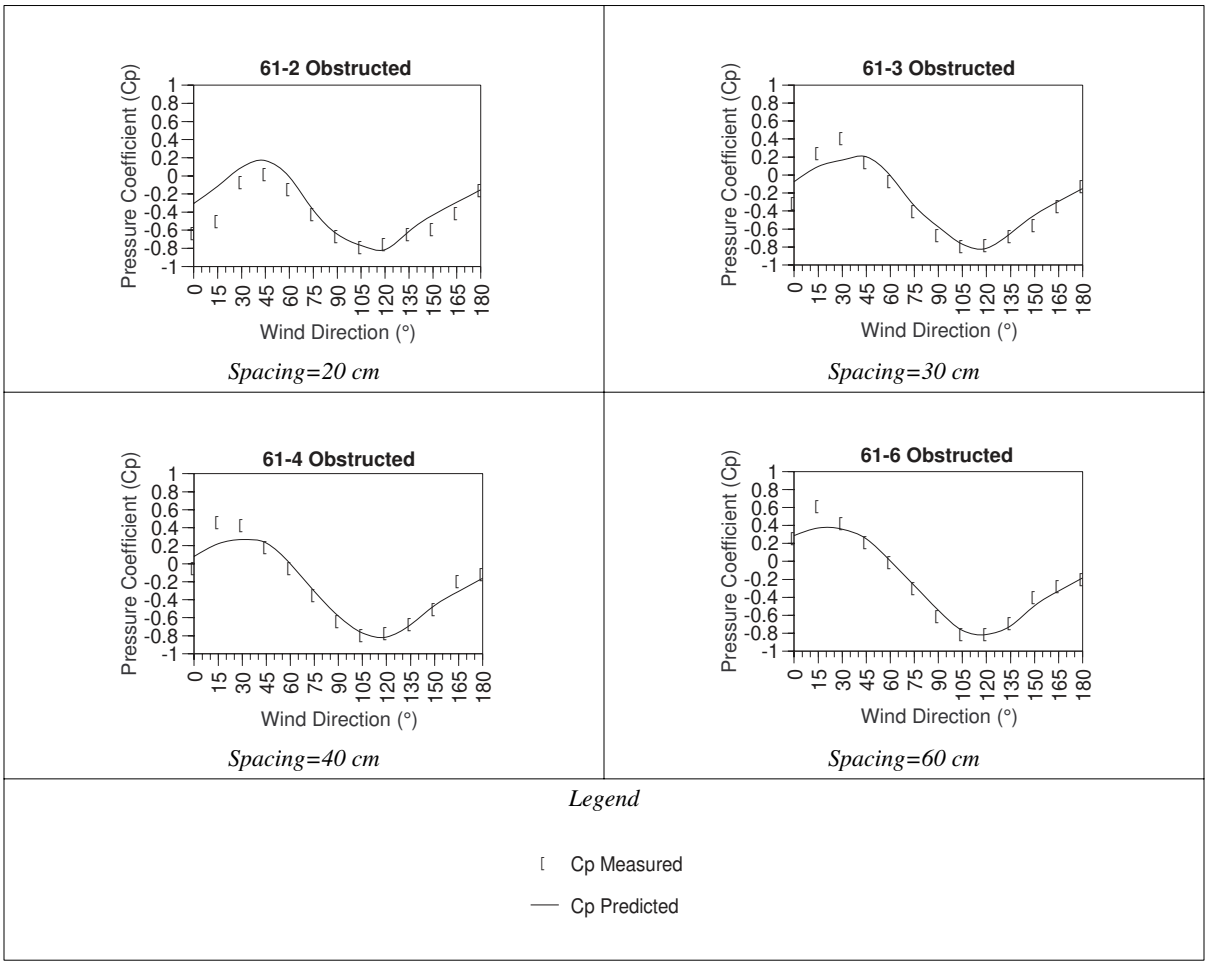

Figure F-5 **Comparison between measured and predicted values of C_p on the obstructed side. (obstruction width=86 cm)**

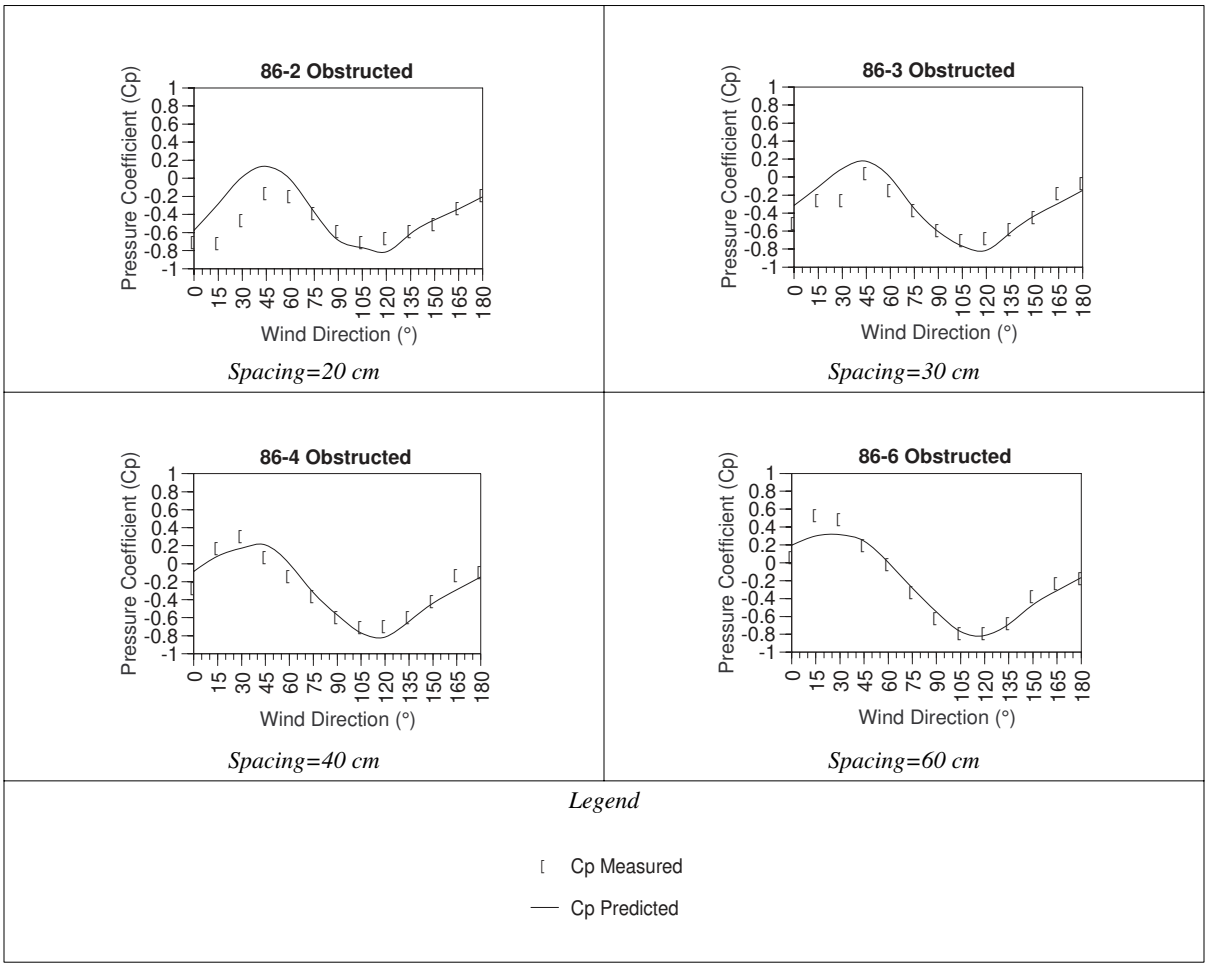

Figure F-6 **Comparison between measured and predicted values of C_p on the unobstructed side. (obstruction width=25 cm)**

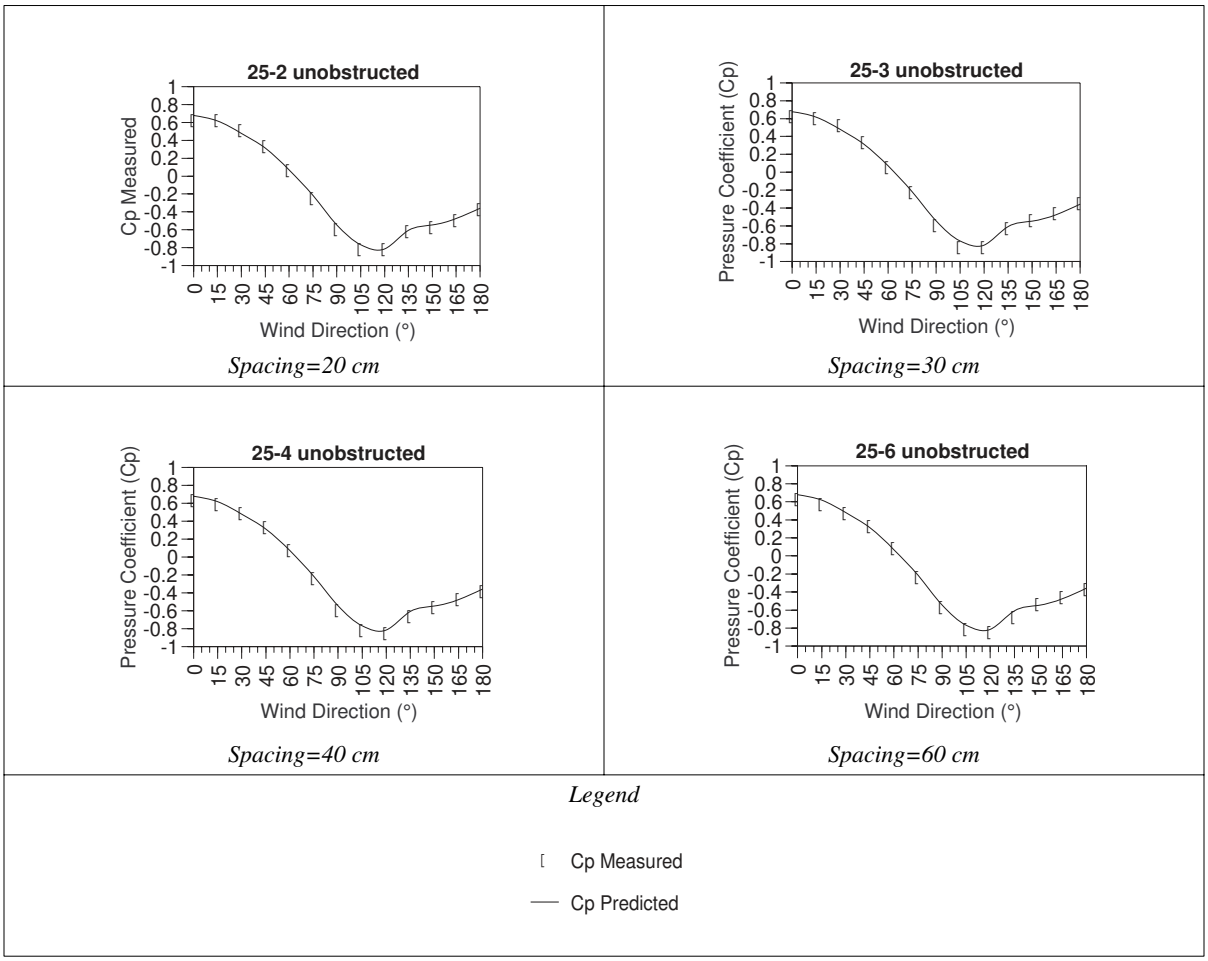

Figure F-7 **Comparison between measured and predicted values of C_p on the unobstructed side. (obstruction width=61 cm)**

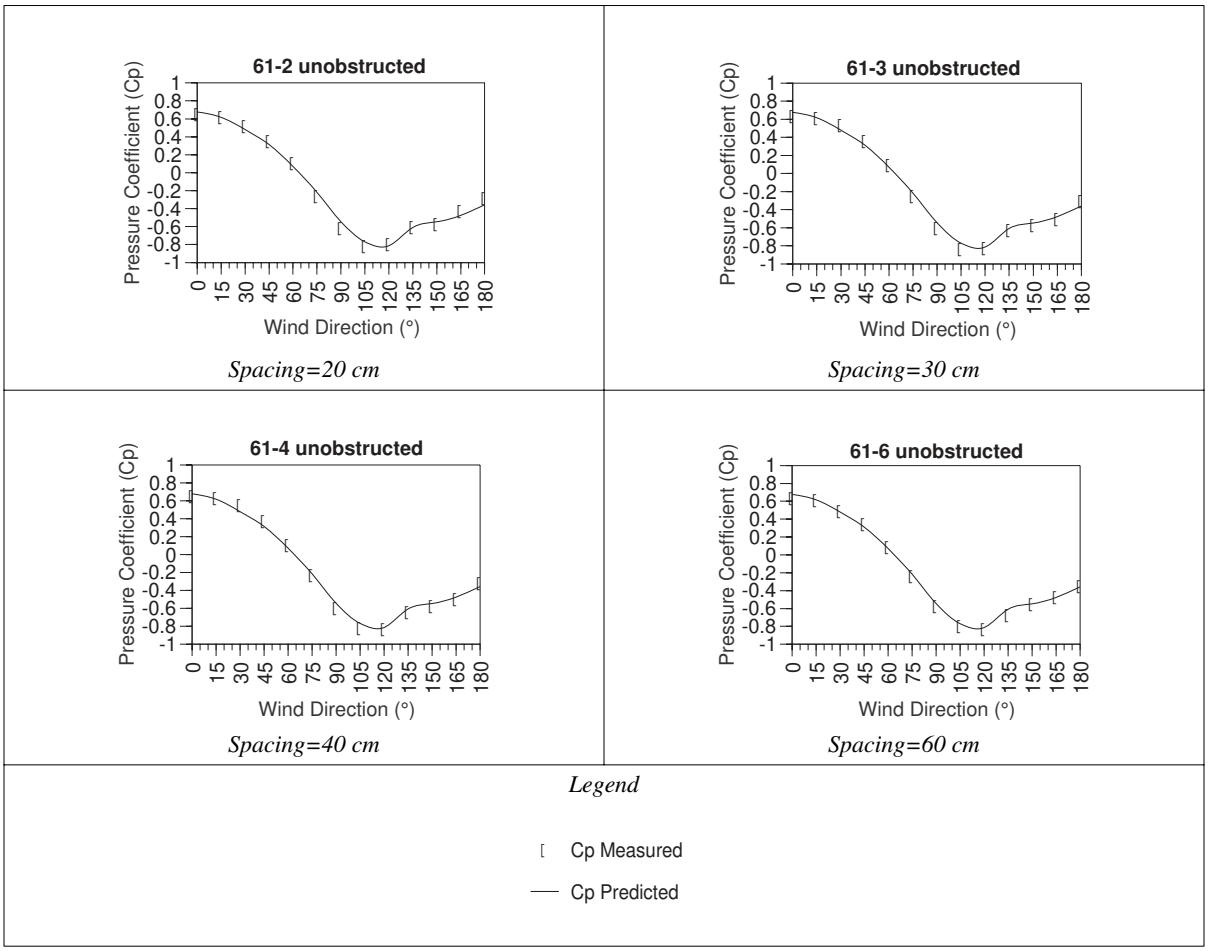

Spacing=20 cm

Spacing=30 cm

Spacing=40 cm

Spacing=60 cm

Figure F-8 **Comparison between measured and predicted values of C_p on the unobstructed side. (obstruction width=86 cm)**

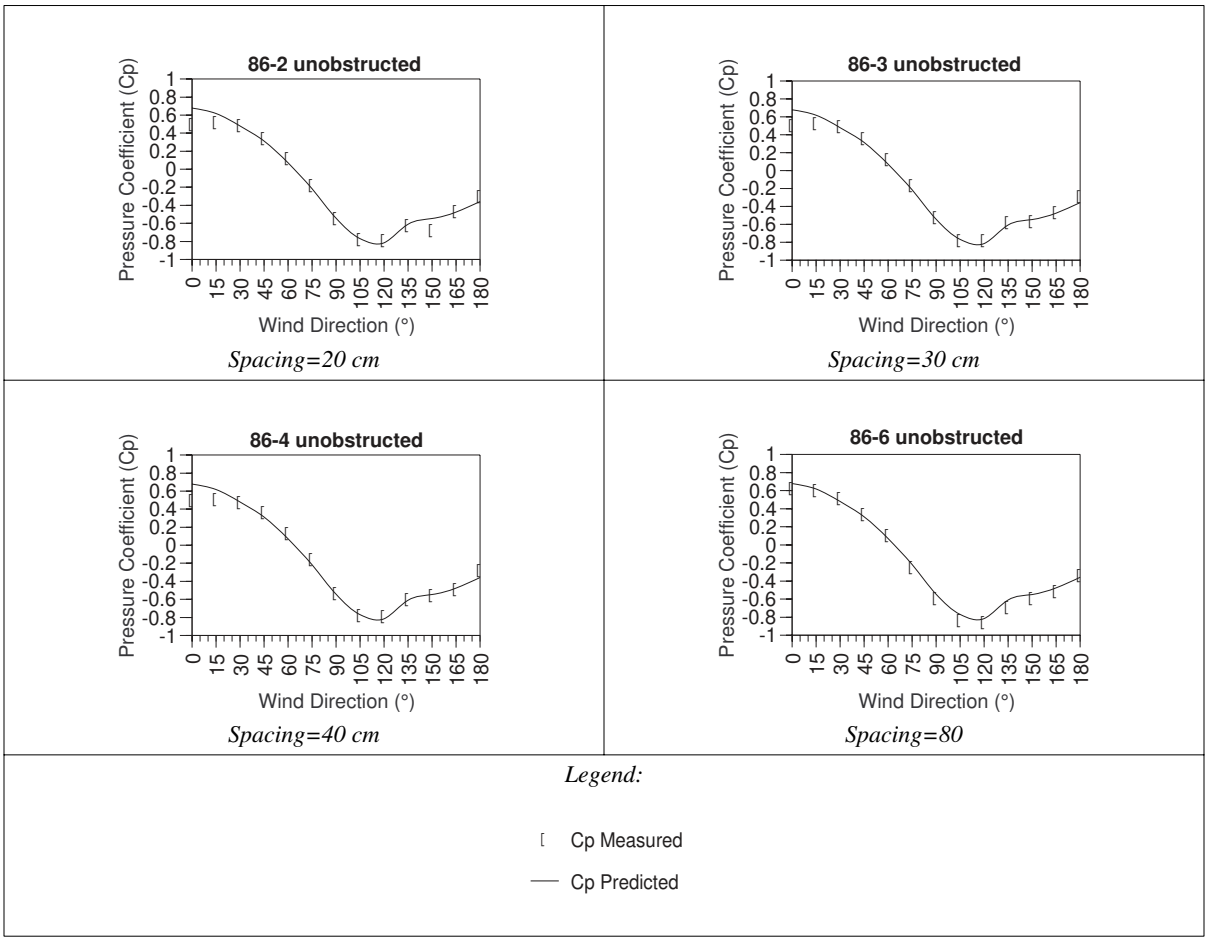

Obstruction is always perpendicular to wind direction:

Figure F-9 **Setup of experiment for scenario II**

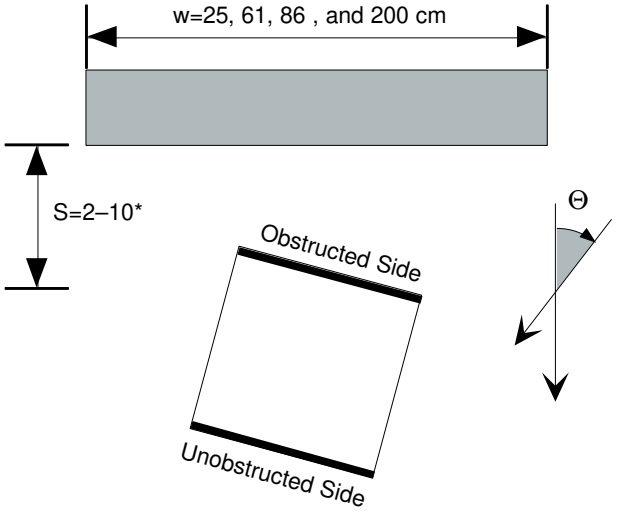

*3, 5, 7, 9 Additional spacing (S) for obstruction width = 200 cm only

Figure F-10 **Effect of changing wind direction-measured data**

a.Effect of changing the wind direction on surface pressure coefficients *(C_p)*

Obstruction Width=25 cm

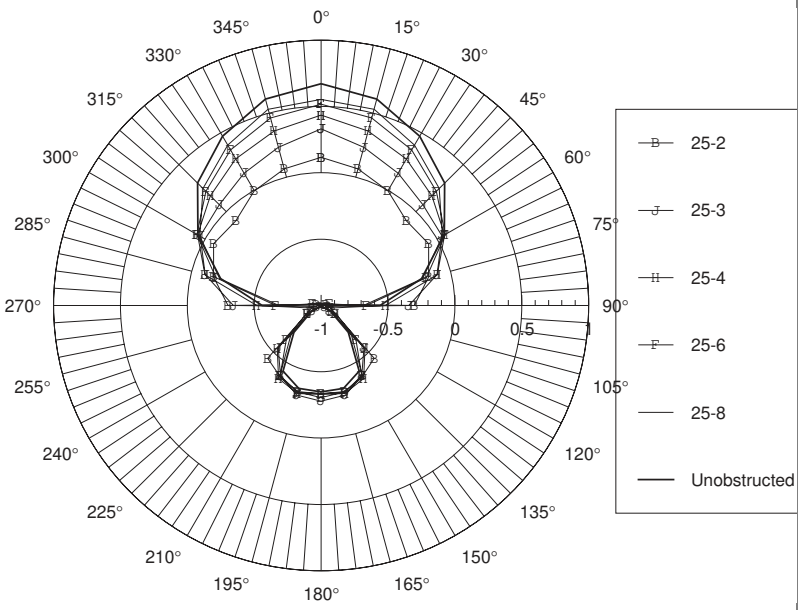

b.Effect of changing the wind Direction on surface pressure coefficients *($C_{p.m}$)*

Obstruction Width=25 cm

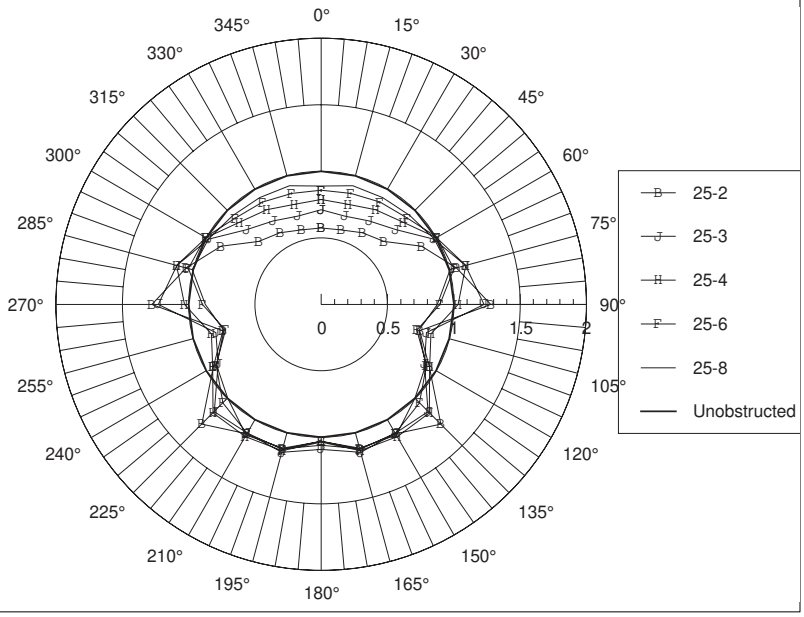

Figure F-10 **Effect of changing wind direction-measured data (Continued)**

c.Effect of changing the wind Direction on surface pressure coefficients *(C_p)*

Obstruction Width=61 cm

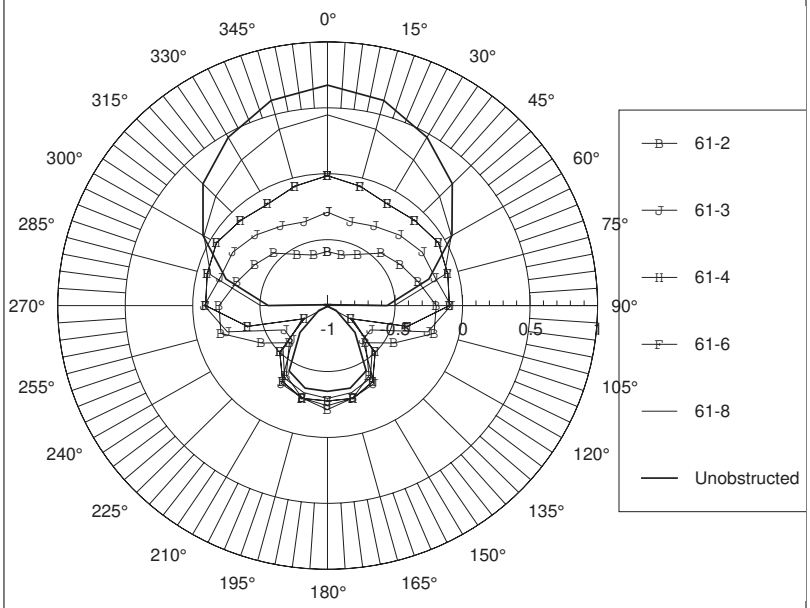

d.Effect of changing the wind direction on surface pressure coefficients *($C_{p.m}$)*

Obstruction Width=61 cm

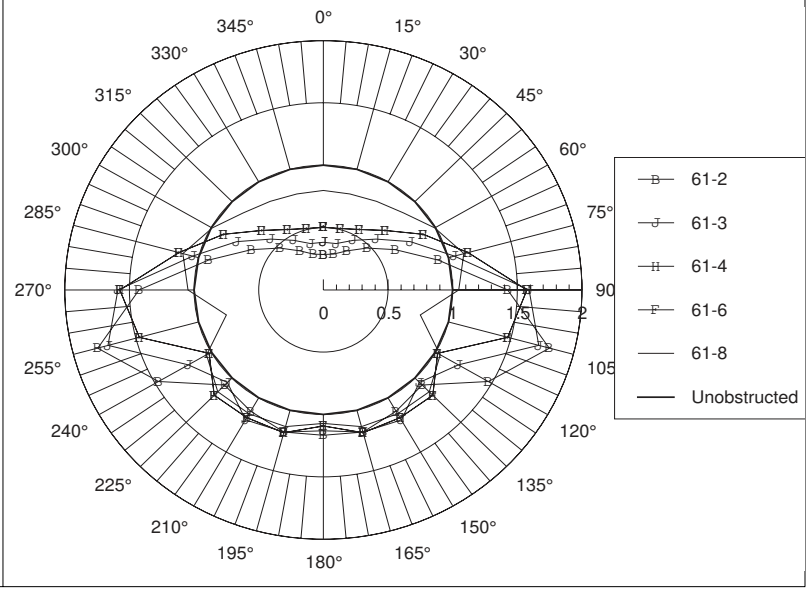

Figure F-10 **Effect of changing wind direction-measured data (Continued)**

e.Effect of changing the wind direction on surface pressure coefficients *(C_p)*

Obstruction Width=86 cm

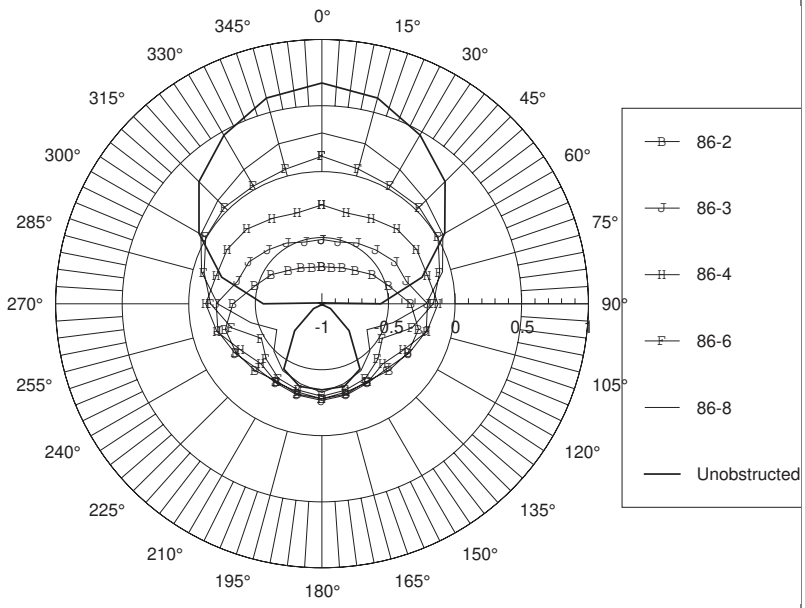

f.Effect of changing the wind direction on surface pressure coefficients *($C_{p.m}$)*

Obstruction Width=86 cm

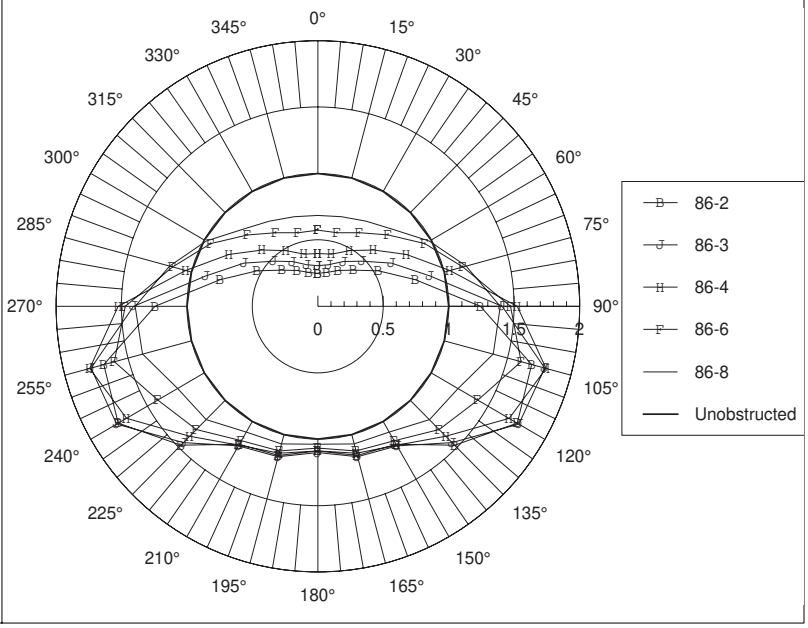

Figure F-10 **Effect of changing wind direction-measured data (Continued)**

g.Effect of changing the wind direction on surface pressure coefficients *(C_p)*

Obstruction Width=200 cm

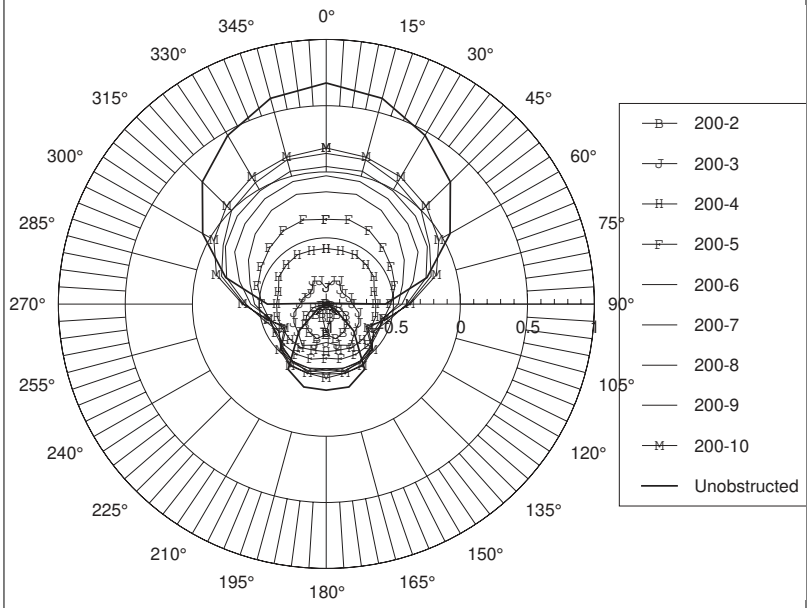

h.Effect of changing the wind direction on surface pressure coefficients *($C_{p.m}$)*

Obstruction Width=200 cm

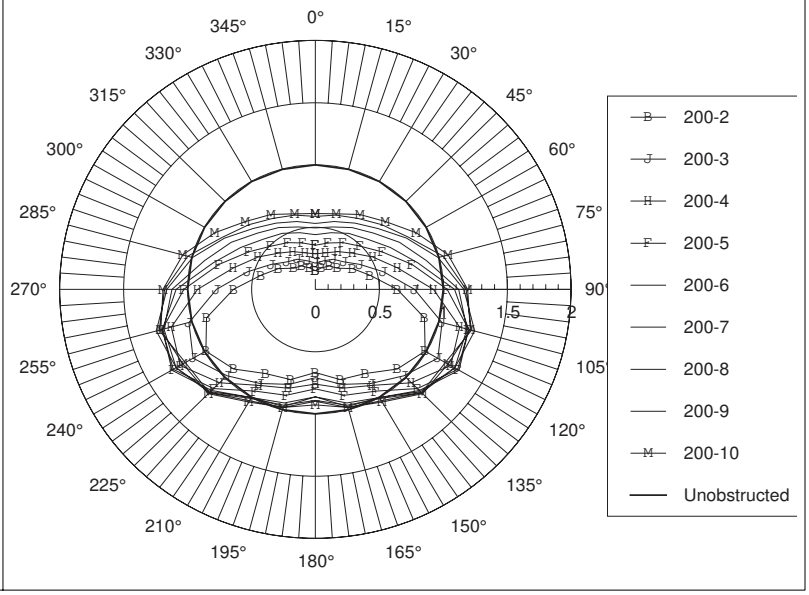

Figure F-11 **Comparison between measured and predicted values of C_p. (obstruction width=25 cm)**

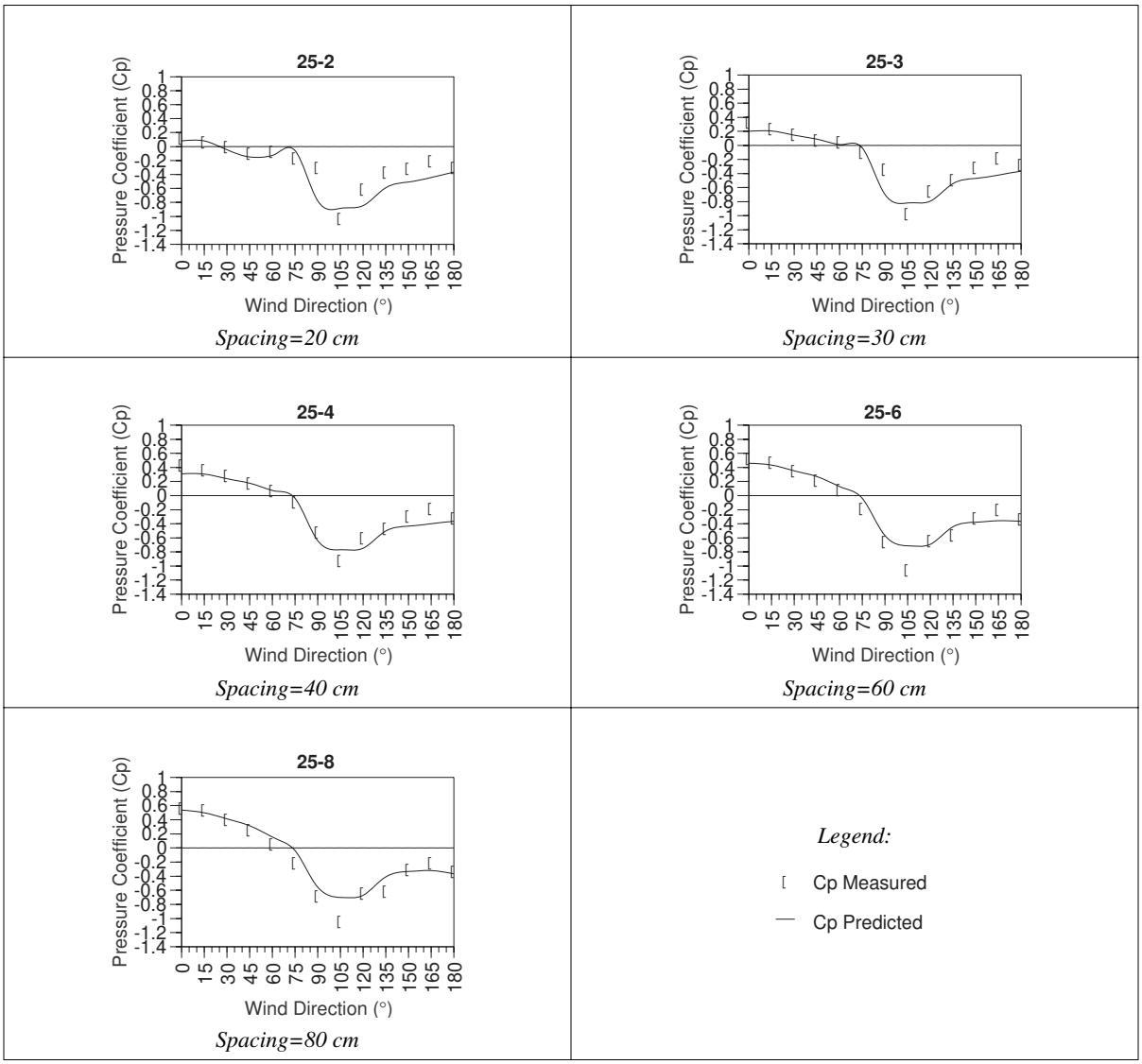

Figure F-12 **Comparison between measured and predicted values of C_p. (obstruction width=61 cm)**

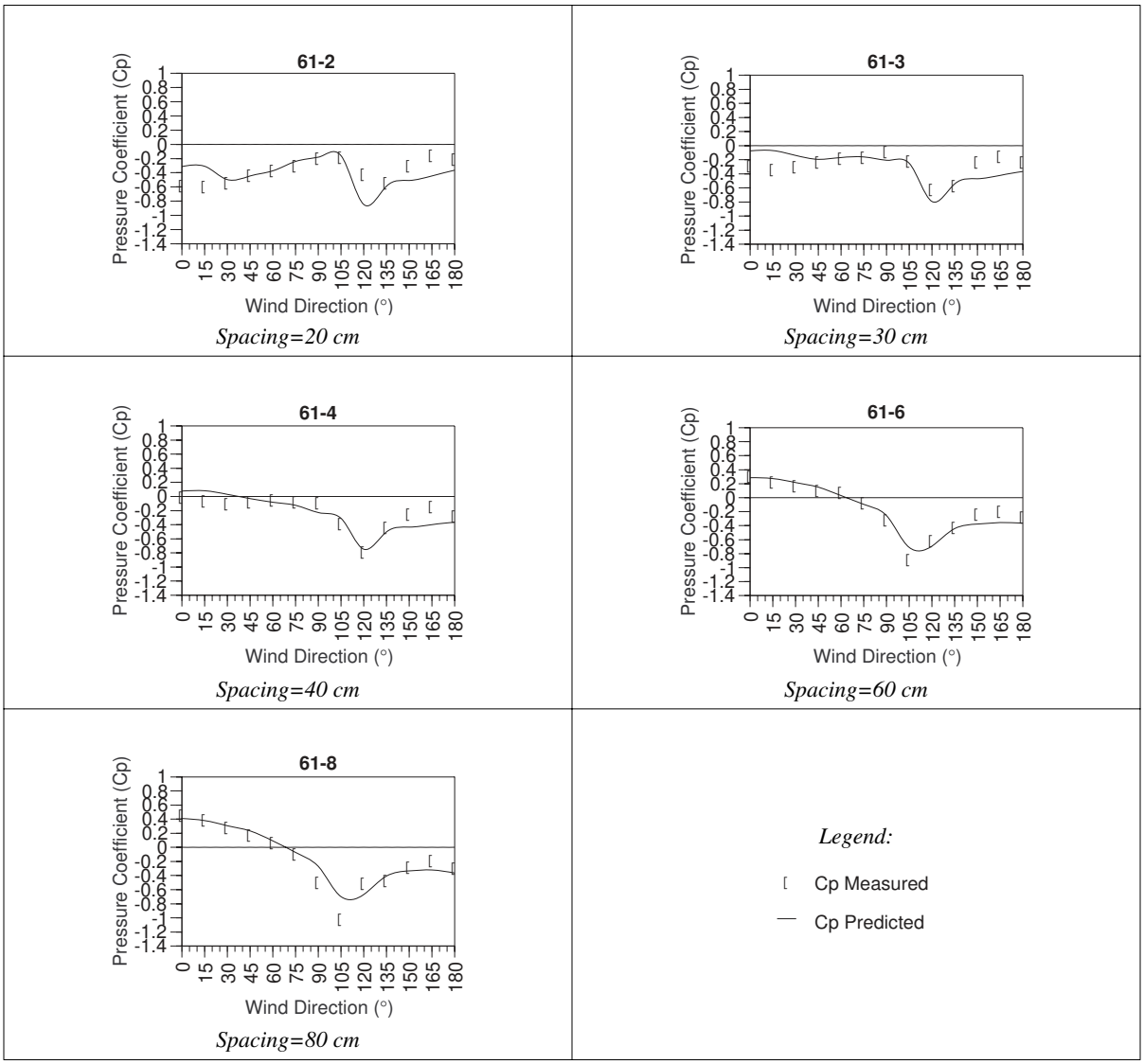

Figure F-13 **Comparison between measured and predicted values of C_p. (obstruction width=86 cm)**

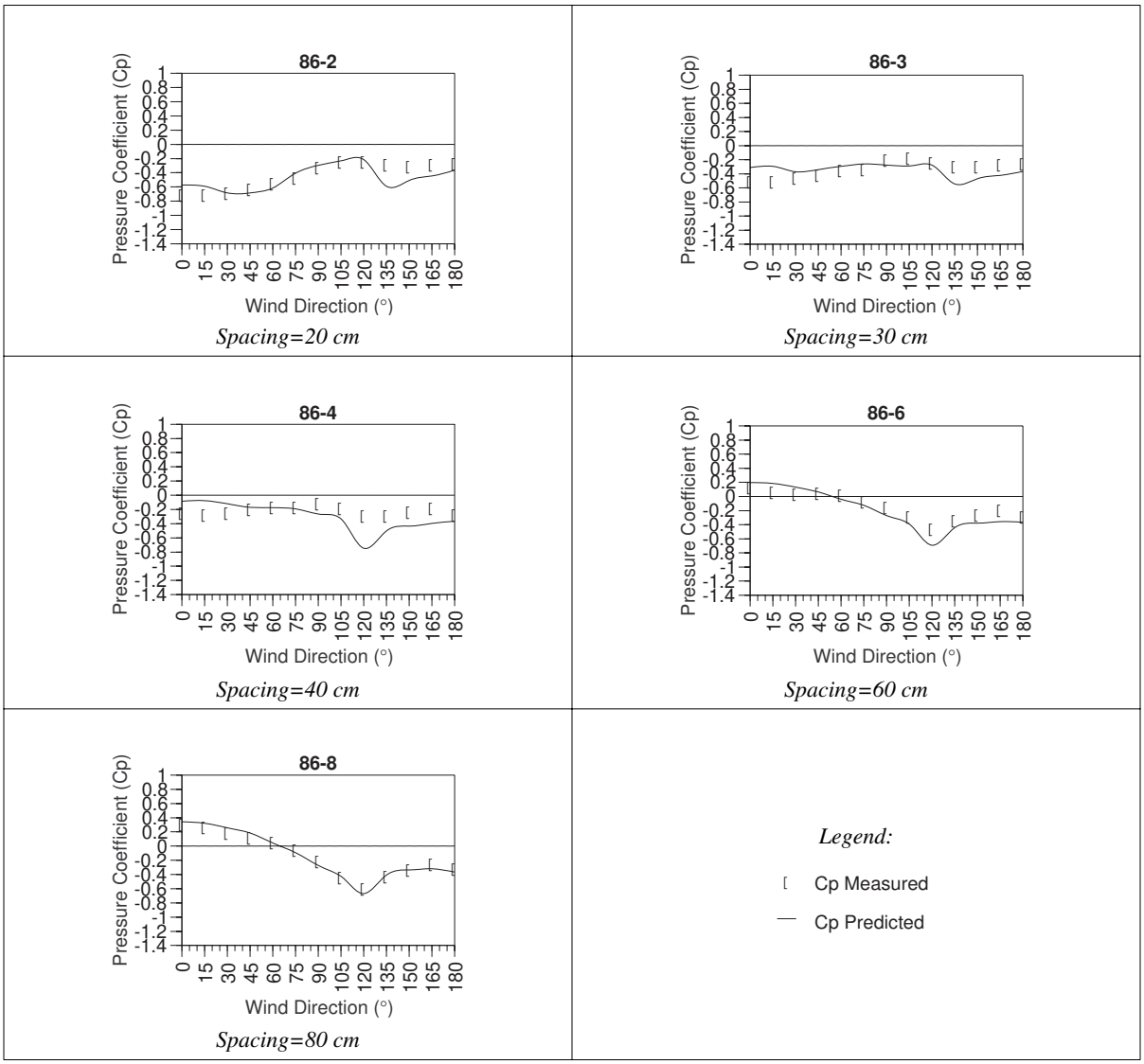

Figure F-14 **Comparison between measured and predicted values of C_p. (obstruction width=200 cm)**

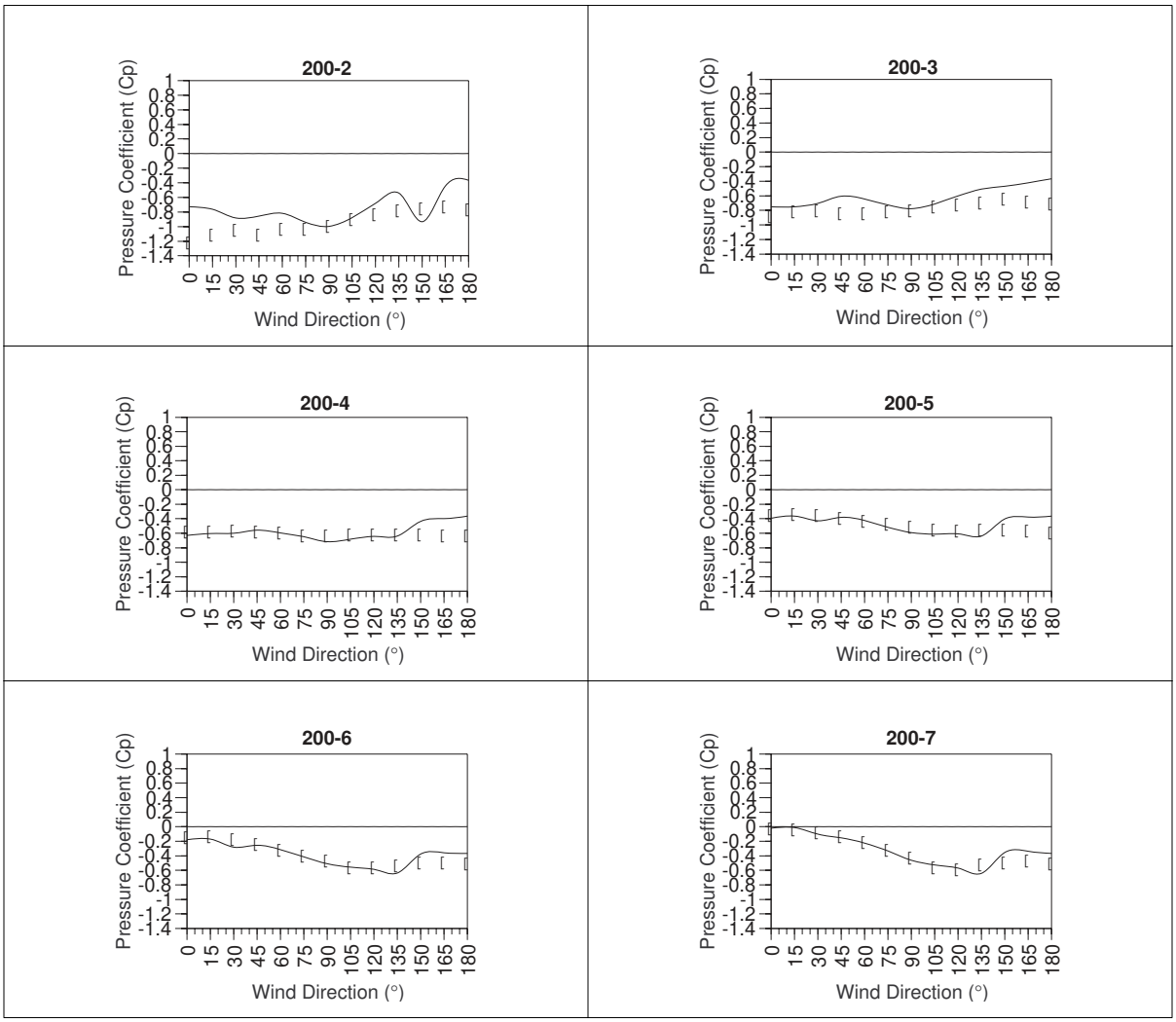

Figure F-14 **Comparison between measured and predicted values of C_p. (obstruction width=200 cm) (Continued)**

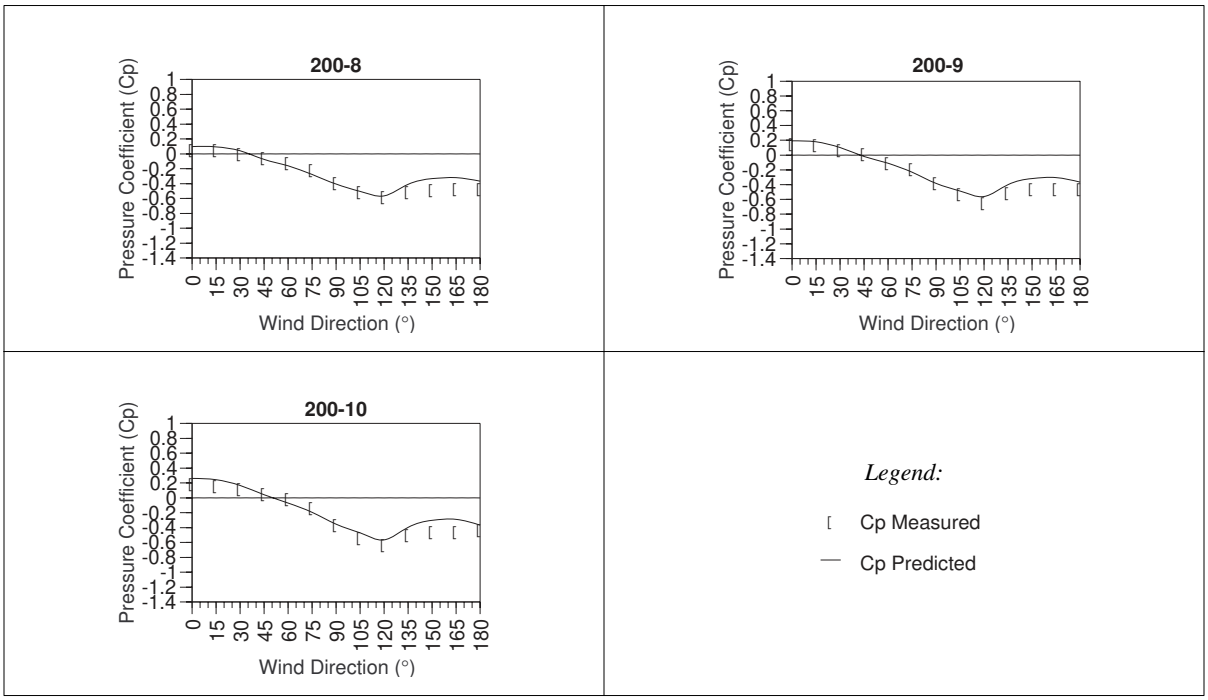

Appendix G

Appendix G

Multiple Obstruction Blocks

This appendix shows the effect of two obstruction blocks positioned on the windward side of the of the instrumented model. Figure G-1 illustrates the variables studied in this set of experiments and these are:

1. The spacing between the obstruction blocks (gap).
2. The spacing between the obstruction blocks and the model.
3. Wind direction.
4. Horizontal shift or changing the position of the two obstruction blocks relative to the instrumented surface.

Figure G-1 **The studied variables**

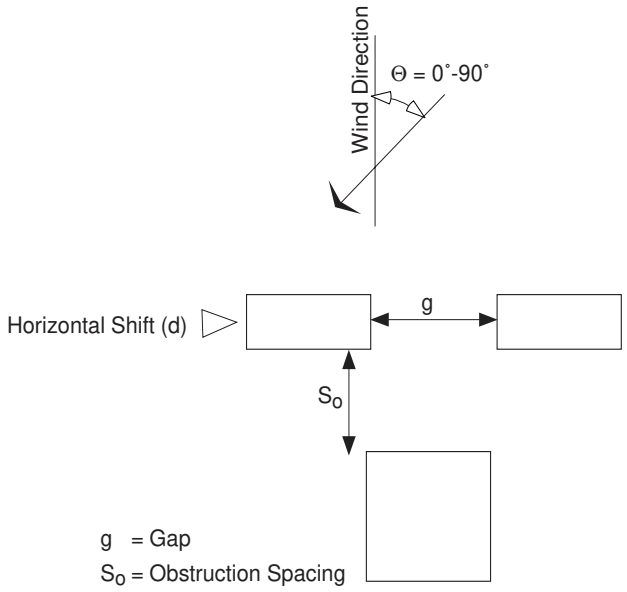

Figure G-2.1 **Pressure modification coefficients C_{pm} profiles as shielded by two obstruction blocks 2 spacings and 12.5 cm between blocks**

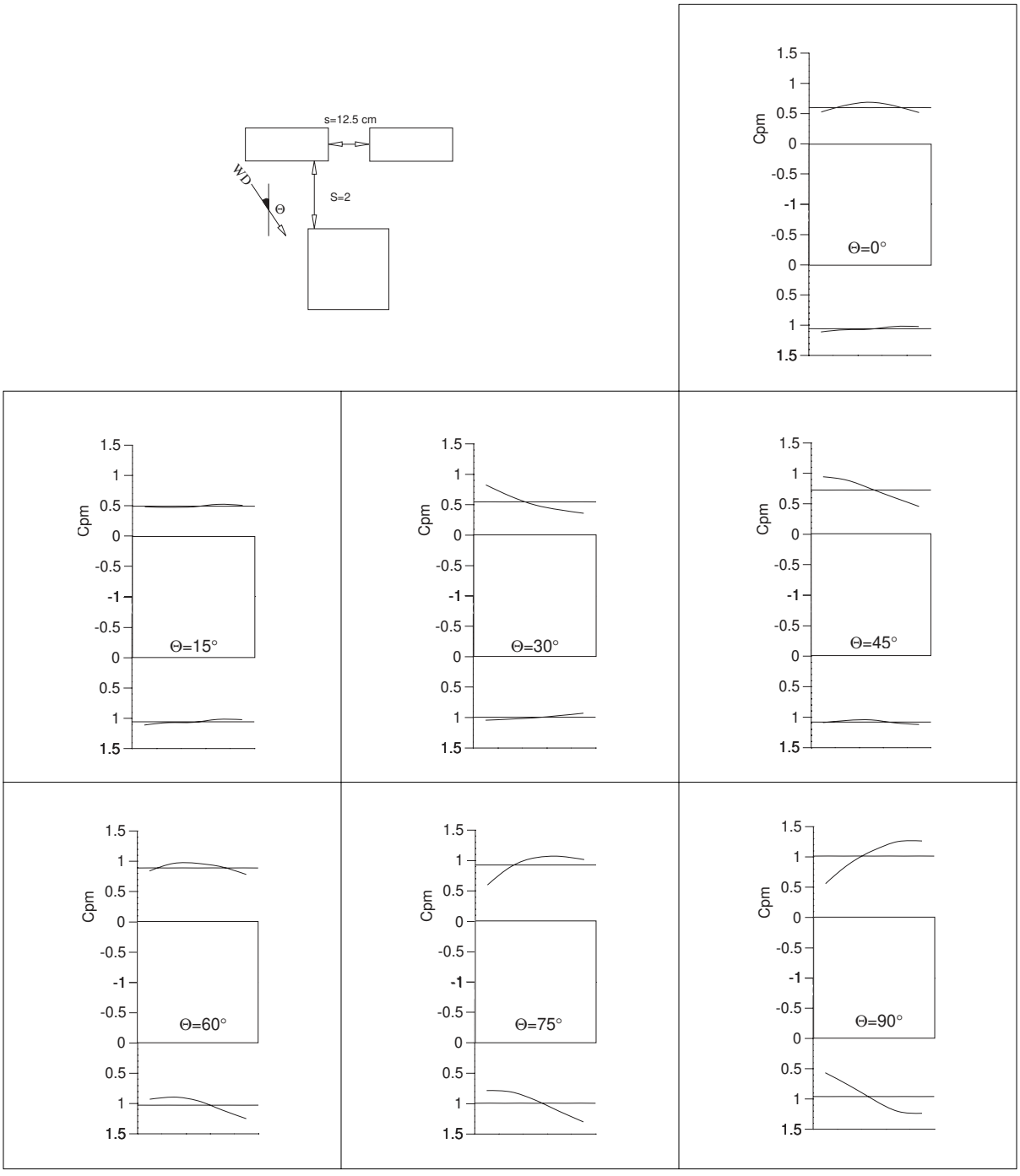

Figure G-2.2 **Pressure modification coefficients C_{pm} profiles as shielded by two obstruction blocks 2 spacings and 25 cm between blocks**

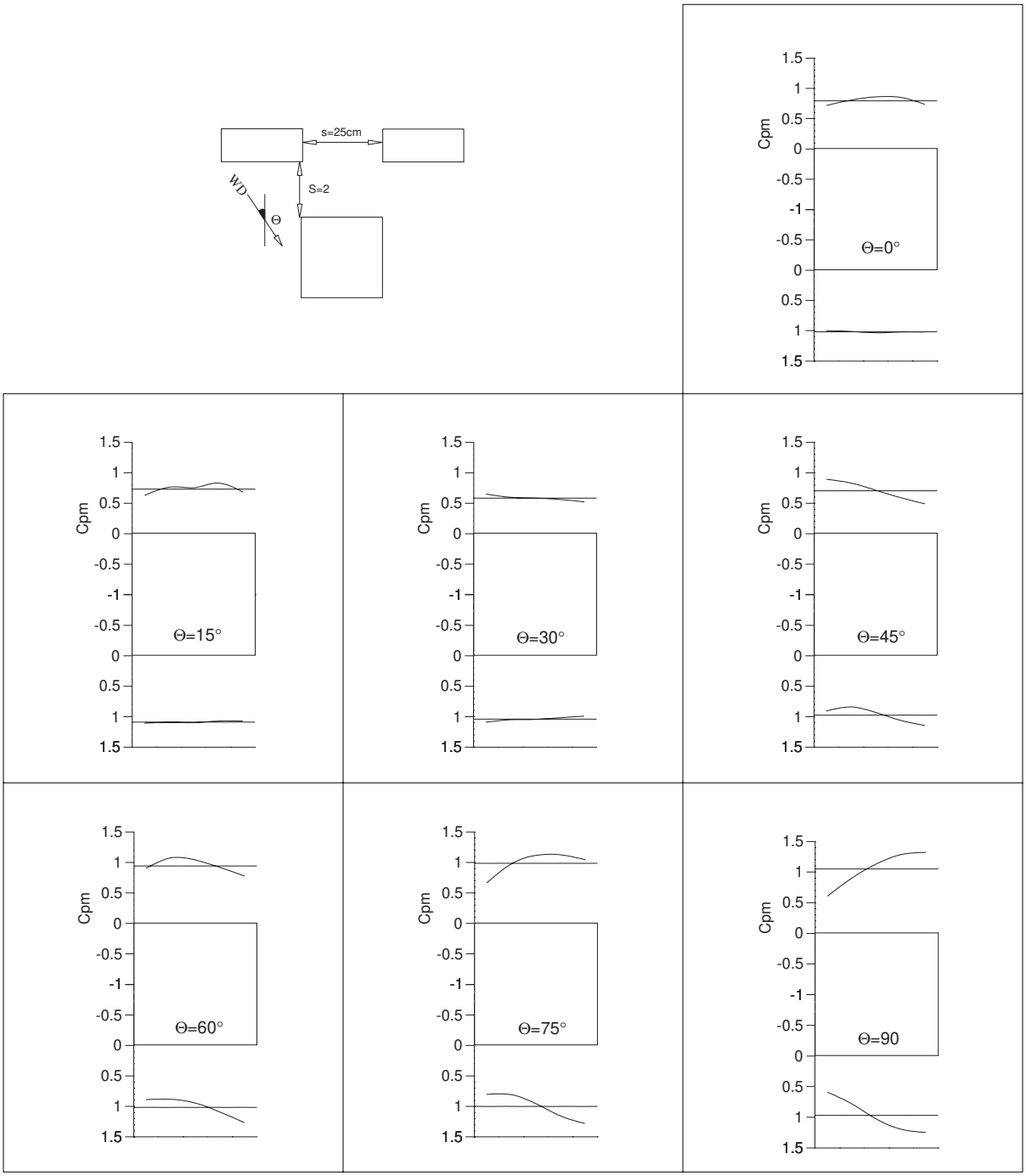

Figure G-2.3 **Pressure modification coefficients C_{pm} profiles as shielded by two obstruction blocks 2 spacings and 37.5 cm between blocks**

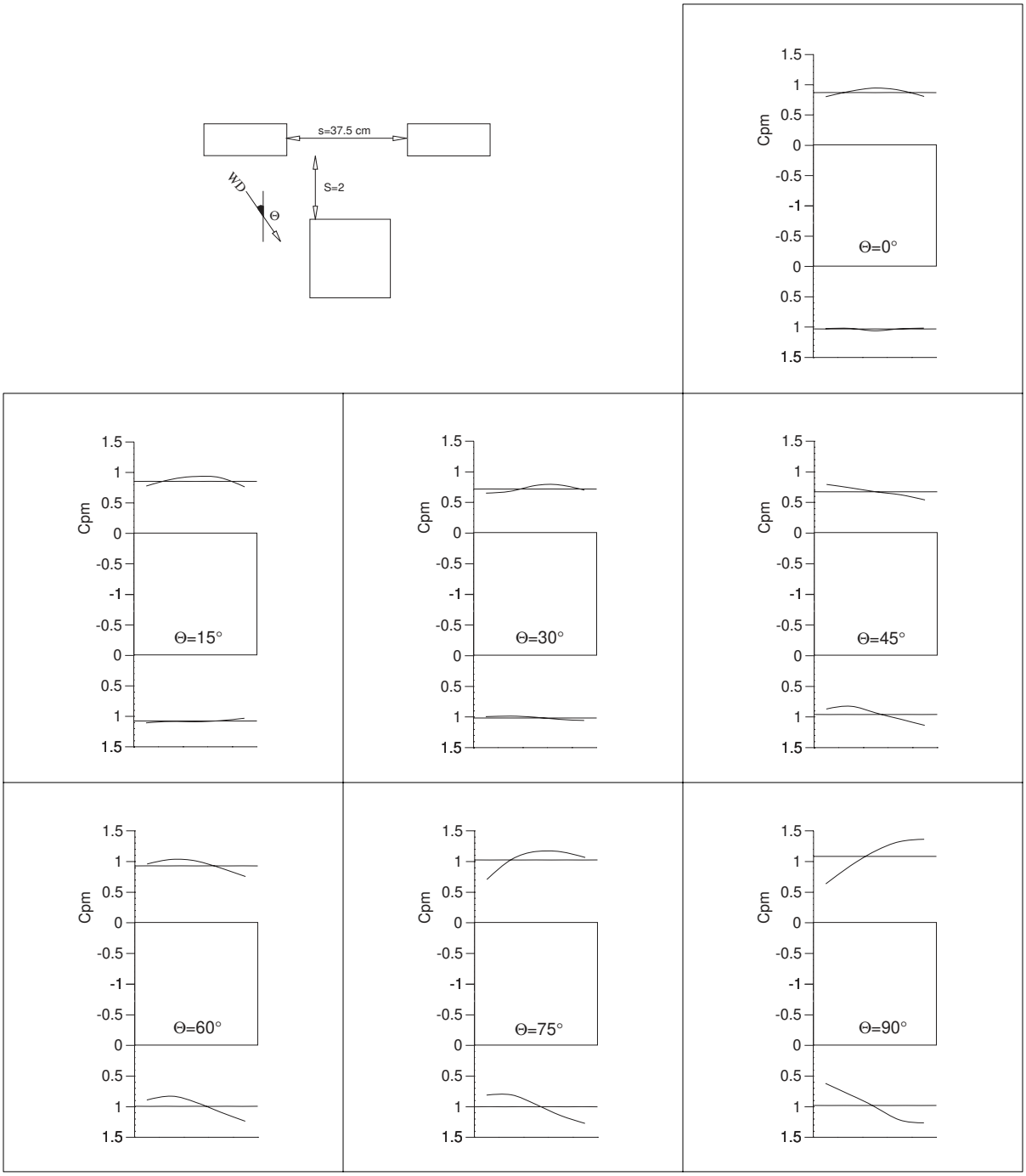

Figure G-2.4 **Pressure modification coefficients C_{pm} profiles as shielded by two obstruction blocks 2 spacings and 12.5 cm between blocks and horizontally displaced**

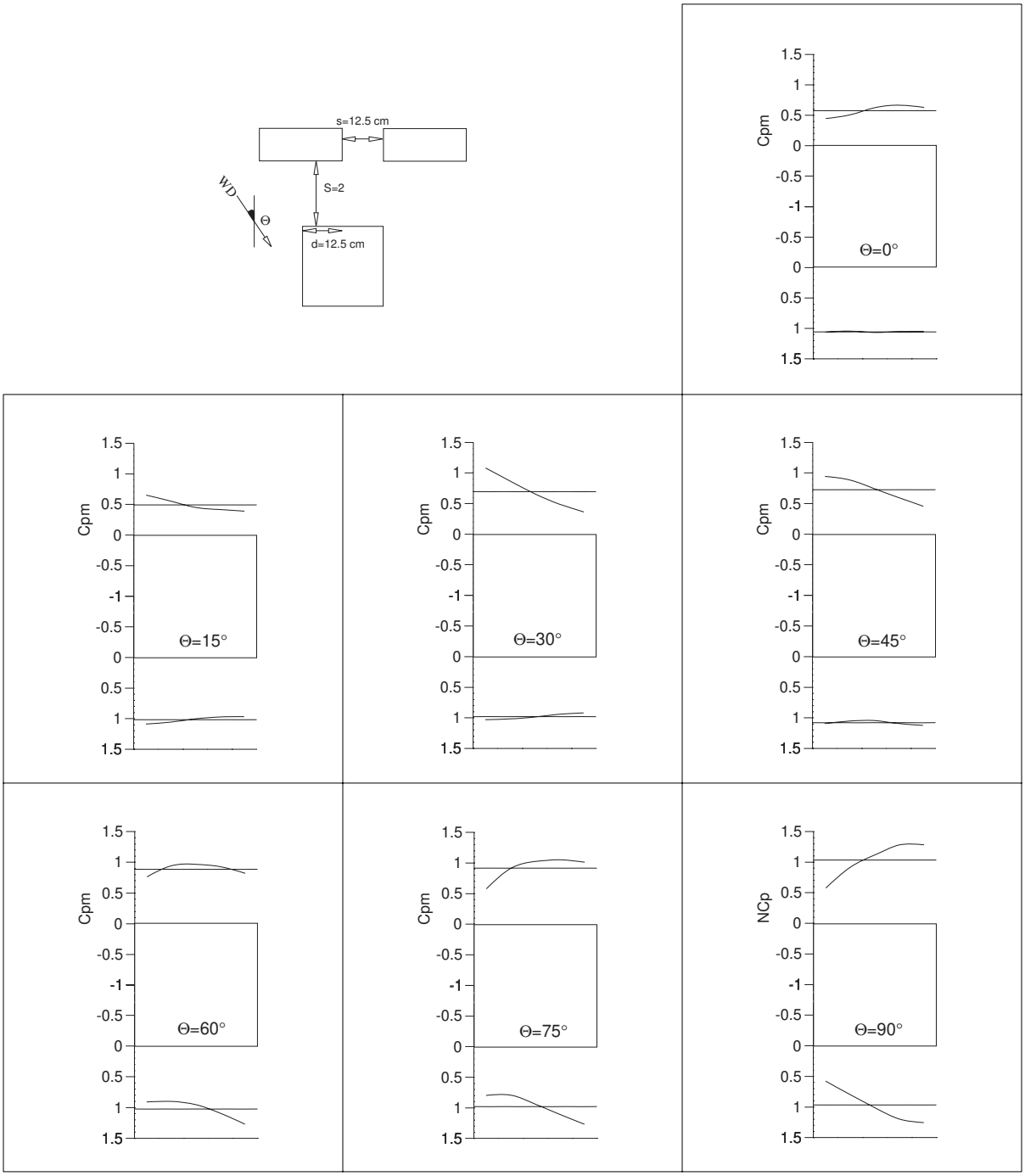

Figure G-2.5 **Pressure modification coefficients C_{pm} profiles as shielded by two obstruction blocks 2 spacings and 25 cm between blocks and horizontally displaced**

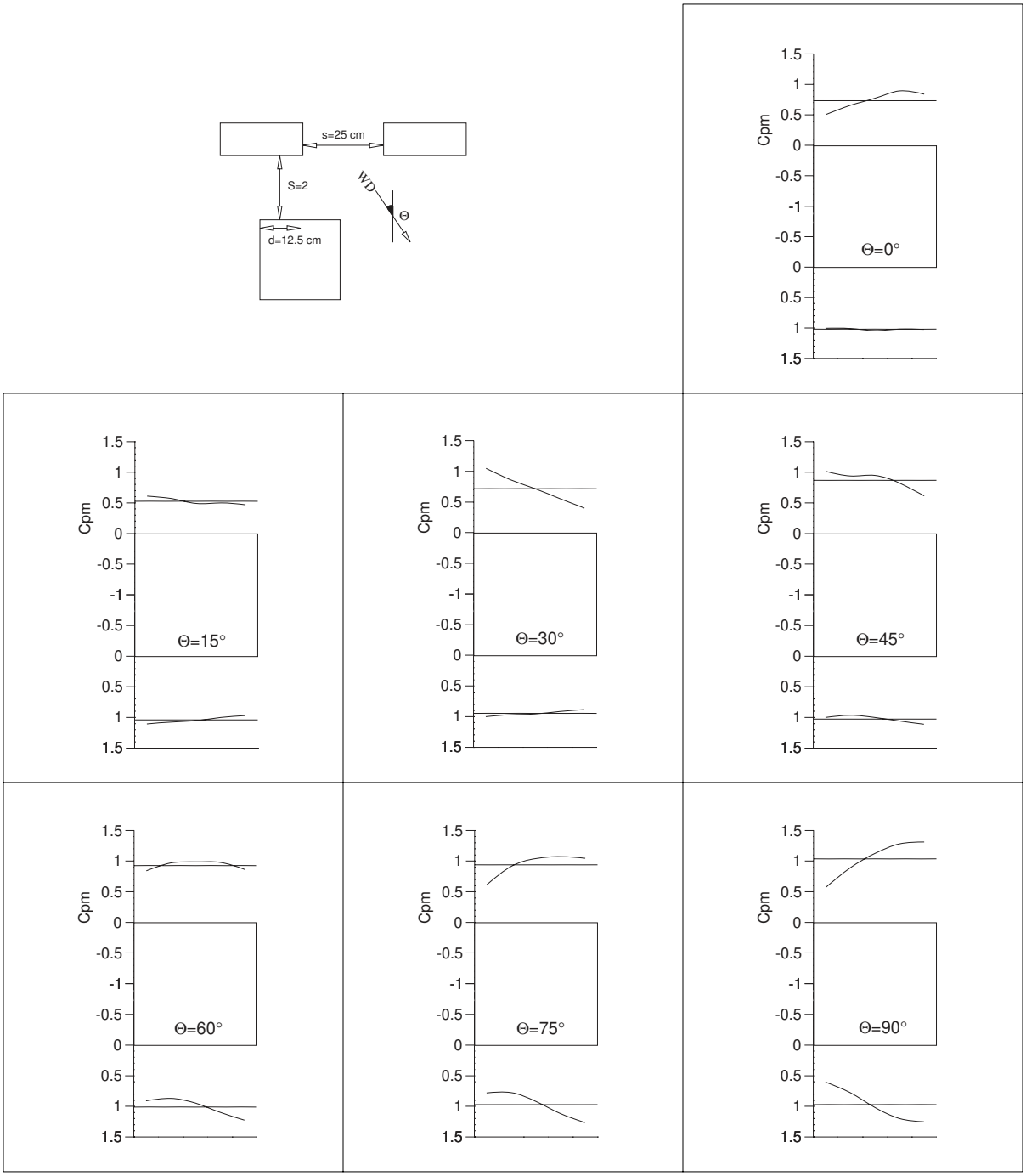

Figure G-2.6 **Pressure modification coefficients C_{pm} profiles as shielded by two obstruction blocks 2 spacings and 37.5 cm between blocks and horizontally displaced**

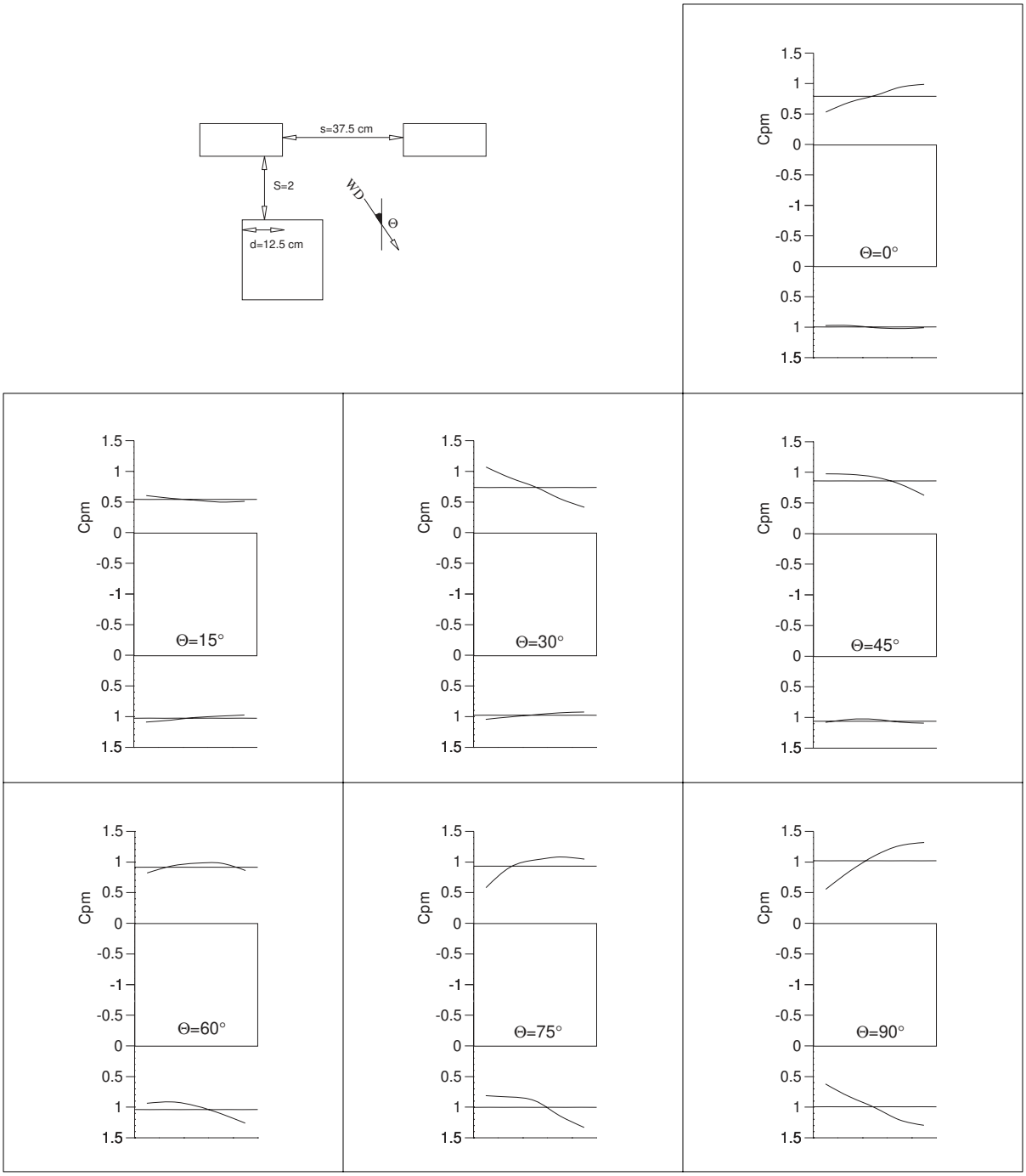

Figure G-2.7 **Pressure modification coefficients C_{pm} profiles as shielded by two obstruction blocks 2 spacings and 12.5 cm between blocks and horizontally displaced**

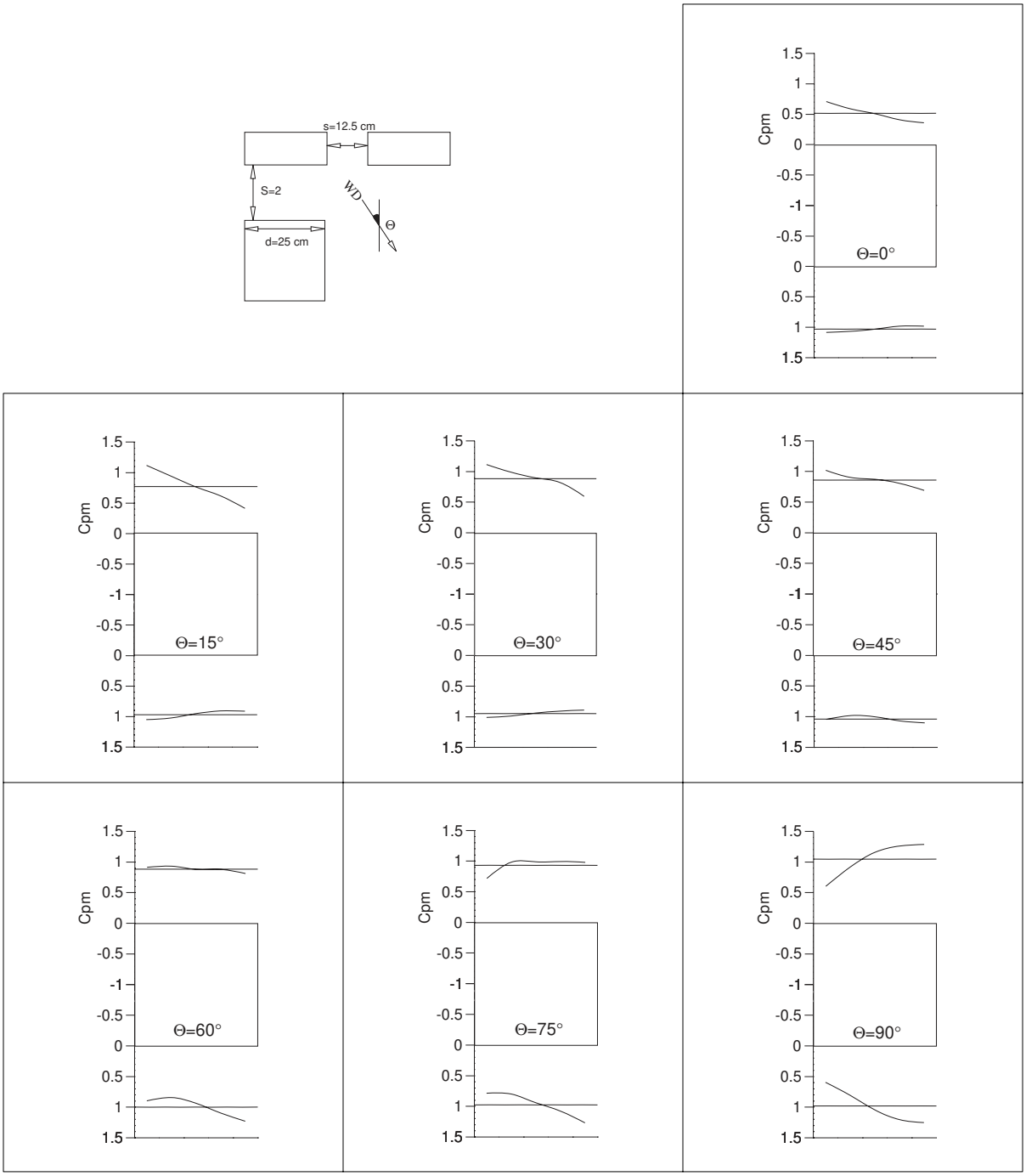

Figure G-2.8 **Pressure modification coefficients C_{pm} profiles as shielded by two obstruction blocks 2 spacings and 25 cm between blocks and horizontally displaced**

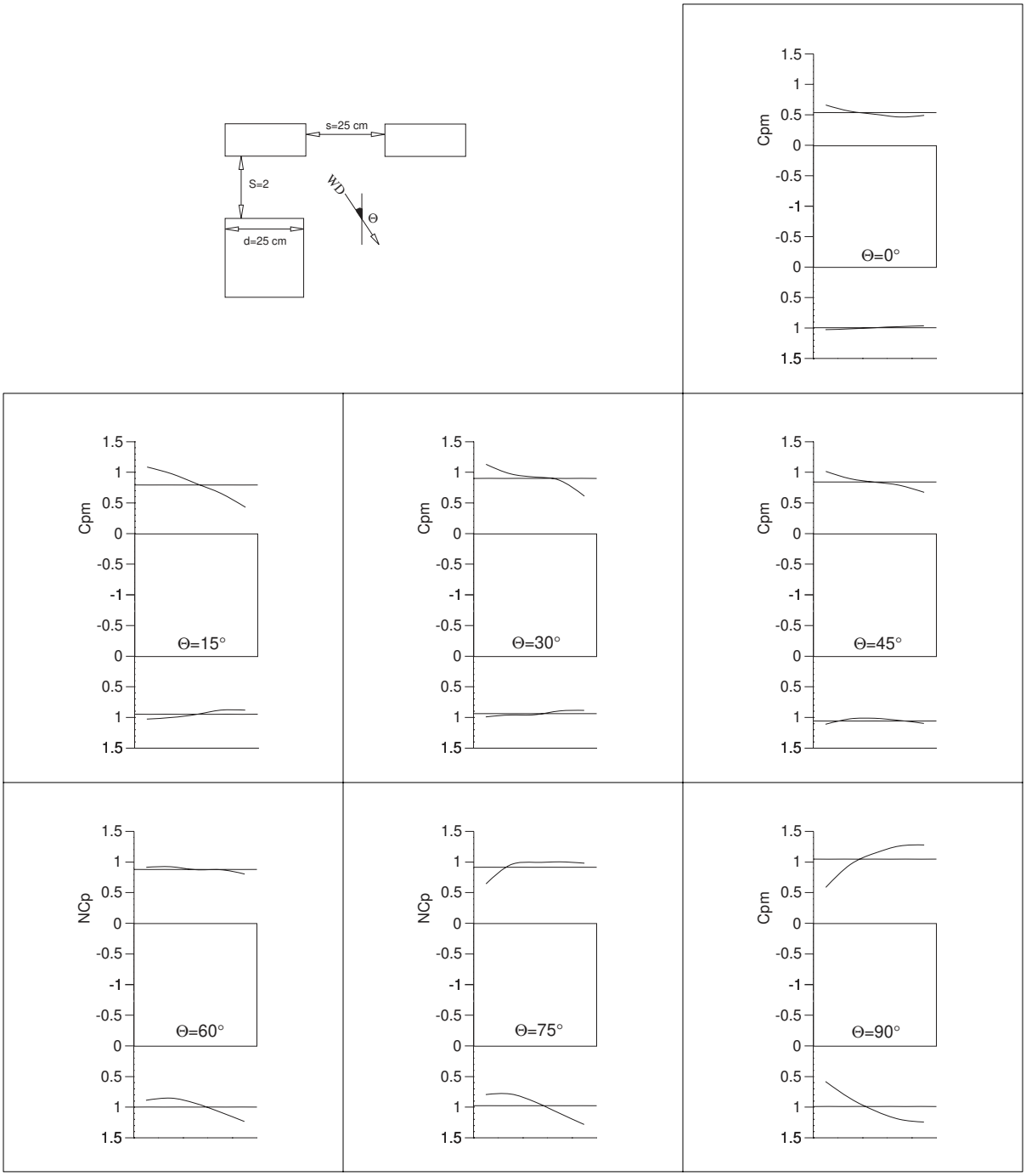

Figure G-2.9 **Pressure modification coefficients C_{pm} profiles as shielded by two obstruction blocks 2 spacings and 37.5 cm between blocks and horizontally displaced**

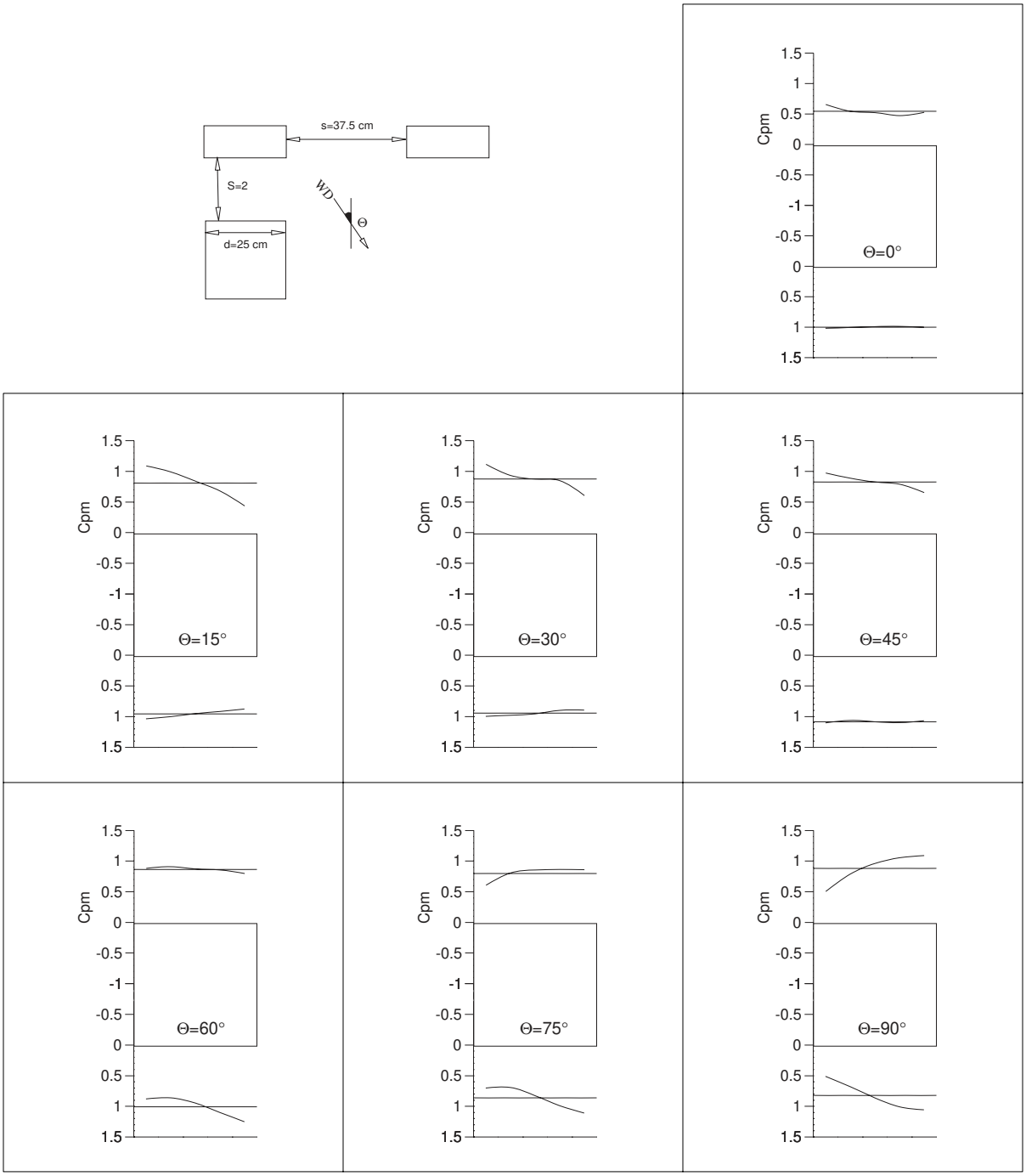

Figure G-2.10 **Pressure modification coefficients C_{pm} profiles as shielded by two obstruction blocks 3 spacings and 12.5 cm between blocks and horizontally centered**

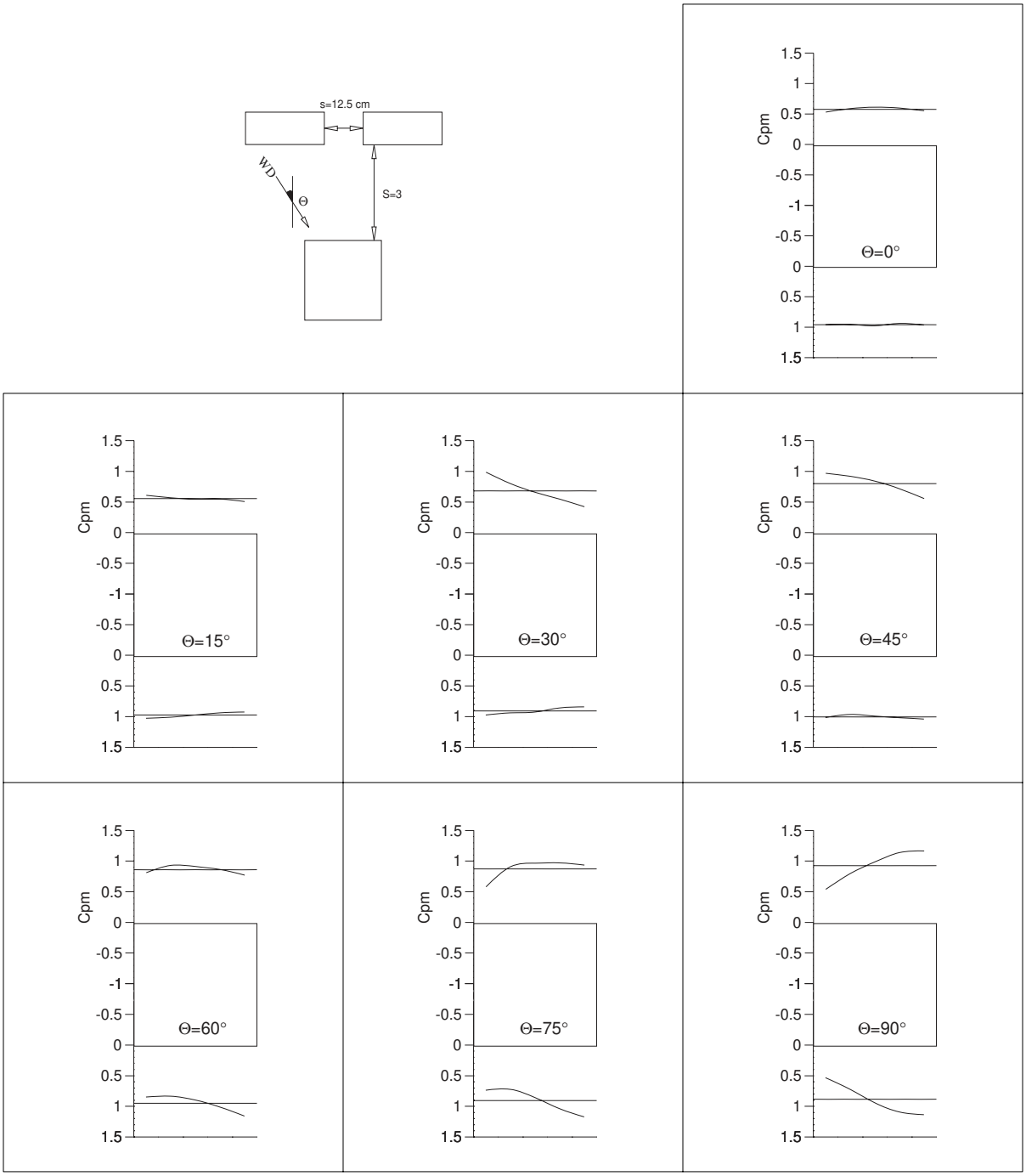

Figure G-2.11 **Pressure modification coefficients C_{pm} profiles as shielded by two obstruction blocks 3 spacings and 25 cm between blocks and horizontally centered**

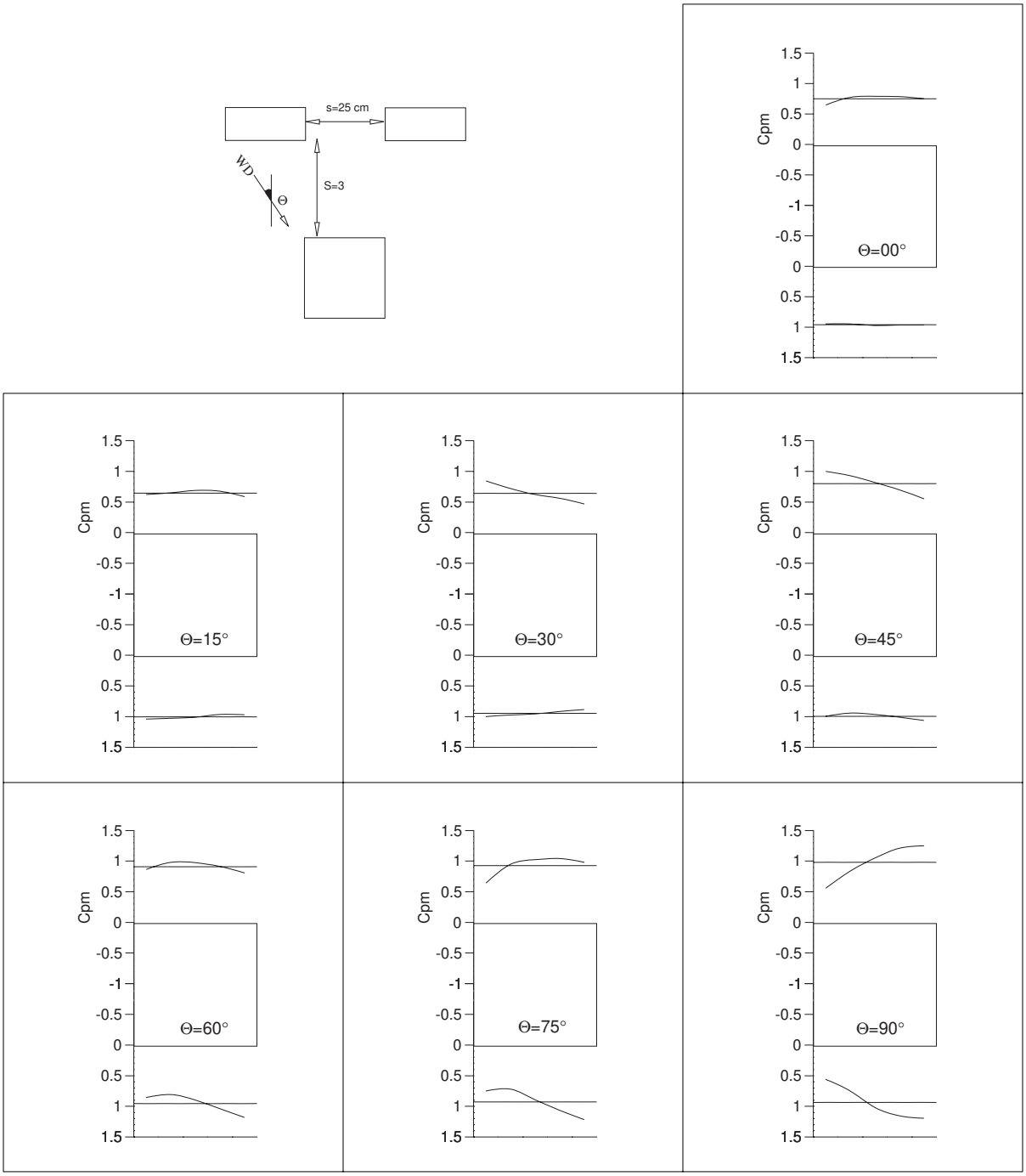

Figure G-2.12 **Pressure modification coefficients C_{pm} profiles as shielded by two obstruction blocks 3 spacings and 37.5 cm between blocks and horizontally centered**

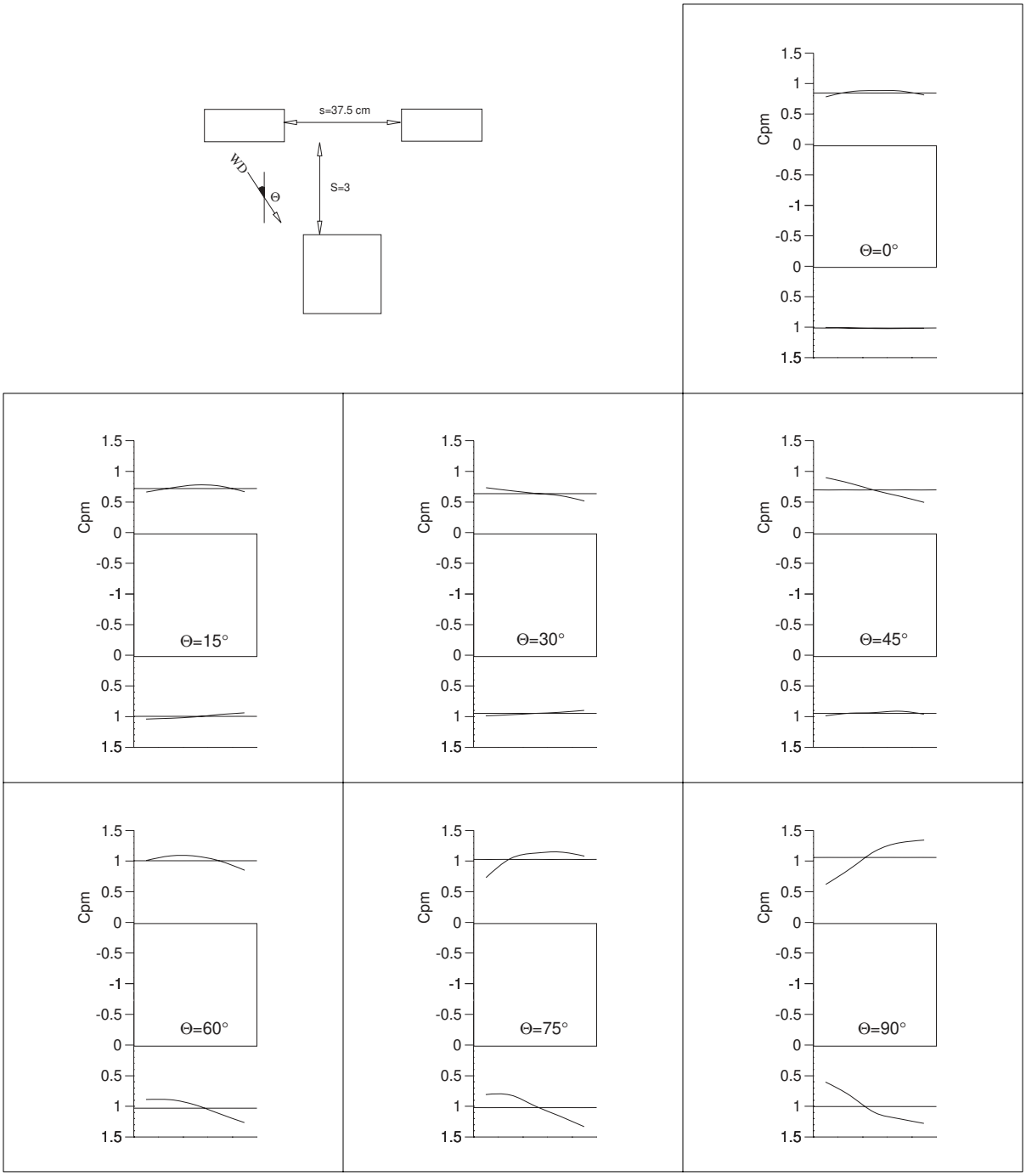

Figure G-2.13 **Pressure modification coefficients C_{pm} profiles as shielded by two obstruction blocks 4 spacings and 12.5 cm between blocks and horizontally centered**

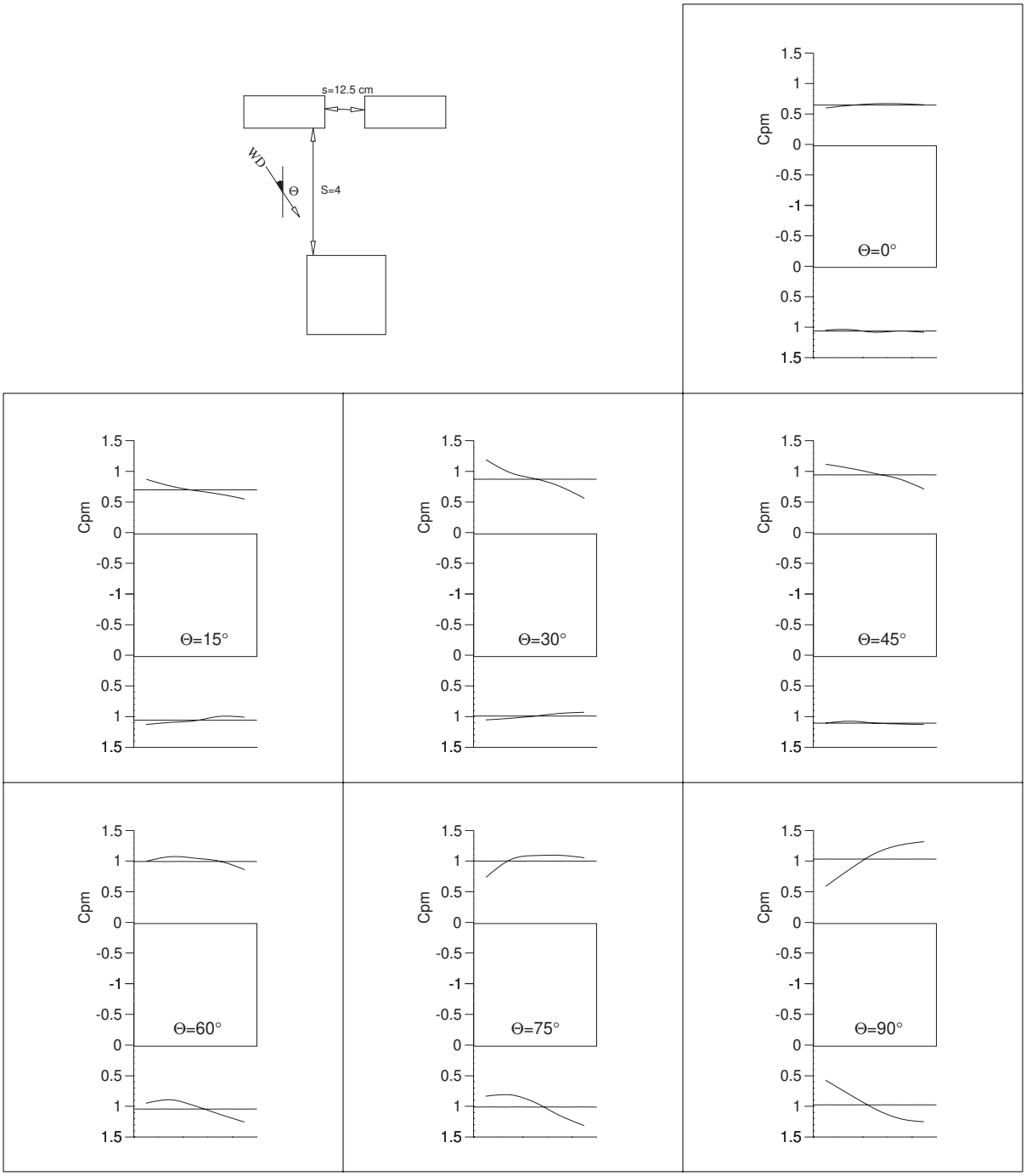

Figure G-2.14 **Pressure modification coefficients C_{pm} profiles as shielded by two obstruction blocks 4 spacings and 25 cm between blocks and horizontally centered**

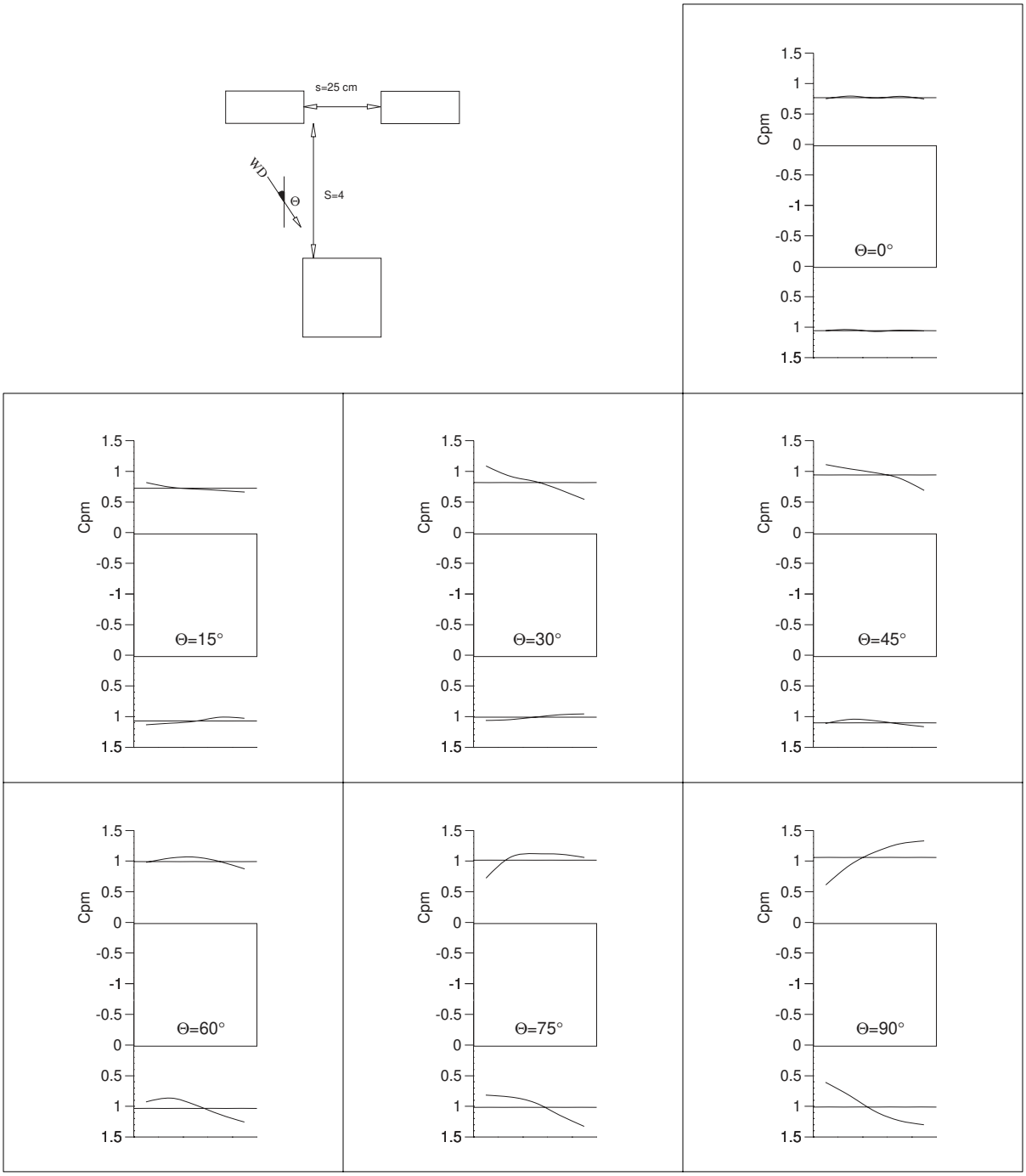

Figure G-2.15 **Pressure modification coefficients C_{pm} profiles as shielded by two obstruction blocks 4 spacings and 37.5 cm between blocks and horizontally centered**

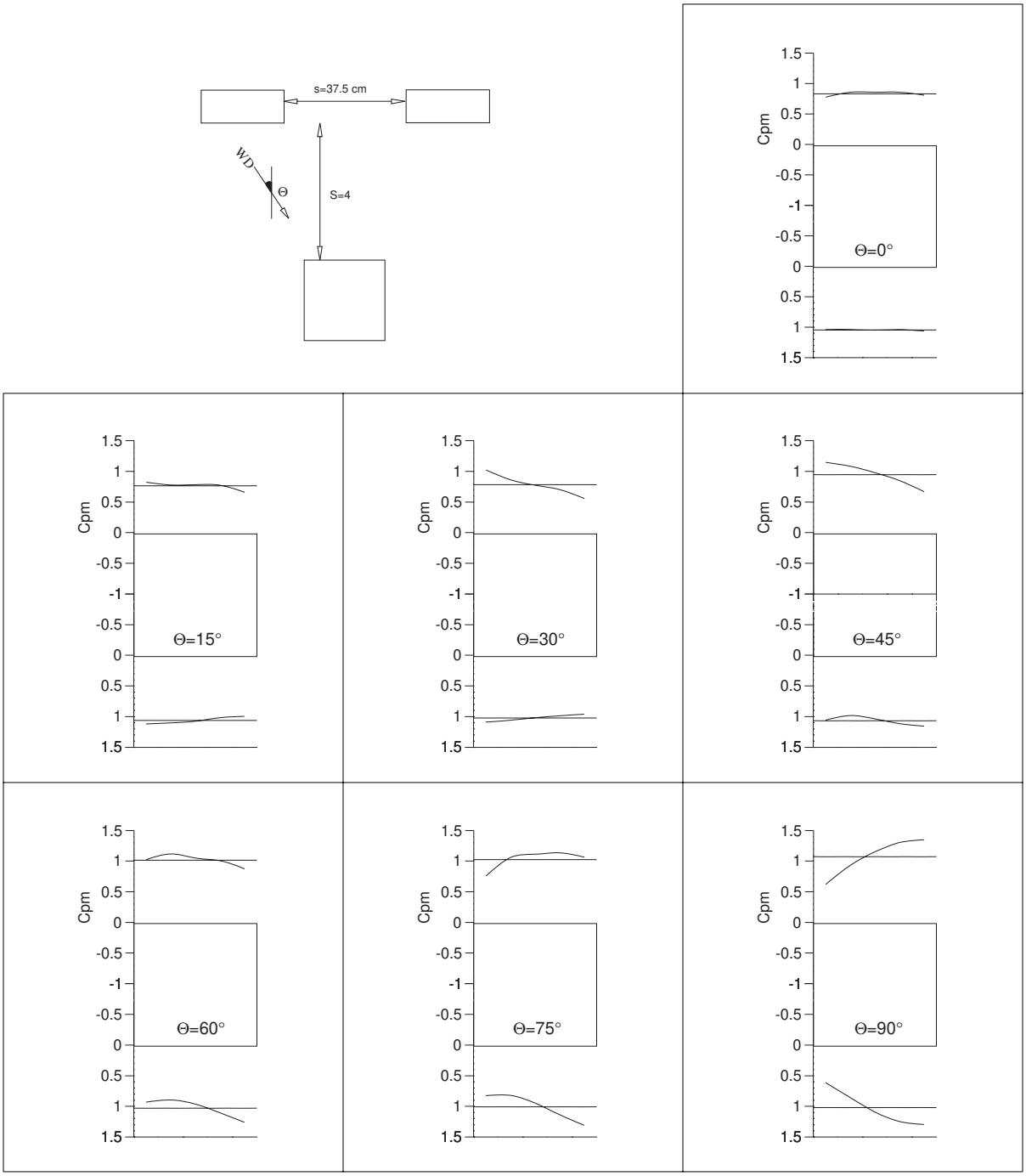

Figure G-3 **Effect of two shielding blocks on obstructed surface of model**

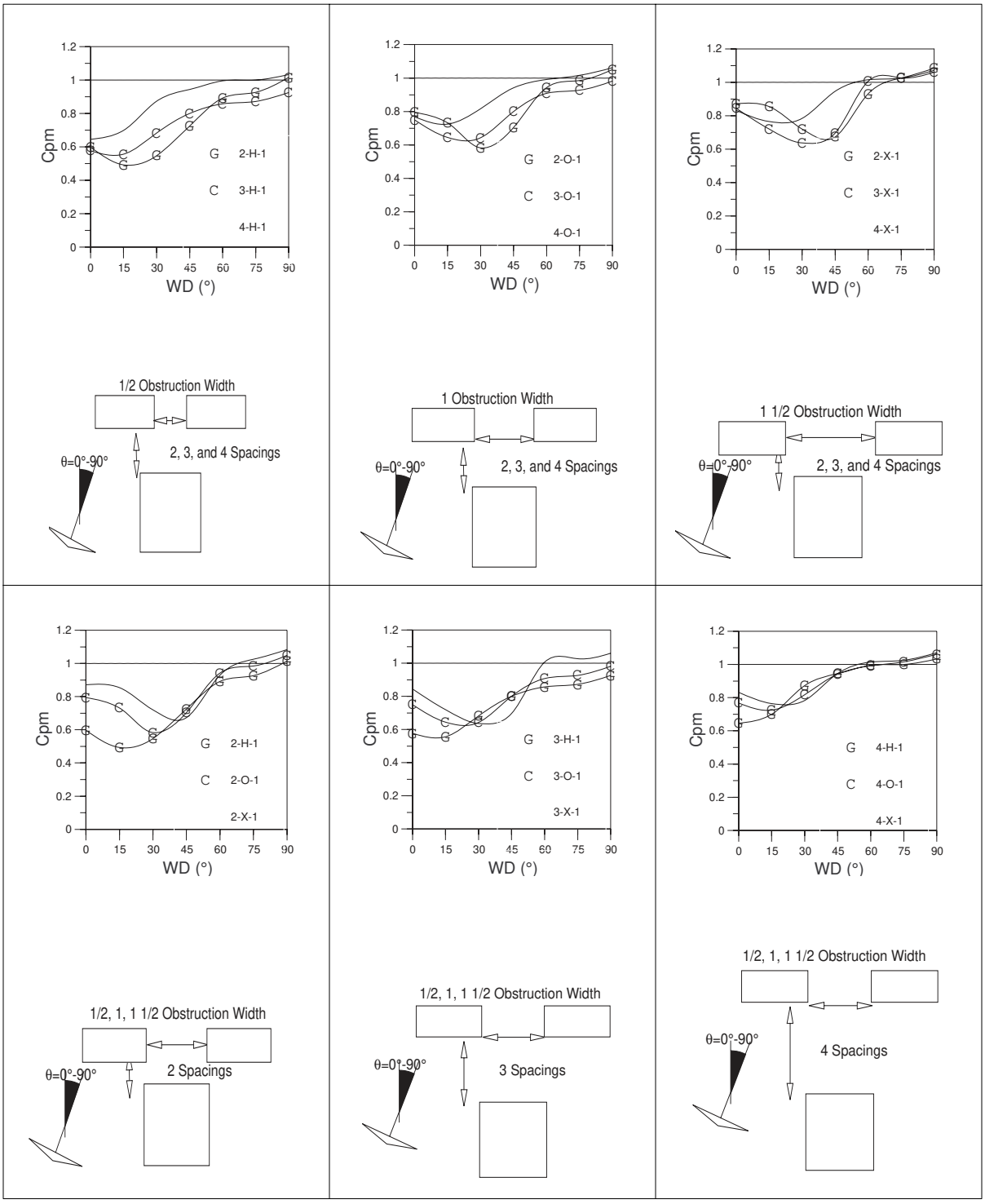

Figure G-3 **Effect of two shielding blocks on obstructed surface of model (Continued)**

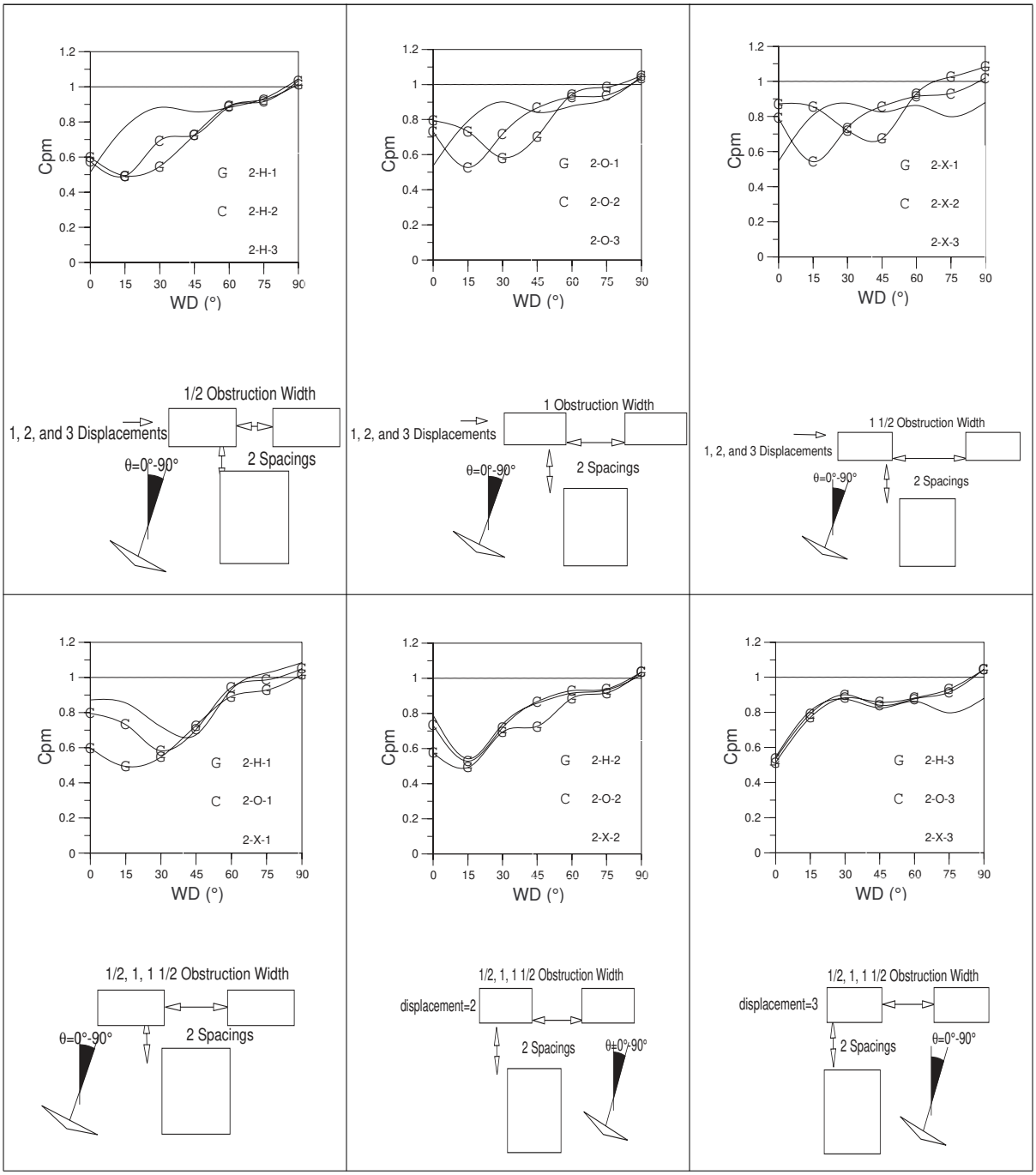

***Figure G-4*. Comparison between the predicted value of C_{pm} for the individual shielding blocks and the measured values.**

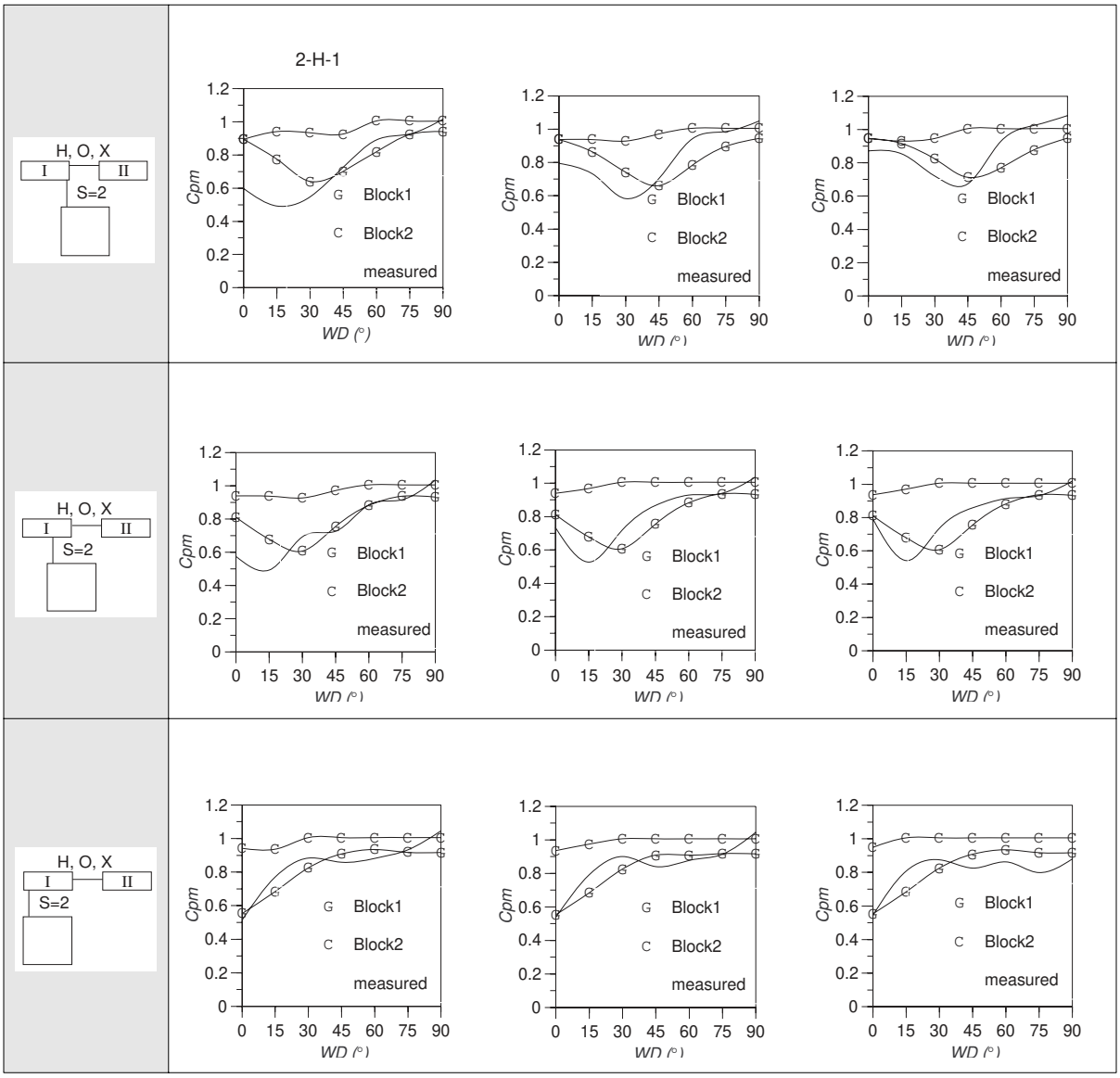

***Figure G-4*. Comparison between the predicted value of C_{pm} for the individual shielding blocks and the measured values. (Continued)**

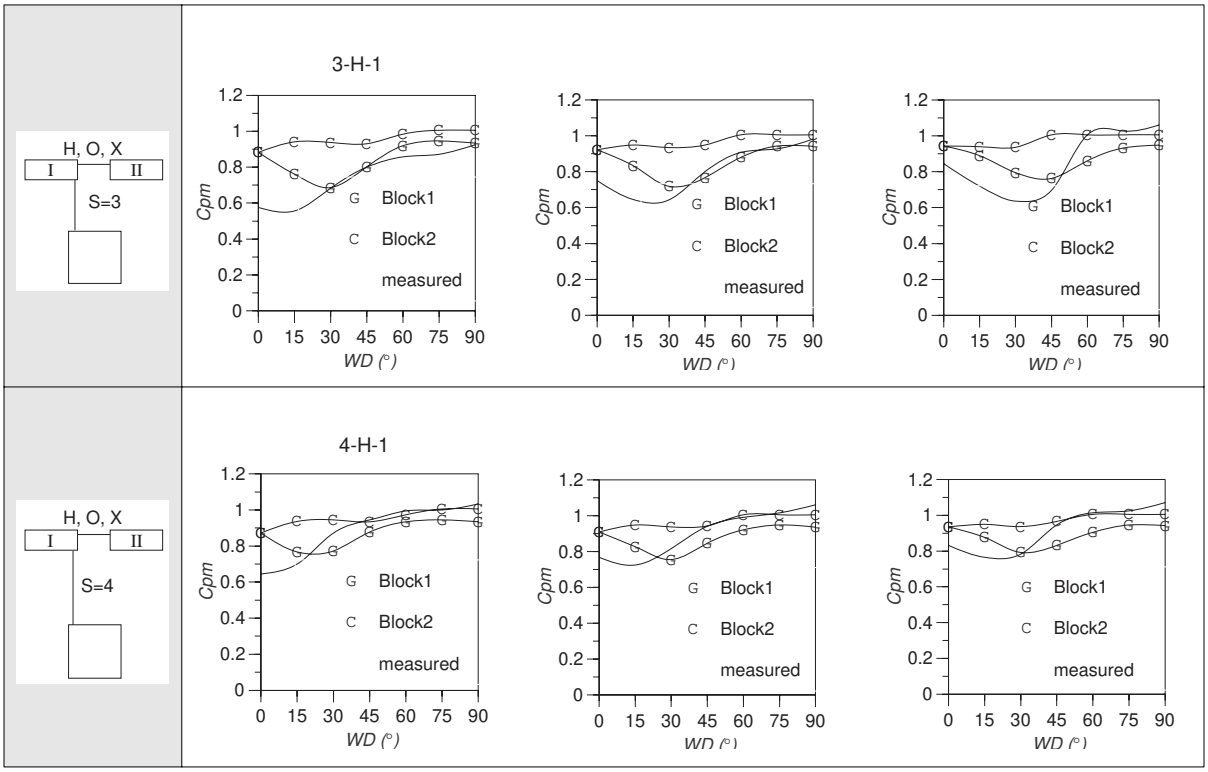

Figure G-5 **Comparison between measured and predicted values of C_{pm}**

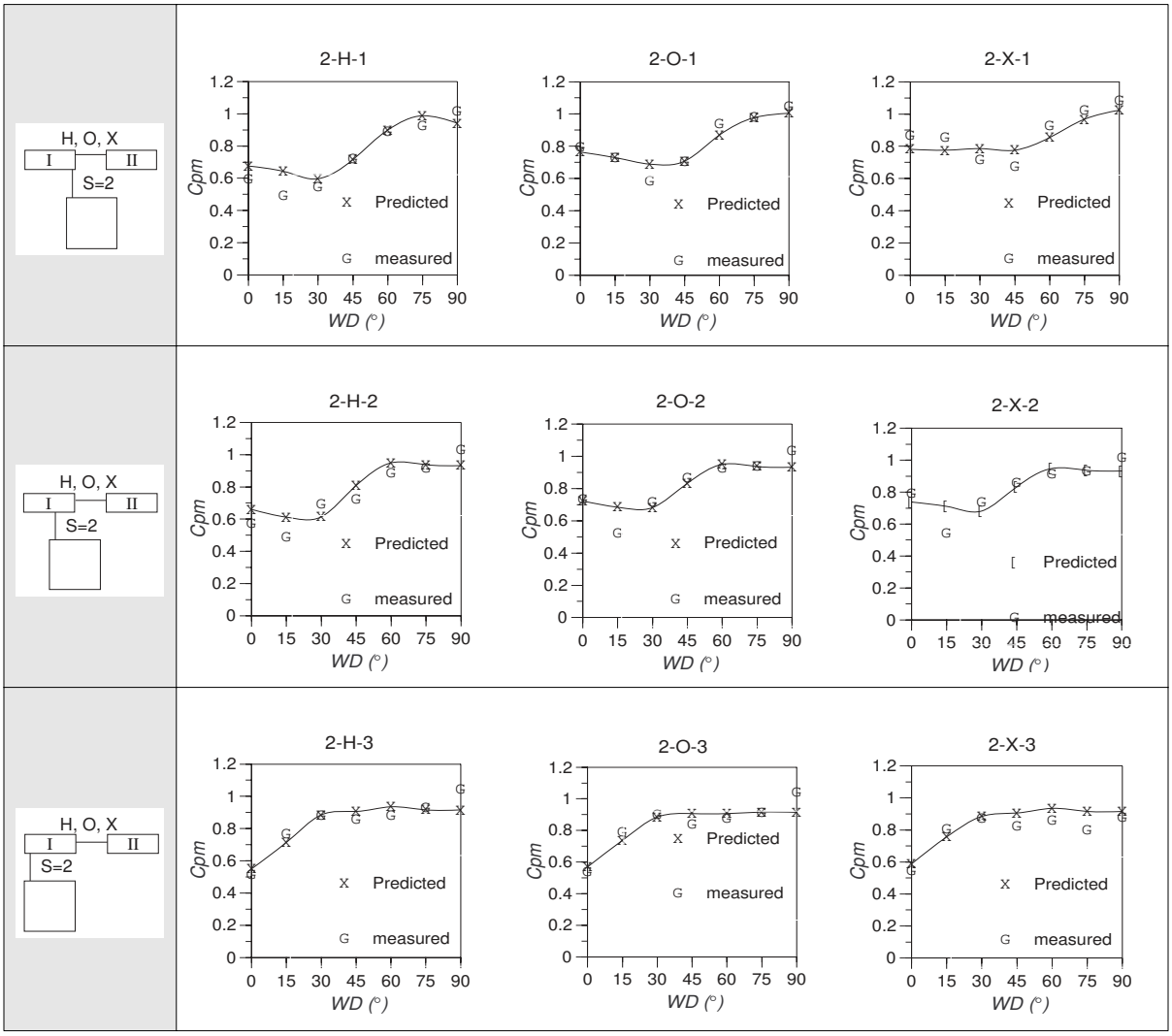

Figure G-5 **Comparison between measured and predicted values of C_{pm} (Continued)**

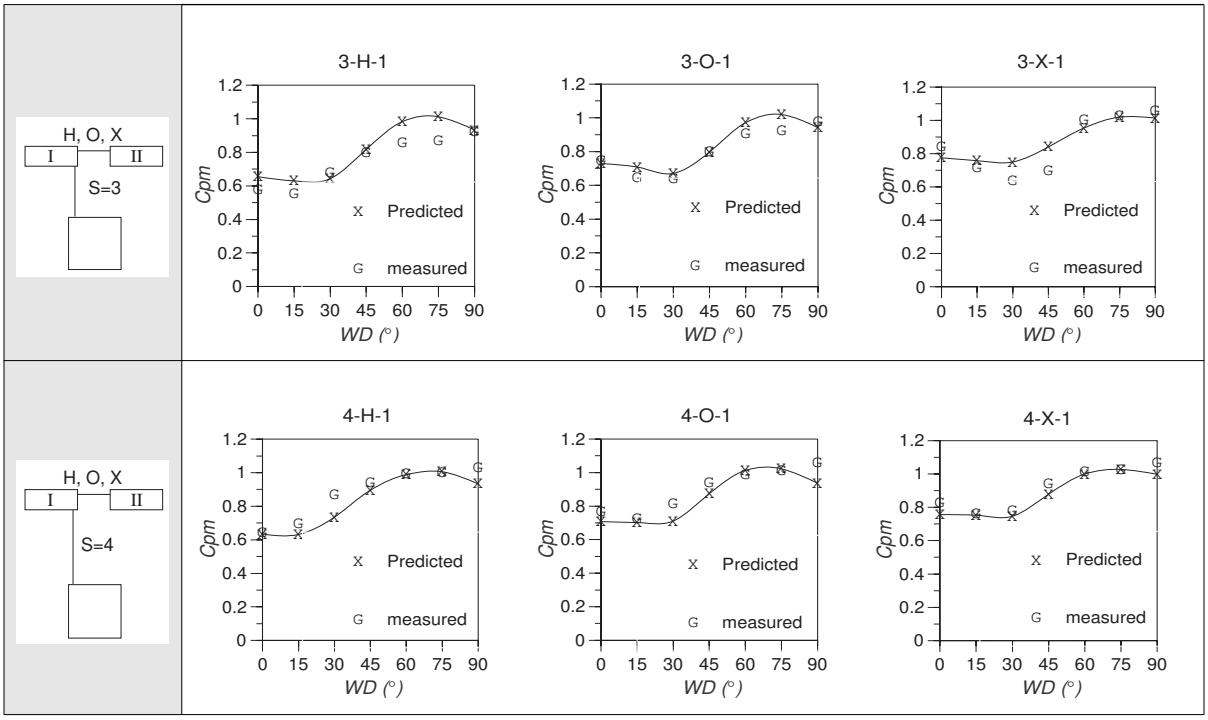

Appendix H

Appendix H

Model Application and Algorithm

H.1 Algorithm

Figure H-1 **Diagram showing the procedural flow of the model for predicting velocity coefficients C_v**

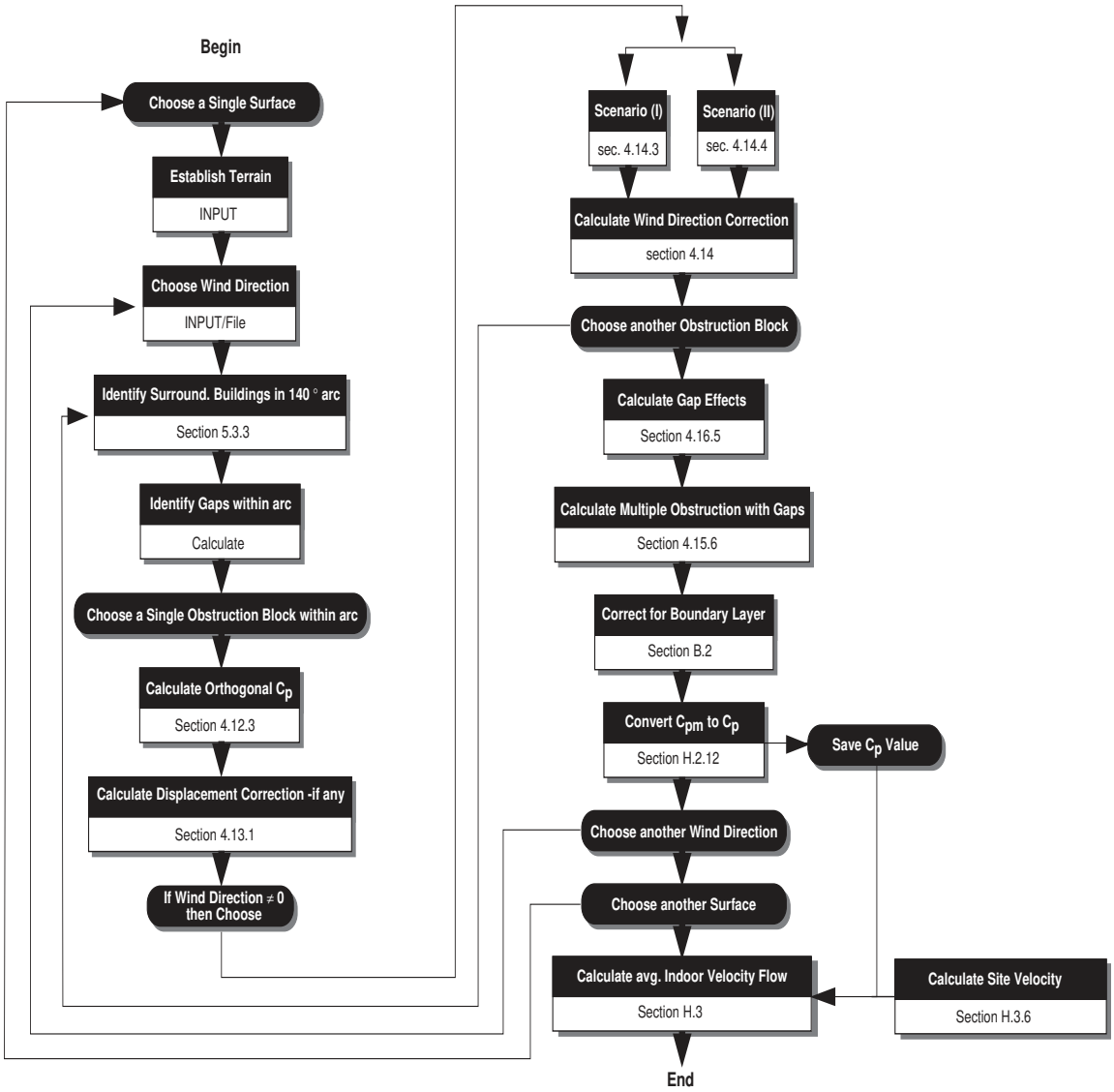

H.2 Sample Calculations

This part contains a sample calculation of the Indoor Ventilation prediction Model (IVM) with a detailed description of the procedure used. The site and model configuration were the same as the ones used for the verification of the model using the complex urban layout[1].

H.2.1 Inputting Terrain Types

The terrain types around the building of concern was identified and input using Table B-1. The terrain information is used in the IVM in two ways:

- Conversion from weather station data to site's street level velocities. Examples of these conversion methods are found in Arens 1985 (Ref. 10), Aynsley 1989. (Ref. 24), ASHRAE (Ref. 16), Swami and Chandra 1987 (Ref. 203). For this example, an adapted version of SITECLIMATE method was used to predict the wind speeds at the site (Section 5.7).
- Correcting C_{pm} value using Table B-1 to account for the difference in terrain type from the one used in deriving the prediction model.

H.2.2 Inputting the Obstruction Coordinates

As discussed in Chapter 5, the input for the model is based on the polar coordinates of the outermost visible corners/edges of each visible obstruction block. Figure H-2 demonstrates how the coordinates of the corners/edges were taken off. A list of the measured polar coordinates of all adjacent blocks for each surface is shown in Table H-1.

H-1. For a more detailed description of the tested model and configuration of the obstruction blocks refer to Section 4.17.4 in page 159.

Figure H-2 **Description of surrounding blocks.**

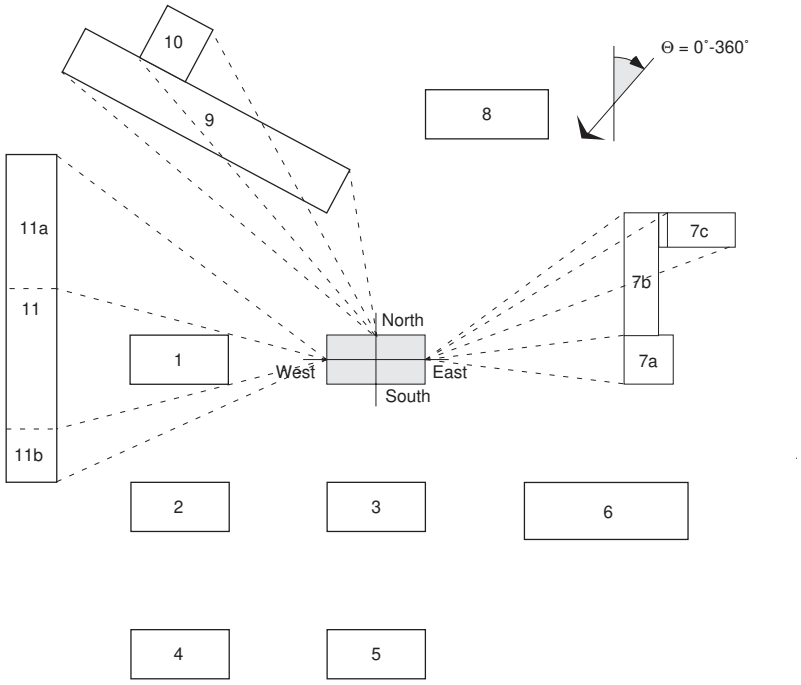

Table H-1 **Polar coordinates of the corners of the surrounding obstruction blocks relative to the four surfaces .**

Surface	Block[a]	Block Height	Point	r (S)[b]	λ [c] (°)
North	*7B*	*7*	*1*	*8.1*	*63.8*
			2	*7.2*	*90*
	7C	*17*	*1*	***3.8***[d]	***67.3***
			2	***4.4***	***76.2***
	8	*25*	*1*	*2.1*	*41.2*
			2	*2.0*	*11.4*
	9	*10*	*1*	***3.4***	***-8.9***
			2	***8.3***	***-50.1***
	10	*24.7*	*1*	***2.9***	***-28***
			2	***3.0***	***-40.3***
	11	*10*	*1*	*7.5*	*-60.4*
			2	*6.5*	*-90*

Table H-1 Polar coordinates of the corners of the surrounding obstruction blocks relative to the four surfaces (Continued).

Surface	Block[a]	Block Height	Point	r (S)[b]	λ [c] (°)
South	*2*	*10*	*1*	*5.4*	*68.1*
			2	*4.2*	*45.2*
	3	*10*	*1*	*2.3*	*26.6*
			2	*2.3*	*-26.6*
	4	*10*	*1*	*7.1*	*44.9*
			2	*6.6*	*27*
	6	*10*	*1*	*6.7*	*-72.4*
			2	*4.4*	*-43.9*
	11	*10*	*1*	*6.8*	*72.8*
			2	*6.5*	*90*
East	*6*	*10*	*1*	*5.9*	*25.1*
			2	*4.2*	*61.2*
	7A	*25*	*1*	*1.6*	*7.0*
			2	*1.6*	*-7.0*
	7B	*7*	*1*	*7.2*	*-36.4*
			2	*5.8*	*-7*
	7C	*17*	*1*	*4.0*	*-20*
			2	*3.4*	*-31.2*
	8	*25*	*1*	*2.1*	*-60.9*
			2	*1.8*	*-90*
West	*1*	*10*	*1*	*2.1*	*13.9*
			2	*2.1*	*-13.9*
	2	*10*	*1*	*4.7*	*-32.1*
			2	*4.0*	*-11.3*
	4	*10*	*1*	*6.3*	*-60.7*
			2	*6.8*	*-73.1*
	9	*10*	*1*	*8.0*	*47.3*
			2	*3.0*	*90*
	10	*24.7*	*1*	*2.9*	*58.1*
			2	*2.9*	*71*
	11a[e]	*10*	*1*	*6.9*	*37.3*
			2	*5.7*	*14.1*
	11b	*10*	*1*	***5.7***	***-14.1***
			2	***6.0***	***-24.4***

a. Refer to Figure H-2.

b. The radial coordinate is measured in terms of obstruction Spacing (S_o).

c. Angular coordinate of visible edge of obstruction block.
d. Refer to Section H.2.3
e. Note that for the west surface, obstruction block has been divided into two sections: 11a and 11b (Figure H-2)

H.2.3 Running a Point Order Check

Following the rules stated in Section 5.3.3.3, the point coordinates in bold font in Table H-1 have been flagged for order errors. The three points were then reversed in the calculation in the next section. However, the corner coordinates of block 9 were kept as ordered in Table H-1. This exception was used to account for the shifted wake effect discussed in Section 4.17.4.4. By selecting point 1 to be the one with the smallest absolute value of the angular polar coordinates, the equivalent obstruction plane appears closer to the north surface, thus decreasing the predicted value of C_{pm}.

H.2.4 Determining the Relative Wind Direction Θ_{rel}

Based on the discussion in Section 5.3.3.1, the relative wind directions for the four facades were determined. At 0˚, the values of Θ_{rel} were 0˚, -90˚, 180˚, and +90˚ for the North, East, South, and West facades respectively[2]. For wind directions $\Theta_{rel} > 0°$, Equations (5-4) and (5-5) were used.

H.2.5 Calculating the Angles of Obstruction

Using the geometric relationships discussed in Chapter 5, the angles of obstructions were calculated [Equations (5-7), (5-14) to (5-20)]. Figures H-3 to H-6 show the result of the calculations of the three angles of obstruction for the four surfaces for the 360 wind directions. As a visual hint, it should be noted that wind direction at max $|\alpha_h|$ roughly coincides with the wind direction at which the shielding effect of that obstruction block is maximum.

H-2. Refer to Equation (5-1).

Figure H-3 **Angles of obstruction for the North facade.**

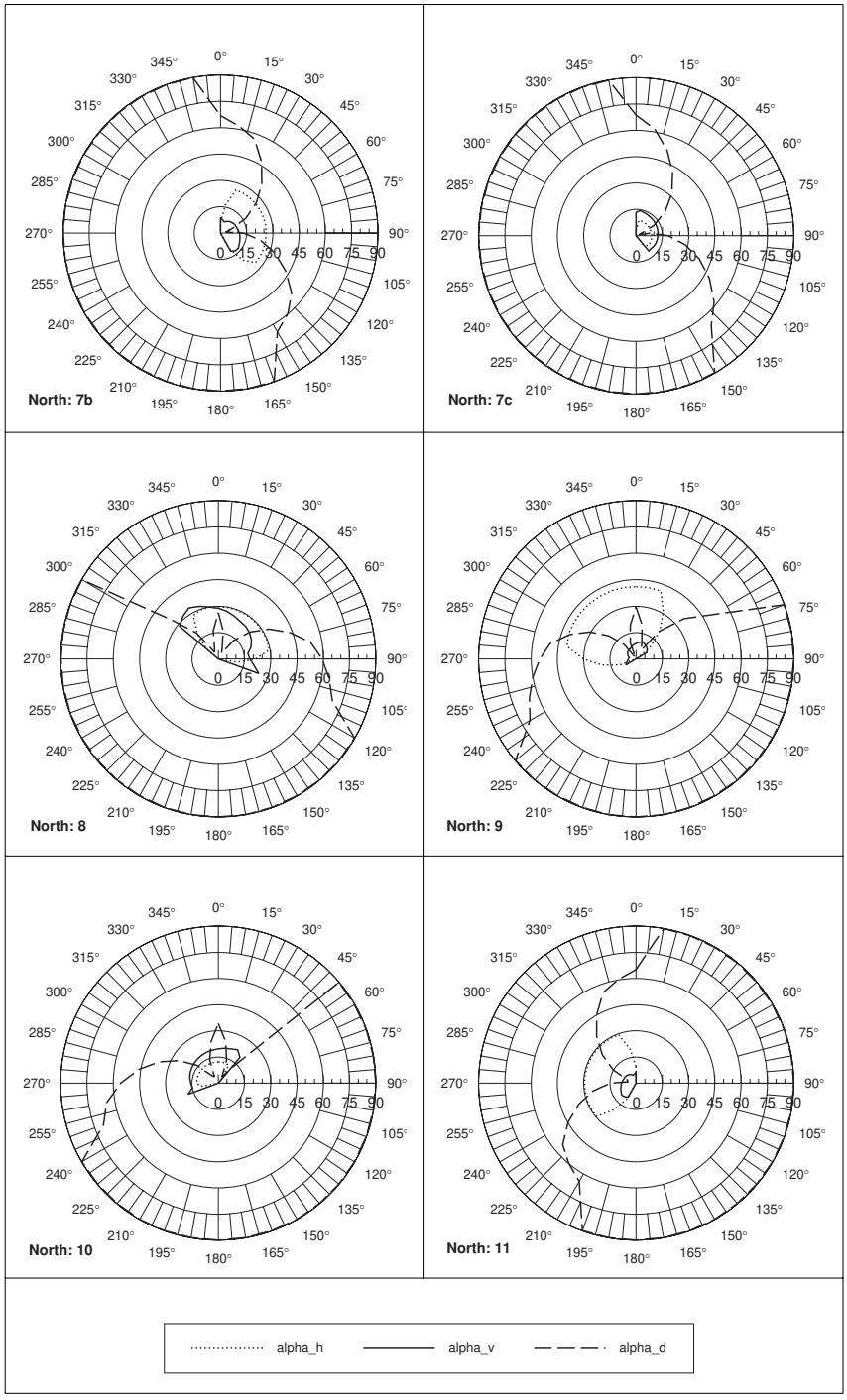

Figure H-4 **Angles of obstruction for the South facade.**

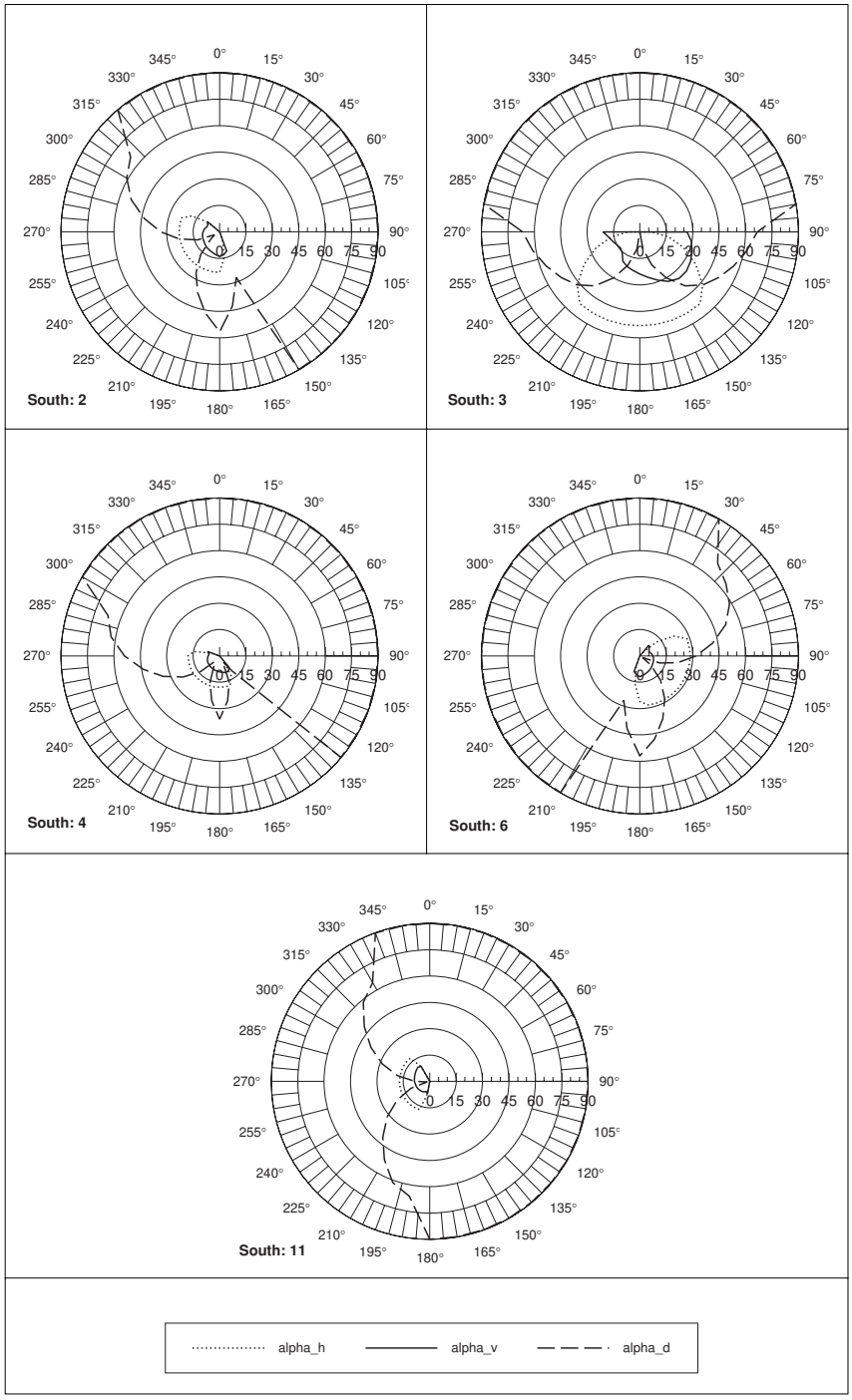

Figure H-5 **Angles of obstruction for the East facade.**

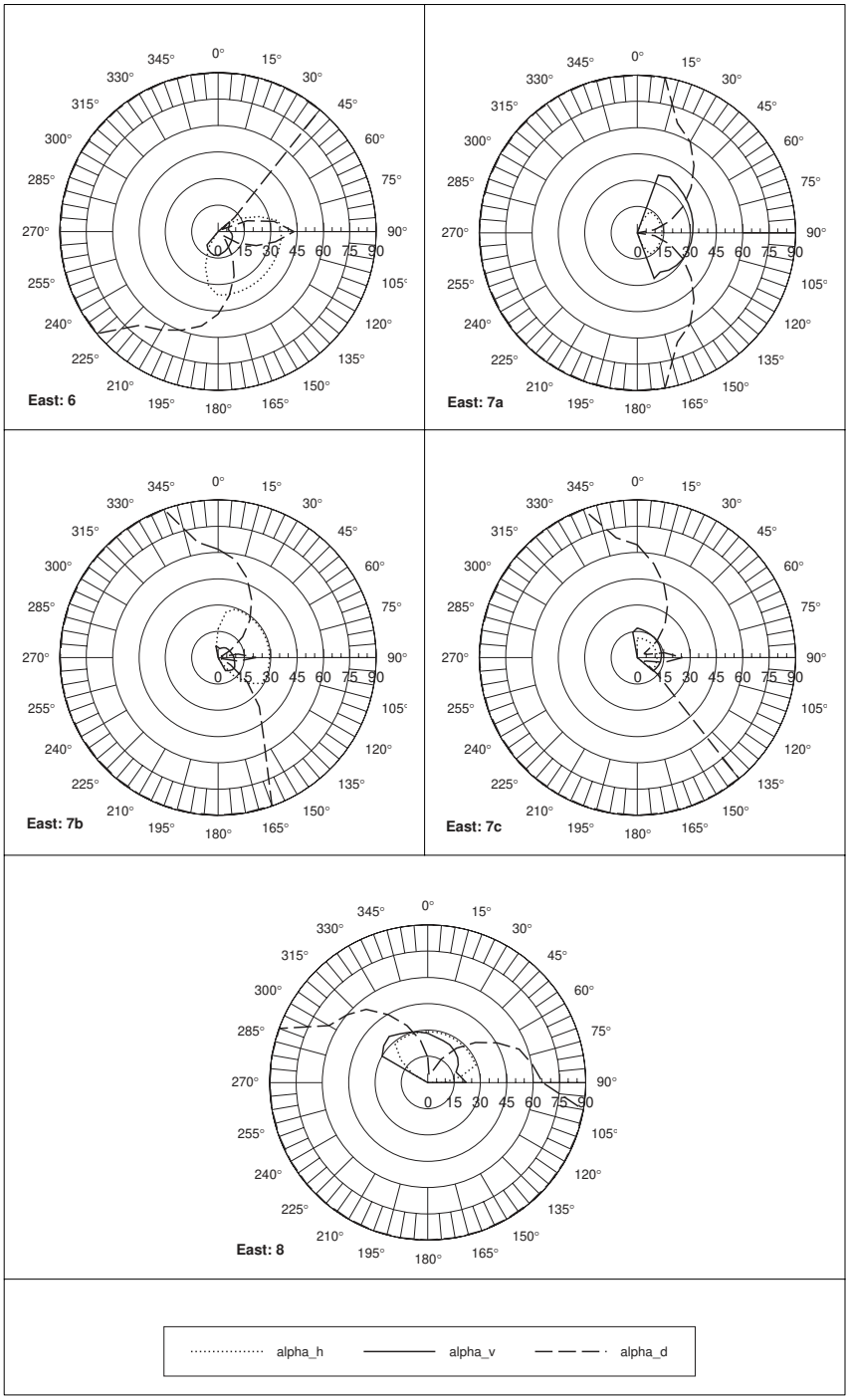

Figure H-6c **Angles of obstruction for the West facade.**

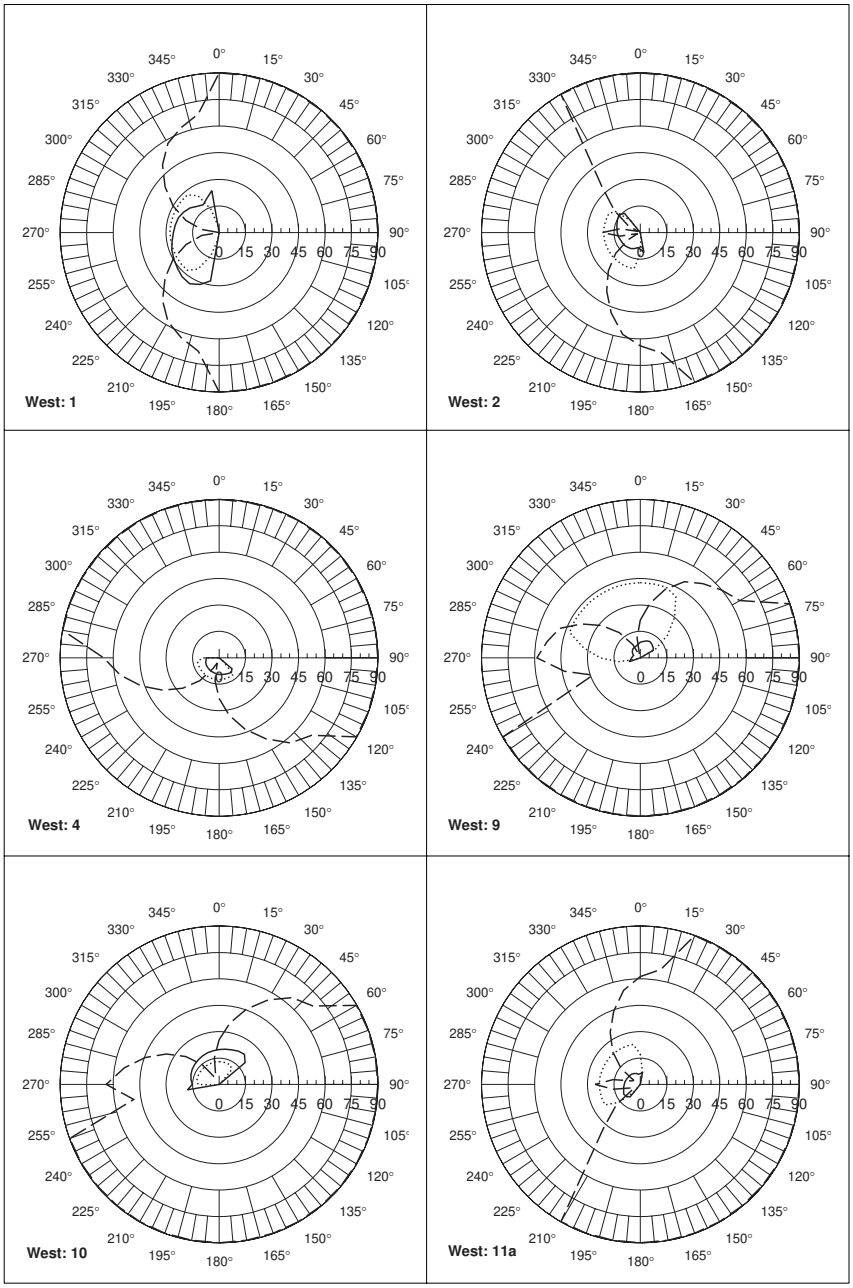

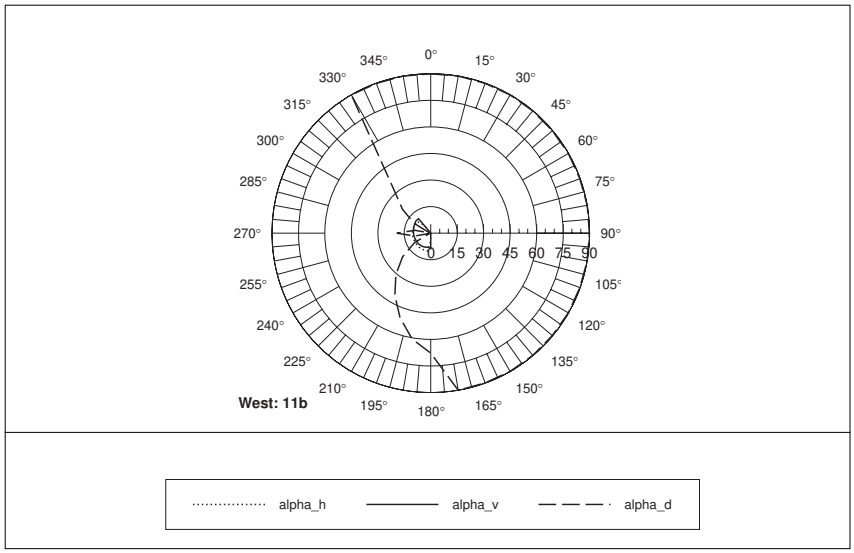

H.2.6 Inputting the Gap Description

As defined in Section 5.3.3.7, the gaps' polar coordinates are taken off from the plan (Figure H-7). Similar to the obstruction blocks, only gaps visible from the surface are considered in determining the overall shielding effect.

Figure H-7 **Determination of the Gaps coordinates**

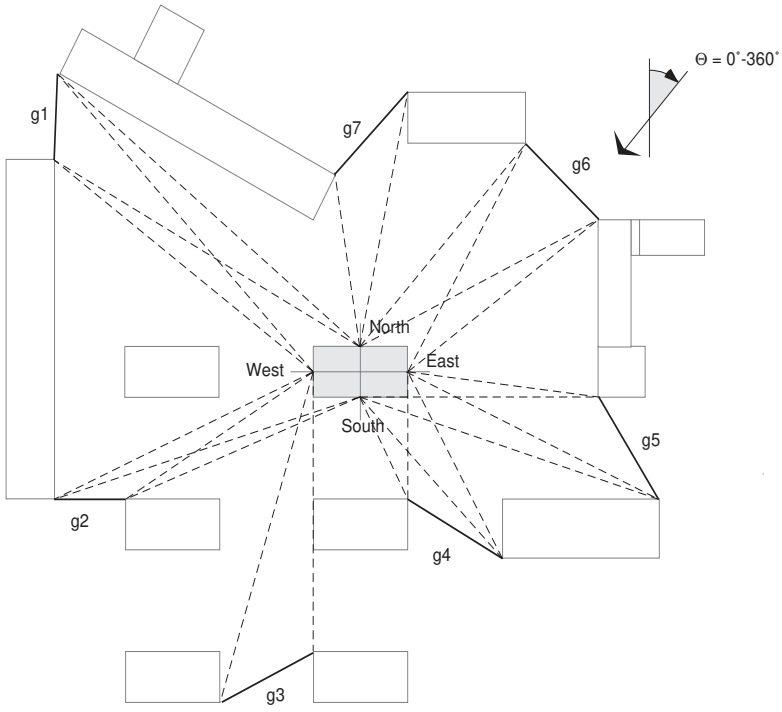

Table H-2 **Coordinates of visible Gaps.**

Surface[a]	Gap	Block Height	Point	r (S)	λ (°)
North	*g1*	*10*	*1*	*8.4*	*-50.1*
		10	*2*	*7.5*	*-60.4*
	g6	*7*	*1*	***8.0***	***63.8***
		25	*2*	***2.1***	***41.2***
	7g	*25*	*1*	*1.7*	*14.1*
		10	*2*	*3.4*	*-8.9*
South	*g2*	*10*	*1*	***5.4***	***68.1***
		10	*2*	***6.8***	***72.9***
	g4	*10*	*1*	***2.3***	***-26.6***
		10	*2*	***4.4***	***-43.7***
	g5	*10*	*1*	***6.7***	***-72.6***
		25	*2*	***2.0***	***-90***
East	*g4*	*10*	*1*	*4.2*	*61.3*
		10	*2*	*2.5*	*90*
	g5	*25*	*1*	*1.7*	*7*
		10	*2*	*5.9*	*25.1*
	g6	*7*	*1*	*7.2*	*-36.4*
		25	*2*	*2.1*	*-60.9*
West	*g1*	*10*	*1*	***6.9***	***37.3***
		10	*2*	***8.0***	***47.3***
	g2	*10*	*1*	*6.0*	*-24.4*
		10	*2*	*4.7*	*-32.1*
	g3	*10*	*1*	*6.8*	*-73.1*
		10	*2*	*5.5*	*-90*

a. Refer to Figure H-7.

H.2.7 Running a Point Order Check for the Gaps

Similar to the procedure discussed in H.2.3, a point order check was run to determine the correct order of the gap coordinates. Gap coordinates in Bold letters in Table H-2 show the points that needed re-ordering.

H.2.8 Determine the Angular Description of the Gaps

The lone parameter needed to define the gap is the displacement angle (α_{dg}) and was calculated using Equation (5-17) and corrected in Equations (5-18) to (5-20). Table H-2 shows the calculated displacement angles of all visible gaps for the four surfaces of the model.

Figure H-8 **Calculated Displacement Angle of visible Gaps.**

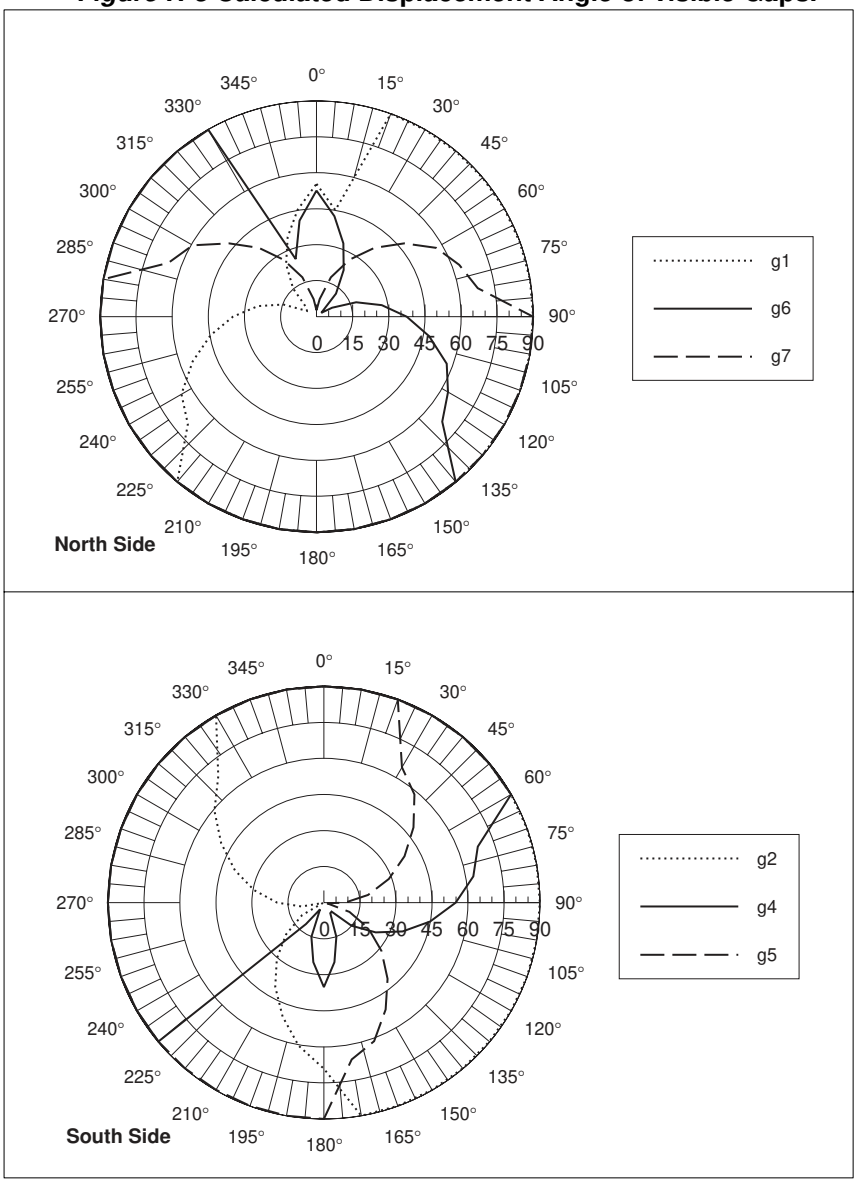

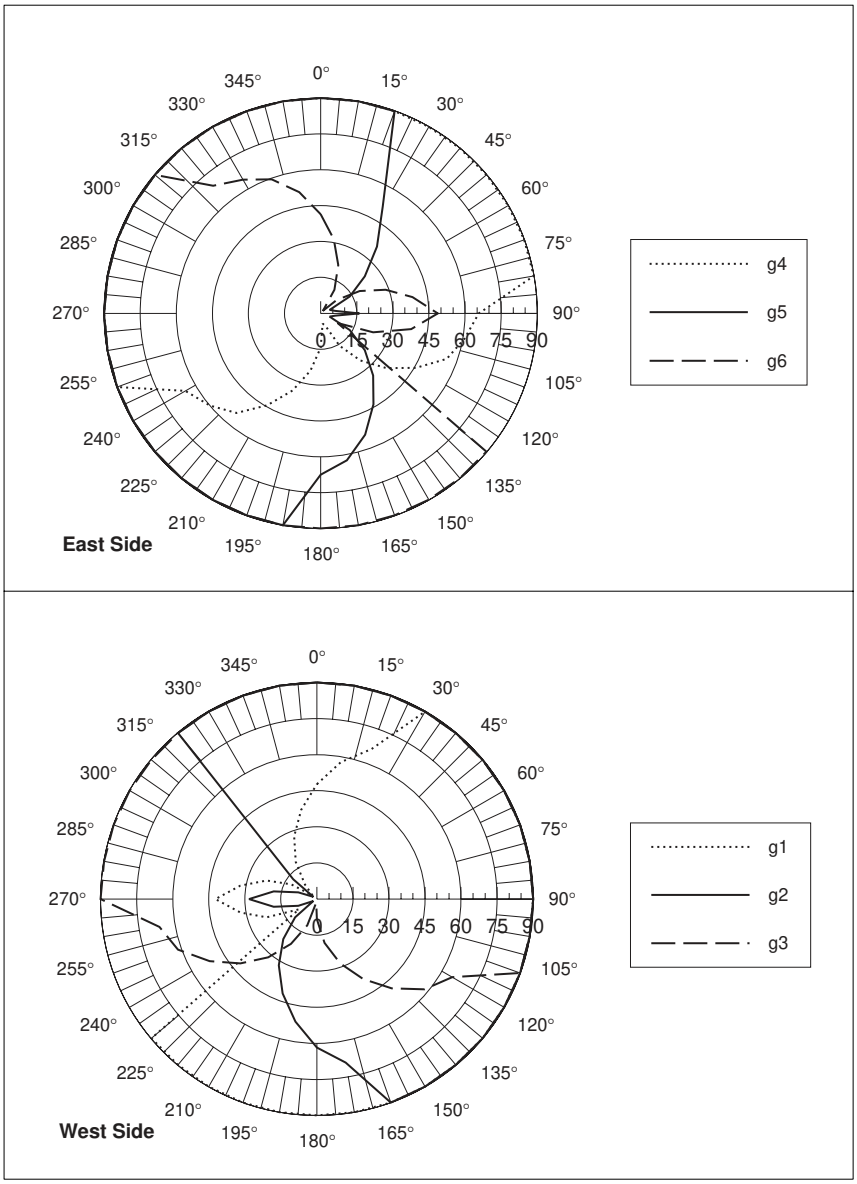

H.2.9 Calculate C_{pm} for Individual Blocks

The determination of the shielding effect of the individual obstruction blocks on the four model surfaces described in the following sections adheres to the algorithm presented in Chapter 4 and illustrated in Figure H-1.

H.2.9.1 Orthogonal Model

This calculation is performed on all obstruction blocks visible from the surface for which C_{pm} was determined. Based on the angles of obstruction determined in STEP H.2.5, formula (D-1)

was used to calculate the value of $C_{pm(ortho)}$ for all surfaces based on the individual shielding of all visible blocks[3].

H.2.9.2 Correction for Displacement

Similarly, the correction for displacement ($C_{pm_{\alpha d(corr)}}$) was implemented using formula (4-13) for all obstruction blocks. The resulting values were then categorized based on the geometric relation between the considered surface and the individual obstruction block.

H.2.9.3 Correction for Wind Direction (Scenario I)

The effect of changing the wind direction for blocks that follow scenario I configuration[4] was performed for all obstruction blocks except for blocks 9 and 10 (Figure H-2). This means that no correction was needed except that was applied when $\alpha_h > 140°$. When this latter condition was met, the correction in Equation (4-17) was applied. However, only blocks 1, 3 and 7a cause the pressurization effect described in Equation (4-17). The other blocks do not cause this pressurization and thus $C_{pm_{\Theta(corr)}} = C_{pm_{\alpha d(corr)}}$ (Figure 4-71)

H.2.9.4 Correction for Wind Direction (Scenario II)

Even though obstruction blocks 9 and 10 fit Scenario III description, the discussion in Section 4.14.1 explained that Scenario II correction was to be used. The applied correction for $\alpha_h > 10°$ was described in Equation (4-19) in Section 4.14.4.3. However, when $\alpha_h < 10°$ the pressurization is non-effectual since blocks 9 and 10 are shifted relative to the considered surface. In these cases, the value of $C_{pm_{\Theta(corr)}} = C_{pm_{\alpha d(corr)}}$ and pressurization is expected (Figure 4-71).

H-3. A simpler version of the relationship was described in Equation (4-11), Section 4.12.3.2.

H-4. Section 4.14.3 on page 114.

H.2.9.5 Correction for Boundary Layer

The boundary conditions under which the model is tested were described in Section 4.17.4. The correction factor for that boundary layer is 0.92 (TABLE B-1). Each value of calculated individual $C_{pm_{\Theta(corr)}}$ was multiplied by the boundary layer correction factor.

H.2.10 Calculating C_{pm} for the Multiple Obstruction

Based on the input from Section H.2.9 and Section H.2.8, the calculated values of $C_{pm_{\Theta(corr)}}$ and α_{dg} were used in Equation (4-22) to determine the average shielding effect of surrounding obstruction blocks ($C_{pm_{\text{multiple}}}$). Figures H-9 to H-12 show the result of calculating the shielding effect of multiple obstruction blocks on each surface.

Figure H-9 **Predicted pressure modification coefficients on the North surface**

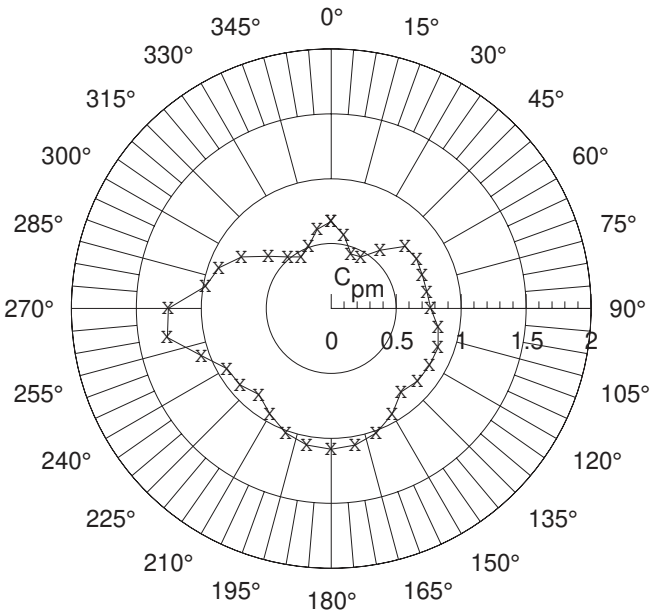

Figure H-10 **Predicted pressure modification coefficients on the South surface**

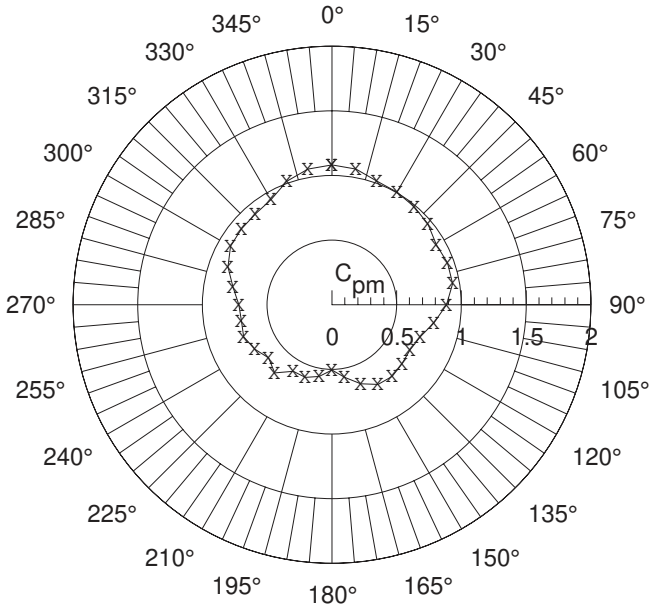

Figure H-11 **Predicted pressure modification coefficients on the East surface**

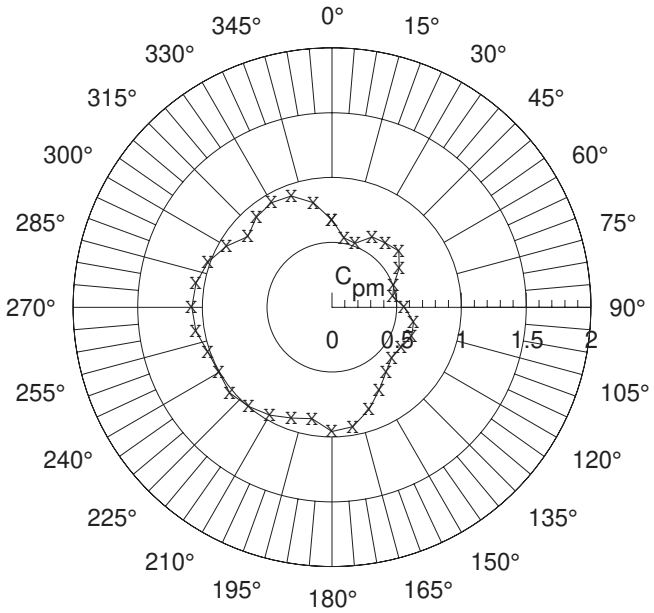

Figure H-12 **Predicted pressure Modification coefficients on the West surface**

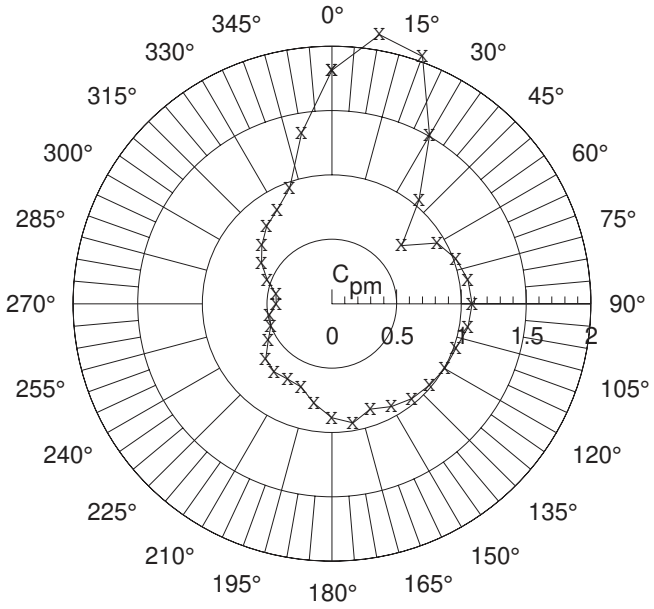

H.2.11 Determination of Unobstructed C_p Values

This section deals with the conversion of the calculated Pressure Modification Coefficients C_{pm} to Pressure Coefficient values that can be used in existing models for predicting indoor airflow. Based on Equation (4-3), the calculated values of C_{pm} were converted to $C_{p(Shielded)}$ using the following relationship;

$$C_{p(Shielded)} = \ln\left[C_{pm} \cdot e^{C_{p(Unshielded)}}\right] \quad \textbf{(H-1)}$$

H.2.11.1 C_p at Wind Direction $\Theta = 0°$

Some of the sources for the unshielded surface pressure coefficients on building surfaces are described in Section 5.6. In addition to these sources, the data from this research are documented in Appendix C, and can also be used.

For this experiment, the values of $C_{p(Unshielded)}$ for all wind directions for the two surfaces (N or long and E or short sides)[5] were measured in the wind tunnel. Figure H-13 shows the values of the pressure coefficient of the unobstructed model used in the determination of C_{pm} values as in Figures G- 14 to G-17.

H.2.11.2 Calculate C_p at Wind Direction $\Theta > 0°$

When the wind direction is larger than 0˚, models such as Swami and Chandra (Ref. 203) or the modified function developed in this research (Section 4.11.2) and illustrated in Equation (4-7) may be used. Figures 4-24 and 4-28 can also be used to provide the designer with the row data needed to establish the value of $C_{p(Unshielded)}$. The latter will be used in the determination of the Pressure Modification Coefficient C_{pm} using the relationship described in Section 4.10 and shown in Equation (H-1). It should be noted that the slight difference between the two curves in Figure H-13 is due to the difference in their respective aspect ratio (A_s). In Equation (4-7), the aspect ratio of the surface under consideration is accounted for in the prediction of the $C_{pm@\Theta}$.

H-5. Refer to Figure 4-100, pp. page 161.

Figure H-13 **Pressure modification coefficients of the unobstructed instrumented model**

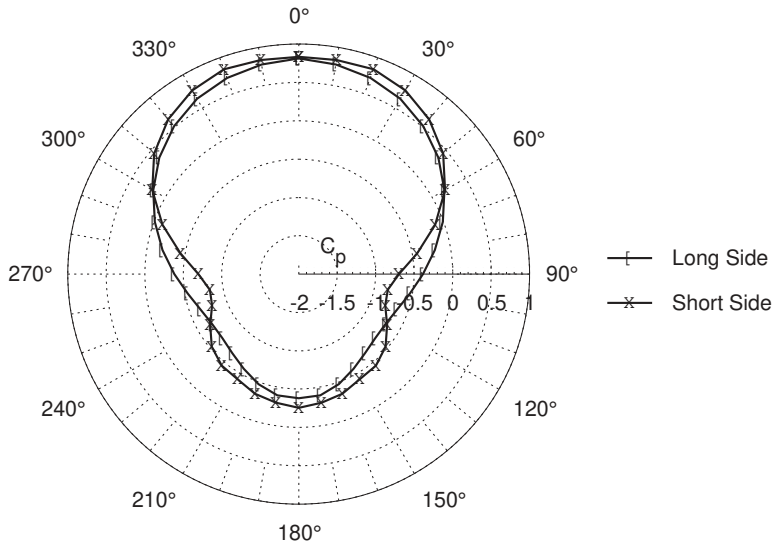

H.2.12 Determination of the Shielded Pressure Coefficients $C_{p(Shielded)}$

Based on the values of C_{pm} calculated in Section H.2.10 and Equation (H-1), the Pressure Coefficients of the shielded mdel ($C_{p(Shielded)}$) were calculated and presented in Figures G- 14 to G-17.

Figure H-14 **Predicted pressure coefficients on the North surface**

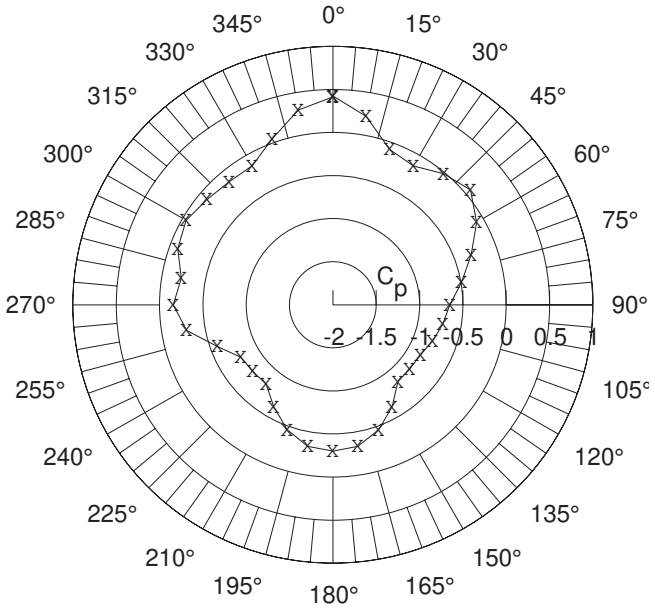

Figure H-15 **Predicted pressure coefficients on the South surface**

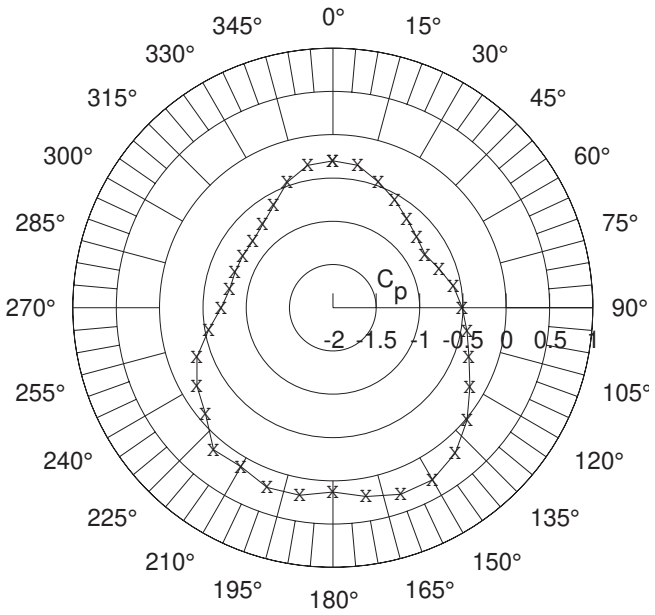

Figure H-16 **Predicted pressure coefficients on the East surface**

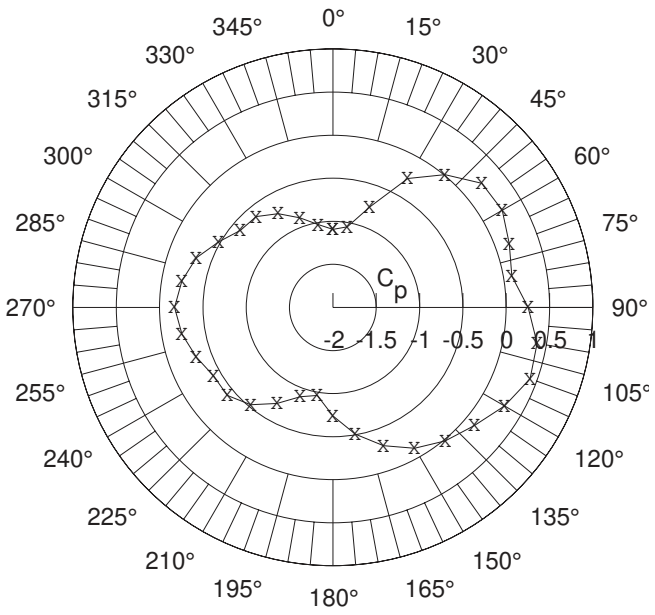

Figure H-17 **Predicted pressure coefficients on the West surface**

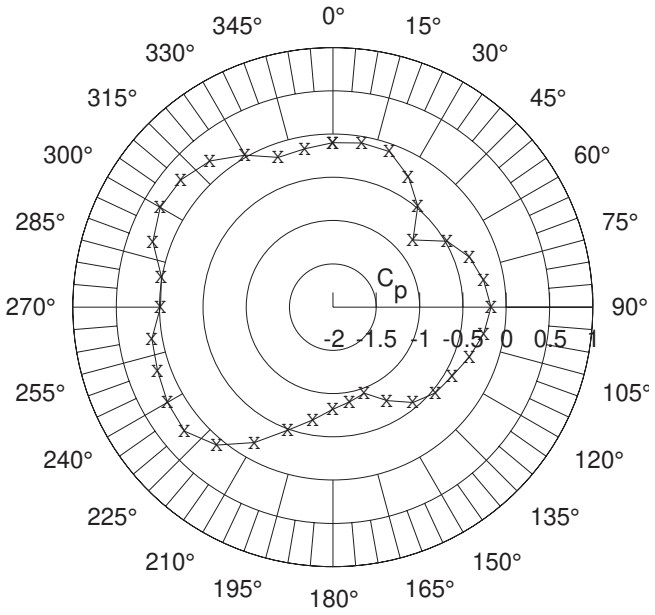

H.2.13 Building Characteristics

The building in our case is a single storey with a flat roof, rectangular plan, and single space with no interior partitions.

As shown in Figure H-18, the windows in the experiment are located on the long sides opposite to each other[6]. The windows in both walls have the same dimensions, location, and surface area (Figure 18).

Figure H-18 **The Windows Configurations**

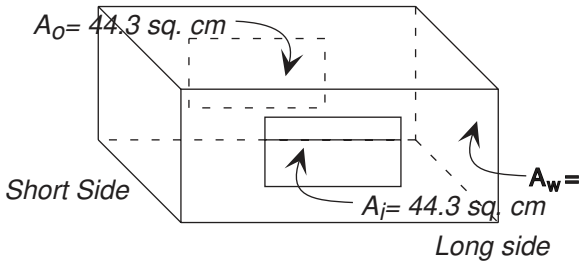

H.3 Determining Indoor Velocity

The transformation of the predicted pressure data involves the implementation of Ernest mathematical model discussed in Section 5.8. The determination of the indoor air velocity of the physical model follows a step-by-step calculation of the different variables described in Equation (5-29).

H.3.1 Effect of Pressure Distribution and Wind Direction (f_1)

The function that is used to determine effect if pressure distribution and wind direction[7] is as follows[8]:

$$f_1(C_p, \Theta) = (C_1 \cdot \Delta C_p + C_2 \cdot C_{pw} \cdot \cos\Theta + C_3 \cdot C_{pl} \cdot \cos\Theta_{ws} + C_4 \cdot \cos\Theta_{ws} + C_5)^{0.5} \quad \textbf{(H-2)}$$

Where

H-6. Surfaces N and S.

H-7. Refer to Equation (5-29).

H-8. Ernest 1991, ((Ref. 74)), Equation A.3-2 pp. 249.

Θ = Wind direction ($0° \le \Theta \le 90°$)

C_{pw} = Pressure coefficient at windward side

C_{pl} = Pressure coefficient at leeward side

$\Delta C_p = \left| C_{pw} - C_{pl} \right|$

The empirical coefficients are:

$C_1 = 0.0203$

$C_2 = 0.0296$

$C_3 = -0.0651$

$C_4 = -0.0178$

$C_5 = 0.0054$

Since Ernest's Model limits wind direction to $0° \le \Theta \le 90°$, wind direction $90° < \Theta_{ws} \le 360°$ had to be broken into three quadrants 90˚ each. In both the first and fourth quadrants where $0° \le \Theta \le 90°$ and $270° \le \Theta \le 360°$ respectively, surface N was the windward surface while S was the leeward side in Equation (H-2). In the second and third quadrants ($90° \le \Theta_{ws} \le 180°$ and $180° \le \Theta_{ws} \le 270°$), surface N becomes the leeward while S is the windward surface in Equation (H-2).

Table H-3 **Result of calculating f_1 (First Quadrant)**

Θ_{ws}	Θ	C_{pw}	C_{pl}	ΔC_p	$f(C_p, \Theta)$
0	*0*	*0.4143*	*-0.3014*	*0.71566*	***0.40591***
10	*10*	*0.21888*	*-0.3295*	*0.54836*	***0.35594***
20	*20*	*-0.0814*	*-0.4554*	*0.37401*	***0.30032***
30	*30*	*-0.1382*	*-0.5658*	*0.42766*	***0.32428***
40	*40*	*-0.0129*	*-0.6684*	*0.65546*	***0.39732***
50	*50*	*0.07248*	*-0.7343*	*0.80675*	***0.4357***
60	*60*	*-0.0867*	*-0.772*	*0.68537*	***0.39935***
70	*70*	*-0.3001*	*-0.6927*	*0.39264*	***0.30233***
80	*80*	*-0.4921*	*-0.5874*	*0.09526*	***0.16049***
90	*90*	*-0.6498*	*-0.5063*	*0.14352*	***0.18583***

Table H-4 Result of calculating f_1 (Second Quadrant)

Θ_{ws}	Θ	C_{pw}	C_{pl}	ΔC_p	$f(C_p, \Theta)$
180	0	0.13062	-0.3014	0.43198	**0.31429**
170	10	0.21498	-0.3295	0.54446	**0.35466**
160	20	0.29556	-0.4554	0.75101	**0.42096**
150	30	0.29906	-0.6343	0.9334	**0.47212**
140	40	0.19773	-0.8326	1.03031	**0.49691**
130	50	0.02241	-0.8431	0.86548	**0.45316**
120	60	-0.1761	-0.8336	0.65751	**0.39307**
110	70	-0.3299	-0.7748	0.44486	**0.32176**
100	80	-0.4269	-0.7113	0.28438	**0.25668**
90	90	-0.5063	-0.6498	0.14352	**0.18583**

Table H-5 Result of calculating f_1 (Third Quadrant)

Θ_{ws}	Θ	C_{pw}	C_{pl}	ΔC_p	$f(C_p, \Theta)$
180	0	0.13062	-0.3014	0.43198	**0.31429**
190	10	0.20101	-0.3295	0.53049	**0.35006**
200	20	0.21157	-0.4554	0.66702	**0.39727**
210	30	0.12107	-0.6343	0.7554	**0.42685**
220	40	0.14458	-0.8015	0.94605	**0.47651**
230	50	-0.0831	-0.7929	0.70978	**0.41188**
240	60	-0.1891	-0.775	0.58585	**0.37129**
250	70	-0.3303	-0.5829	0.25267	**0.24544**
260	80	-0.5458	-0.287	0.25886	**0.23515**
270	90	-0.7129	-0.1583	0.55466	**0.3435**

Table H-6 Result of calculating f_1 (Fourth Quadrant)

Θ_{ws}	Θ	C_{pw}	C_{pl}	ΔC_p	$f(C_p, \Theta)$
360	0	0.4143	-0.3014	0.71566	**0.40591**
350	10	0.29602	-0.3295	0.62551	**0.38026**
340	20	0.05105	-0.4554	0.5065	**0.34753**
330	30	-0.1376	-0.6343	0.49673	**0.35079**
320	40	-0.137	-0.7405	0.60357	**0.38486**
310	50	-0.1001	-0.7958	0.69574	**0.40815**
300	60	-0.0425	-0.7999	0.75742	**0.41912**
290	70	-0.0948	-0.7981	0.7033	**0.39861**
280	80	-0.2226	-0.788	0.56539	**0.35334**
270	90	-0.1583	-0.7129	0.55466	**0.3435**

Since it is assumed in this example that the reference velocity was measured at eave height, the ratio of V_e/V_r should equal unity and no correction for the value of f_1 was needed.

H.3.2 Effect of Window Size (f_2)

In Section H.2.13, the porosity (φ) of the two walls were established (Figure 18). The effect of window size is determined based on the following function[9]:

$$\varphi = \frac{2 \cdot A_i \cdot A_o}{\left[A_w \cdot (2 \cdot A_i^2 + 2 \cdot A_o^2)^{0.5}\right]} \quad \textbf{(H-3)}$$

Where;

φ = Building porosity
A_i = Open inlet area
A_o = Open outlet area
A_w = Interior of wall containing opening

The resulting value of is;

$$\varphi = \frac{2 \times 44.3 \times 44.3}{[192 \cdot (2 \times 44.3^2 + 2 \times 44.3^2)^{0.5}]}$$

$$= 0.23$$

The derived value of porosity φ is within the limits i.e $0.06 \le \varphi \le 0.25$.

The function accounting for building porosity is[10]:

$$f_2(\varphi) = C_1 \cdot \varphi + C_2 \quad \textbf{(H-4)}$$

Where;

H-9. Ernest, D. Op. Cit, Equation A.3-3 on pp. 250.
H-10. Ibid. Equation A.3-4 on pp. 250.

$$C_1 = 3.48$$

$$C_2 = 0.42$$

The resulting f_2 for the model is 1.22.

H.3.3 Effect of Interior Partitions (f_3)

Since no partitions were inside the model, the value of f_3 is 1.0.

H.3.4 Effect of Window Accessories (f_4)

Since no insect screen or awning is specified f_4 will be 1.0.

H.3.5 Calculating Velocity Coefficient (C_v)

Based on Equation (5-29), the values of C_v were calculated and shown in Figure H-19.

Figure H-19 **Calculated velocity coefficient *(C_v)***

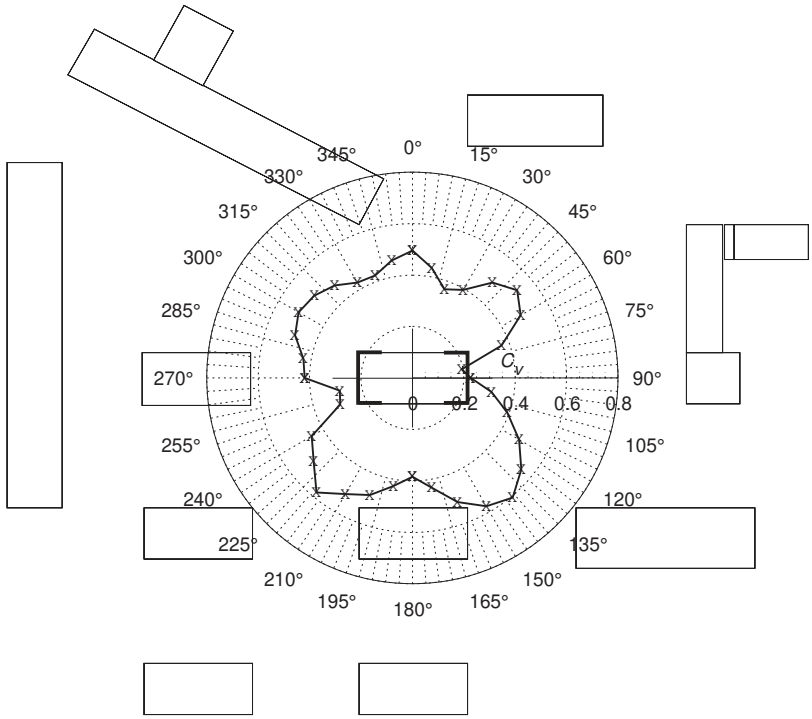

Other indoor airflow characteristics can be predicted based on the velocity coefficient values. Based on Ernest's model, the calculated velocity coefficient values can be used to determine the indoor turbulence[11] and indoor velocity distribution[12] of the building for which indoor airflow was to be studied[13].

H.3.6 Determining the Wind Speed at Site

Wind data can be in hourly, tri-hourly, daily, monthly formats. In all cases the wind speeds are associated with cardinal wind direction. The indoor velocity prediction routine can use all these formats resulting in indoor airflow predictions related to seasonal variation as well as diurnal in the case of hourly data.

Based on a hypothetical wind rose[14] and an adapted site wind velocity prediction routine from SITECLIMATE (Section 5.7), a year-round wind speed and corresponding probability of exceedance was determined (Figure H-21). For ventilation purposes, the 1% and 5% exceedance lines were reasonable levels for design.

Section 5.7 discusses the correction of weather station wind data to the specific site conditions for use by the Indoor Velocity Model (IVM). The two correction factors applied to the data from hypothetical wind rose mentioned above, are calculated below;

H-11. Turbulence Coefficient (C_t).

H-12. Coefficient of Spatial Variation (C_{sv}).

H-13. Ernest op. cit. pp. 254-261.

H-14.Reference: ASHRAE Handbook of Fundamentals 1989, pp. 14.8.

H.3.6.1 Effect of Terrain and Height

Arens *et al* (Ref. 10) state that if the reference is located in an open terrain[15] –typical airport weather station conditions–, equation (5-21)[16] can be rewritten as:

$$\text{ROGRAT} = 0.2p \cdot \ln\left(\frac{z}{z1_0}\right) \quad \textbf{(H-5)}$$

Where

$$p = \left(\frac{u_f}{u_{f1}}\right)$$

z = height of eave (m)

The boundary conditions of the tested model were equivalent to those of a small town or a suburban development ($z1_0 = 0.3$ m). From Table H-7, the value of p in equation (H-6) is equal to 1.15. Since the eave height was taken to be 2.5 m, therefore;

$$\therefore \text{ROGRAT} = 0.2 \times 1.15 \times \ln\left(\frac{2.5}{0.3}\right)$$

$$= 0.49$$

Table H-7 **Mean Wind Profile Parameters[17]**

z_0	$p = \left(\frac{U_f}{U_{f1}}\right)$
0.005	*0.83*
0.07	*1.00*
0.3	*1.15*
1.00	*1.33*
2.50	*1.46*

In the example, the assumption is that the boundary conditions at the eight cardinal wind direction to be the same. Therefore, the

H-15. or $z1_0 = 10$ m and $z_0 = 0.07$.

H-16. page 199.

H-17. Source: Bietry *et al* (Ref. 36).

value of ROGRAT=0.49 should be multiplied by the wind data for all wind directions (Figure H-20).

Figure H-20 **Application of SITECLIMATE: eight cardinal wind directions to correspond with different boundary layers and topography around the site**

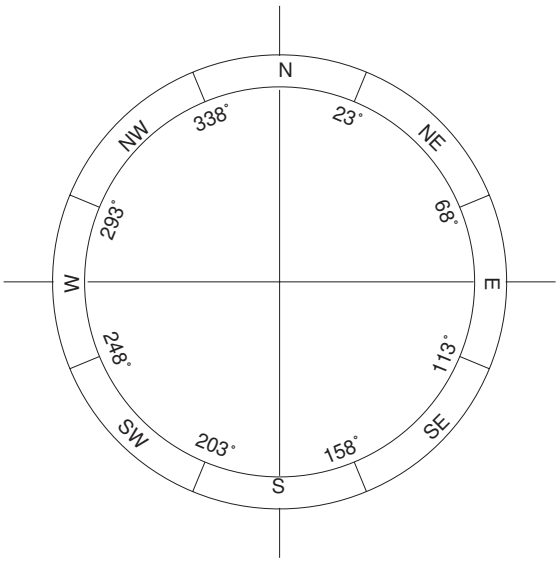

H.3.6.2 Effect of Topography

The effect of topography was not included in this example since the urban layout was assumed to be flat. Therefore, SLPFAC is taken to be 1.0.

Figure H-21 shows the result of weather station wind data conversion to site wind speeds at a point located in the middle of the considered model[18].

H-18. The location of the point is take without the model in place.

Figure H-21 **Wind Speeds and probability of exceedance at the Building Site.**

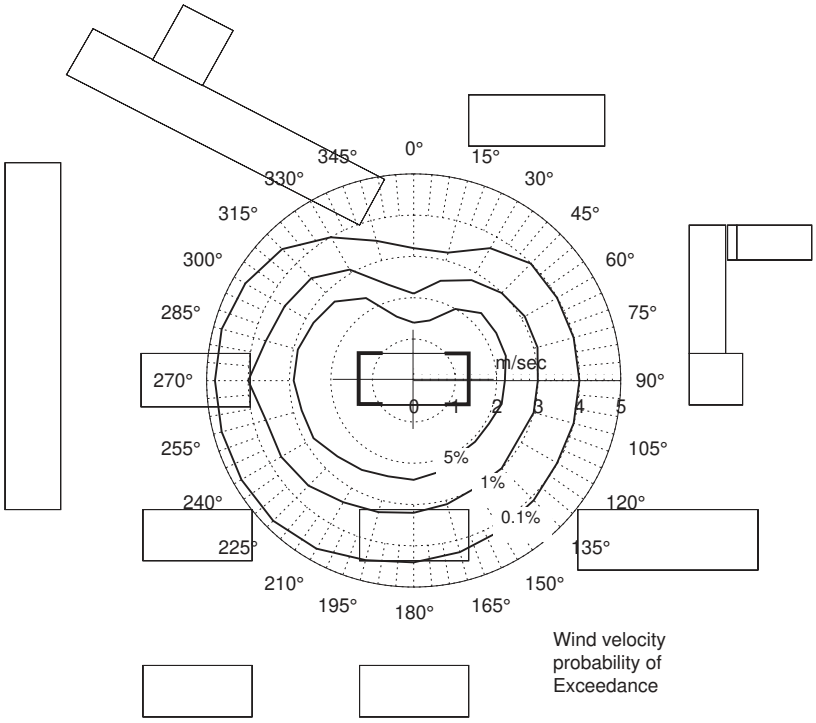

H.3.7 Determining Indoor Wind Velocity

Figure H-22 demonstrates the result of calculating the predicted interior velocity of the space[19].

$$V_i = C_v \times V_o \quad \textbf{(H-6)}$$

Where

V_i = Indoor air speed m/s

V_o = Wind speed at site m/s

The polar diagram shows that indoor wind speeds were at minimal levels when wind direction is parallel to the windows (90˚ and 270˚). However, at wind direction equals to 270˚, the surrounding buildings were lower in height that those facing the eastern side

H-19. Based on Equation (3-1).

(90˚). The mathematical model was able to predict these difference resulting in lower indoor wind speeds at corresponding wind angles.

The wind directions at which the space experienced the highest indoor air speeds coincided with the gaps between the buildings. This proves that the model can handle complex urban geometries where multiple surrounding buildings of various sizes, forms, interacting with each other.

Figure H-22 **Predicted interior wind velocities.**